An X-ray Tube Focal Spot Size Measurement Technique Using A Digital Imaging Computer Method

by

Konstantinos Chantziantoniou

A thesis
submitted to the Faculty of Graduate
Studies in partial fulfillment of the
requirements for the degree
of

Master of Science

Department of Physics

Winnipeg, Manitoba

ISBN 0-315-76601-8

AN X-RAY TUBE FOCAL SPOT SIZE MEASUREMENT TECHNIQUE USING A DIGITAL IMAGING COMPUTER METHOD

BY

KONSTANTINOS CHANTZIANTONIOU

A thesis submitted to the Faculty of Graduate Studies of the University of Manitoba in partial fulfillment of the requirements of the degree of

MASTER OF SCIENCE

DEDICATION

I dedicate this work to my wife Connie Rose and children Dimitrios John and Alexander Nicolas.

ABSTRACT

The image quality of radiographs is continually of concern to radiologists. In the radiographic imaging chain, it is the finite size of the focal spot that is one of the major contributors to this quality. Difficulties can arise when the focal spot dimensions enlarge and image quality deteriorates below a level acceptable to radiologists thus making the use of the diagnostic x-ray equipment unacceptable for certain radiographic examinations. To maintain quality assurance standards, methods of measuring the manufacturers' indicated focal spot size have been established of which the pinhole camera and star resolution test pattern methods are the currently acceptable techniques. Since both of these techniques have certain drawbacks - the pinhole camera technique requires generator settings that are much higher than those generally used during diagnostic x-ray examinations and the star resolution pattern involves a subjective interpretation of the exact resolution of the test tool film image by the individual that is performing the focal spot measurement, it was decided to develop a new, more objective technique that can be used to evaluate the size of the focal spot at clinically used x-ray machine settings. For this purpose, a computer algorithm was devised to be used in conjunction with digital imaging techniques to extract the focal spot's horizontal and vertical dimensions from a

digitized image of an x-ray film image of a specially designed parallel wire focal spot test tool. This new technique not only produces results that are in agreement with both the star resolution test tool pattern and pinhole camera methods, but also typically provides results to an overall accuracy of ± 6%, over a wide range of x-ray generator settings.

ACKNOWLEDGEMENTS

I would like to express my deepest gratitude to professor A.M. Sourkes for his undivided attention during those frequent discussions concerning the experimental techniques and data analysis. I am indebted to him for the knowledge and experience that I have gained. I would also like to thank him for enduring so patiently the division of my attention during the preparation of this work.

I wish to express thanks to Dr. S. Shalev for allowing me to use his focal spot test tools and digital imaging equipment. His contribution to this work was greatly appreciated. Particular thanks are due to K. Leszczynski, S. Cosby and T. Chu for their valuable suggestions relating to the analysis of the digital imaging test tool film images. I would also like to thank R. Kowaluk, G. Philippot and C. Neduzak for their valuable discussions concerning the utilization of the focal spot test tools and other quality assurance test equipment. It is also a pleasure to thank D. Elcheshen, R.T.(R) and S. Hereman, R.T.(R) from the Health Sciences Center Department of Radiology and E. Zemianski, R.T.(R) from Radiology Consultants of Winnipeg for their assistance in the collection of the diagnostic and mammographic x-ray tube focal spot data.

I would also like to express many thanks to the University of Manitoba's Dental College for providing the special x-ray

film that was used with the pinhole camera tests, to the Health Sciences Centre General Hospital's Department of Radiology for the use of their film processing equipment, and to the Manitoba Cancer Foundation's mechanical devices shop for constructing the parallel wire focal spot test tool.

Special thanks are reserved for my wife, Connie Rose, who has given me continuing encouragement during this work and without whose support it could have not have been completed. I would also like to thank all my family members for both their emotional and financial support.

Last but not least I would like to thank the Manitoba Cancer Treatment and Research Foundation for the financial support provided via a graduate studies studentship.

TABLE OF CONTENTS

LIST OF FIGURES

LIST OF TABLES

CHAPTER I

INTRODUCTION

Radiologists are continually concerned with the image quality of diagnostic radiographs, whose quality is dependent upon adequate performance of the x-ray imaging chain of which the x-ray tube is an integral part. In particular, in the radiographic imaging system it is the finite size of the x-ray tube focal spot that leads to a type of image blurring called geometrical unsharpness [Fig. 1]. For this reason, it is recommended that radiology departments include a routine evaluation of the "effective" focal spot size in their equipment quality assurance programs [Ref. 1,2]. The "effective" focal spot size will henceforth be referred to as the focal spot.

It is known and expected that upon x-ray tube installation the dimensions of most focal spots are generally larger than the nominal size quoted by the manufacturers. In fact the National Electrical Manufacturers' Association (NEMA) [Ref. 3] specification standard for focal spots allows the actual focal spot dimension to exceed the specified dimension by up to 50% when measured using the pinhole camera technique [Ref. 4]. It is also known that after a period of time, the x-ray tube focal spot dimension may grow to such a degree that it

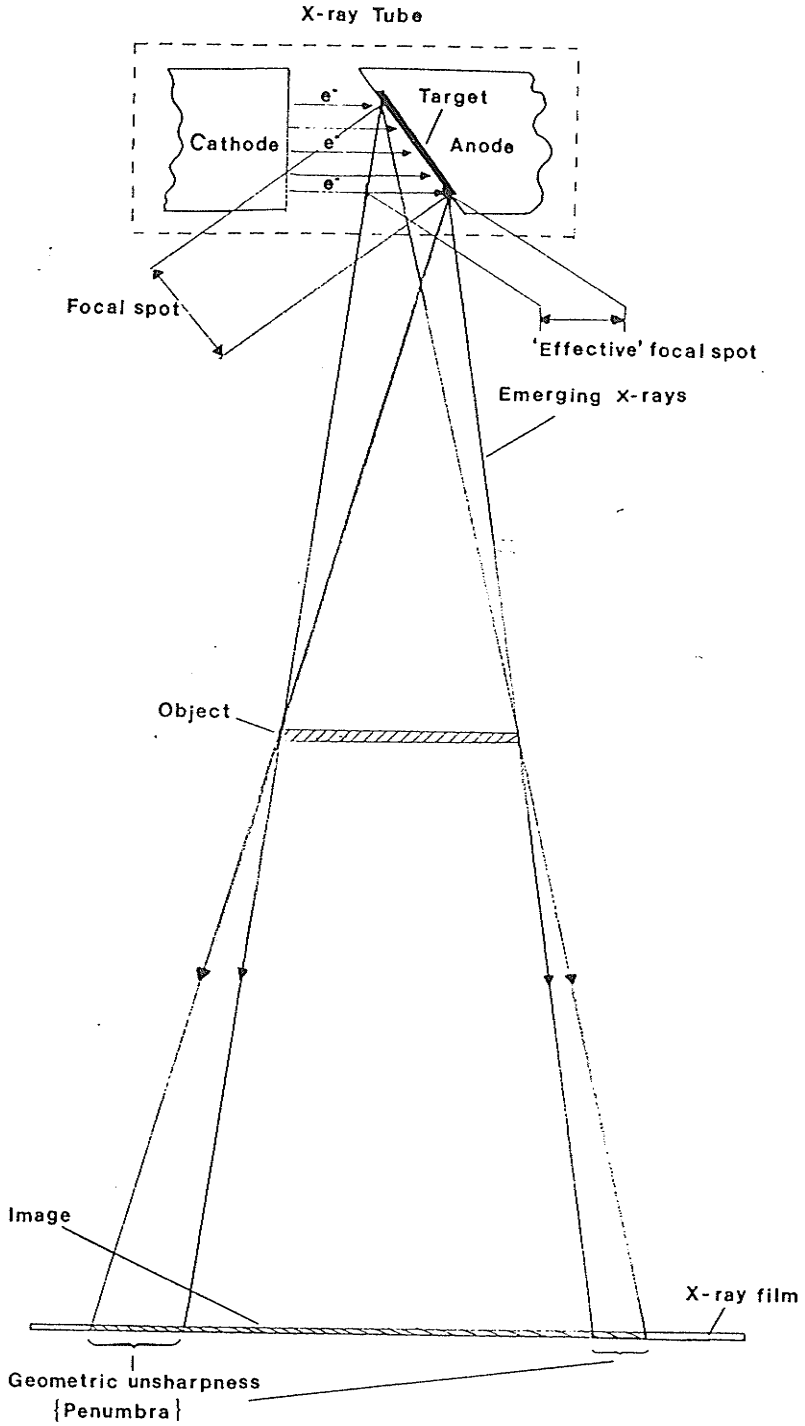

[Fig. 1]

Geometric unsharpness (penumbra) illustration for a typical x-ray tube. Diagram is not to scale.

compromises certain types of radiographic imaging. This is particularly so for magnification radiography [Ref. 5], which requires the use of the smallest practical focal spot size, usually no larger than 0.3 mm [Ref. 6]. To maintain quality assurance, various international organizations such as:

(a) the International Commission on Radiological Units and Measurements (ICRU) [Ref. 7]; and

(b) the National Electrical Manufacturers Association (NEMA) [Ref. 3]

have recommended or established standard methods for evaluating the focal spot size.

At present, ICRU recommends that the focal spot dimensions be determined by means of a pinhole camera [Ref. 4,8], with a pinhole diameter [Table 1] that depends on the focal spot size being measured. To reduce the uncertainty in this focal spot measurement, the penumbra region of the focal spot image on the x-ray film (radiograph) - which is unavoidable due to the finite size of the pinhole - has to be reduced. This is accomplished by using a pinhole diameter that is considerably smaller than the focal spot. One difficulty that arises from the ICRU recommended method occurs due to the use of a pinhole with a diameter of 0.03 mm, for example, in the x-ray imaging of focal spots with a nominal size below 1 mm. Because such pinholes allow very little radiation to pass, the investigator must resort to setting long exposure times, or, less desirably, multiple exposures of the pinhole, both of which are clinically atypical. In addition the use of

[Table 1]

ICRU Recommendations

Pinhole Diameter (mm)	Focal Spot Size (mm)
0.030	below 1.0
0.075	1.0 to 2.5
0.100	above 2.5

large value x-ray tube mAs settings could damage the x-ray tube, rendering such pinhole diameters as impractical for certain x-ray tube capacities. To compensate for this difficulty, NEMA recommends use of a star pattern [Ref. 9,10] for measurement of focal spots with a nominal size of 0.3 mm or less with pinhole cameras utilized for focal spots larger than 0.3 mm [Table 2].

Even though the pinhole camera is regarded as the "standard" method of measuring the focal spot sizes, it has the following problems:

(a) the size of the x-ray image of a 0.3 mm focal spot is so small that accurate measurement requires special equipment;

(b) because the x-ray intensity of the focal spot image about its length (along the x-ray tube cathode-anode axis) peaks near the center of the focal spot and fades towards the edges, an accurate measurement of the length of the focal spot is observer dependent;

(c) the accuracy of the 0.7 correction factor to the long dimension of the focal spot, which is used to compensate for the uneven focal spot intensity distribution, is somewhat arbitrary; and

(d) when the pinhole camera is positioned the pinhole must be aligned to the central beam of the x-ray tube. In those cases where the light field indicator is inaccurate, this location may be difficult to determine.

As a result of these difficulties with the pinhole camera method, the star resolution pattern method has gained increasing acceptance. It should be noted that a pinhole image of the focal spot gives more insight into the actual focal spot size, configuration and intensity distribution, while a star pattern image provides directional information

[Table 2]

NEMA Recommendations

Pinhole Diameter (mm)	Focal Spot Size (mm)
Star pattern	below 0.3
0.030	0.3 to 1.2
0.075	1.2 to 2.5
0.100	above 2.5

on the resolving capacity of the focal spot, which is a function of both its size and radiation intensity distribution within the 360° pattern.

The drawbacks in using star pattern images to determine the focal spot size are twofold: 1) is that it is somewhat dependent on the film optical density of the test tool's film image and 2) it strongly depends on the individual that is performing the test (this will be illustrated in chapter IV). It is the purpose of this work to devise a more versatile and objective method of determining focal spot sizes.

In order to remove the observer subjectiveness in a focal spot measurement, a computer-automated algorithm has been devised that uses digital imaging techniques to extract the focal spot length and width from a digital image of an x-ray film image of a parallel wire test tool.

Chapter II will present the radiographic imaging system from x-ray production within the x-ray tube to image formation on the x-ray film, and Chapter III presents the experimental apparatus and the procedures employed to obtain a film image of the focal spot when using a star resolution pattern, a bar resolution pattern [Ref. 11], a pinhole camera and a parallel wire test tool. Chapter IV will describe the analysis that was done to measure the focal spot dimensions from the various test tool film images. Finally, Chapter V compares the focal spot dimensions obtained using the digital imaging method to those obtained from the more conventional

measuring techniques, and comments on the effectiveness of the digital imaging technique to determine the focal spot size.

CHAPTER II

THE RADIOGRAPHIC SYSTEM

II.a The Discovery and Nature of X-rays

The German physicist, Wilhelm Conrad Roentgen, discovered x-rays on November 8, 1895 [Ref. 12] during his investigations of "cathode rays" (electrons) in gaseous discharge tubes. A number of studies of this historic discovery have been published [Ref. 13-16]. In recognition of his outstanding contribution to science, Roentgen was awarded the fist Nobel Prize for Physics in 1901.

The application of x-rays to the field of medicine was perhaps first realized by Roentgen when he placed his hand between the discharge tube and a fluorescent screen, and to his surprise saw an image of his hand's skeleton on the screen. This observation later inspired Roentgen to make the first radiograph while using his wife's hand as the subject on December 22, 1895, but it was not until the time of the first world war that the application of x-rays in medicine was first fully appreciated.

It had been known for some time now that x-rays are a form of electromagnetic radiation [Table 3][Ref. 17]. Thus they too behave as a wave in space and are emitted and absorbed in the form of discrete particles of energy, known as photons. The properties of x-rays that make them ideal for their use in medical radiology are as follows:

[Table 3]

The Electromagnetic Spectrum[1]

	Frequency (Hz)	Wavelength	Photon Energy	Type of Radiation
from	1.0×10^{5}	3 km	413 peV	Radiowaves
to	3.0×10^{10}	0.01 m	124 μeV	
from	3.0×10^{12}	100 μm	12.4 meV	Infrared
to	3.0×10^{14}	1 μm	1.24 eV	
from	4.3×10^{14}	700 nm	1.77 eV	Visible light
to	7.5×10^{14}	400 nm	3.1 eV	
from	7.5×10^{14}	400 nm	3.10 eV	Ultraviolet
to	3.0×10^{16}	10 nm	124 eV	light
from	3.0×10^{16}	10 nm	124 eV	Soft x-rays
to	3.0×10^{18}	100 pm	12.4 eV	
from	3.0×10^{18}	100 pm	12.4 keV	Diagnostic
to	3.0×10^{19}	10 pm	124 keV	x-rays
from	3.0×10^{19}	10 pm	124 keV	Deep therapy
to	3.0×10^{20}	1 pm	1.24 MeV	x-rays/gamma rays
from	1.0×10^{21}	310 fm	4 MeV	Radiation from
to	1.0×10^{22}	31 fm	40 MeV	LINAC

[1]It should be noted that the regions in the spectrum overlap and there is no sudden changes in properties in the propagation from one region to the next.

(a) they can penetrate matter;

(b) when they interact with matter they can produce ionization and/or excitation of the atoms;

(c) they produce fluorescence (and hence visible light) from certain materials;

(d) they affect photographic emulsions; and

(e) they produce biological effects in living tissues.

In the area of diagnostic radiology the production of x-rays is achieved by the use of an x-ray tube, whose various components will be discussed below in some detail.

II.b The Diagnostic X-ray Tube

X-rays are produced whenever a fast stream of electrons is suddenly decelerated as occurs in the "target" anode of an x-ray tube. The requirements to produce x-rays efficiently are:

(a) a source of electrons;

(b) a large potential difference to accelerate the electrons to usable ionizing energies;

(c) an evacuated space to contain the accelerated electrons and to allow them to move essentially unimpaired from the cathode to the anode;

(d) a target to efficiently absorb the accelerated electrons and produce x-rays; and

(e) a glass envelope to enclose the x-ray tube cathode and anode assembly and to maintain the vacuum.

The major components of a diagnostic x-ray tube have been illustrated in [Fig. 2].

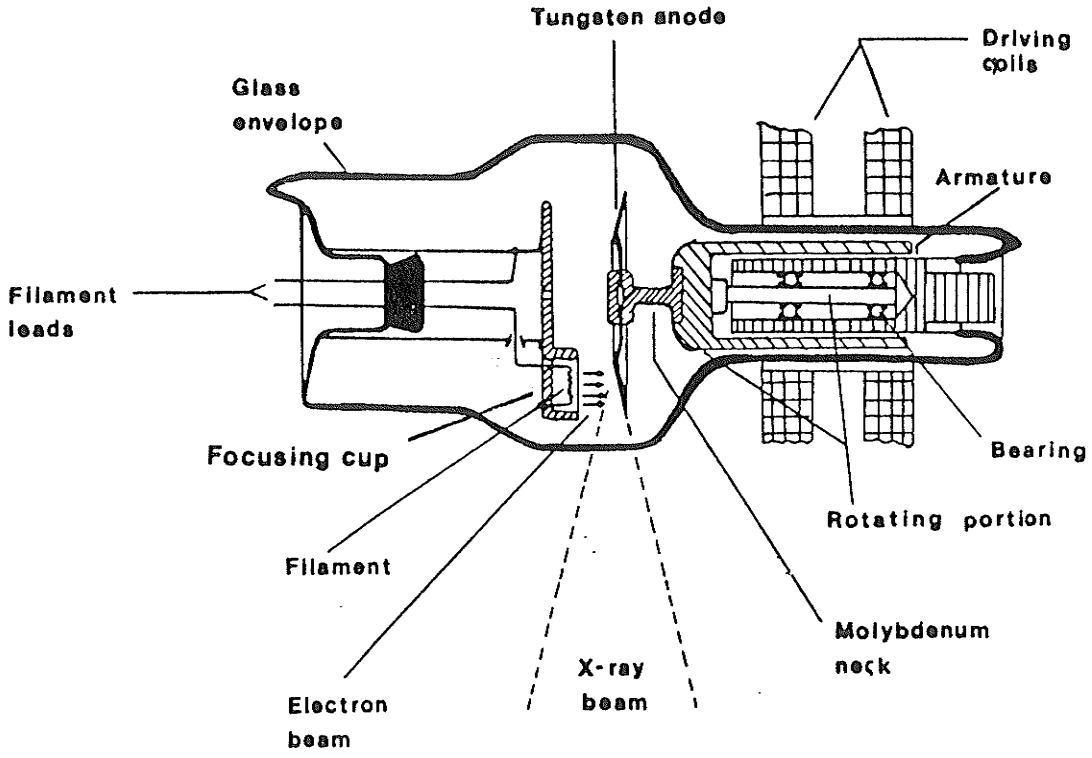

[Fig. 2]

The major components of a diagnostic x-ray tube [Ref. 18].

II.b.1 Cathode Assembly

The negative terminal of an x-ray tube is called the cathode, whose assembly [Fig. 2] consists of a filament which may be heated and thereby acts as the source of electrons in the x-ray tube, connecting wires that supply the amperage and voltage to heat the filament and a metallic electron focusing cup.

II.b.1.i Filament

The filament is typically made of a 0.2 mm diameter tungsten wire that is coiled to form a vertical spiral of 2 mm in diameter and 1 cm or less in length. The fine resistive tungsten wire is heated when an electric current is made to flow through it. As it is heated, the atoms in the metal absorb thermal energy and some of their electrons (in particular those near the surface of the filament) acquire enough energy to be "boiled" off the surface of the filament. Their escape is often referred to as the process of thermionic emission or the Edison effect. The filament must be heated to a temperature of at least 2200°C to emit a useful number of electrons (thermions).

Even though tungsten may not be as efficient in emitting electrons as some other known materials, it was chosen for its high melting point (3370°C), its ability to be drawn into thin wires that are quite durable, and its tendency not to vaporize. The use of tungsten as a filament material

therefore ensures a reasonably long life.

The electrons that have been emitted from the tungsten filament via thermionic emission will form an electron cloud in the immediate vicinity of the filament. The net effect of this cloud of electron "space charge" will be to repel the electrons that have been emitted from the filament back to the filament (since the loss of electrons causes the filament to acquire a positive charge), thus preventing the emission of other electrons from the filament surface until they have obtained sufficient thermal energy to overcome the forces caused by the space charge. The tendency of the space charge to limit the emission of more electrons from the filament is called the space charge effect.

II.b.1.ii Focusing Cup

When the electrons are "boiled" out of the filament, they are emitted in all directions. To focus these emitted electrons in a particular direction and onto a specific location on the positive anode (to be discussed in section II.b.5), a focusing "cup" [Fig. 2] is placed behind (and around) the filament to deflect and steer the emitted electrons. When the x-ray tube is in operation the focusing "cup" is maintained at the same negative potential as the filament. The design of the focusing "cup" then allows the emitted electrons to converge onto the "target" anode. The focusing "cup" is usually made of molybdenum.

To increase the versatility of the x-ray tube, the focusing "cup" is usually fitted with two filaments [Fig. 3]. The differences between the two filaments lie in their length, spiral diameter and tungsten wire diameters. The larger (smaller) filament of the two is often referred to as the coarse (fine) filament. The coarse filament is designed to focus the emitted electrons onto a larger area of the "target" anode and is used when the x-ray tube is to be loaded heavily (during long or high current exposures). The finer filament is used to focus the emitted electrons onto a relatively smaller area of the "target" anode and is used to produce radiographs with higher detail (resolution). It should be noted that only one of the two filaments is used during any single exposure.

II.b.2 X-ray Tube Circuit

The main components of the x-ray tube circuit are illustrated in [Fig. 4]. The circuit is essentially composed of two sections: a high voltage circuit to supply the accelerating potential to the cathode emitted electrons and a low voltage circuit to supply the current to the filament.

II.b.2.i Low Voltage Circuit

To heat the filament to its emission temperature a potential difference of approximately 10 V is required. This produces a filament current of between 3 and 5 A. Because the

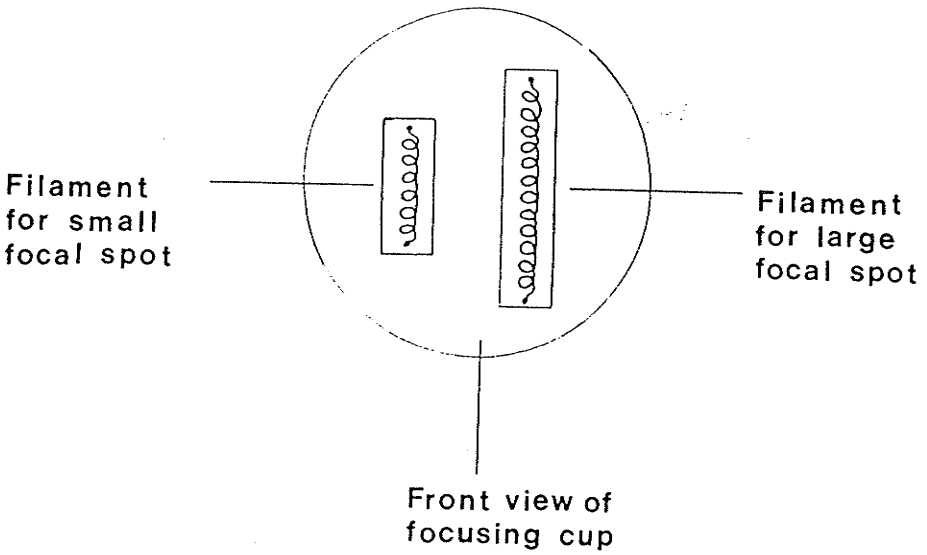

[Fig. 3]

Illustration of a focusing "cup"
fitted with two filaments [Ref. 19].

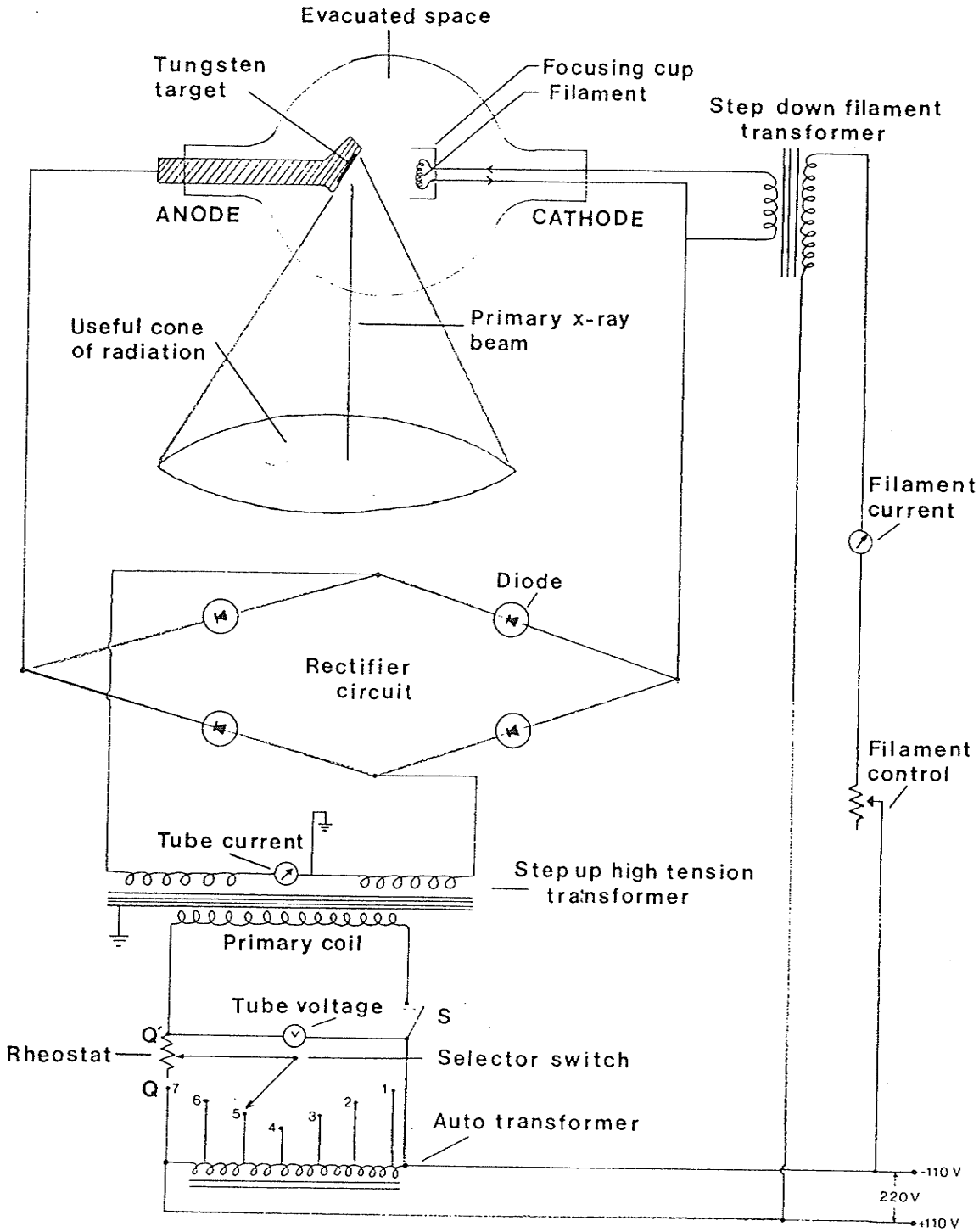

[Fig. 4]

Simplified circuit diagram of a full wave rectified x-ray tube.

potential difference in the main power supply is typically 220 V [Fig. 4], a step-down transformer is used to reduce the potential across the filament.

The variable resistor filament control in the step-down transformer circuit adjusts the current that flows through the filament. Increasing (decreasing) the resistance would have the net effect of decreasing (increasing) the number of electrons that can be emitted from the surface of the filament, which decreases (increases) the x-ray tube current (the current in the circuit due to the flow of electrons across the tube). The mA (milliampere) selector switch in [Fig. 4] corresponds to the current that is being passed through the step-down transformer's primary coil.

II.b.2.ii **High Voltage Circuit**

The voltage that is applied across the x-ray tube is supplied by a step-up transformer, whose primary coil is connected to an autotransformer via a rheostat [Fig. 4]. The function of the autotransformer is to divide the main power line's voltage in a step wise fashion. The voltage across the primary coil of the step-up transformer is selected by means of the selector switch. The rheostat, which is essentially a variable resistor, then varies the voltage in a continuous manner. The x-ray tube's kVp (peak kilovoltage) setting corresponds to the voltage set across the primary coil of the step-up transformer.

In addition to the mA and kVp controls, the x-ray tube control panel also contains two meters: one to measure the x-ray tube current (often referred to as the tube mA setting) and another for the x-ray tube kVp. The connection of these two meters to the x-ray tube circuit is also illustrated in [Fig. 4].

The switch S in [Fig. 4], opens and closes the high voltage supply to the primary coil of the step-up transformer. The x-ray tube exposure time setting corresponds to the time the switch is to be opened. The switch is kept open for a pre-selected exposure time by a timer mechanism [Ref. 20].

II.b.2.iii High Voltage Circuit Rectification

If the circuit in [Fig. 4] were not rectified, the voltage across the anode and cathode would have a waveform similar to that of the main power line, which is depicted in [Fig. 5a]. This would imply that during the positive voltage cycle the polarity of the anode would be positive and the cathode would be negative, thus the electrons emitted from the cathode will be travelling from cathode to anode. As these emitted electrons impinge on the "target" anode, the anode would heat up, produce x-ray radiation and subsequently emit electrons in the same way as does the filament. In the negative voltage cycle, the polarities of the anode and cathode would be interchanged. The electrons emitted from the anode would now

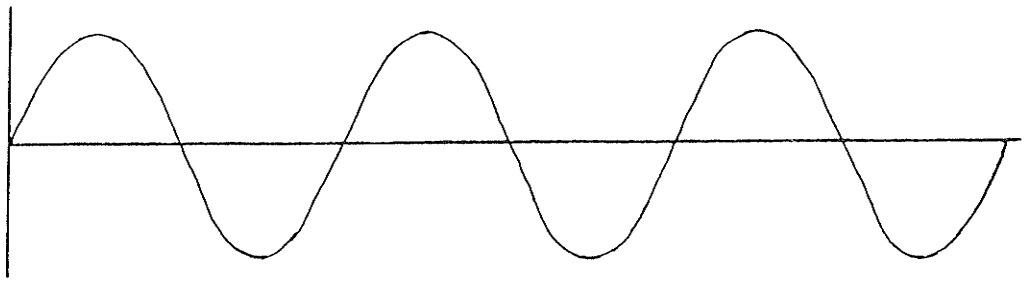

(a) Main power supply voltage waveform.

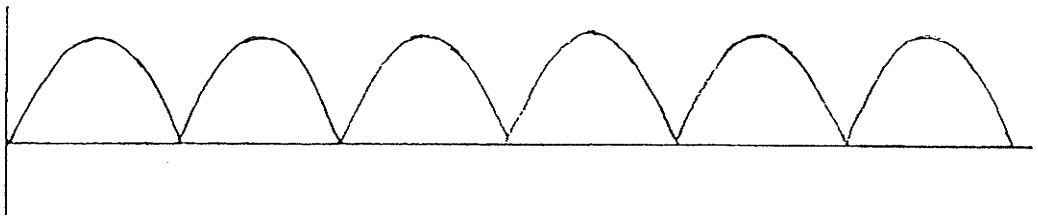

(b) X-ray tube voltage waveform after full wave rectification.

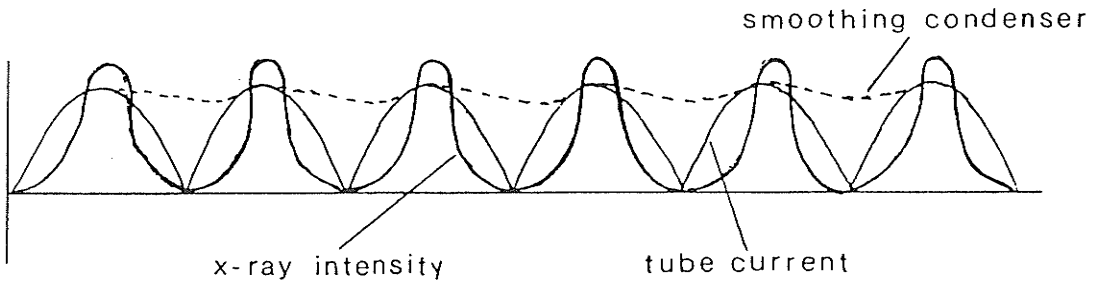

(c) X-ray tube current and x-ray intensity.

[Fig. 5]

Electrical waveforms for full wave rectification [Ref. 21].

bombard the filament and perhaps destroy it. To prevent this, rectifiers must be placed in the x-ray tube circuit to act as a switch to block the current during the negative voltage cycle. The x-ray tube voltage waveform of the circuit as illustrated in [Fig. 4] is depicted in [Fig. 5b]. Note that the use of the four semi-conductor (diode) rectifier [Ref. 22] arrangement allows the cathode polarity to remain negative with respect to the anode during both half cycles of the voltage waveform, utilizing the full potential of the main power supply. This type of rectification is known as full wave rectification.

As it is seen in [Fig. 5c], the x-ray radiation that is produced from the "target" anode is pulsed. This indicates that a considerable portion of the exposure time is lost while the x-ray tube voltage is between peaks of two successive pulses. To minimize this, the x-ray tube voltage should be kept as constant as possible.

In addition to full wave rectification, the voltage across the tube may be kept nearly constant by:

(a) placing a smoothing condenser (high capacitance) across the x-ray tube (illustrated in [Fig. 5b] by a dashed line); or

(b) by using three phase power and three phase x-ray tube generators of which there are the 6 pulse and 12 pulse system types [Ref. 23]; or

(c) by using high frequency converters that operate in the range of 10 kHz to supply the power to the x-ray generator as is done in the more modern x-ray generators.

II.b.3 X-ray Tube Current Characteristics

The variation of the electron current between the cathode and anode, henceforth referred to as the tube current, with tube kVp setting, is illustrated in [Fig. 6]. It is seen that for low kVp values the accelerating voltage across the tube is not sufficient for the emitted electrons to completely overcome the space charge effect surrounding the cathode, thus limiting the tube currents. As the tube kVp is increased the tube current increases as well, since the space charge effects are gradually overcome. As the tube kVp is increased further a point will be reached where the tube current will no longer increase as fast as in the low kVp region. This is because the filament is emitting almost all of the available electrons. The voltage at which little or no increase in tube current is observed is known as the saturation voltage. Diagnostic x-ray tubes operate at high tube currents in the kVp region above the space charge effect and below the saturation voltage. The exact width of this tube current region will depend on the filament current that is being used.

Because of the residual space charge effect, as the tube kVp is increased above the saturation voltage there will be a slight increase in the tube current, which is undesirable because the tube current cannot be precisely controlled. In the x-ray tube's low voltage circuit, additional resistors are added to the filament control circuit that automatically

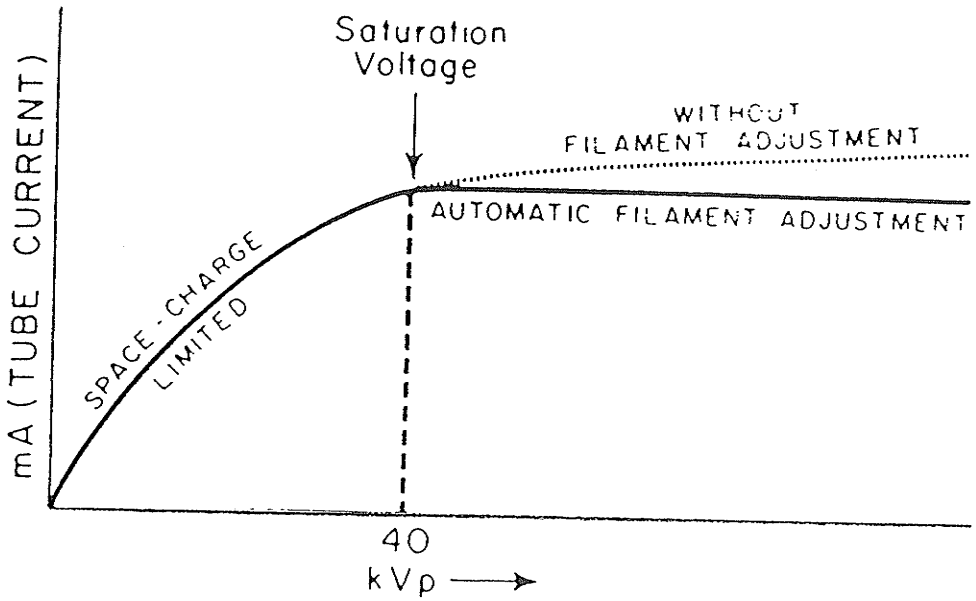

[Fig. 6]

X-ray tube current as a function of tube voltage [Ref. 24].

compensate for this residual charge by slightly decreasing the filament heating. One should note though, that this compensation will vary with x-ray tube and filament current.

II.b.4 X-ray Tube Efficiency

The efficiency (ϵ) of an x-ray tube is defined as:

$$\epsilon = \frac{\text{energy emerging as x-ray radiation from target}}{\text{energy deposited by electrons impinging on target}} \quad . \quad (1)$$

The rate at which the electrons are depositing energy in the target can be expressed as

$$P = VI \quad (2)$$

where P is the power (in W), V is the tube voltage (in V) and I is the tube current (in A). The rate at which energy (P') is released as x-ray radiation from the target has been shown to be [Ref. 25]:

$$P' = 0.9 \times 10^{-9} ZV^2I \quad (3)$$

where Z is the atomic number of the target material. Substituting [Eq. 2] and [Eq. 3] into [Eq. 1] we find the x-ray tube efficiency to be expressed as:

$$\epsilon = P'/P$$

$$= 0.9 \times 10^{-9} ZV \quad . \quad (4)$$

It can be seen from the factor in [Eq. 4], that x-ray production in a x-ray tube is a relatively inefficient process which depends upon the target material's atomic number and the tube voltage (kVp). If we take a tube voltage of 100 kV and the target material to be tungsten (Z = 74), then from [Eq. 4] we find the x-ray tube's efficiency to

produce x-rays is no more than 0.7% . This implies that 99.3% of the incident electron energy is converted to heat and light when the electrons impinge on the "target" anode.

II.b.5 "Target" Anode Assembly

The anode is the positive electrode of the x-ray tube as is illustrated in [Fig. 2] for a diagnostic x-ray tube. The anode has basically two functions: to produce the x-ray radiation when the cathode emitted accelerated electrons impinge upon the target (that has been embedded in the anode), and to serve as a means of removing the heat build up that has resulted from the electron bombardment. Both of these functions will be discussed below.

II.b.5.i Target

The target material that is often used is tungsten or a tungsten-rhenium alloy. Tungsten was chosen for its high atomic number, thus optimizing the x-ray tube efficiency [Eq. 4], and the fact that it has the following characteristics:

(a) high melting point;

(b) high conductivity of heat; and

(c) reasonable cost.

When the incident electrons impinge upon the tungsten target, they can lose their energy (as they interact with the atoms of the target) by two fundamentally different energy loss processes, referred to as collisional losses and

radiation losses.

II.b.5.i.1 Electron Collisional Energy Losses

As an electron penetrates the surface layers of the tungsten target, it can undergo a large number of collisions with the target atoms before it loses all of its energy and comes to rest in the target. During a collision the incident high speed electron can do one of two things: the electrons can excite the tungsten atom by moving one of the valence electrons to an optical orbit [Fig. 7a]. But, because the target material is in a solid form, the excited electron will not emit optical radiation when it returns to the ground state (as would be the case for atoms in a gaseous state). Instead it transfers the energy to the lattice (atom) vibrations called phonons. The energy loss of the incident electron during this process is only a few electron volts (eV). On the other hand, if the incident electron energy is high enough, it can remove the valence electron of the tungsten atom entirely, thus ionizing the atom. The energy loss of the incident electron in this process is much greater than the above case, but this too will eventually appear as heat. If the energy loss is of the order of 100 eV, the ejected valence electron (called a delta ray) would then undergo interactions similar to the incident electron.

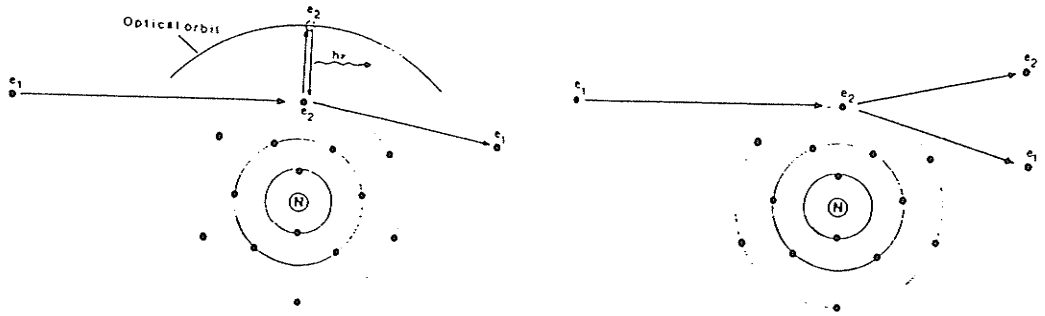

(a) Electron interacting with valence shell.

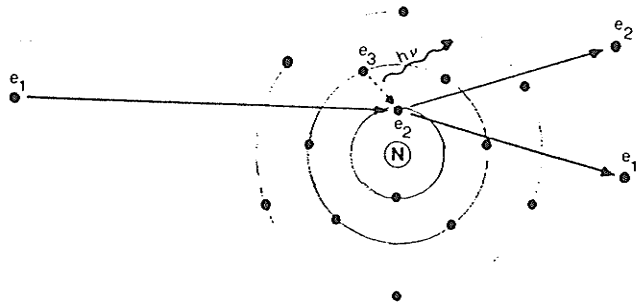

(b) Electron interacting with inner shell.

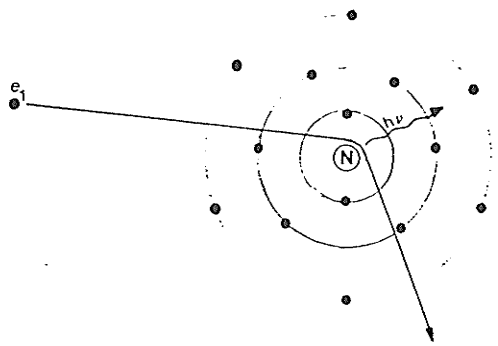

(c) Electron interacting near nucleus.

[Fig. 7]

Incident electron interaction with tungsten atom.

II.b.5.i.2 Electron Radiation Energy losses

When the incident electrons have an even higher energy, they could eject one of the inner-most bound electrons [Fig. 7b]. If a K shell electron is ejected, the tungsten atom will become unstable; and to place itself in a lower energy state, one of the L, M or N shell electrons will have to undergo a transition to the K shell. But because the L, M or N shell electrons are at an energy state greater than the K shell electrons, energy will be given off during the transition as radiation in the form a photon. The photon energies that result from electron transitions from either L, M or N (M or N) shells to the K (L) shell are in the x-ray energy range. Because these photons have sufficient energy to leave the target material, it is possible to identify the target material from the characteristic emitted photon energies. That is, each type of atom will have distinct K, L, M and N shell energy separations. For this reason, this type of radiation is called characteristic radiation. In the case of a tungsten target, the principle emission lines have been summarized in [Table 4][Ref. 26].

To observe any of the tungsten K shell emission lines the incident electron must have an energy of at least 69.51 keV which is the energy of the K shell electrons.

If we consider once again the incident electron but this time with energy greater than 69.51 keV, the electron can approach very close to the nucleus of the target atoms

[Table 4]

Principle Emission Lines of Tungsten

Transition[2]	Symbol	Photon Energy (keV)	Relative Number
$K-N_{II}N_{III}$	$K\beta_2$	69.081	7
$K-M_{III}$	$K\beta_1$	67.244	21
$K-M_{II}$	$K\beta_3$	66.950	11
$K-L_{III}$	$K\alpha_1$	59.321	100
$K-L_{II}$	$K\alpha_2$	57.984	58
L_I-N_{III}	$L\tau_3$	11.674	10
$L_{II}-N_{IV}$	$L\tau_1$	11.285	24
$L_{III}-N_V$	$L\beta_2$	9.962	18
L_I-M_{III}	$L\beta_3$	9.817	37
$L_{II}-M_{IV}$	$L\beta_1$	9.670	127
L_I-M_{II}	$L\beta_4$	9.523	29
$L_{III}-M_V$	$L\alpha_1$	8.395	100
$L_{III}-M_{IV}$	$L\alpha_2$	8.333	11

[2]The roman numerals specify the shells sub-shell.

[Fig. 7c]. Because the electron has negative charge and the nucleus is positive, the electron partially orbits around the nucleus due to the strong coulomb attraction. The electron will then recede from the interaction with a reduced energy. The loss of energy will appear as a photon with energy $h\upsilon$ and the incident electron will recede with energy $E - h\upsilon$, where E is the initial electron energy. This type of radiation is termed Bremsstrahlung radiation, which means "braking" radiation in German. The word "braking" is analogous to the electron sudden deceleration or "braking." The emitted photon energies from this process can be less than or equal to the incident electron energy. Because in this type of radiation the photon energies can have many values - like that of white light radiation - it is also called "white" radiation.

Between the two energy loss processes, the incident electrons lose most of their energy via collisions within the target atoms. Only at high incident electron energies will the radiation loss process be more probable than the collisional process.

II.b.5.ii Anode

It was shown in [section II.b.4] that approximately 1% of the incident electron's energy is utilized in x-ray production within an x-ray tube, whereas the remaining 99% is delivered to the tungsten target (anode) as heat. This implies that if the anode is not cooled off by some means it

will quickly reach a temperature above its boiling temperature and vaporize.

The cooling of the anode in a diagnostic x-ray tube is often achieved by using the following techniques:

(a) a system is used to re-circulate oil around the outside of the x-ray tube's glass envelope (discussed in next section) thus removing the unwanted heat build up;

(b) the heating of the target is reduced by enlarging the target area (that is, the heat load delivered per unit target area is reduced). A means of doing this is by using the "line focus" principle and "rotating" anode; and

(c) heat is also removed by passive radiation by coating the back of the anode with a good radiative material such as graphite.

II.b.5.ii.1 Line Focus Principle

The theory of the line focus principle is illustrated in [Fig. 8]. Instead of having the incident electrons impinging upon a flat surface of the tungsten target, the electrons are made to strike an area that is much larger, thus delivering less energy per unit target area. This is achieved by tilting the tungsten target at some angle, θ, with respect to the incident electron trajectories. The area on the tungsten target which the electron "pencil" beam bombards is called the "actual" focal spot. The resulting beam of x-ray radiation, though it subtends an area that is much smaller, is referred to as the "effective" focal spot or just the focal spot. Diagnostic x-ray tubes typically use target tilt angles that vary from 6° to 20°.

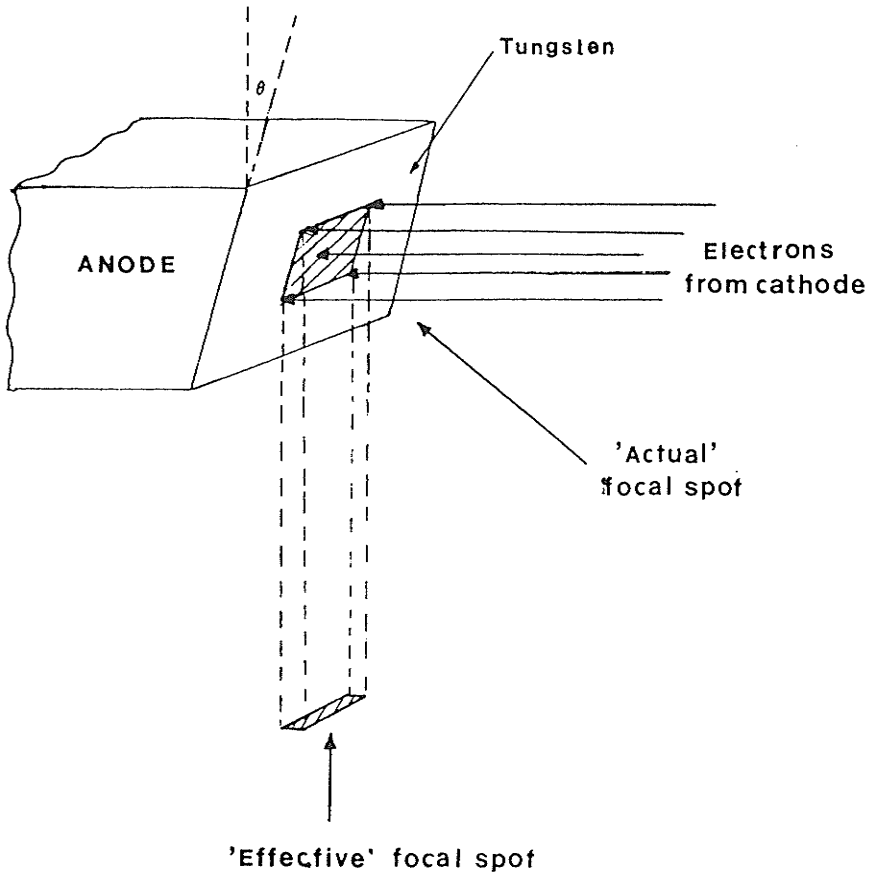

[Fig. 8]

Illustration of the line focus principle [Ref. 27].

The incorporation of the "line focus" principle into the anode design not only aids in reducing the heat load on the target, but the "effective" focal spot size can also be made quite small with respect to the "actual" focal spot size by utilizing large target tilt angles. This makes it possible to achieve radiographic images of highest quality which is of paramount importance in diagnostic radiology.

It should be noted that the "effective" focal spot of an x-ray tube will be directly proportional to the physical size of the cathode filament and target tilt angle. The small (large) focal spot of an x-ray tube refers to the use of the fine (coarse) cathode filament. The "effective" focal spot is the x-ray tube parameter that is to be determined in this work.

II.b.5.ii.2 Rotating Anode

Even with the incorporation of the "line focus" principle into the anode design it is still very difficult to get a sharp picture of a thick biological object in a very short time and with sufficient anode cooling. For this reason, the rotating anode [Fig. 9] was introduced. By rotating the anode, the electrons incident on the target actually bombard an area of length L and width ab; yet they appear to come from a region of area (ab x cd). With this arrangement, the primary x-ray beam intensity can be greatly increased by increasing the tube current. This is made possible by the

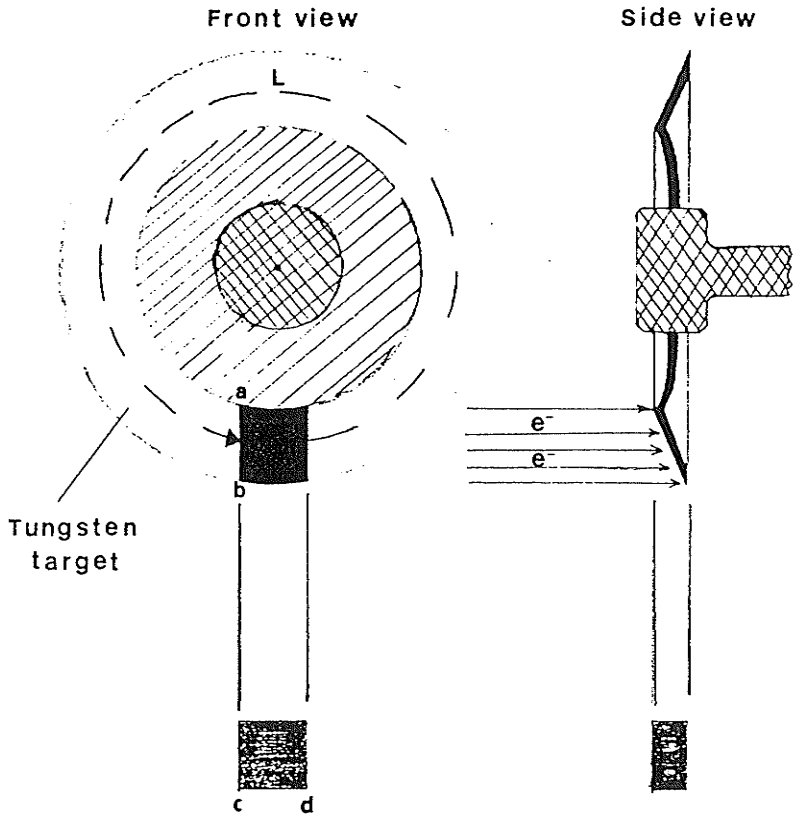

[Fig. 9]

Illustration of rotating anode design [Ref. 28].

fact that the incident electron beam heat loading is now delivered to a much larger target area and thus is much lower.

In the anode assembly the tungsten target is machined into a disk with a diameter that is typically in the range of 7.5 to 10.0 cm. The disk is usually laminated with a molybdenum backing and is attached to a molybdenum rotor which in turn is connected to an induction motor. Molybdenum was selected for its high melting temperature (2600°C) and poor heat conductivity. Before the x-ray tube is used to take an exposure, the induction motor is energized for about 1 sec, ensuring that the electrons do not bombard the tungsten target before it reaches its operational rotational speed which is generally between 3,500 and 10,000 rpm.

The life span of the anode disk is limited due to the roughening and pitting of the target surface by the incident electron bombardment, which will reduce the x-ray yield and change the spatial distribution. For this reason, the target is often made of a tungsten alloy (90% tungsten and 10% rhenium). The incorporation of rhenium reduces surface roughening and increases the anode heat capacity.

II.b.6 Glass Envelope

The function of the glass envelope [Fig. 2] is to keep the surrounding environment of the anode and cathode

assembly of the x-ray tube under vacuum. If gas were present inside the tube, the accelerated electrons would collide with the gas molecules, lose energy and cause secondary electrons to be ejected from the gas molecules via ionization. These secondary electrons would then be accelerated by the tube's potential difference thus contributing to the tube's current. Because this ionization process cannot be entirely controlled, the presence of secondary electrons will cause a wide variation in the tube current and in the energy of the electrons that are impinging on the "target" anode (and thus the energy of the x-rays produced). Independent control of the accelerated electron current and kinetic energy is thus achieved by evacuating the space surrounding the anode and cathode assemblies.

The wires that connect to the tube's cathode and anode assemblies must be sealed into the glass envelope's wall to ensure the integrity of the vacuum. When the tube is operating, both the glass envelope and the connecting wires are heated to high temperatures. If this heating were not done, the different coefficients of expansion for glass and metal would break the glass-metal seal, destroying the vacuum. Pyrex glass is most often used as envelope material.

II.b.7 Tube Housing

The various x-ray tube components enclosed within the

glass envelope are mounted inside a metal housing which is electrically grounded and contains oil. The oil, which is recirculated, absorbs the radiated heat from the anode and also electrically insulates the housing from the tube's high voltage. In addition to the oil, the metal housing contains a lead sheath that attenuates x-ray radiation that has emerged from the anode in undesired directions. Two bellows, one placed at each end of the x-ray tube, are also built into the housing that allow the heated oil to expand when the tube is in operation. The primary x-ray radiation emerges from the x-ray tube housing via a small beryllium window.

II.b.8 Spectra of Primary X-ray Beam

[Fig. 10] illustrates the spectral distribution of the primary x-rays produced when 150 keV electrons bombard a tungsten target. The atomic number of the target material will determine the energy position of the characteristic x-ray radiation (sharp peaks in diagram) and the amount (area under curve) of bremsstrahlung radiation that is produced. The end point energy corresponds to the maximum energy the x-ray photons can achieve, which is at the x-ray tube's kVp setting. The dashed line indicates bremsstrahlung radiation that would have been present in the primary x-ray beam if the glass envelope of the x-ray tube and internal tube filtration (oil and housing window) were not present.

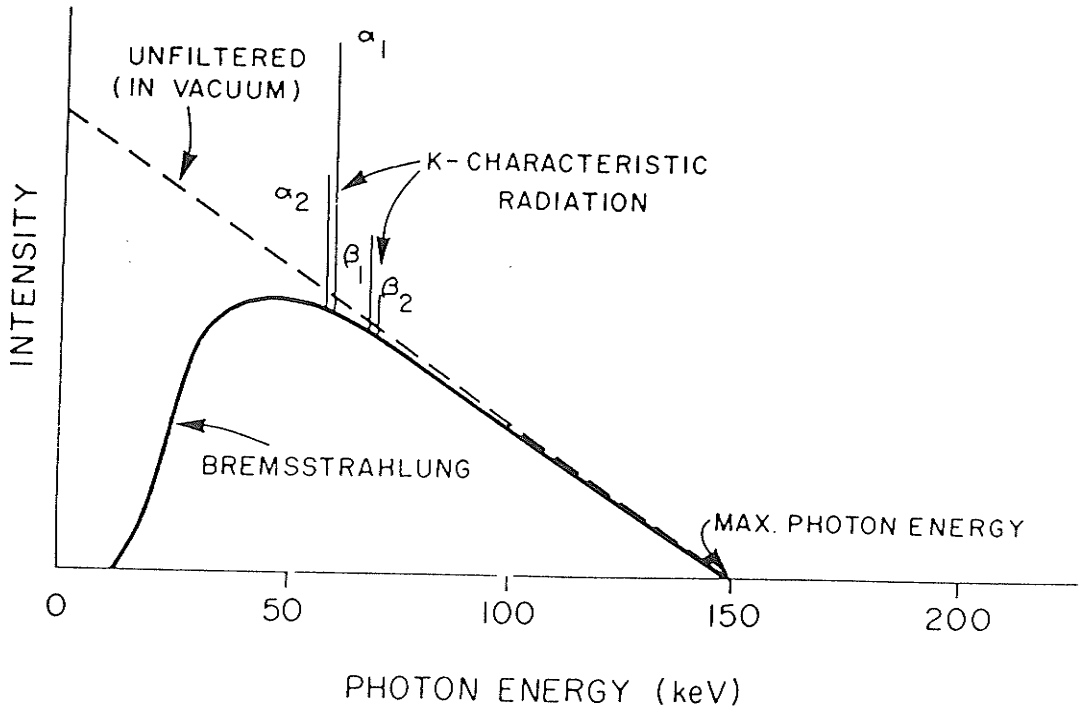

[Fig. 10]

Primary x-ray beam intensity spectrum [Ref. 29].

II.b.9 Primary X-ray Beam Angular Distribution

The intensity distribution of the primary x-ray beam [Fig. 11] is not uniform throughout the beam, rather it depends on the angle at which the x-rays are emitted from the focal spot. This observation can be explained as follows: as the incident electrons impinge upon the target material they can produce x-rays from both the surface and at depth within the target. In both cases, the x-ray photons will be partially absorbed by the target material depending on the angle and location at which the photon is emitted from the target, thus diminishing their intensity. The maximum of the intensity distribution is not at 0° since the photons that are emitted at 90° to the incident electrons trajectory must pass through a portion of the target as well. This reduced photon intensity on the anode side is called the heel effect, which has the net effect of shifting the intensity distribution away from the anode (that is a shift of the intensity maximum away from 0°).

II.c The X-ray Film

When an x-ray tube is used in a diagnostic examination, the emerging x-ray beam itself contains no useful medical information about the patient. Only after the x-ray beam passes through and interacts with the tissues of the patient, will it contain all the information that can be revealed relating to the examination. The information within

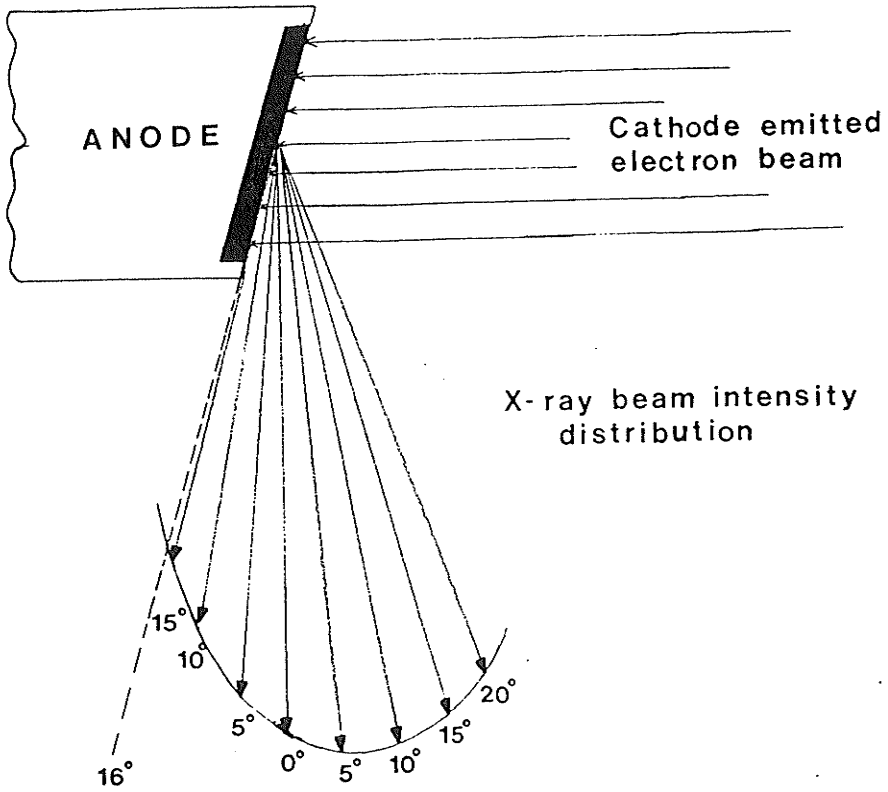

[Fig. 11]

The heel effect [Ref. 30].

the patient-emergent x-ray beam is represented by the variation of the number of x-ray photons in the different areas of the beam. The information in this form can not be used directly but must be transferred to a medium suitable for viewing by the eye. The material most often used to view the information carried by the attenuated x-ray beam is photographic emulsion x-ray film which is ideal for diagnostic radiology due to its excellent spatial resolution. It is often referred to as x-ray film or just film.

II.c.1 Physical Characteristics of X-ray Film

X-ray film [Fig. 12] consists of a photographically active emulsion coating on one side (single emulsion film) or both sides (double emulsion film) of a transparent sheet of plastic called the base. The emulsion layer is firmly attached to the base by the use of a thin layer of adhesive. A supercoating layer is then used to protect the emulsion layer from physical or mechanical damage.

II.c.1.i Film Base

The base, whose only function is to provide support for the delicate photographic emulsion, is made of either triacetate or polyester. Because both of these compounds are clear and colorless, a blue dye is often added to the base to tint the x-ray film, making it easier to look at and

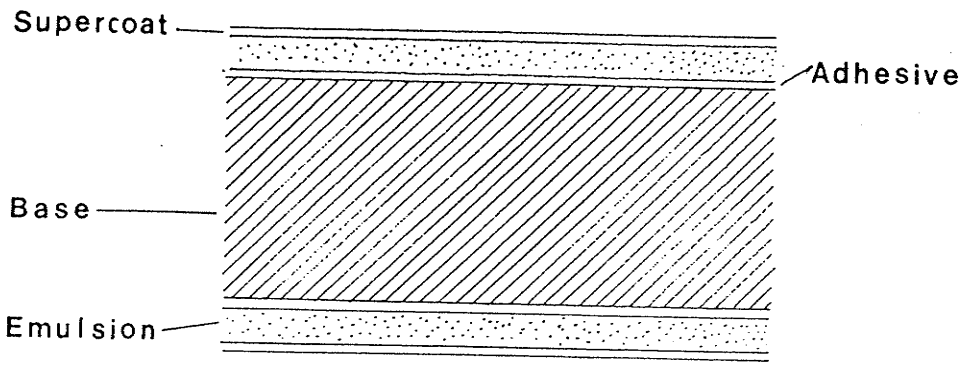

[Fig. 12]

Cross section of a double emulsion x-ray film [Ref. 31].

causing less eye strain. The thickness of the base is about 8 mils (0.008 inches) for triacetate and 7 mils for polyester. The difference in the base thickness is due to the fact that a slightly thinner polyester base is required to produce handling properties that are similar to that of a triacetate base.

Since the emulsion cannot adhere to the finished base directly, a thin layer of adhesive is applied between base and emulsion.

II.c.1.ii Photographic Emulsion

The x-ray film emulsion layer is manufactured by adding in total darkness a potassium bromide (KBr) solution and a silver nitrate ($AgNO_3$) solution to a solution of gelatin. The creamy solution is then heated and cooled into a jelly-like solution. The unwanted potassium nitrate (KNO_3) which results from the following reaction:

$$AgNO_3 + KBr \rightarrow AgBr + KNO_3 \qquad (5)$$

is washed out of the material prior to the reheating and coating of the base.

It is the silver halide (AgBr) in the form of small crystals suspended in the gelatin that is the light sensitive material in the emulsion. A crystal is formed when ions of silver (Ag^+) and bromide (Br^-) are arranged in a cubic lattice. The size of these halide crystals or grains will depend on the concentration of the various reactants,

the sequence and rate at which these chemicals are added, and the temperature at which the reaction [Eq. 5] takes place. To increase the emulsion sensitivity to light a small amount of potassium iodide (KI) is also added to the gelatin solution prior to the heating. The incorporation of KI produces the halide, silver iodide (AgI) and has the net effect of introducing point defects within the halide crystal [Fig. 13]. The halides in x-ray film emulsions are typically 90 to 99% AgBr and about 1 to 10% AgI.

Sulfur containing compounds such as allythiourea are also added to the emulsion to chemically sensitize the crystals. The allythiourea compound reacts with the silver halide and forms silver sulfur (AgS) which is embedded on the surface of the crystal. It is the presence of AgS that initiates the image formation on film (see following section).

The emulsion layer, which is no thicker than 0.5 mil, contains crystals that have average diameters between 1.0 and 1.5 μm with about 6.3×10^9 grains per cubic centimeter of emulsion, and each grain contains on the average 1×10^6 to 1×10^7 silver ions.

The incorporation of gelatin in the emulsion layer keeps the silver halide grains well dispersed and prevents the clumping of grains. The developing and fixing solutions which are used in film processing can also penetrate the gelatin easily without destroying its strength and/or structure.

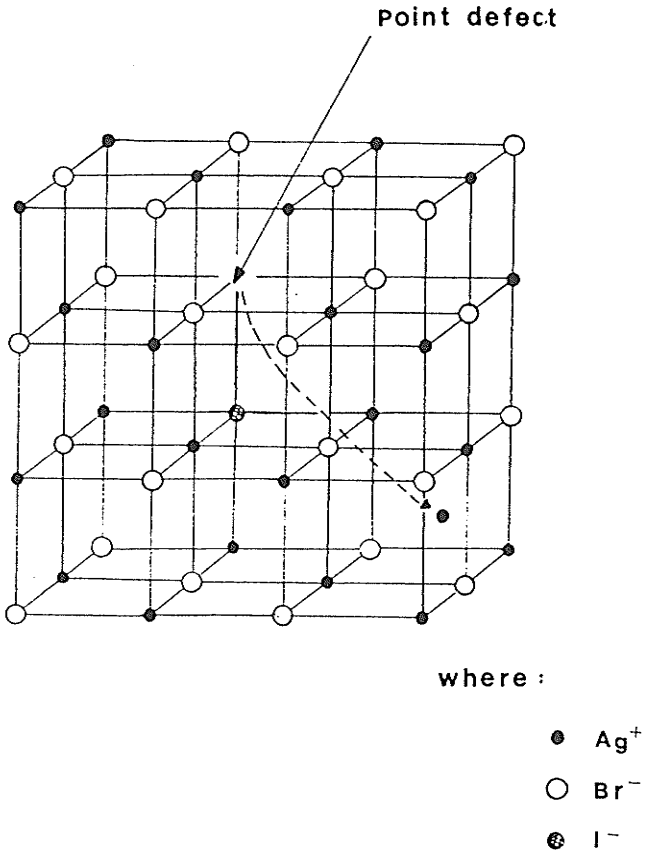

[Fig. 13]

The silver iodo-bromide crystal lattice with point defect [Ref. 32].

II.c.2 X-ray Film Image Formation

To best describe the image formation process on film, consider [Fig. 14]. When a light photon interacts with a silver halide crystal, the energy of the photon is absorbed by the Br^- ion which gives the extra valence electron enough energy to escape the ion entirely. That is,

$$Br^- + \text{light photon} \rightarrow Br + \text{electron} \quad . \qquad (6)$$

The neutral Br atom then leaves the crystal and is taken up by the gelatin of the emulsion. The free electron, on the other hand, is then captured and temporarily trapped by the AgS sensitivity speck that is on the surface of the silver halide crystal. The electron that has been captured then gives the AgS sensitivity speck a net negative charge which then attracts the interstitial Ag^+ ions within the crystal. Once an Ag^+ ion has migrated to the speck, it is then neutralized to atomic (metallic) silver by the trapped electron. That is,

$$Ag^+ + \text{electron} \rightarrow Ag \quad . \qquad (7)$$

When a second light photon interacts with the silver halide crystal the electron that has escaped from a second Br^- ion via [Eq. 6] will then be trapped by the silver atom at the sensitivity speck, which in turn will attract a second interstitial Ag^+ ion to produce a second silver atom. The collection of silver atoms at the location of a single AgS sensitivity speck will continue to increase via the above mechanism as was hypothesized by Gurney and Mott. This clump

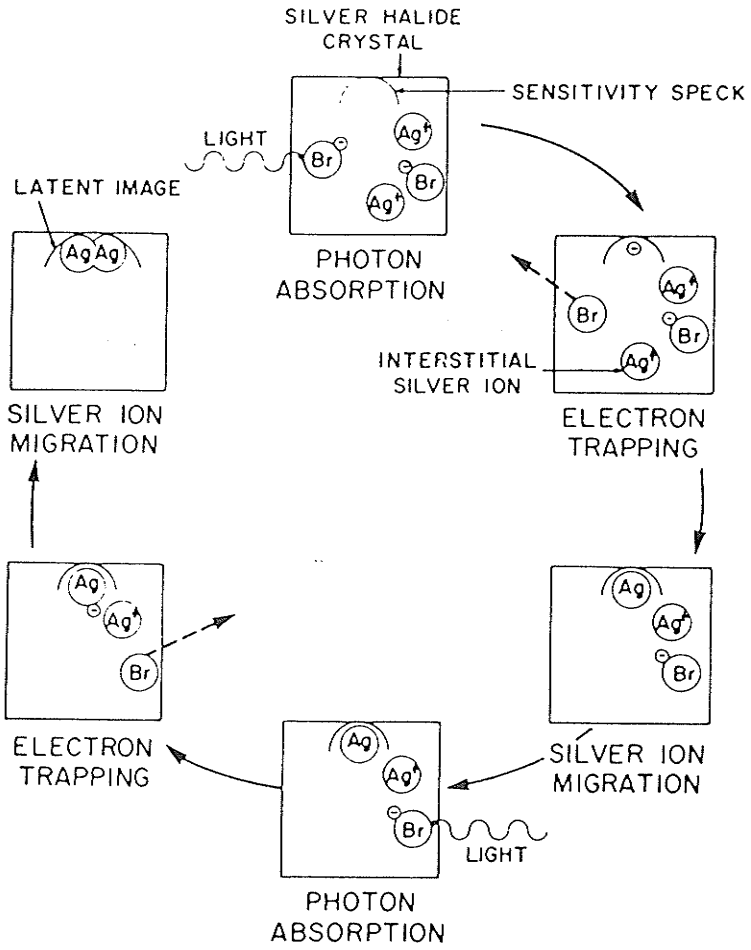

[Fig. 14]

Formation of the latent image [Ref. 33].

of atomic silver near a sensitivity speck is referred to as the latent image center. There could be one or more of these centers on a single halide crystal.

As was shown above, a single light photon allows a single silver atom to be deposited at the sensitivity speck. When an x-ray photon is incident on the halide crystal, it is the electrons that have been emitted from the x-ray photon's interaction (photoelectric absorption [Ref. 33] and Compton scattering [Ref. 34]) with the free silver halide in the emulsion that causes the Br^- ion's electron to be emitted thus initiating latent image center formation. Because the electrons emitted by the x-ray photon have rather long ranges they can interact with many silver halide crystals (grains) within the emulsion, making the image formation process more efficient (that is producing thousands of silver atoms at latent image sites in one or more crystals).

When x-ray radiation is used to expose the film, the information in the beam is transmitted to the film via the deposition of metallic silver at the various latent image centers located on the crystal surfaces. The amount of atomic silver deposited in each latent image center is proportional to the amount of exposure - heavier exposures (when x-rays pass through less opaque material such as soft tissue within the patient) produce much silver, lesser exposure (when x-rays pass through bone within the patient) cause a smaller deposit of silver at the latent image

center. Since these changes in the silver halide grains are not visible to the naked eye, the film is processed to make the latent image centers visible.

II.c.3 X-ray Film Processing

The entire film processing procedure is done in a darkroom. The exposed film is first placed in a developing solution whose function is to convert activated silver halide crystals to silver (black metallic silver) grains. The more metallic silver present at a latent image site the blacker the film will be in that region. Therefore, portions of the film that were directly exposed by x-ray radiation will appear as black and those regions where the x-ray radiation has been filtered by passage through the patient will have a reduced exposure and thus will appear as shades of gray.

Once the film has been developed, the film is rinsed to neutralize or greatly dilute the various chemicals in the developing solution that may be present on the film. To make a permanent image on film the latent image centers are fixed in the gelatin by hardening the emulsion. This is accomplished by placing the developed film in a fixing solution, which also removes any unexposed and undeveloped silver halide that might be present. The film is then washed to remove any chemicals remaining in the emulsion after processing, and dried.

The film processing procedure that is briefly summarized above is explained in some detail in [Ref. 35,36]. In this work, an automatic film processor was used, whose entire cycle from the time the exposed film enters the machine until it emerges as a viewable finished radiograph takes as little as 45 to 90 seconds.

II.c.4 Photographic Characteristics of X-ray Film

To accurately represent the information of a diagnostic examination on film, it is imperative to understand the relationship between the exposure a film receives and the way the film responds to this exposure. In the following discussion it will be assumed that exposure on film is via x-ray photons.

II.c.4.i X-ray Air Kerma

X-ray air kerma (Kinetic Energy Released per unit Mass) [Ref. 37] is a quantity that is used to define the radiation output of an x-ray tube and is defined as:

$$\text{X-ray air kerma } (K) = dE_{tr}/dm \qquad (8)$$

where dE_{tr} is the total of the initial kinetic energies of all the charged ionizing particles liberated by uncharged ionizing particles in a volume element of air having a mass dm. The unit of x-ray kerma is the Gray (Gy), defined as

$$1\text{Gy} = 1\ \text{J/Kg in air at STP.} \qquad (9)$$

The "exposure" of an x-ray film will depend on the number

of x-ray photons that interact with the film emulsion layer, which in turn will determine the size and lengths of the various developed silver halide grains. It would then be logical to assume that the film exposure will be proportional to the product:

$$\text{Film exposure} \propto \text{mA}\cdot\text{s} \qquad (10)$$

where mA is the x-ray tube current and s is the exposure time, since after all, the higher the x-ray tube current the more x-rays that will be produced. Thus an x-ray tube current of 100 mA for 1 sec produces a (film) exposure of 100 mAs. Note, a similar film exposure can be achieved when using a tube current of 50 mA and exposure time of 2 seconds. At a given kVp, the greater the x-ray tube mAs value, the greater the extent of film blackening or density.

A more practical quantity to the radiologist and/or technologist is the relative film exposure which allows corrections of overexposed or underexposed films to be made by adjusting the tube's mAs value, without any knowledge of the true exposure [Eq. 8].

II.c.4.ii Film Optical Density

The degree of film darkening (or density) is directly related to the intensity of the light (or x-ray) radiation that is reaching the film. The measurement of this parameter, which is often referred to as the film optical density (O.D.), is obtained from the relation

$$\text{Optical density} = \text{Log}_{10}(I_0/I_t) \qquad (11)$$

where I_0 is the intensity of light incident on the film and I_t is the intensity of light transmitted by the film [Fig. 15]. A film optical density of 2 means that from 100 incident photons only 1 of these photons on average will be transmitted by the film.

II.c.4.iii X-ray Film Characteristic Curve

The relationship between the film's optical density and relative exposure is plotted as a curve [Fig. 16] and is called the film's characteristic curve or the H - D (after Hurter and Driffield) curve, named after the individuals who first published this curve. The curve is essentially comprised of three regions: the toe region, the shoulder region and a straight line (linear) region in between.

Even at zero exposure, the curve indicates that the film optical density will be about 0.2 and not zero. This intrinsic film density is due to the base density (which results from the absorption of light by the plastic and blue dye that comprise the base) and the fog density (development of unexposed or heat or background radiation induced exposure of silver halide grains within the emulsion). Thus, to determine the optical density of the film produced by the exposure itself it is necessary to subtract the intrinsic film density (typically about 0.15 for a new film) from the total film density. The toe and

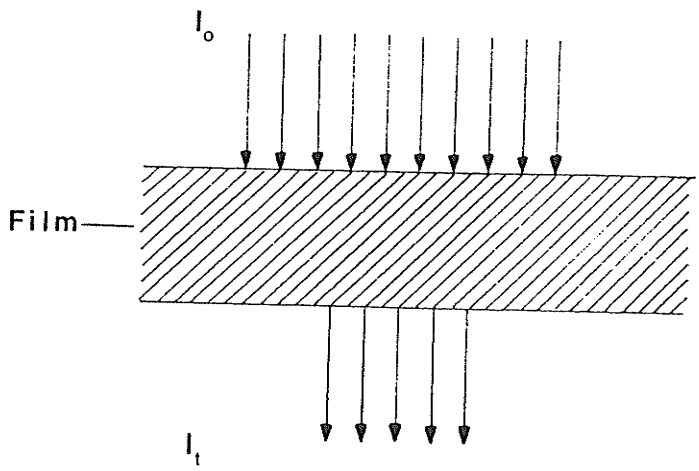

[Fig. 15]

Film optical density.

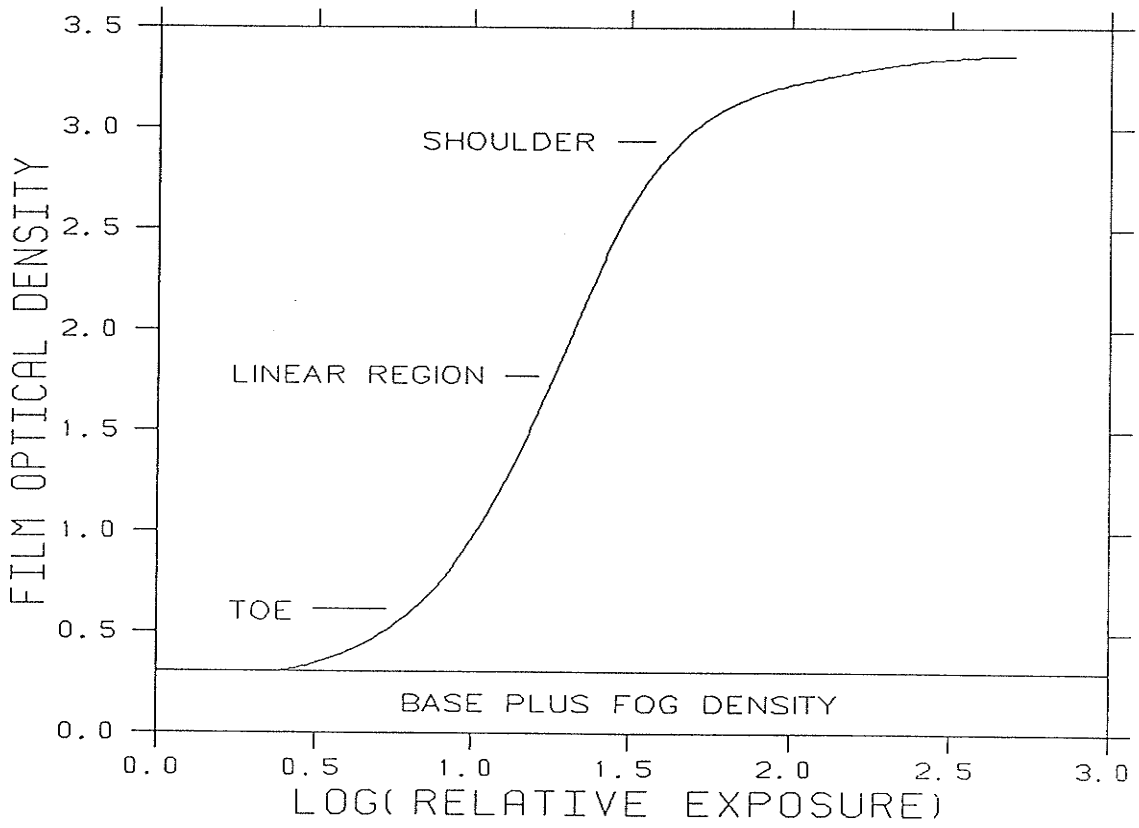

[Fig. 16]

A typical x-ray film characteristic curve.

shoulder indicate the regions where the change in the film's optical density is small even though the change in the log relative exposure is relatively large.

In diagnostic radiology, the log relative exposures are supposed to be kept in the region where they produce film optical densities that lie in the relatively straight (linear) portion of the curve (often between 1 and 2). In this region a small change in exposure will produce a proportional change in film density. This ensures maximum film contrast, which is defined as the difference in film density existing between adjacent regions on the film.

II.c.5 Intensifying Screen

In order to reduce the direct x-ray exposure of a patient during an examination, the x-ray film is first sandwiched in a film cassette that has a fluorescent x-ray intensifying screen [Ref. 38] on each side before it is exposed.

The purpose of the cassette is to provide a rigid support for the two intensifying screens so that a film can be sandwiched in between the two screens. The front of the cassette is usually made of a plastic material that introduces minimum filtration effects to the passage of the x-ray radiation. The back of the cassette on the other hand is usually made of metal, either aluminum or steel, with a thin sheet of lead foil attached to the inner surface of the back of the cassette, so as to assist in preventing back-

scattering radiation from penetrating the x-ray film within the cassette. Each intensifying screen is a sheet of plastic (base) that is coated on one side with an emulsion of a finely powdered phosphor (such as calcium tungstate or barium lead sulphate) suspended in some carrier. The base of the screen, which is evenly coated with a white reflecting surface on which the layer of phosphor is coated, is attached inside the cassette to either the front or back by double-sided adhesive tape.

Because when each intensifying screen is struck by x-ray radiation the screen fluoresces with a blue-violet light (light radiation to which blue-sensitive x-ray film emulsion is most sensitive), this implies that as a single x-ray photon traverses the screen it can result in the liberation of many light photons. These light photons in turn can expose the x-ray film within the film cassette. The net effect of a single screen is then to intensify the action of x-ray radiation on the x-ray film. Because of this effect and the fact that two intensifying screens are used (one in front and one behind the x-ray film), the incident x-ray radiation exposure of the patient can be substantially reduced.

Even though intensifying screen cassettes are normally used during patient examinations, they were not used during the collection of the focal spot test tool film images. This was done to eliminate film unsharpness that results when

using intensifying screens, since each screen will emit light photons in various directions above or below the x-ray film in some interwoven pattern, resulting in some unsharpness in detail within the image of the object that is cast on the film.

CHAPTER III

EXPERIMENTAL APPARATUS

The goal of this thesis was to determine the focal spot dimensions by using a digital imaging technique and then to have its findings compared to the more conventional measurement techniques:

(a) bar resolution pattern;

(b) star resolution pattern; and

(c) pinhole camera.

In each of these methods the focal spot dimensions were determined (see chapter IV) from an x-ray film image of the test tool that was used, whether it was a bar pattern, a star pattern, a pinhole or two thin parallel wires (used in the digital imaging technique). This chapter will describe the equipment and experimental procedures that were used.

III.a Experimental Procedure and Equipment used to Obtain Focal Spot Test Tool Images

III.a.1 Bar Resolution Pattern

III.a.1.i Test Tool

The x-ray focal spot test tool which was manufactured by Radiation Measurements Incorporated (RMI) [Ref. 39], is a metal plate that is machined with eleven pair of bar pattern groups each of a different size. Each bar pattern group consists of three rectangular slots (bars) in one direction and three slots at right angles to the first group. The

spacing of the slots in the eleven bar pair groups [Table 5] varies from 0.6 line pairs·mm^{-1} to 3.35 line pairs·mm^{-1} (a line pair consists of one slot and one space between two consecutive slots). This machined metal plate is mounted in the center of a 10.2 cm by 10.2 cm square Plexiglass plate which contains a fluorescent screen and a lead shield. This plate in turn is mounted at the top of a 15.2 cm high cylindrical Plexiglass base.

III.a.1.ii Experimental Procedure

The focal spot of the diagnostic x-ray tube (whose location is often identified by a red or black dot on the tube housing) was positioned 60.9 cm above the surface of the x-ray (patient) table and a cardboard cassette[3] containing a double emulsion Kodak TMG x-ray film was placed on the table beneath the x-ray tube. The test tool was then placed on top of the cardboard cassette and was aligned with respect to the x-ray beam central axis by utilizing the x-ray collimator alignment light field source. The focal spot-to-film distance (FFD) was 60.9 cm (24"), which gave a bar pattern test tool image magnification of 1.33X (see chapter IV for definition of magnification). The x-ray tube collimator opening was adjusted using the collimator alignment light so that the x-ray field was within the

---

[3]A cardboard cassette was used instead of a cassette containing intensifying screens [Ref. 38] to eliminate intensifier screen related image blurring.

[Table 5]

Bar Pattern Line Pair Frequencies

Bar Group Number	Line Pairs·mm^{-1}
1	0.60
2	0.70
3	0.85
4	1.00
5	1.15
6	1.40
7	1.70
8	2.00
9	2.50
10	2.80
11	3.35

dimensions of the fluorescent screen of the test tool. The x-ray film was then exposed to produce an image of the test tool. [Table 6] summarizes typical x-ray tube techniques that were used during the experiment.

III.a.2 Star Resolution Pattern

III.a.2.i Test Tool

The test tool is distributed by Nuclear Associates division of Victoreen Incorporated [Ref. 40] and was identified by the model number 07-510. The star pattern consists of a circular array of lead wedges of 0.05 mm thickness, that are radially arranged like the spokes of a wheel with gaps between the lead wedges of the same size. In a 2° pattern, each lead wedge (and spacing between adjacent wedges) diverges at an angle of 2°. The entire wedge arrangement is embedded in a circular plastic plate having a diameter of 45 mm.

The star resolution pattern differs from the previously described bar resolution pattern in the following way. In the bar pattern test tool each of the eleven bar groups has a distinct line pair frequency; the star pattern on the other hand defines a continuously variable line pair frequency whose resolvable frequency depends on the distance from the center of the wedge pattern (location where all lead wedges converge) to the nearest location of resolution. To illustrate this, consider the following: since the star

[Table 6]

Bar Pattern X-ray Tube Techniques

Tube kVp	Focal Spot Size	Exposure Time (ms)	Tube mAs	Film Optical Density
For a Picker diagnostic x-ray tube (test run 1):				
70	Small	100.0	10	0.84
	Large	50.0	10	0.80
80	Small	125.0	12.5	1.20
	Large	66.7	13.3	1.19
90	Small	150.0	15	1.37
	Large	66.7	13.3	1.32
For a Siemens fluoroscopic x-ray tube (test run 4):				
70	Small	21.0	10	0.88
	Large	10.0	10	1.00
80	Small	29.5	12.5	1.20
	Large	12.5	12.5	1.37
90	Small	43.0	16	1.46
	Large	18.0	16	1.81

pattern contains lead wedges with angular separation of 2° and exactly similar blank spaces between them, the pattern contains 90 spokes of lead and 90 spokes of plastic within a given circle, in other words 90 line pairs per circle (where a single line pair consists of two spokes one of lead and one of plastic). At the periphery where the diameter is 45 mm and the circumference is 45π mm, the line pair frequency will be $90/45\pi = 0.637$ line pairs·mm^{-1}. At any smaller diameter (D mm), the line pair frequency of the star pattern will be given by $0.637(45/D)$ line pairs·mm^{-1}.

III.a.2.ii Experimental Procedure

The first thing that was done was to adjust the x-ray tube mount to the center position, perpendicular to the x-ray table. Once this was done the focal spot-to-film distance (FFD) was set at 101.6 cm (40"). Once again a cardboard cassette was used to enclose the double emulsion Kodak TMG x-ray film. The star pattern was placed midway between the focal spot and film to give a test tool image magnification of 2X. The star pattern was held at the FFD midpoint by resting it on a clear plastic plate that was in turn held by a clamp attached to a stand. The clear plastic plate had a square hole of slightly smaller dimensions than the star pattern diameter to eliminate x-ray beam attenuation through the clear plastic plate. The x-ray field was adjusted via the collimator alignment light-source

indicator to insure that the total star pattern was within the field. The star pattern was also centered with respect to the x-ray beam central axis. Once the star pattern was set in place the x-ray film was exposed to produce the test tool image.

Star pattern x-ray images were also taken using a focal spot-to-film distance of 182.9 cm (72"). At this FFD setting the star pattern was also placed midway between the focal spot and film to give an image magnification of 2X. Single emulsion Kodak OM1 x-ray film was used at both FFD settings during test run 1. [Tables 7-10] summarize typical x-ray tube techniques that were used during the experiment.

III.a.3 Pinhole Camera

III.a.3.i Test Tool

The pinhole camera was obtained from the Nuclear Associates division of Victoreen Incorporated [Ref. 40] and was identified by the model number 07-610. The pinhole assembly that was used had a pinhole diameter of 0.075 mm (model number 07-617). The camera consists of a metallic stand with four telescopic legs attached to a top and bottom plate. The top part of the stand consists of two plates: a metallic one and a lead one underneath. Each of these plates has a center hole with machined threads to allow the pinhole assembly to be accurately screwed into place. On either side of the central threaded hole is a single hole that has been

[Table 7]

Star Pattern X-ray Tube Techniques
When Using Double Emulsion Film at FFD of 101.6 cm (40")

Tube kVp	Focal Spot Size	Exposure Time (ms)	Tube mAs	Film Optical Density
For a Picker diagnostic x-ray tube (test run 1):				
70	Small	800.0	80	1.55
	Large	400.0	80	1.52
80	Small	600.0	60	1.55
	Large	300.0	60	1.46
90	Small	500.0	50	1.59
	Large	250.0	50	1.52
For a Siemens fluoroscopic x-ray tube (test run 4):				
70	Small	190.0	80	1.96
	Large	80.0	80	2.01
80	Small	165.0	63	1.93
	Large	63.0	63	2.11
90	Small	147.0	50	1.92
	Large	56.5	50	1.99

[Table 8]

Star Pattern X-ray Tube Techniques
When Using Single Emulsion Film at FFD of 101.6 cm (40")

Tube kVp	Focal Spot Size	Exposure Time (ms)	Tube mAs	Film Optical Density
For a Picker diagnostic x-ray tube (test run 1):				
70	Small	3000.0	300	2.26
	Large	1500.0	300	2.19
80	Small	2000.0	200	2.17
	Large	1000.0	200	2.09
90	Small	1200.0	150	2.12
	Large	800.0	160	2.02

[Table 9]

Star Pattern X-ray Tube Techniques
When Using Double Emulsion Film at FFD of 182.9 cm (72")

Tube kVp	Focal Spot Size	Exposure Time (ms)	Tube mAs	Film Optical Density
For a Picker diagnostic x-ray tube (test run 1):				
70	Large	1500.0	300	1.58
80	Large	1000.0	200	1.47
90	Large	800.0	160	1.38
For a Siemens fluoroscopic x-ray tube (test run 4):				
70	Large	372.0	320	2.15
80	Large	228.0	200	1.96
90	Large	201.0	160	1.90

[Table 10]

Star Pattern X-ray Tube Techniques
When Using Single Emulsion Film at FFD of 182.9 cm (72")

Tube kVp	Focal Spot Size	Exposure Time (ms)	Tube mAs	Film Optical Density
For a Picker diagnostic x-ray tube (test run 1):				
70	Large	5000.0	1000	2.11
80	Large	3000.0	600	1.65
90	Large	2000.0	400	1.39

drilled through both of the top plates. The 14.3 mm separation distance between these two side holes aids in the determination of the pinhole image magnification on film. The bottom plate is made of clear plastic and on the surface of the plate nearest to the pinhole is attached a fluorescent screen with cross hairs, which aids in pinhole alignment prior to film exposure.

The pinhole assembly consists of a metallic screw that is filled with gold. A fine pinhole is then drilled through the center. To protect the pinhole from dust and dirt a piece of transparent tape is used to cover the pinhole.

III.a.3.ii Experimental Procedure

Once the x-ray tube mount was adjusted to the center, perpendicular position, the focal spot-to-film distance (FFD) was set at 92.7 cm (36.5"). The pinhole camera was then placed on the x-ray table beneath the x-ray tube. The camera was then checked to see if it was level by using the bottom surface of the x-ray tube collimator as the reference. Once the pinhole camera was levelled the pinhole assembly was carefully removed. The four telescopic legs of the camera were fully extended and the x-ray tube was brought as close as possible to the center hole. The x-ray tube housing was aligned and the camera was centered by eye. Camera alignment was verified by darkening the room, taking a test exposure at 10 kVp and 15 mAs, and observing the

location of the spot on the camera's fluorescent screen. When the image of the hole was not centered on the cross-hairs of the fluorescent screen the camera was moved and the process repeated. Once the camera was aligned, the x-ray tube housing was raised vertically and the pinhole assembly was inserted. The x-ray tube was then moved to its original vertical position and a 5.7 cm by 7.6 cm fine grain Kodak dental occlusal film was placed on the camera base centering it to the fluorescent screen cross hairs. The film was then exposed to produce an image of the pinhole. [Table 11] summarizes typical x-ray tube techniques that were used during the experiment.

III.a.4 Digital Imaging Technique

III.a.4.i Test Tool

The test tool was constructed at the Manitoba Cancer Treatment and Research Foundations workshop, where it took about 2 hours to build. The estimated cost of construction was $70.00 .

The test tool [Fig. 17] consisted of two components: a base and two parallel wires. The 15 cm by 15 cm base was constructed out of acrylic with a thickness of 5 mm. The base material was chosen for its low x-ray attenuation, convenient machining characteristics and its availability. At the center of the base a 5 cm by 5 cm square hole was cut out to further minimize x-ray attenuation through the test

[Table 11]

Pinhole Camera X-ray Tube Techniques

Tube kVp	Focal Spot Size	Exposure Time (ms)	Tube mAs	Film Optical Density
For a Picker diagnostic x-ray tube (test run 1):				
70	Small	7500.0	750	0.87
	Large	3800.0	760	0.85
80	Small	5000.0	500	1.00
	Large	2500.0	500	0.93
90	Small	4000.0	400	1.01
	Large	2000.0	400	0.90
For a Siemens fluoroscopic x-ray tube (test run 4):				
70	Small	2274.0	710	1.24
	Large	1377.0	710	1.16
80	Small	1723.0	500	1.21
	Large	1010.0	500	0.97
90	Small	1547.0	400	1.12
	Large	902.0	400	0.98

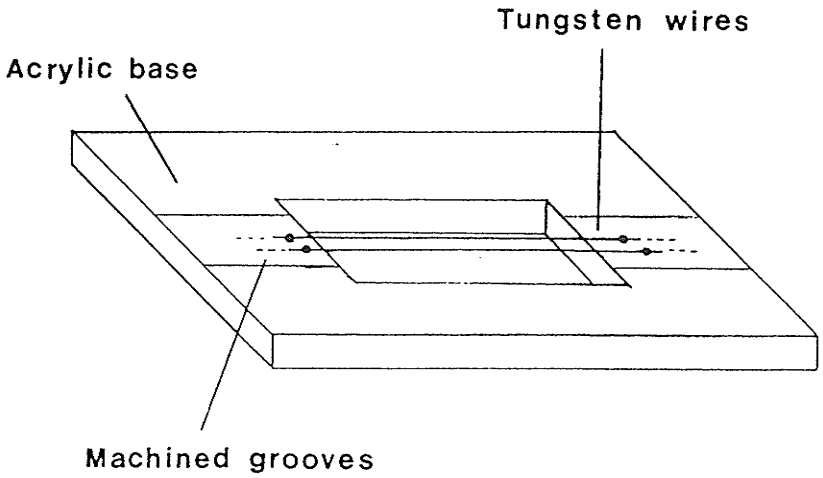

[Fig. 17]

Illustration of parallel wire focal spot test tool.

tool. Two parallel grooves (with a separation of 5 mm) were machined on the base to guide the wires when they were mounted. The two wires had a diameter of 0.05 mm and were made of tungsten. The wire diameter was purposely chosen to be very small in comparison with the focal spot dimensions that were to be measured, to minimize the penumbra region on film which in turn minimized the focal spot unsharpness. The wire material was chosen for its high atomic number which minimized radiation transmission through the wires to optimize the contrast in the image. After the two wires had been mounted by gluing the ends to the base with acrylic cement, the wire separation distance[4] within the 5 cm by 5 cm square hole region was measured and was found to vary from 4.70 to 4.90 mm along the 5 cm wire separation distance.

III.a.4.ii Experimental Procedure

To duplicate the experimental conditions as much as possible the parallel wire test tool images were taken with the same x-ray tube techniques as those used for the star pattern test tool. The geometrical conditions were also duplicated by replacing the star pattern test tool with the parallel wire test tool once the star pattern test tool images had been taken. Once the test tool was centered, the

---

[4]The measurement was performed by using a 7X magnifier with reticle scale in 0.1 mm divisions. The uncertainty in each individual measurement was ± 0.05 mm.

[Table 12]

Parallel Wire Test Tool X-ray Tube Techniques
When Using Double Emulsion Film at FFD of 101.6 cm (40")

Tube kVp	Focal Spot Size	Wire Orientation w.r.t c-a Axis	Exposure Time (ms)	Tube mAs	Film Optical Density
For a Picker diagnostic x-ray tube (test run 1):					
70	Small	Parallel	800.0	80	1.57
		Perpendicular	800.0	80	1.60
	Large	Parallel	400.0	80	1.47
		Perpendicular	400.0	80	1.46
80	Small	Parallel	600.0	60	1.55
		Perpendicular	600.0	60	1.59
	Large	Parallel	300.0	60	1.46
		Perpendicular	300.0	60	1.49
90	Small	Parallel	500.0	50	1.60
		Perpendicular	500.0	50	1.61
	Large	Parallel	250.0	50	1.53
		Perpendicular	250.0	50	1.55
For a Siemens fluoroscopic x-ray tube (test run 4):					
70	Small	Parallel	190.0	80	2.06
		Perpendicular	190.0	80	2.01
	Large	Parallel	80.0	80	2.07
		Perpendicular	80.0	80	2.01
80	Small	Parallel	165.0	63	2.04
		Perpendicular	165.0	63	2.00
	Large	Parallel	63.0	63	2.08
		Perpendicular	63.0	63	2.04
90	Small	Parallel	147.0	50	2.03
		Perpendicular	147.0	50	1.96
	Large	Parallel	56.5	50	2.06
		Perpendicular	56.5	50	2.03

[Table 13]

Parallel Wire Test Tool X-ray Tube Techniques
When Using Single Emulsion Film at FFD of 101.6 cm (40")

Tube kVp	Focal Spot Size	Wire Orientation w.r.t c-a Axis	Exposure Time (ms)	Tube mAs	Film Optical Density
For a Picker diagnostic x-ray tube (test run 1):					
70	Small	Parallel	3000.0	300	2.25
		Perpendicular	3000.0	300	2.27
	Large	Parallel	1500.0	300	2.36
		Perpendicular	1500.0	300	2.39
80	Small	Parallel	2000.0	200	2.21
		Perpendicular	2000.0	200	2.21
	Large	Parallel	1000.0	200	2.28
		Perpendicular	1000.0	200	2.28
90	Small	Parallel	1200.0	150	2.13
		Perpendicular	1200.0	150	2.19
	Large	Parallel	800.0	160	2.28
		Perpendicular	800.0	160	2.30

[Table 14]

Parallel Wire Test Tool X-ray Tube Techniques
When Using Double Emulsion Film at FFD of 182.9 cm (72")

Tube kVp	Focal Spot Size	Wire Orientation w.r.t c-a Axis	Exposure Time (ms)	Tube mAs	Film Optical Density
For a Picker diagnostic x-ray tube (test run 1):					
70	Large	Parallel	1500.0	300	1.55
		Perpendicular	1500.0	300	1.49
80	Large	Parallel	1000.0	200	1.44
		Perpendicular	1000.0	200	1.46
90	Large	Parallel	800.0	160	1.43
		Perpendicular	800.0	160	1.47
For a Siemens fluoroscopic x-ray tube (test run 4):					
70	Large	Parallel	372.0	320	2.19
		Perpendicular	372.0	320	2.16
80	Large	Parallel	228.0	200	1.95
		Perpendicular	228.0	200	1.92
90	Large	Parallel	201.0	160	1.95
		Perpendicular	201.0	160	1.91

[Table 15]

Parallel Wire Test Tool X-ray Tube Techniques
When Using Single Emulsion Film at FFD of 182.9 cm (72")

Tube kVp	Focal Spot Size	Wire Orientation w.r.t c-a Axis	Exposure Time (ms)	Tube mAs	Film Optical Density
For a Picker diagnostic x-ray tube (test run 1):					
70	Large	Parallel	5000.0	1000	2.12
		Perpendicular	5000.0	1000	2.14
80	Large	Parallel	3000.0	600	1.97
		Perpendicular	3000.0	600	1.99
90	Large	Parallel	2000.0	400	1.86
		Perpendicular	2000.0	400	1.85

adjusted to a focal spot to table distance of 88.9 cm (35"), which was the distance at which the meter was calibrated. The x-ray field size was then adjusted via the collimator opening and its alignment adjusted via the collimator and its alignment light source to only include the meter's active region. The meter provided a digital readout upon exposure that was accurate to ± 2 kV in the range between 50 and 150 kVp. The reproducibility of the meter was experimentally determined to be ± 0.1 kV (one standard deviation).

When a comparison was made between the kVp values set on the x-ray generator control panel to the kVp values measured by the digital KV meter, it was observed that the KV meter values were consistently slighter higher (highest observed difference were typically 2.7% at 70 kVp). Because the error bars of the measured kVp values included the set kVp values, all of the quoted x-ray tube kVp values in this work are the kVp values that were set on the x-ray tube generator control panel.

III.b.2 X-ray Tube Exposure Time Measurement

After the kVp measurement, the digital KV meter was replaced by a model 3036 Dosimeter·Ratemeter·Timer digital meter [Ref. 42], constructed by Radcal Corporation [Ref. 43]. The meter's radiation sensor is a 40 mm diameter air ionization chamber that has an active air equivalent volume

of 10.4 cm^3 whose midplane is located 40 mm from the upper surface. Prior to exposure the x-ray tube was set at the appropriate FFD and the collimator was adjusted to produce a field that included the 40 mm diameter ion chamber (which was delineated by a circle at the top of the meter). The meter upon exposure provided a digital readout of the exposure time that was accurate to ± 1 ms. The reproducibility of the meter was indicated as ± 5% in the instruction manual and was experimentally found to be within ± 0.25 ms (one standard deviation).

When a comparison between the x-ray generator control exposure time settings and the measured values was made, it was found that the digitally measured values were consistently slightly lower (the largest observed difference was 4 ms (8%) at the lowest generator control setting used, 50 ms [1/20 s]). This can be understood by the way in which the meter functions, including only that portion of the waveform during which the exposure rate exceeds 10 mR/s, thus losing about 2 ms at each end of the waveform. All of the exposure time technique settings quoted in this work are those set on the x-ray generator control panel.

The digital meter was also utilized to enable production of test tool film images of approximately equal optical density for the various x-ray tubes that were used. This was done by testing the x-ray tube output exposure prior to taking a test tool film image. Adjustments to the x-ray tube

mAs values were then made to compensate for any changes in exposure from that required. This test was particularly useful when making the transition from single phase (1ϕ) Picker generators to three phase (3ϕ) high frequency Siemens generators.

III.c Test Tool Film Image Collection Procedure

With the exception of the pinhole camera occlusal films where a single test was performed on each (3.2 cm by 7.6 cm) film, six test tool images were collected on a single 20.3 cm by 27.9 cm medical x-ray film to optimize data collection and x-ray film usage. This was done by masking off the regions of the cardboard cassette (which contained the x-ray film) that were not inside the x-ray field with lead sheets of 0.3 cm thickness. Lead numbers were placed on the cardboard cassette in the x-ray field region to identify each test tool image procedure. The anode-cathode orientation with respect to the test tool image direction as recorded on the run data sheets.

III.d X-ray Film Processors

All of the x-ray films were developed in a Kodak RP X-OMAT processor. The first 7 test runs used the M4 model type that had a film processing time of 90 s. The basic operation of the processor is illustrated in [Fig. 18]. The film was removed from the cardboard cassette in the dark room and fed

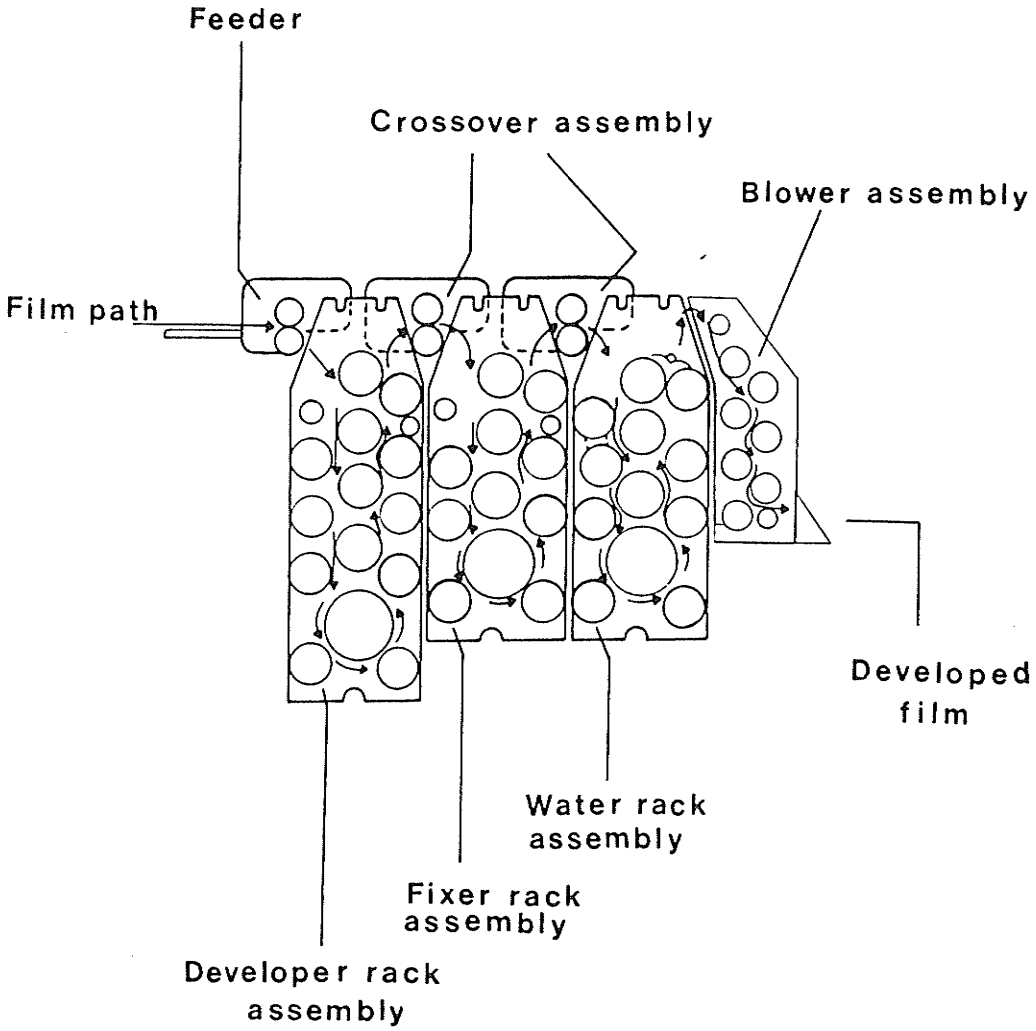

[Fig. 18]

Basic operation of an automatic film processor.

into the processor via the feeder tray entry slot also located in the darkroom. The film was positioned in the feeder so that its length was perpendicular to the direction of travel. This minimized the effect of the developer chemical induced gradients on the film that might occur due to film processing. Once the film had entered the processor it passed through a developer rack assembly that contained 65 cm^3 of developer kept at a temperature of 34.4 ± 0.5 °C. The developed film then entered a fixer rack assembly that contained 110 cm^3 of fixing solution kept at a temperature of 31.7 ± 0.5 °C. To wash the developer and fixing solutions off the film, the film was passed through water held at a temperature of 31.7 ± 0.5 °C all via a rack assembly. The processed film was then dried by a blower set at a temperature of 51.7 ± 0.5 °C. Because the x-ray tubes and corresponding processors used in test runs 8, 9 and 10 were dedicated to the performance of mammography the film processing took place at a much longer time interval to bring out contrast in the film image. For this reason, an M7B model type processor was used that had a total film processing time of 175 s. This processor operated under conditions similar to those of the M4 model type described above, with the following two exceptions: the water temperature was set at 18.3 ± 0.5 °C and 60 cm^3 of developer was used.

III.e X-ray Tubes

Test tool images were collected of ten different x-ray tubes [Table 16]. The manufacturer's specified focal spot sizes (also referred to as the nominal focal spot sizes) were obtained from the labelling on the individual x-raytube housing or technical specifications that accompanied the x-ray tube.

III.f Digital Imaging System

Before the focal spot dimensions could be determined from the parallel wire test tool image on the film, the film image had to be first captured by a frame grabber, digitized, with the resulting digital image stored in computer memory. The digitized image of the two parallel wires then is subject to a software algorithm operation that was devised for the purpose of extracting the focal spot dimensions (see following chapter).

III.f.1 Hardware and Software

The computer system was an IBM personal computer AT clone manufactured by Mind [Ref. 44], with a single diskette drive capable of reading double-sided, double-density 5¼" diskettes and a 25.4 cm (10") monochrome display terminal manufactured by Packard Bell. The computer included 1 Mbyte RAM system memory and a 60 Mbyte hard disk storage capacity.

The direct connection of a single PCVISIONplus Frame

[Table 16]

X-ray Tube General Information

Test Run Number	Dedication	Generator Type	Tube Make	Anode Angle[5]	Focal Spot Sizes (mm) Small/Large
1	Diagnostic Radiology	1ϕ	Picker	13.5°	0.7/1.4
2	Diagnostic Radiology	1ϕ	Picker	13.5°	0.7/1.4
3	Diagnostic Radiology	1ϕ	Picker	13.5°	0.7/1.4
4	Fluoroscopy/ General Radiography	3ϕ	Siemens	13°	0.6/1.2
5	Fluoroscopy/ General Radiography	3ϕ	Siemens	13°	0.6/1.3
6	Tomography	1ϕ	Picker	13.5°	0.7/1.4
7	Fluoroscopy/ General Radiography	3ϕ	Siemens	13°	0.6/1.0
8	Mammography	3ϕ	CGR	7.5°/12°	0.1/0.3
9	Mammography	3ϕ	CGR	7.5°/12°	0.1/0.3
10	Mammography	1ϕ	Lorad	16.5°	0.1/0.3

[5]The x-ray tubes that were dedicated to mammography had an anode with two different tilt angles. The small (large) tilt angle was used for the small (large) focal spot. Also during test run 10 the beam angle used for the small (large) focal spot was 8.5° (12.5°).

Grabber board [Ref. 45] to an expansion slot in the Mind computer and the utilization of ITEX PCplus software [Ref. 46] provided the computer configuration with the required digital image processing capabilities. The PCVISIONplus Frame Grabber board contained a video digitizer capable of digitizing a standard video input signal of 512 lines by 512 lines of digitizing information per single frame, a 0.5 Mbyte on-board frame memory that was capable of storing the digitized image and a display logic module that could simultaneously display the stored image on a video monitor. The PCVISIONplus Frame Grabber board required access to a computer memory space consisting of a single contiguous block of 64 kbytes of RAM. The ITEX PCplus software was a library of image processing and graphics display subroutines written for use with the PCVISIONplus Frame Grabber board and designed for use with an IBM personal computer AT (or equivalent). The ITEX PCplus software package was distributed as an object code library that could be linked to applications programs written in the C computer language.

III.f.2 Digitization Procedure

The description of the overall digitizing process can be simplified by referring to [Fig. 19]. The 20.3 cm by 27.9 cm medical x-ray film containing the six parallel wire test tool images was placed on a 35.6 cm by 43.2 cm clear glass plate that was positioned on top of a light box. The glass

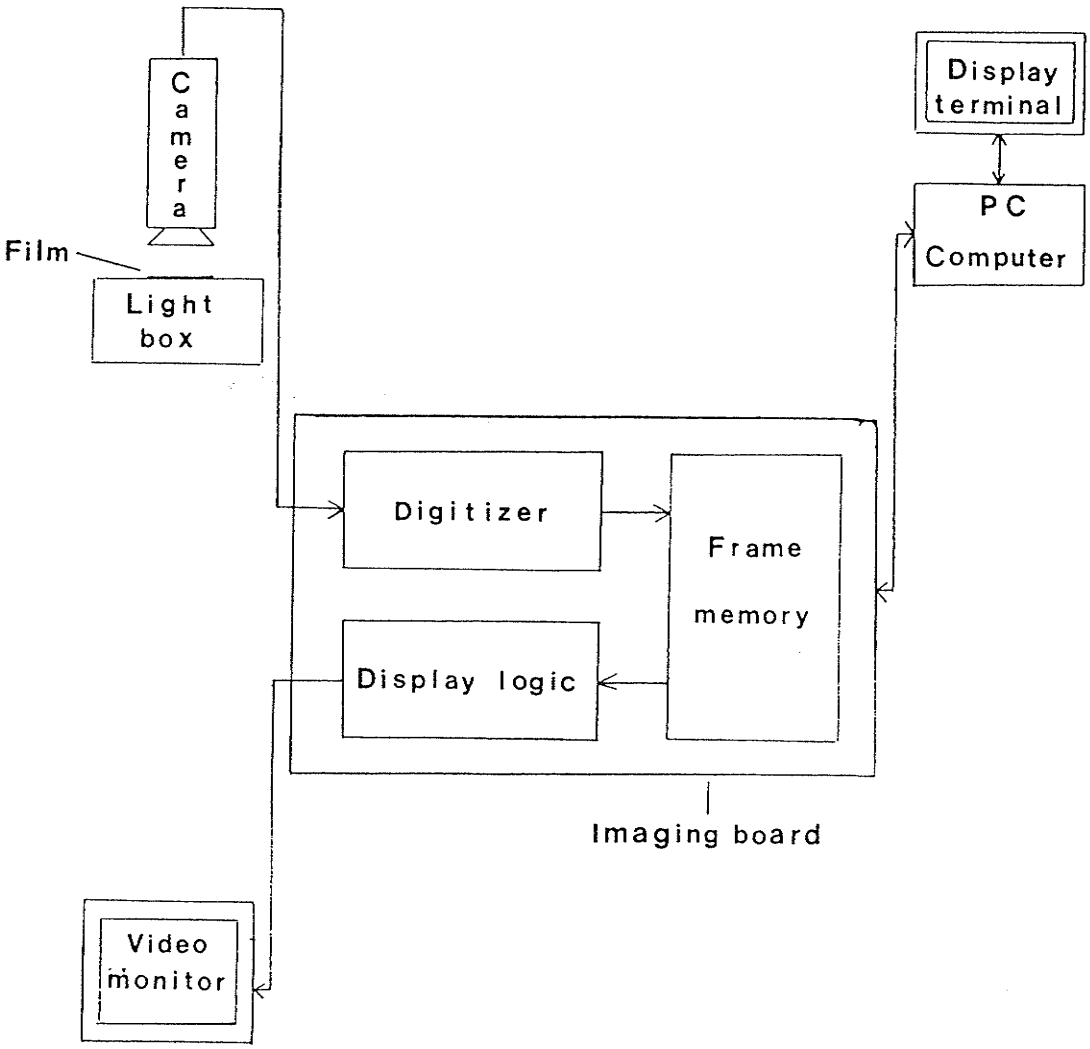

[Fig. 19]

Components of the digital image processing system.

plate just covered the top face of the light box. A 35.6 cm by 43.2 cm milky colored plastic diffuser plate of 5 mm thickness was placed just beneath the glass plate to reduce and equalize the intensity of the emerging light. A 35.6 cm by 43.2 cm overexposed (black) film with a 5 cm by 5 cm center hole cut out was placed on top of the test tool film. This had two functions: one to physically block off regions of the film that were not to be digitized and two, to provide easy centering of the test tool film image of interest. The light box contained a single 600 W incandescent bulb that was placed 30.5 cm below the top glass plate. An 11.4 cm by 19.0 cm black metal plate was centered 10.2 cm above the light bulb to ensure provision of a nearly uniform light intensity distribution. Once the light box was turned on, a Cohu 5000 series television camera was used to produce an analog video signal of the film image (called a frame) to be captured by horizontally scanning the entire image. The video information in each horizontally scanned line was kept separate by the placement of timing information between adjacent lines. The horizontally scanned lines were divided into two groups (called fields): an even field and an odd field, which consisted of the even and odd numbered horizontal scan lines of the frame respectively. The analog signal produced by the camera was then transformed into a digital signal via the PCVISIONplus Frame Grabber board's digitizer. The

digitization process involved the sequential sampling of the analog signal at discrete time intervals and the conversion of each sample, or pixel, to a digital value. The resulting pixels were then stored in the frame memory at individually specified memory locations. Each pixel in the frame memory was assigned one of 256 possible intensities or gray levels. The parallel wire test tool film image was then stored in the frame memory as a 512 pixel by 512 pixel image. Once the entire frame had been digitized and stored in the frame memory, it was displayed on a NEC/Multisync II [analog red-green-blue (RGB) color] video monitor via the PCVISIONplus Frame Grabber board's display logic module which transformed the digital values of the individual pixels back into an analog format (which could then be manipulated by the video monitor). Because of the monitor's limiting vertical screen dimensions, the stored image was viewed as a 480 pixel by 512 pixel image with 32 vertical lines being omitted. The individual pixel coordinate assignments on the screen were such that the y-coordinate (vertical) axis increased from top to bottom and the x-coordinate (horizontal) axis increased from left to right. This type of assignment placed the pixel coordinate systems origin at the top left hand corner of the screen. It should be noted that the 512 pixel by 512 pixel image in memory was not compressed into a 480 pixel by 512 pixel displayed image, but rather had the top 32 pixels in the vertical dimension cut off. Each pixel on

the monitor screen was rectangular in shape with its smaller vertical dimension being $4/5^{th}$ of the horizontal dimension.

On a further note, when the parallel wire test tool film image was placed on the light box's top glass plate, the two parallel wires were orientated so that they ran from top to bottom on the displayed digitized image. To magnify the parallel wire test tool film image further, a Tamron 28 to 80 mm variable focal length telephoto lens was mounted on the video camera. The distances from the film to the center of the lens and camera were always kept at 36.8 cm and 55.9 cm respectively. At a focal length of 80 mm and film-to-lens center distance of 36.8 cm, the zoom lens produced a secondary magnification (as opposed to the primary geometric test tool magnification) of 3.4X. During the data analysis of the parallel wire test tool images the zoom lens was set to either a focal length of 50 or 80 mm depending on the wire thickness on the film to be analyzed.

CHAPTER IV

DATA ANALYSIS

This chapter will present the analysis that was performed to determine the focal spot dimensions from the various focal spot test tool film images. Because the concept of magnification arises quite frequently in this chapter, it will be discussed first.

IV.a Magnification

IV.a.1 Geometric Magnification

It is well known that when an object of size S_0 is placed in the x-ray beam between the focal spot and film, as illustrated in [Fig. 20], the emerging x-rays will cast a "shadow" of size S_i of the object on the film. This "shadow" is referred to as the image of the object. The magnification of the object on the film is then defined as

$$\text{Magnification} = S_i/S_0 \quad . \tag{12}$$

The geometric magnification (M) can be written as

$$M = \frac{d + d'}{d}$$

$$= 1 + \frac{d'}{d} \tag{13}$$

where d is the object distance (distance between the focal spot and the object) and d' is the image distance (distance between the object and film). [Eq. 13] was derived from

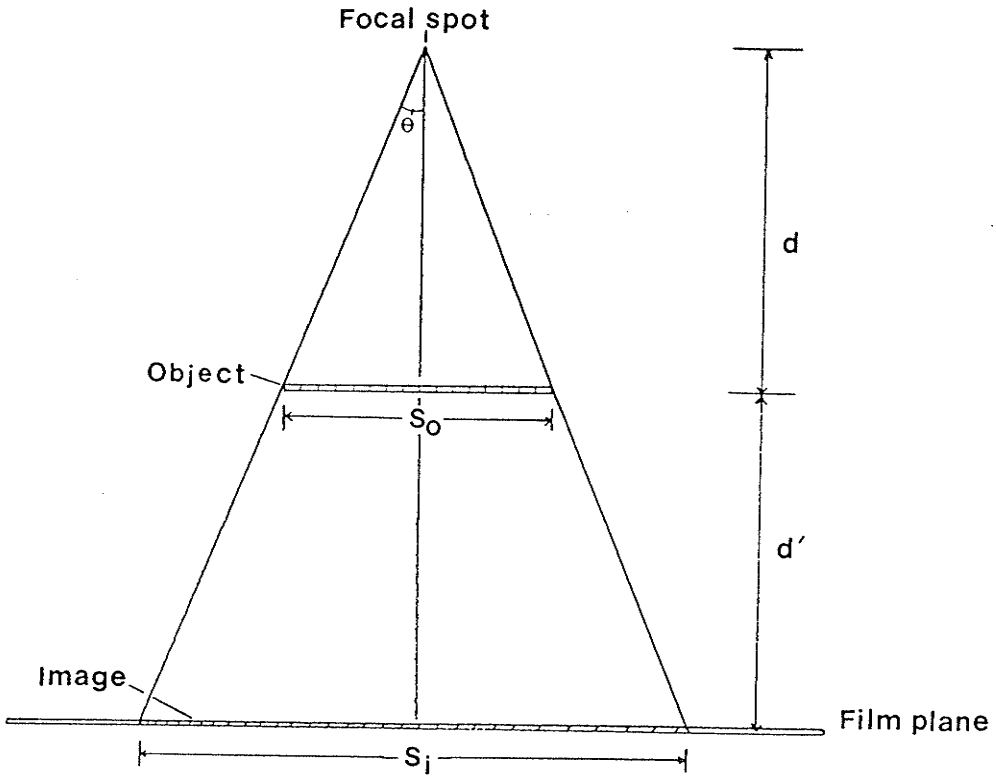

[Fig. 20]

Geometry of a magnified image produced by a point source focal spot.

[Eq. 12] via the following relation

$$\tan(\theta) = \frac{S_0}{2d} = \frac{S_i}{2(d + d')} \qquad (14)$$

which was derived from the geometry in [Fig. 20]. The two assumptions made during the derivation of [Eq. 13] was that the focal spot was a point source and emulsion thickness is negligible.

IV.a.2 Enlargement Factor

The degree of enlargement of the image with respect to the object is known as the enlargement factor and is given by the second term in [Eq. 13] that is:

$$\text{Enlargement factor} = \frac{d'}{d} = M - 1 \quad . \qquad (15)$$

IV.a.3 True Magnification

A more realistic expression of the object's magnification on film can be determined (see Appendix A) by considering a focal spot of a finite size. This true magnification (m) is then related to the geometric magnification (M) by the following expression

$$m = M + (M - 1)\cdot\frac{f}{S_0} \qquad (16)$$

where f is the finite size (diameter) of the focal spot.

It is seen from [Eq. 16], that the true magnification will be equal to the geometric magnification only when the

focal spot size is very small in comparison to the dimensions of the object.

IV.b Focal Spot Calculations Using Conventional Measuring Techniques

IV.b.1 Bar Resolution Pattern

The small focal spot's film image of the bar resolution test tool pattern has been illustrated in [Fig. 21]. In this film image it is seen that some sets of bars can be seen clearly and some can not. The explanation of this observation can be simplified by the consideration of [Fig. 22] which utilizes a test tool magnification of 2X. Since the focal spot has a finite size for this analysis, it can be approximated by two point sources located at opposite edges. When the bars and spaces between the bars are wider than half the focal spot dimensions [Fig. 22a], the images of the bars as seen on film will be separated, that is, bars will be resolved. If on the other hand, the bars and spaces are narrower than half the focal dimensions [Fig. 22b], the images of the bars on film will appear to be overlapped, thus bar separation will not be possible.

To eliminate repetition the focal spot dimensions will be defined here. The dimension of the focal spot perpendicular to the x-ray tube's cathode-anode axis will be referred to as the width (f_w) and the dimension of the focal spot that is parallel to the cathode-anode axis will be referred to as the length (f_l).

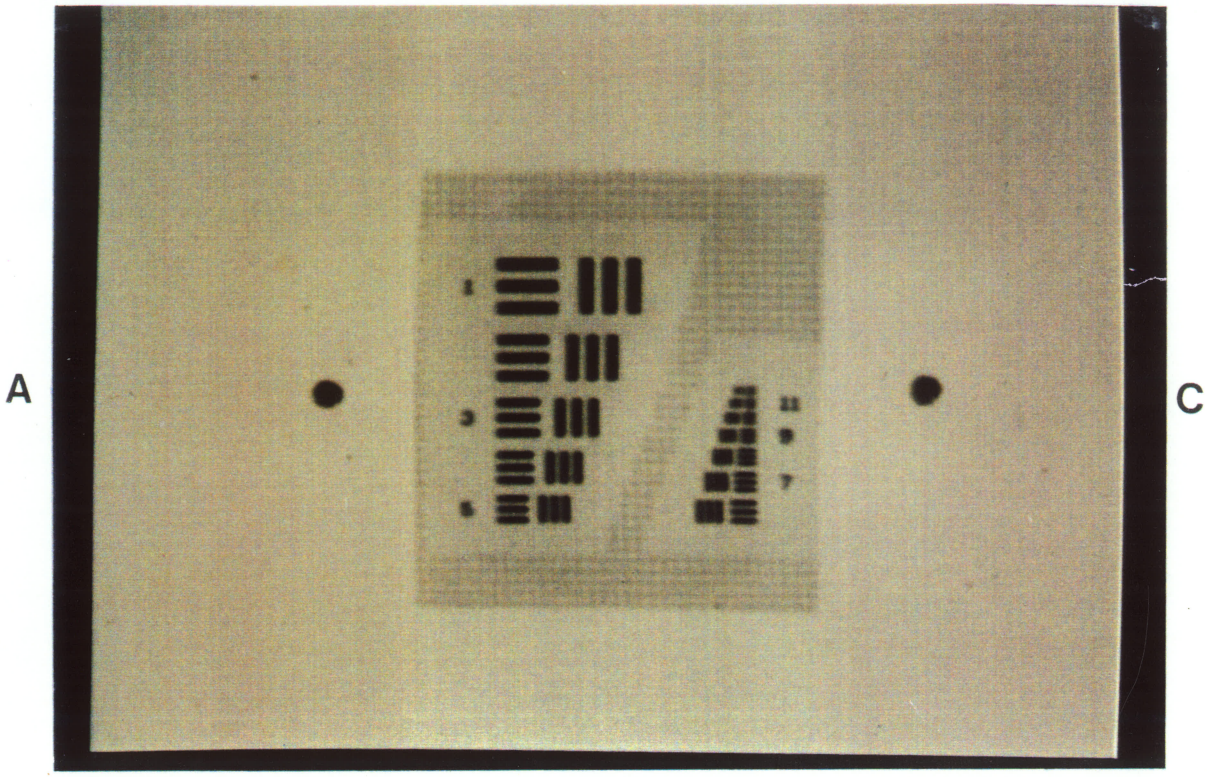

[Fig. 21]

Bar resolution test tool pattern film image of the small focal spot of test run 2, when using a 70 kVp tube voltage. The letters C and A above illustrate the cathode - anode axis with respect to the focal spot test tool (this convention will also be used in the remaining radiographs as well).

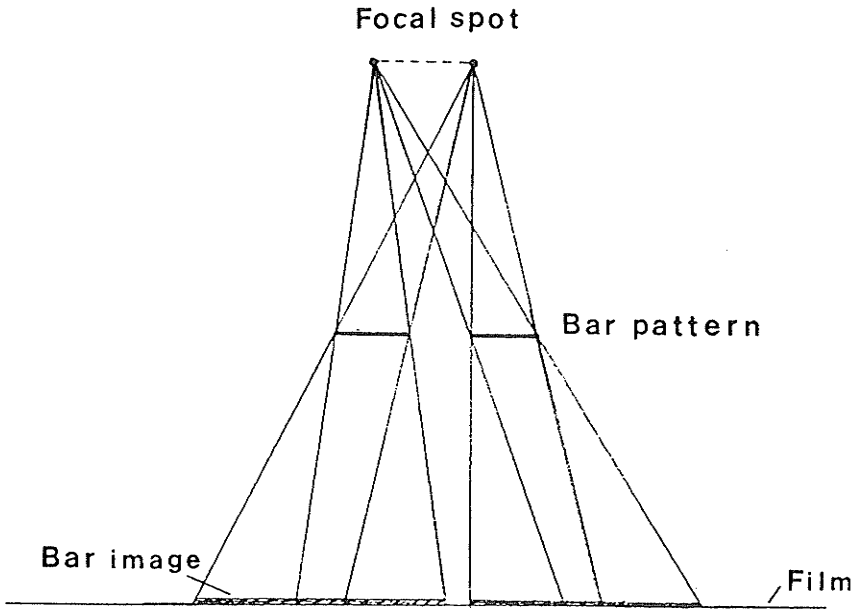

(a) For bars or spaces wider than half the focal spot.

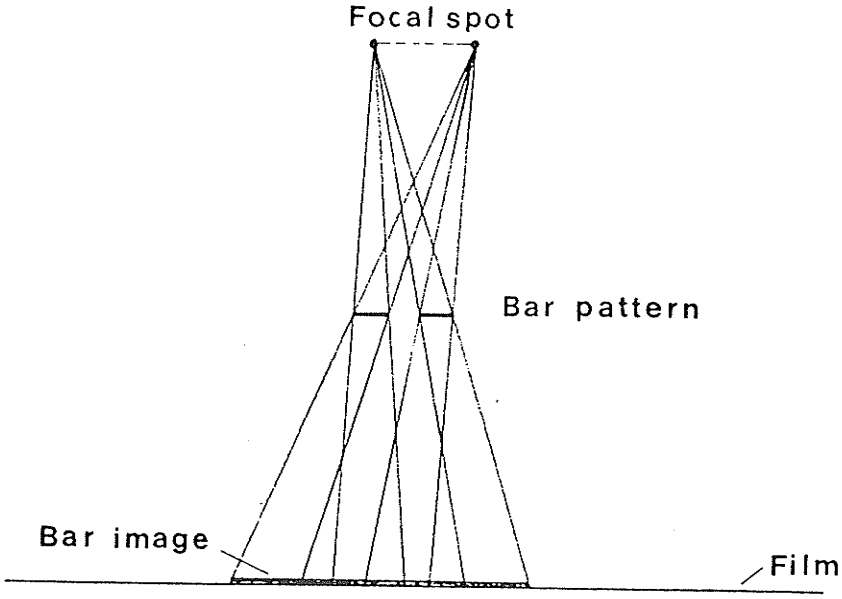

(b) For bars or spaces narrower than half the focal spot.

[Fig. 22]

Geometric considerations in determining the focal spot.

Because the test tool was constructed of eleven bar groups with each bar group containing two sets of three bars, one set perpendicular to the other, both focal spot dimensions can be determined from a single test tool film image. The focal spot length and width were calculated from the following equation

$$f = \frac{M}{2l_f} \cdot \frac{1}{(M - 1)} \qquad (17)$$

where l_f is the highest bar group line pair frequency resolved from those tabulated in [Table 5] and M is the test tool's geometric magnification. The derivation of [Eq. 17] is indicated in [Appendix B].

Because [Eq. 17] gives the focal spot dimensions from the line pair frequencies (which is the reciprocal of twice the width of an individual bar), only the set of bars that was parallel (perpendicular) to the cathode-anode axis as considered in the determination of the focal spot width (length). l_f is the line pair frequency corresponding to the bar group that had the three bars just resolvable. To illustrate this point, [Table 17] tabulates the bar group assignment that was used in the analysis of the bar pattern test tool image of [Fig. 21]. M was determined from [Eq. 12] via the measurement of the separation distance between the two alignment screws (shown in [Fig. 21] as two dark spots) both on the film and on the test tool.

[Table 17]

Bar Group Assignment for Test Run 2
When Using a 70 kVp Tube Voltage

Focal Spot Size	Focal Spot Dimensions	Bar Group Assignment
Small	Width	10
	Length	8

The uncertainty in the focal spot dimension (δf) as calculated from [Eq. 17] was determined from

$$\delta f = \left[(\delta l_f)^2 \cdot \left(\frac{dl_f}{df} \right)^2 + (\delta M)^2 \cdot \left(\frac{dM}{df} \right)^2 \right]^{1/2}$$

$$= f \left[\left(\frac{\delta l_f}{l_f} \right)^2 + \left(\frac{\delta M}{M(M-1)} \right)^2 \right]^{1/2} \qquad (18)$$

where δl_f and δM are the uncertainties in the assigned line pair frequency and test tool magnification respectively.

The uncertainty in l_f was estimated to be half the difference between the assigned bar groups line pair frequency and the line pair frequency of the next lower bar group. This estimate is justified by the fact that we are considering the bar group that has the three bars just resolvable (whose spaces between the bars may not be perfectly clear) as opposed to the bar group (next higher bar group set) that will have the three bars clearly visible (spaces between bars much more clearly visible). The true focal spot resolution is likely between these two bar groups line pair frequencies. Since M was determined using [Eq. 12], its uncertainty is calculated from

$$\delta M = \left[(\delta S_0)^2 \cdot \left(\frac{dS_0}{dM} \right)^2 + (\delta S_i)^2 \cdot \left(\frac{dS_i}{dM} \right)^2 \right]^{1/2}$$

$$= M \left[\left(\frac{\delta S_0}{S_0} \right)^2 + \left(\frac{\delta S_i}{S_i} \right)^2 \right]^{1/2} . \qquad (19)$$

S_0 and S_i are now the separation distances between the two alignment holes as measured on the test tool and on the film

respectively. The uncertainty in each measurement, that is δS_0 and δS_i, was estimated to be ± 0.7 mm.

IV.b.2 Star Resolution Pattern

The small focal spot film image of the star resolution test tool pattern has been illustrated in [Fig. 23]. In this image it is seen that a region exist about the center of the pattern where the "rays" of the star pattern gradually disappear. This region, which depends on the focal spot size and radiation intensity distribution, is termed the area of failure of resolution. The origins of this region on the star pattern's film image can be explained by the consideration of [Fig. 24]. Once again, when a focal spot of finite size (f) is used to irradiate a star pattern that has been placed a distance "d" away, the emitted radiation can be considered to originate from two point sources at opposite edges. Also, for the sake of simplicity, only a small portion of the star pattern has been considered: this entails two absorbing strips each of width "w", that are separated by a gap also of width "w". The dimensions of "w" have been assumed to be smaller than the focal spot dimensions. The various planes in [Fig. 24] illustrate the images of the star pattern's two absorbers as a function of distance from the focal spot. It is seen from planes A and B that the image of the gap between the two absorbers is still present. Plane C on the otherhand is at a distance where the

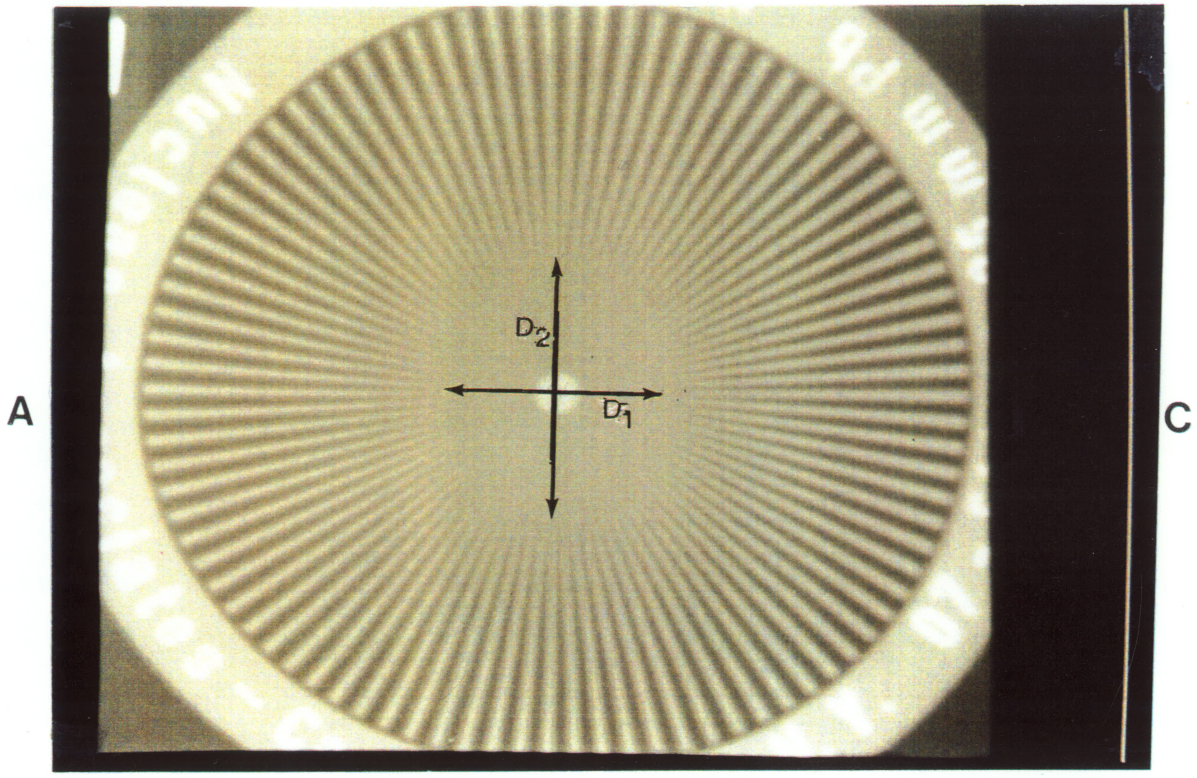

[Fig. 23]

Star resolution test tool pattern film image of the small focal spot of test run 2, when using a 70 kVp tube voltage.

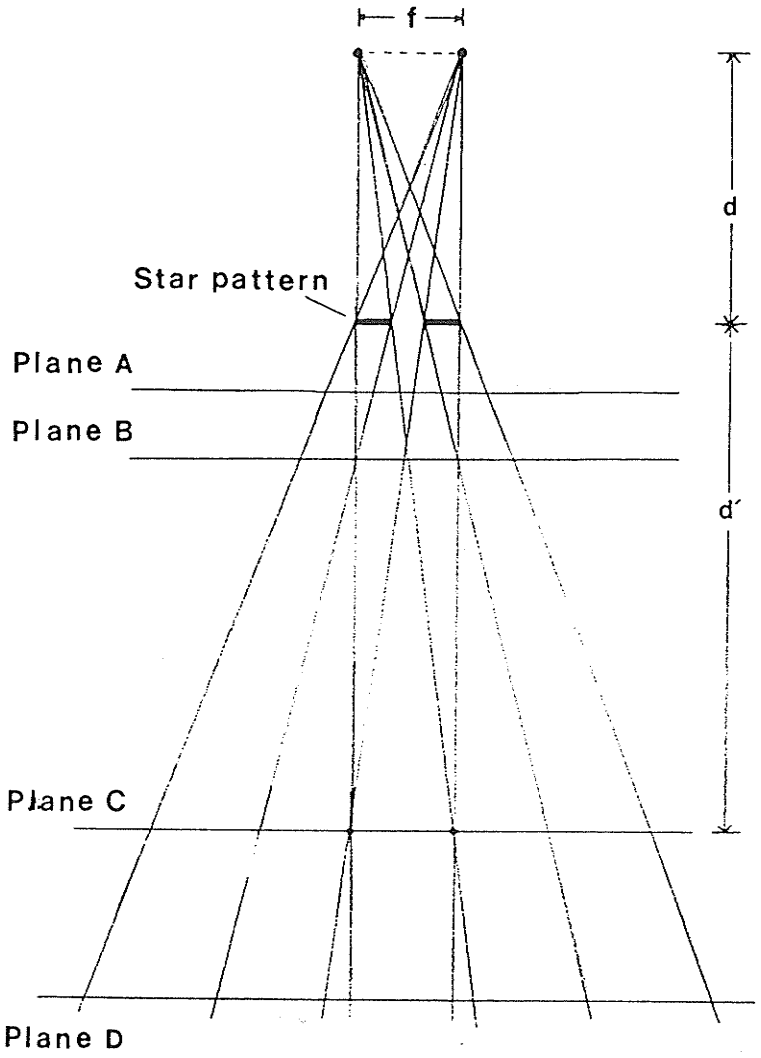

[Fig. 24]

Star pattern images as a function of distance from the test tool.

penumbra regions of the two absorbers overlap and blur the image of the gap. This is the region where the star pattern's resolution fails. For this region to exist, the magnified image of the gap between the two absorbers has to be equal to the penumbra of the absorbers. Plane D contains the penumbra regions of the two absorbers interacting in such a way as to have the resulting radiation field within the gap at a minimum as a opposed to a maximum as it was in planes A and B.

Both focal spot dimensions f_w and f_l, were calculated from a single film image of the test tool via the following equation

$$f = \frac{N}{57.3} \cdot \frac{D}{(M - 1)} \qquad (20)$$

where N is the spoke angle of the star pattern (2°), M is the test tool's geometric magnification and D is the diameter of the zero contrast region (in mm). [Eq. 20] is derived in [Appendix C].

Prior to the calculation of the focal spot dimensions, the two variables D and M in [Eq. 20], had to be determined from the film image of the test tool [Fig. 23]. The geometric magnification (M) of the test tool was determined from

$$M = \frac{D'}{D'_0} \qquad (21)$$

where D' is the diameter of the radiographic image of the

star pattern (in mm) and D'_0 corresponds to the physical diameter of the test tool (45 mm). When calculating the width of the focal spot, the zero contrast diameter (D in [Eq. 20] and D_1 in [Fig. 23]) was determined by first scanning the star pattern on the radiograph along the corresponding cathode-anode axis, inward from the periphery, to find the two outermost regions in which the images of the spokes first seem to disappear and then measuring the distance between these two regions. The contrast diameter (D in [Eq. 20] and D_2 in [Fig. 23]) perpendicular to D_1 was then measured in a similar fashion and subsequently used to compute the length of the focal spot.

The uncertainty in the geometric magnification [Eq. 21] of the test tool was calculated from

$$\delta M = \left[(\delta D'_0)^2 \cdot \left(\frac{dD'_0}{dM} \right)^2 + (\delta D')^2 \cdot \left(\frac{dD'}{dM} \right)^2 \right]^{1/2}$$

$$= M \left[\left(\frac{\delta D'_0}{D'_0} \right)^2 + \left(\frac{\delta D'}{D'} \right)^2 \right]^{1/2} . \qquad (22)$$

The uncertainty in the D'_0 measurement, $\delta D'_0$, was taken to be ± 0.7 mm. Because of the unsharpness of the outer edges of the test tool film image, the uncertainty in the D' measurement, $\delta D'$, was taken to be ± 1.0 mm.

The uncertainty in the focal spot measurement was determined from the following expression

$$\delta f = \left[(\delta D)^2 \cdot \left(\frac{dD}{df} \right)^2 + (\delta M)^2 \cdot \left(\frac{dM}{df} \right)^2 \right]^{1/2}$$

$$= f\left[\left(\frac{\delta D}{D}\right)^2 + \left(\frac{\delta M}{M(M-1)}\right)^2\right]^{1/2} \qquad (23)$$

where δD and δM are the uncertainties in the assigned zero contrast diameter and test tool magnification respectively. Because of the image unsharpness at the edges of the zero contrast region, δD was taken to be $\pm$ 1.0 mm.

The subjectiveness in using the star pattern test tool to determine the focal dimensions arises from the determination of the parameter D in [Eq. 20], which may be estimated slightly differently by each individual that is performing the focal spot measurement.

IV.b.3 Pinhole Camera

The small focal spot test tool film image as obtained from pinhole camera imaging has been illustrated in [Fig. 25]. The intensity distribution of the focal spot as seen in [Fig. 25] is somewhat of a surprise, in that it is not uniform in intensity as one could expect from the line focus principle [Fig. 8] but rather appears to have two maxima located at opposite edges. An explanation of this observation has been illustrated in [Fig. 26], which indicates that the two intensity maxima are a result of the focusing cup's influence on the trajectories of the cathode emitted electrons. The deflections in the electron trajectories then cause the emitted electrons to focus onto the two vertical "line" regions on the target anode.

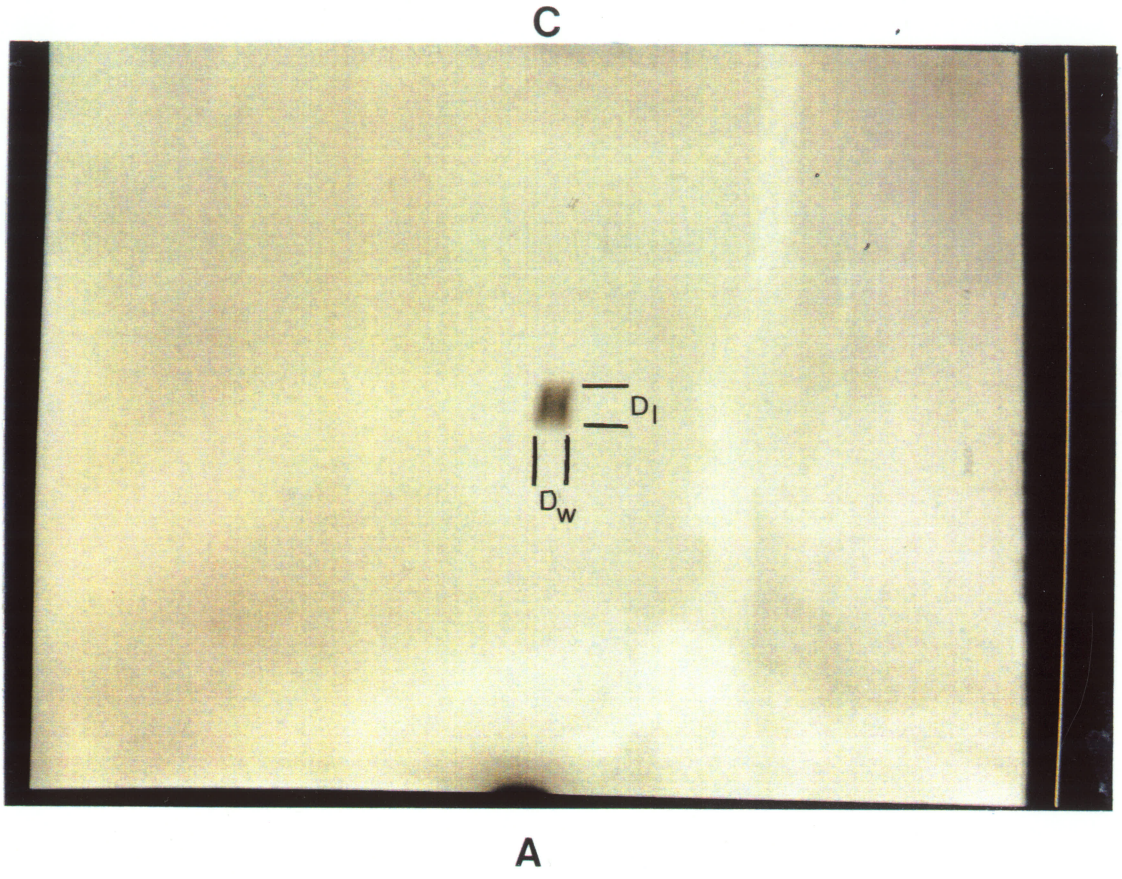

[Fig. 25]

Pinhole camera film image of the small focal spot of test run 2, when using a 70 kVp tube voltage. It should be noted that this pinhole camera image has been magnified to best show the shape of the focal spot image.

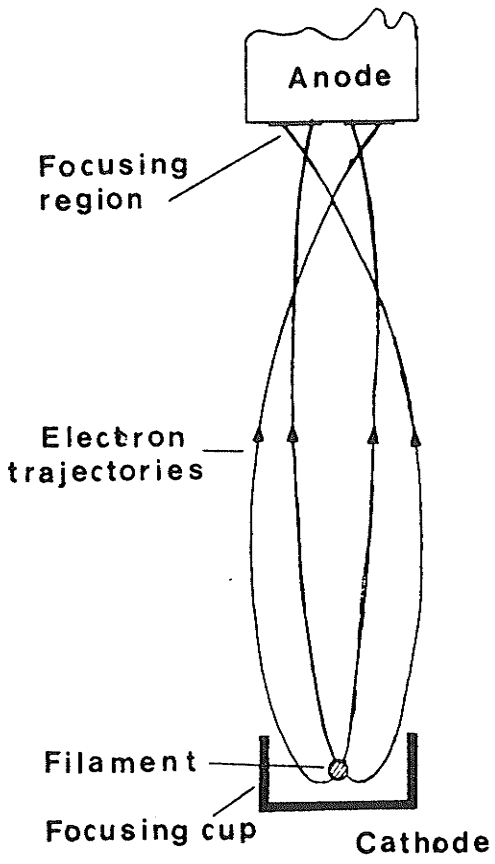

[Fig. 26]

Schematic of focusing cup's induced deflections on cathode emitted electron trajectories. The focusing cup and filament are viewed from above.

The width and length of the focal spot as determined from a single pinhole camera image [Fig. 25] was calculated from

$$f_W = \frac{D_W - D_h \cdot M}{(M - 1)} \qquad (24)$$

and

$$f_l = \frac{0.7 \cdot D_l}{(M - 1)} \qquad (25)$$

where M is the geometric magnification of the pinhole, D_h is the diameter of the pinhole (in mm); D_W and D_l are the width and length of the pinhole camera focal spot image (in mm). The derivation of [Eq. 24] is indicated in [Appendix D]. The length of the focal spot was determined differently than was the width due to the observed decrease in radiation from the ends of the pinhole camera's focal spot image. The 0.7 correction factor in [Eq. 25] is there to compensate for this effect.

The geometric magnification of the pinhole was determined from [Eq. 21] where D' is now the distance between the two alignment screws on the film pinhole test tool image (one of which is indicated as a dark spot on [Fig. 25]) and D'_0 is the distance between the two alignment screws on the upper plate of the pinhole camera (14.3 mm). The uncertainty in the magnification was determined from [Eq. 22]. The uncertainties in the measurements of D' and D'_0, $\delta D'$ and $\delta D'_0$, were taken as ± 1.0 mm and ± 0.7 mm respectively (the uncertainty in $\delta D'$ was larger than that set for $\delta D'_0$ due to the uncertainty in determining the exact centers of the two

that in the uncertainty calculation of f_1 [Eq. 25 and 27], an uncertainty was not assigned to the 0.7 correction factor because this factor was specified by the formalism in the pinhole camera focal spot evaluation method [Ref. 47].

IV.c Focal Spot Calculation Using Digital Imaging Technique

To determine the width or length of a given focal spot as determined via the parallel wire test tool, the film image of this test tool had to be first "grabbed", digitized and then stored in computer memory. The width (length) of the focal spot, which was determined from test tool film images that had the two parallel wires on the test tool parallel (perpendicular) to the x-ray tube cathode-anode axis, was then extracted from the digitized image by using the analysis program FSPOTCAL (see Appendix E).

IV.c.1 The Analysis Program FSPOTCAL

The program FSPOTCAL was written and compiled in the C computer language and was used:

(a) to reconfigure the computer, so that the software knows where the hardware registers and frame memory are mapped;

(b) to initialize the PCVISIONplus hardware;

(c) to specify the size of the PCVISIONplus frame memory;

(d) to digitize the parallel wire test tool film image and to store the digitized image in frame memory;

(e) to recall the digitized image from frame memory and to displayed it on the video monitor screen as a 480 pixel by 512 pixel image;

(f) to enhance the digitized image by utilizing the

appropriate ITEX PCplus software subroutines; and

(g) to calculate the dimensions of the focal spot and their associated statistical and systematic errors.

The sequence of events that the program FSPOTCAL followed to calculate the focal spot dimensions from a parallel wire test tool film image (that had already been digitized and stored in frame memory), are summarized in [Fig. 27]. A description of each of these steps will be provided below. Because steps (a) through (e) as listed above, were performed by the program FSPOTCAL simply by calling the appropriate ITEX PCplus subroutines [Ref. 46], these steps will not be discussed any further.

IV.c.1.i **Displayed Digital Film Images**

Digitized film images of the parallel wire test tool as displayed on the monitor's screen are illustrated in [Fig. 28] and [Fig. 29]. Both of these illustrations were results of the small focal spot of test run 2, using a 70 kVp tube voltage. The FFD was set at 101.6 cm (40") and Kodak TMG double emulsion film was used.

The "noisy" background on the test tool images, see [Fig. 28] and [Fig. 29], resulted from radiographic mottle and in particular quantum mottle, which is defined as the variation in density of a uniformly exposed radiograph (film) that results from the random spatial distribution of the x-ray quanta (within the x-ray beam) absorbed by the film. It

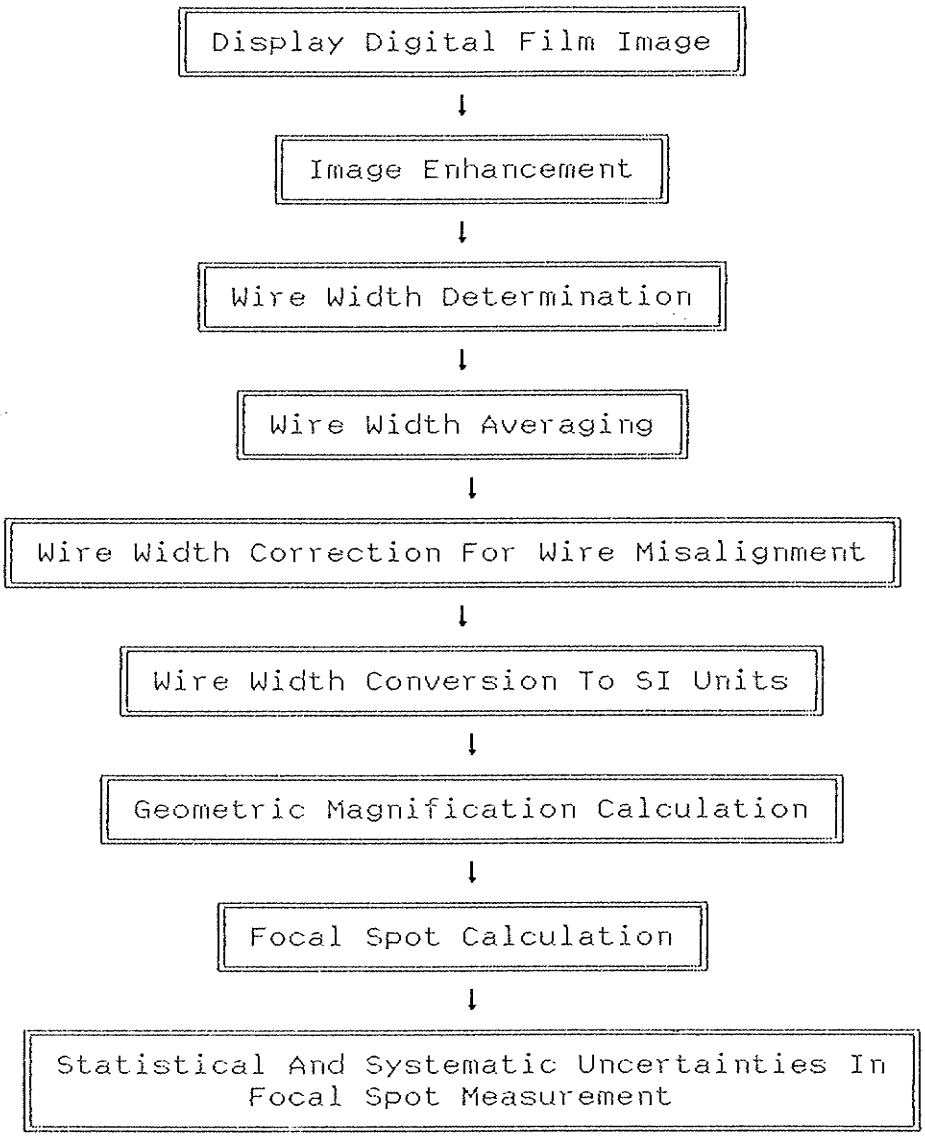

[Fig. 27]

Block diagram of the FSPOTCAL program's algorithm.

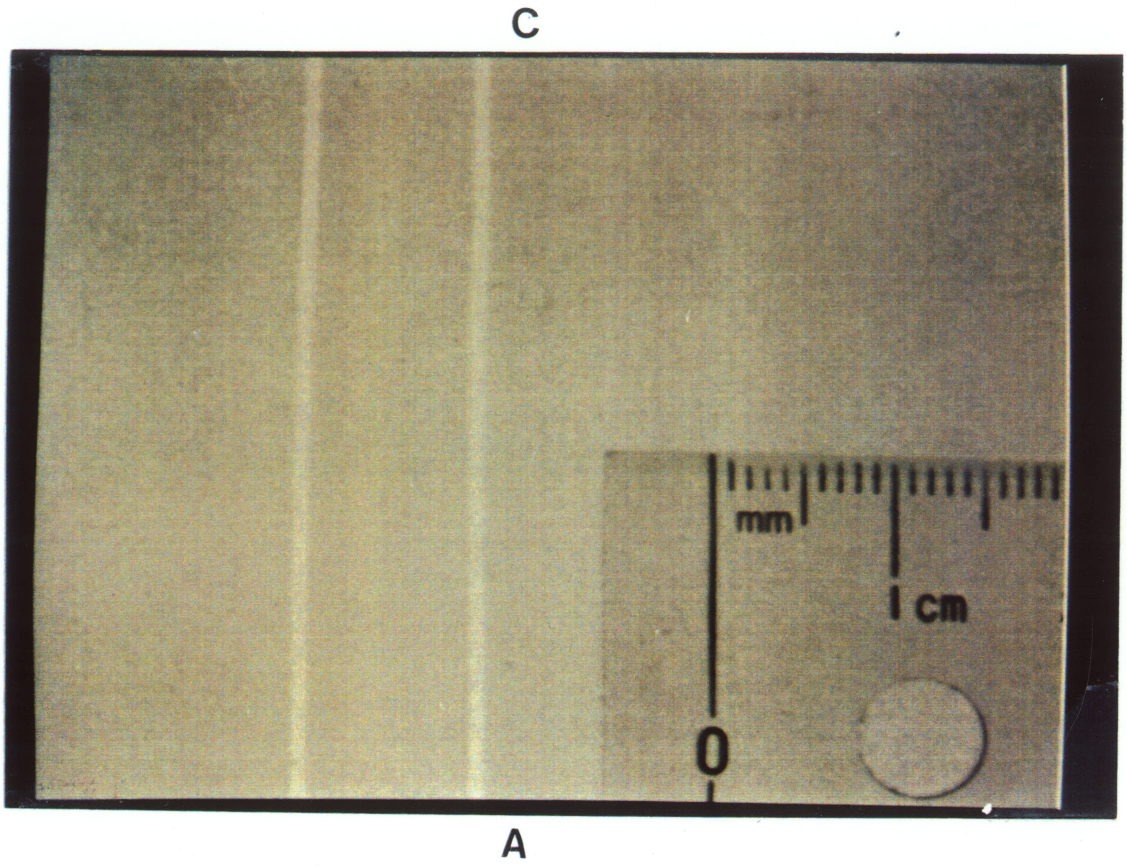

[Fig. 28]

Small focal spot digitized image of the parallel wire test tool during test run 2, when using a 70 kVp tube voltage and and a FFD of 101.6 cm (40"). The test tool's wires were orientated such that to have the wires parallel to the tube's c-a axis, so as to calculate the focal spot's width.

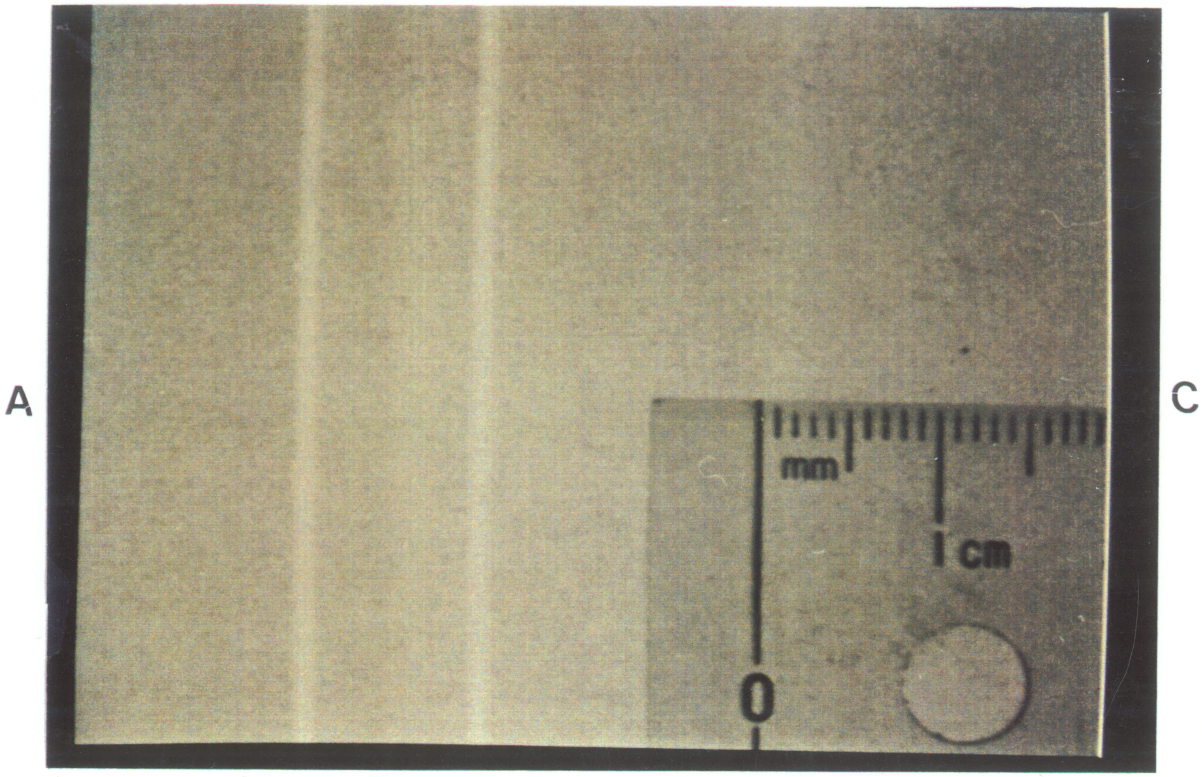

[Fig. 29]

Small focal spot digitized image of the parallel wire test tool during test run 2, when using a 70 kVp tube voltage and and a FFD of 101.6 cm (40"). The test tool's wires were orientated such that to have the wires perpendicular to the tube's c-a axis, so as to calculate the focal spot's length.

should be noted that because no intensifying screens were used screen mottling was not present. Film graininess on the other hand, which also contributes to radiographic mottle and is due to the random distribution of the deposits of developed silver halide grains in the emulsion layer, was not seen on film due to the overwhelming extent of quantum mottling. The bright and dark regions in the test tool images, were caused by the Heel effect on the film prior to digitization. Because the test tool's film images were magnified by a magnification that varied between 2.1X and 3.4X, the magnified quantum mottling effect on film images caused the edges of the wires of the test tool as seen on the digitized image to appeared irregular.

The secondary magnification, as a opposed to the primary geometric test tool magnification which was kept constant at 2.0X, was either 2.1X or 3.4X (which corresponded to choosing telephoto lens focal lengths of 50 mm or 80 mm respectively) for the following reasons. If the secondary magnification was much higher than 3.4X, both the width of the wires and the film mottling would have been magnified to such an extent that the variation in the wire width would have increased substantially, increasing the overall percent uncertainty in the focal spot measurement. If the secondary magnification was much lower than 2.1X, the variation in the wire width would have decreased (due to a smaller magnification of the film mottling), but the magnitudes of

the wire widths would have also decreased, thus again increasing the overall percent uncertainty in the focal spot measurement. This range between 2.1X and 3.4X was experimentally determined to minimize the percent error in the focal spot measurements. In the above discussion the percent uncertainty in the focal spot measurement was taken to be

$$\text{Percent uncertainty} = \frac{\delta f}{f} \times 100\ \% \qquad (28)$$

where f and δf in the above equation is the average focal spot size and the statistical variation of the focal spot respectively as calculated by the program FSPOTCAL and as described in (section IV.c.1.viii) and (section IV.c.2.iii).

The film image quality (defined as the ability of the film to record each point on the object as a point on the film) in the parallel wire test tool film image was influenced by:

(a) radiographic mottle;

(b) unsharpness; and

(c) film resolution.

Because no intensifying screens[6] were used, the only component that contributed to radiographic mottle, which is the irregular mottled appearance of the film caused by small

---

[6] A cardboard cassette was used instead of a cassette containing an intensifying screen [Ref. 38] to reduce image blurring.

optical density differences on the film, was quantum mottle.

The major contributor to the reduction of film sharpness (which is the ability of the film to define sharp edges) was due to the geometric unsharpness of the test tool image [Fig. 1]. This in turn was due to the finite dimensions of the focal spot and the primary magnification of the test tool. Absorption and parallax unsharpness were also present, but made negligible contributions to the net image unsharpness. Absorption unsharpness is due to the fact that the wires in the test tool had a circular cross section which meant that x-ray attenuation would have been different depending on the path length through the wire. Parallax unsharpness results from the fact that double emulsion film was used. This effect can be explained as follows: when double emulsion film is irradiated with x-ray photons both emulsions layers will form an image of the object, but since these two layers are separated by some small distance, a parallax will exist when these images are viewed from some angle (that is, the edges of the two images will not necessary overlap).

Film resolution, which is the ability of the film to record separate images of small objects that are placed very close together, not only depends on film graininess but also on the light-scattering properties of the emulsion and on the contrast with which the film reproduces fine detail (fine grain film with thin emulsions yield the highest

resolving power).

Film resolution is often quoted in terms of the Modulation Transfer Function (MTF) [Ref. 48] or the Contrast Transfer Function (CTF) [Ref. 48], which is a graphic description of the film's ability to image an MTF test object with a sinusoidal pattern or a CTF test object with a line pair (or dot) pattern with varying spacial frequencies. It should be noted that in an MTF test tool the frequencies are defined as the number of cycles (peaks and valleys) per millimeter length whereas for a CTF test tool the frequencies are in terms of the number of lines and spaces (line pairs) per millimeter. The modulation or contrast transfer function then measures the ability of the film to detect the lowest possible contrast differences between adjacent regions and to reflect an image that duplicates the actual object pattern as closely as possible. A typical MTF spectrum of a film is shown in [Fig. 30], and it is apparent from this figure that both single and double emulsion films have spatial resolutions that are not only in excess of 30 cycles/mm but also exceed the visual resolution range. The MTF function, which is defined as the image contrast to object contrast ratio, will have a value of 1.0 when the film resolution is perfect and a value of 0.0 when film blurring is maximum or when film contrast is zero.

In the digital imaging system, both the TV camera and the display monitor influenced image contrast. The resolution of

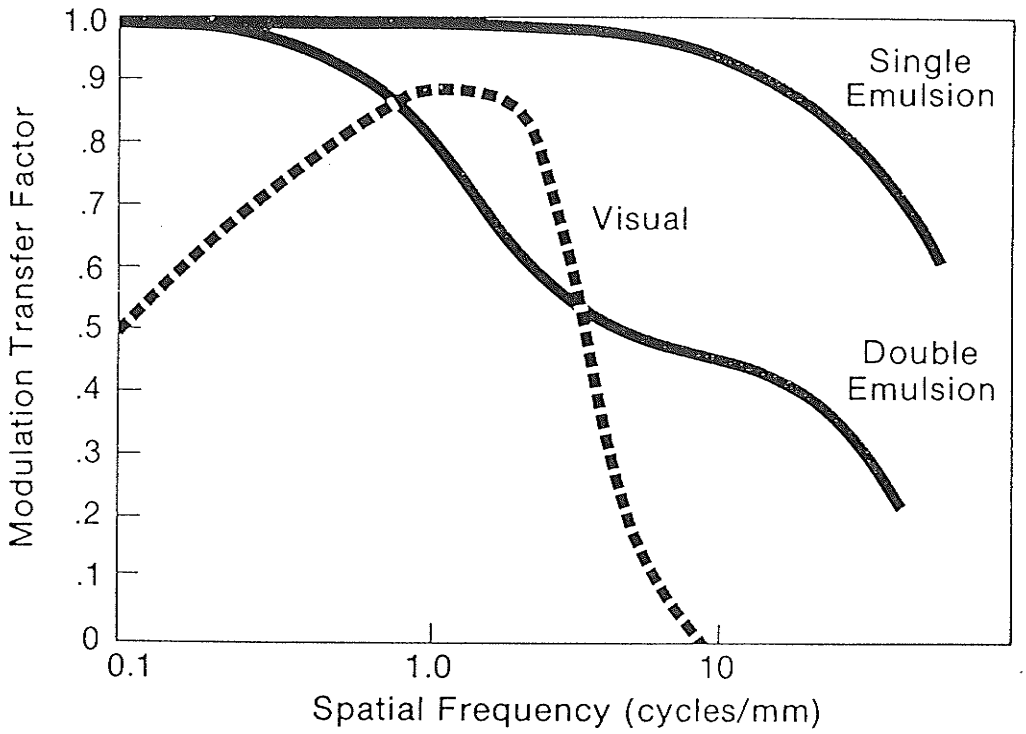

[Fig. 30]

Modulation Transfer Function spectrum of film.

this system was determined by three effects: the number of horizontal scan lines utilized by the television camera to record the film image in frame memory (which in this system was 512 lines/frame), the resolution of each horizontal scan line (that is the number of pixels per horizontal line), and the resolution of the individual system components.

Because each image that was stored in frame memory was "grabbed' by the digitizer which operates at a rate of 30 frames/s (with each frame having information for a 512 by 512 pixel screen), the digitizer was operated at a video band width of 10 MHz [Ref. 45]. The break down of a typical video band width, as in the case of the digitizer, is as follows: the number of pixels that had to be "grabbed" by the digitizer in 1 second would have been at a rate of $512 \cdot 512 \cdot 30 = 7.9$ MHz, the remaining 2.1 MHz was necessary to compensate for the video signal timing information of each pixel and the time it takes the camera to wrap around two adjacent horizontal lines. The video band width of the Cohu 5000 series TV camera and the display monitor were 15.75 MHz [Ref. 49] and 30 MHz [Ref. 50] respectively.

The resolution of the display monitor was at 800 dots per horizontal line [Ref. 50], and since the monitor had an active display screen width of 250 mm then the monitor's resolution was 3.2 dots/mm (0.3 mm dot pitch) or 1.6 line pairs/mm. The Cohu 5000 series TV camera had a horizontal resolution of 600 lines [Ref. 49].

The overall resolution of the digital imaging system, which was found to be in the order of 6 line pairs/mm, was determined by digitizing a film resolution pattern and then displaying the patterns image on the system monitor. Because films have typical resolutions over 20 line pairs/mm, [Fig. 30], the quality of the displayed image was limited not by the film resolution but by the overall resolution of the digital imaging system.

When a comparison is made between [Fig. 28] and [Fig. 29], it is seen that the individual wire images of [Fig. 28] appear to have a double projection as if produced by two separate focal spots in addition to their overall reduced width. This observation, which was evident in all of the small focal spot parallel wire test tool images (when the test tool was placed parallel to cathode-anode axis), resulted from a focal spot that had two intensity maxima each located at either side of the intensity distribution (for more details see section IV.b.3).

IV.c.1.i.1 Active Region of Displayed Image

The program FSPOTCAL was used to calculate the focal spot dimensions from the average wire width of both wires (see section IV.c.1.viii). To simplify the algorithm that was to be used to determine the average wire width, the background image noise (due to quantom mottle) and any gradient effects had to be minimized. This was achieved by considering only

the portion of the image that was in the immediate vicinity of the wire. This enclosed region, whose boundaries are illustrated in [Fig. 31] by the white rectangle, was set by the program at 55 pixels in width and 475 pixels in length and was referred to as the active region. The width of the active region was experimentally determined to minimize the overall percent uncertainty in the focal spot measurement (see Chapter V for more details). The length was chosen to include as much of the wire image as possible so as to improve statistics. [Fig. 31] is identical to [Fig. 29] with the exception of the superimposed delineation of the active region.

To simplify the discussion of how the average width of a given wire image was extracted by the program FSPOTCAL from the image data within a selected active region, only the image manipulation of the left wire of [Fig. 29] will henceforth be illustrated. The program used a similar technique to extract the average width of the right wire of [Fig. 29].

IV.c.1.ii Image Enhancement

As seen from [Fig. 29], the wire image within the active region does not stand out very clearly from the background image noise, thus making it hard to detect the two edges. Since the wire width was to be determined for each of the 475 horizontal scan lines in the active region from position

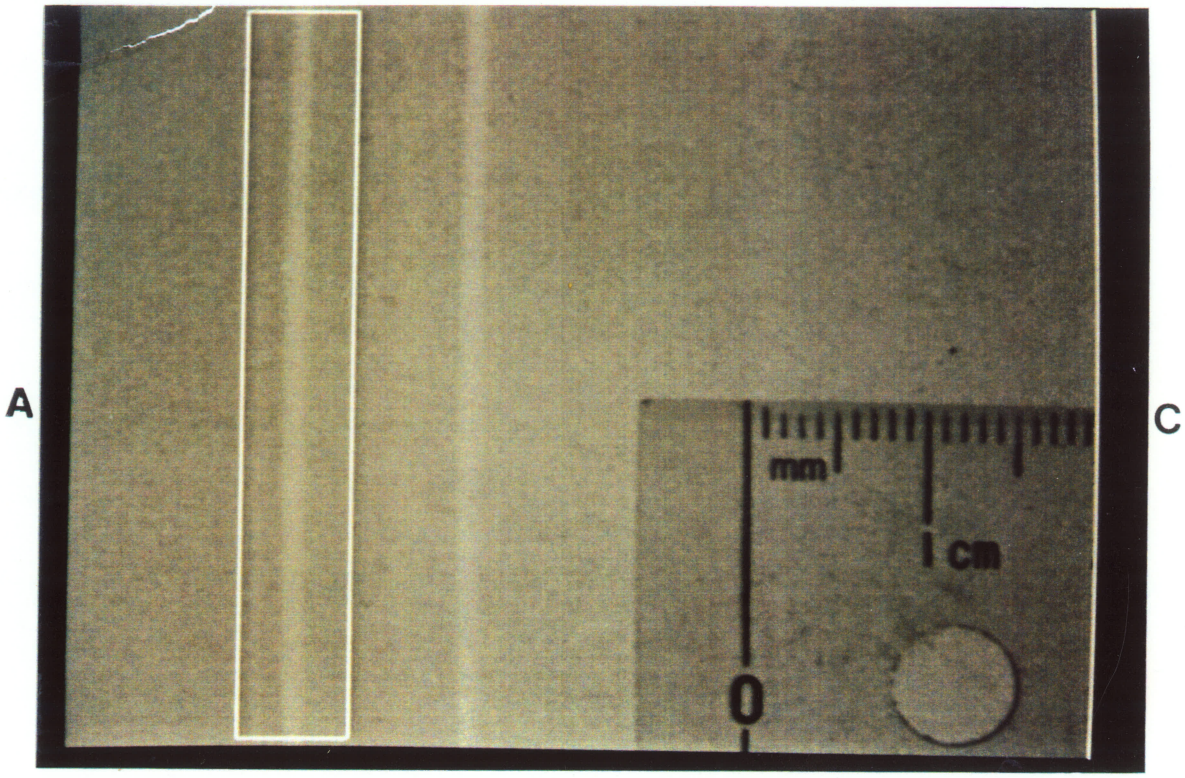

[Fig. 31]

Active region superposition on digitized test tool image.

estimates of the two edges of the wire, the uncertainty in some of these estimates created a problem. To overcome this difficulty, image processing enhancement was performed by using the technique of histogram equalization which modified the appearance of the wire in the active region. [Fig. 32] illustrates [Fig. 31] after the application of histogram equalization. It is seen in [Fig. 32] that when histogram equalization was used to enhance the wire image, it also blurred the wire image width by approximately 2 pixels.

X-ray tubes used for mammography and having smaller focal spot sizes enabled production of digitized parallel wire test tool images in which the edges of the two wires were very clearly defined, making image enhancement unnecessary. In doing this, wire image blurring by enhancement was eliminated.

Due to the x-ray tube heel effect [section II.b.9], a film density gradient was apparent in the active region of [Fig. 32].

IV.c.1.ii.1 Histogram Equalization

When all of the pixels within the active region of a typical parallel wire test tool image are considered and a histogram is made of their pixel values, it can be shown that the range of the pixel values or gray levels is quite small, typically no more than 30. The enhancement of these pixels by histogram equalization [Ref. 51] is achieved by

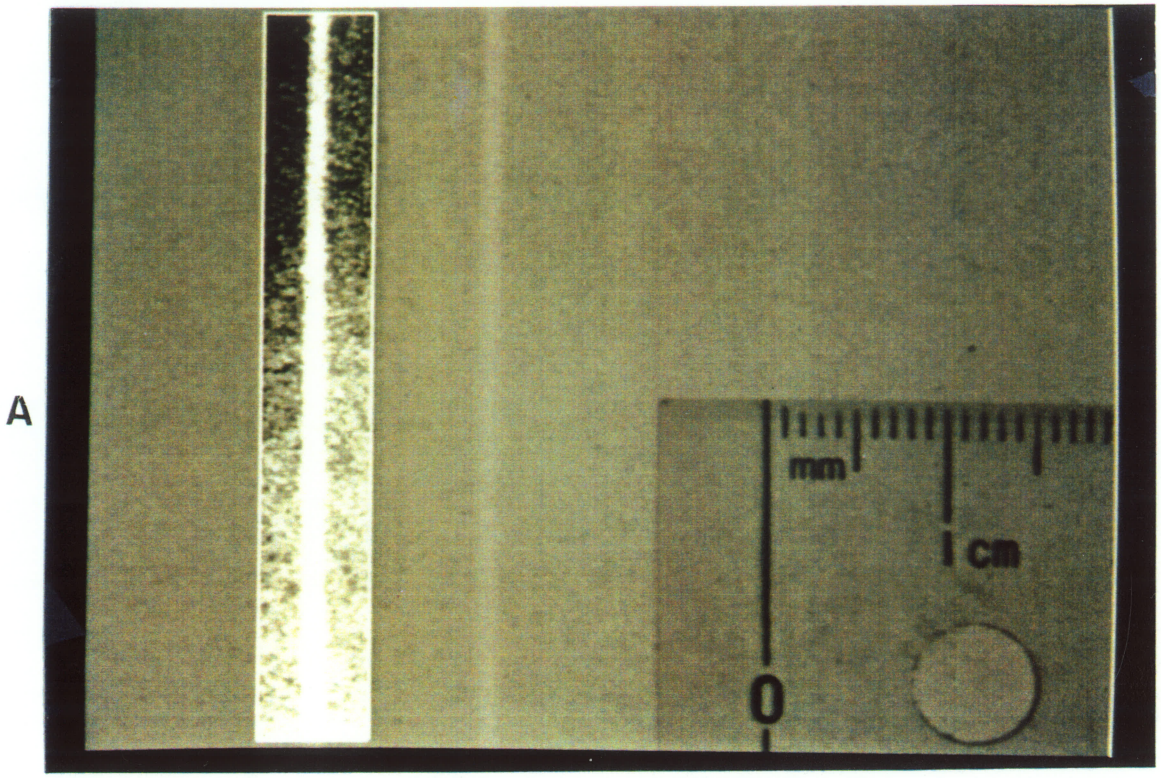

[Fig. 32]

[Fig. 31] after image enhancement by the technique of histogram equalization.

expanding this pixel value or gray level range. This is illustrated in [Fig. 33], which is a horizontal cross section of the active region in [Fig. 31], before (a) and after (b) image enhancement. [Fig. 33] also illustrates the pixel value distribution of a single horizontal row of pixels, which shows the wire image to be a broad peak.

IV.c.1.iii Wire Width Determination

The program FSPOTCAL was used to calculate the width of the wire from the pixel value distribution of each horizontal row of pixels within the selected active region. This meant that the wire width was determined 475 times. This greatly improved statistics, minimizing the corresponding uncertainty. The wire width was defined as the full width at half maximum (FWHM) of the wire image pixel value distribution.

The following section will utilize [Fig. 33b], to illustrate the methods that were employed to extract the width of the wire from the pixel value distribution of a given horizontal row of pixels.

IV.c.1.iii.1 Maximum of Pixel Value Distribution

Before the wire width can be determined from a single horizontal row of pixels the maximum of the distribution must be determined.

Because some of the wire images had a double projection

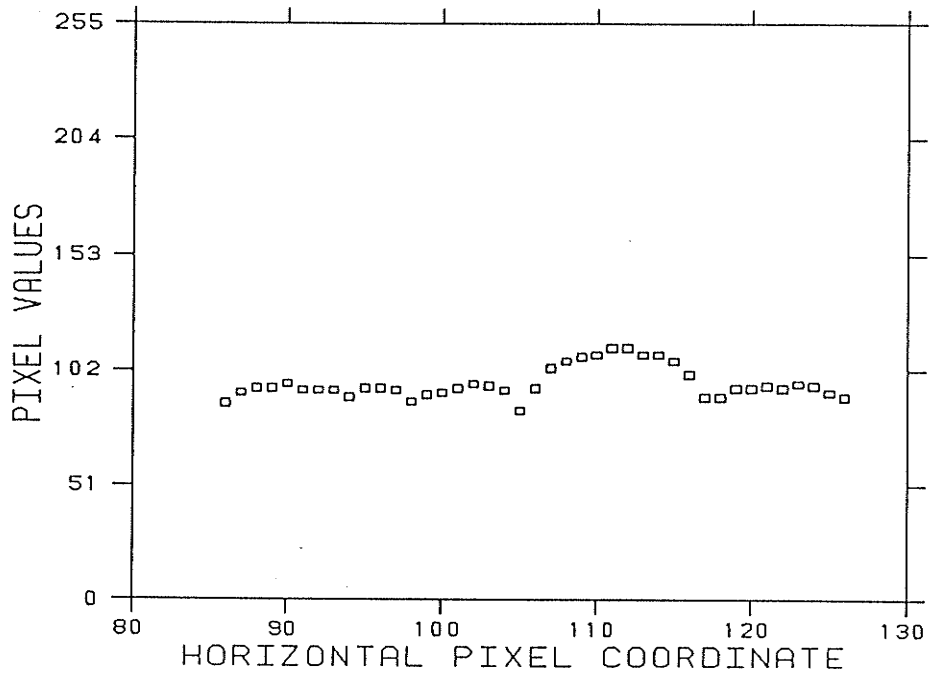

(a) Horizontal row of pixels before image enhancement.

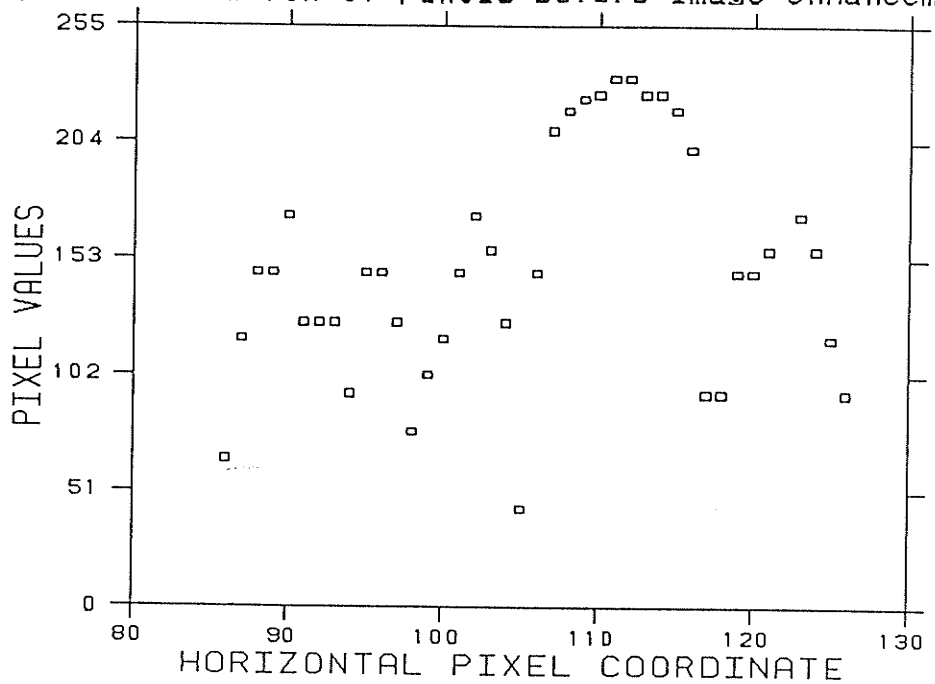

(b) Horizontal row of pixels after image enhancement.

[Fig. 33]

Active region cross section before and after histogram equalization.

(and hence their single wire pixel value distributions would have been composed of two maxima) the maximum of the main peak was determined by smoothing the distribution. This was achieved by first blurring the wire image within the active region in the vertical direction by vertical pixel averaging and then blurring the image in the horizontal direction by horizontal pixel averaging. These are generally utilized digital-image processing techniques.

IV.c.1.iii.1.a **Vertical Pixel Averaging**

The image within the active region was vertically blurred by performing the following operation on to each of the 55 vertical rows of pixels. Consider the first 17 pixels in the first vertical row of pixels (pixel number increasing from top to bottom and the first pixel location was at position 1). The gray level value or pixel value of the pixel in position 9 was first set to 0 and then the pixel values of the remaining 16 pixels were summed. The sum was then divided by 16 and the pixel at position 9 received a value equal to the average pixel value of the remaining 16 pixels. The above described procedure was then re-applied to the next 17 pixels in the vertical row which were located at positions 2 to 18. This technique was then re-iterated for all of the 475 pixels that comprised a single vertical row. [Fig. 34] illustrates [Fig. 31] after image enhancement and vertical pixel averaging.

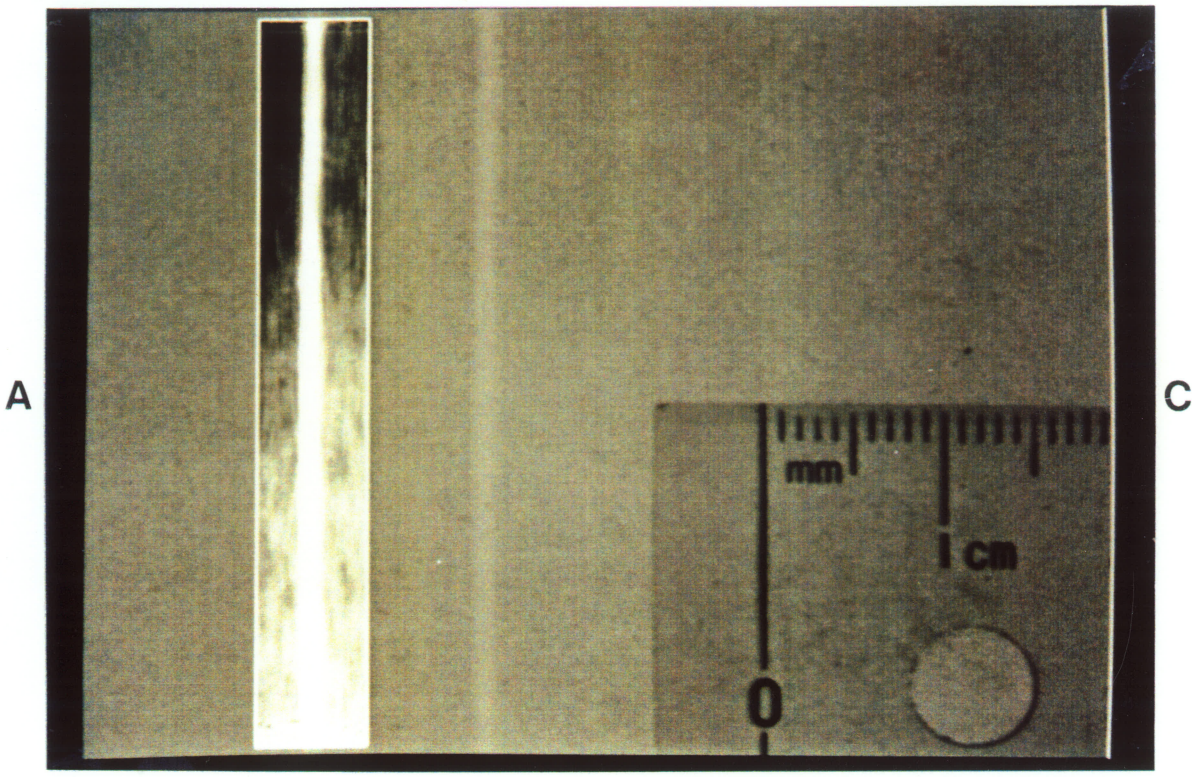

[Fig. 34]

[Fig. 31] after image enhancement by the technique of histogram equalization and vertical pixel averaging.

Because of the above averaging technique the first 8 pixels and the last 16 pixels of the 475 pixels in each vertical row of pixels do not get averaged, see [Fig. 34], and thus the wire width calculation is not performed on the first 8 or last 16 horizontal pixel rows in the active region. This implies that over the entire active region, the wire width is determined 451 times and not 475 times as previously mentioned.

The application of vertical pixel averaging to the already enhanced wire image introduced blurring of the image [Fig. 34]. This blurring was greatly dependent on the alignment of the two wires in the digitized image with the vertical pixel coordinate axis of the display monitor. The alignment of the test tool's film image prior to digitization was such that blurring of the wire image width by vertical pixel averaging was typically of the order of 2 pixels (see section IV.c.1.v for more details).

Because the broad peak of the distribution may not have been completely smoothed over to produce a single peak after the application of vertical pixel averaging [Fig. 35a] (it should be remembered that sometimes the broad peak in the pixel value distribution had double maxima), further blurring of the image was necessary. Additional blurring was achieved by performing horizontal image blurring to the active region of [Fig. 34]. The effect of this type of blurring on [Fig. 35a] has been illustrated in [Fig. 35b].

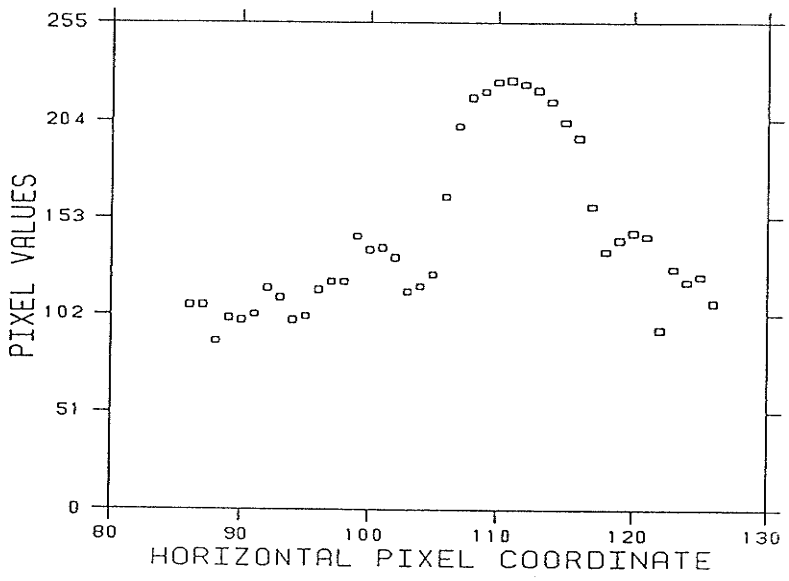

(a) Horizontal row of pixels after image enhancement and with vertical pixels averaging.

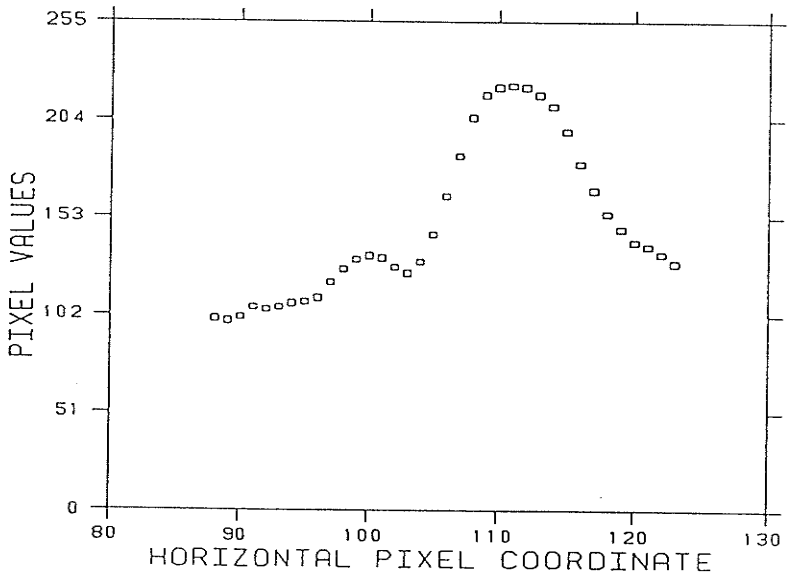

(b) Horizontal row of pixels after image enhancement and after vertical and horizontal pixel averaging.

[Fig. 35]

Active region cross section after histogram equalization and after the various types of image blurring.

IV.c.1.iii.1.b **Horizontal Pixel Averaging**

Horizontal image blurring was achieved by performing horizontal pixel averaging to each of the 451 horizontal rows of pixels that were contained within the active region of [Fig. 34]. The technique used to average the 55 pixels that comprised a single horizontal row of pixels was very similar to that used for vertical pixel averaging.

The number of pixels that was averaged at any one time (during vertical pixel averaging this number was fixed at 17) was taken to be half the width of the left wire as it was seen in the active region (prior to image enhancement). The wire width was estimated as follows: a single cursor (shaped like a cross hair) was superimposed on the digitized image first at the left and then at the right edge of the left wire and the corresponding horizontal pixel coordinates were recorded (the vertical pixel coordinate was kept fixed). The difference between the cursor's horizontal pixel coordinates at the two edges was then taken to be the wire width. In this example the width was determined to be 10 pixels. Cursor coordinate selection was adjusted interactively via the program FSPOTCAL. The left wire's width was also used when performing horizontal pixel averaging on the right wire.

[Fig. 35b] was obtained from [Fig. 35a] by averaging the pixel values 5 pixels at a time (half of the width of the wire as determined from the above method). Averaging was

performed by the following technique. The pixel values of the first 5 pixels (pixel numbering increased from left to right with the first pixel considered to be located at position 1) were averaged and the value of the pixel at position 3 was replaced by the average pixel value of all 5 pixels. The next 5 pixels (ranging from positions 2 to 6) were then averaged and the value of the pixel at position 4 was replaced with the newly calculated pixel value average. This averaging was consecutively applied to the remaining pixels.

The pixel value distribution in [Fig. 33b] had the maximum of the broad peak determined from [Fig. 35b] by scanning the distribution from left to right and locating the pixel with the highest pixel value. In [Fig. 35b] this corresponded to the pixel which had a horizontal pixel coordinate of 111 (henceforth this pixel will be referred to as pixel P).

IV.c.1.iii.2 Full Width Half Maximum of Pixel Value Distribution

Because horizontal pixel averaging can introduce additional blurring of the wire image width (typically about 2 pixels) thus introducing additional error to the wire width estimate, the width of the wire as determined from a single horizontal row of pixels was estimated from [Fig. 35a] and not [Fig. 35b]. [Fig. 35a] was also chosen over

[Fig. 33b] because it had a smooth pixel value distribution (which could be easily manipulated by the computer algorithm).

The steps that were followed by the program FSPOTCAL to extract the FWHM value of the broad peak in [Fig. 35a] can best be explained from the consideration of [Fig. 36]. Before the full width at half maximum could be determined from the pixel value distribution, the base line of the distribution had to be estimated. This was done by scanning to the left and right of pixel P and then determining the first two pixel locations where the pixel values are at a minimum (these two pixels locations have been labelled in [Fig. 36] as P_1 and P_2). The distribution's base line was then taken to be the straight line [Fig. 36] that passed through these two pixel locations. The base line was determined by fitting a linear equation to the coordinates of pixels P_1 and P_2. The pixel value of pixel P at half maximum was then calculated from

$$\text{Pixel value at half maximum} = \frac{P_{max} - P_{base}}{2} + P_{base} \qquad (29)$$

where P_{max} was the pixel value of pixel P and P_{base} is the pixel value of pixel P at the base line. P_{base} was extrapolated from the fitted base line equation. The full width of the distribution at half maximum was calculated from

$$\text{Full width at half maximum} = P_{edge,2} - P_{edge,1} + 1 \qquad (30)$$

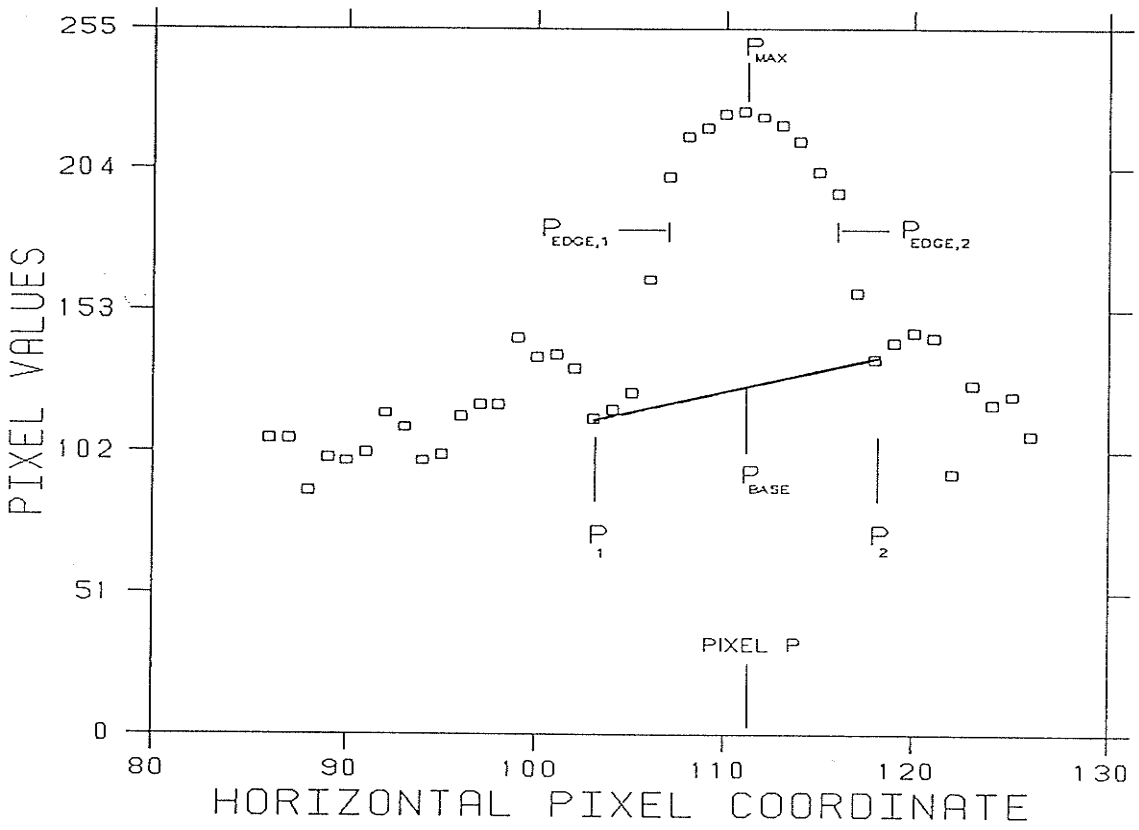

[Fig. 36]

Manipulation of [Fig. 35a] to extract the full width at half maximum of the pixel value distribution.

where the two terms in the above equation are the horizontal pixel coordinates of the pixels that correspond to the two edges of the wire image as determined from the FWHM method. The pixel whose location was at $P_{edge,1}$ (which corresponded to the left edge of the wire image) was determined by scanning to the left of pixel P and then finding the pixel whose adjacent pixel (pixel located further to the left) had a pixel value that was less than the distribution's pixel value at half maximum [Eq. 29]. The horizontal pixel coordinate corresponding to the right edge of the wire image ($P_{edge,2}$) was determined in a similar fashion by scanning to the right of pixel P. The width of the wire image in [Fig. 36] as determined from the FWHM method was 10 pixels.

The effectiveness of program FSPOTCAL to determine the two edges of the wire image and thus in turn the wire width [Eq. 30], for each of the 451 horizontal rows of pixels, is illustrated in [Fig. 37]. The value of the pixels at locations $P_{edge,1}$ and $P_{edge,2}$ were changed to 255 (giving the pixel a white appearance) to bring out the two edges in the left wire image. [Fig. 37] is identical to [Fig. 31] with the only exception being the left wire edge enhancement.

IV.c.1.iv **Wire Width Averaging**

Because the wire width for a single wire image was determined for each of the 451 horizontal rows of pixels that were contained within its active region, the wire width

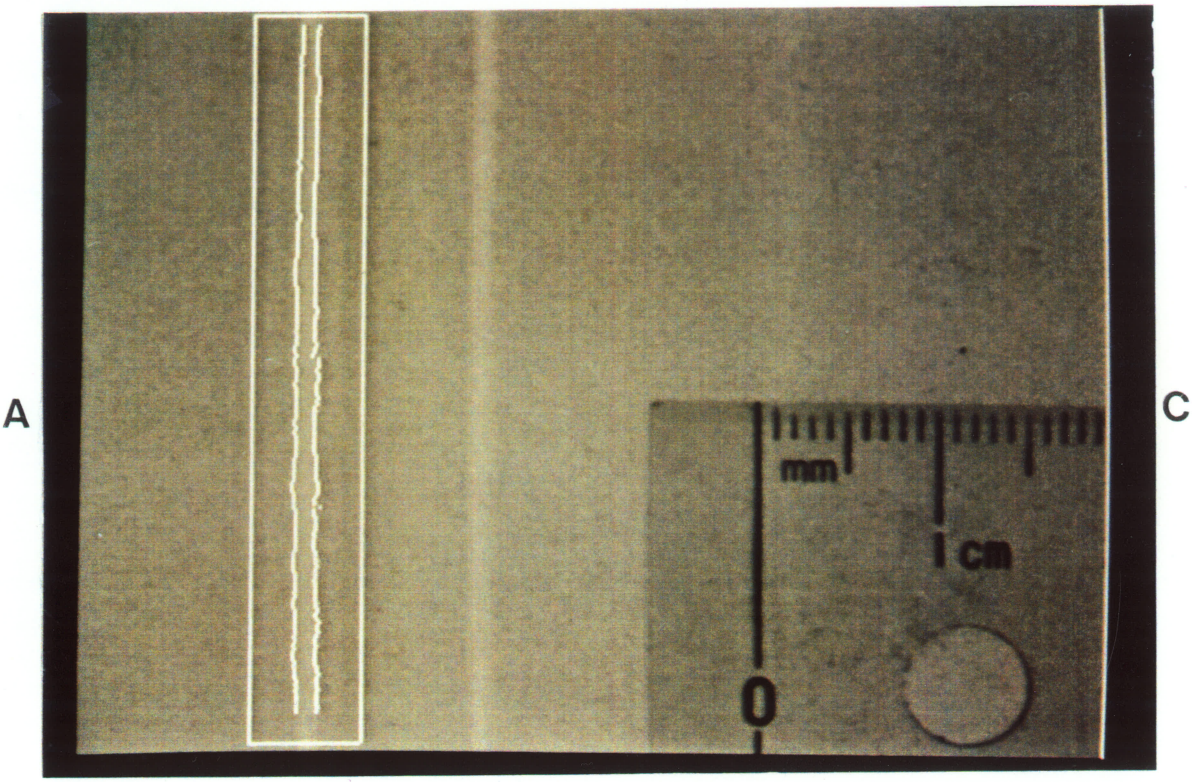

[Fig. 37]

Image edge enhancement illustration of [Fig. 31].

average for the left wire was calculated from

$$w_{image,left} = \frac{\sum_{i=1}^{451} w_i}{451} \qquad (31)$$

where w_i corresponded to the wire width [Eq. 30] as calculated from the i^{th} horizontal row of pixels within the left wires active region. The associated statistical variation in the above average wire width estimate was calculated from

$$\delta w_{image,left} = \left[\frac{\sum_{i=1}^{451} (w_i - w_{image,left})^2}{450} \right]^{1/2} . \qquad (32)$$

To further improve statistics, the overall width of the two wire images in the digitized image was then taken to be the weighted mean of the average wire width of both wires, that is:

$$w_{image} = \frac{\dfrac{w_{image,left}}{(\delta w_{image,left})^2} + \dfrac{w_{image,right}}{(\delta w_{image,right})^2}}{\dfrac{1}{(\delta w_{image,left})^2} + \dfrac{1}{(\delta w_{image,right})^2}} . \qquad (33)$$

The statistical uncertainty of δw_{image} was then calculated from the following equation

$$\delta w_{image} = \left[\frac{1}{\dfrac{1}{(\delta w_{image,left})^2} + \dfrac{1}{(\delta w_{image,right})^2}} \right]^{1/2} . \qquad (34)$$

IV.c.1.v Wire Width Correction for Wire Misalignment

Prior to the digitization of the test tool's film image the film was adjusted so that the wires were vertical on the monitor's screen. But because the wires could not be precisely aligned to the monitor's vertical pixel coordinate axis, the calculated width of the wire [Eq. 33] had to be corrected for this misalignment. The net effect of the wire's misalignment was to broaden the wire's width (see [Fig. 38] for illustration).

The two dark lines in [Fig. 38] represent the wire edges and illustrate a wire which is parallel to the monitor's vertical pixel coordinate axis. The two dashed lines in turn indicate the same wire when rotated by some misalignment angle, θ_{mis}. It is seen then in [Fig. 38], that when the analysis program FSPOTCAL first determined the wire width from a single horizontal row of pixels, the calculated wire width corresponded to the illustrated distance, a. In actual fact, it should have been distance, b. Because distance, b, is a projection of distance, a, the misalignment correction to the calculated wire width was taken to be

$$w_{image,corr} = w_{image} \cdot \cos(\theta_{mis}) \quad . \qquad (35)$$

Because the term w_{image} in [Eq. 35] was determined from both test tool wire images, the cosine of the misalignment angle was calculated from

$$\cos(\theta_{mis}) = \frac{\cos(\theta_{mis,l}) + \cos(\theta_{mis,r})}{2} \qquad (36)$$

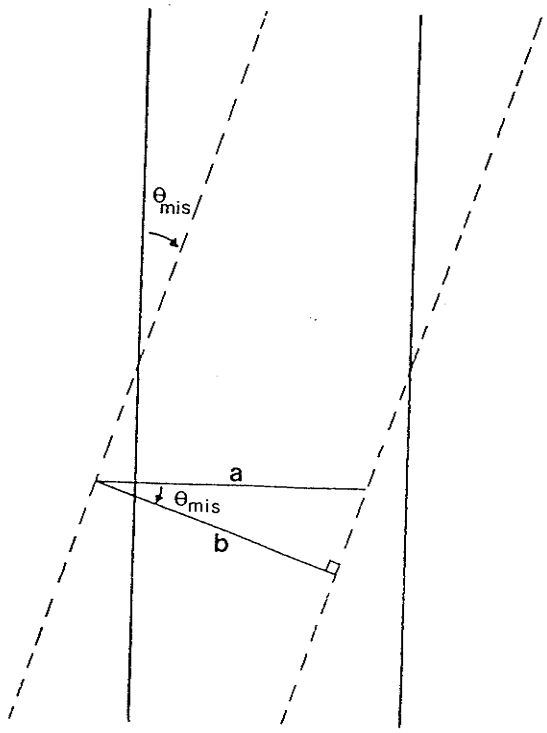

where :

$a = w_{image}$

[Fig. 38]

Illustration of wire misalignment.

where $\theta_{mis,l}$ and $\theta_{mis,r}$ are the individual misalignment angles of the left and right wires. The uncertainty in $\cos(\theta_{mis})$ was then calculated from

$$\delta\cos(\theta_{mis}) = \left[\left[\delta\cos(\theta_{mis,l}) \cdot \frac{d\cos(\theta_{mis})}{d\cos(\theta_{mis,l})}\right]^2 + \left[\delta\cos(\theta_{mis,r}) \cdot \frac{d\cos(\theta_{mis})}{d\cos(\theta_{mis,r})}\right]^2\right]^{1/2}$$

$$= \frac{\sin(\theta_{mis})}{2}\left[(\delta\theta_{mis,l})^2 + (\delta\theta_{mis,r})^2\right]^{1/2} \qquad (37)$$

where $\delta\theta_{mis,l}$ and $\delta\theta_{mis,r}$ are the uncertainties in the individual misalignment angles.

The misalignment angle for a given wire image was determined by the following: once the two edges of the wire for a given horizontal row of pixels was calculated, the center of the wire was determined and the coordinates of the pixel at the wire center were recorded. This procedure was then repeated for all of the 451 horizontal rows of pixels within the active region. The wire's central axis was then represented by a straight line after performing a least squares fit. The misalignment angle for say the left test tool wire image was then determined from

$$\theta_{mis,l} = \tan^{-1}(m_l) \qquad (38)$$

where m_l is the slope of the fitted line. The uncertainty in $\theta_{mis,l}$ was then determined from

$$\delta\theta_{mis,l} = \delta m_l \cdot \frac{d\theta_{mis,l}}{dm_l}$$

$$= \frac{\delta m_1}{1 + m_1^2} \quad . \qquad (39)$$

The method that was used to calculate the fitted equation's slope and associated uncertainty, δm_1, has been summarized in [Ref. 52]. It should be noted though, that during this calculation the vertical pixel coordinates (i.e. the y-coordinates) were multiplied by 0.8, to take into account the fact that the vertical dimensions of a given pixel were $4/5^{th}$ of its horizontal dimensions.

IV.c.1.vi Wire Width Conversion to SI Units

The average width of the wires, $w_{image,corr}$, as it was determined from the digitized test tool image, was in the units of pixels. In order to incorporate this width in the calculation of the focal spot, (see section IV.c.1.viii), the screen's horizontal pixel coordinate and in turn the wire's width had to be converted to SI units.

The procedure that was used to determine the conversion factor will be indicated below. When the program FSPOTCAL was used to digitize a test tool film image, the program first cleared the monitor's screen and then displayed a blank screen with a superimposed cross hair. A thin piece of clear plastic with a cross hair marked on it was then taped on the screen so that both cross hairs were aligned. This was done to have a physical representation of the screen's horizontal and vertical axis when the test tool film image was viewed on

the monitor screen prior to digitization. The film that contained the various test tool images was then placed on top of the light box and the test tool film image to be analyzed was isolated. Once the test tool film image was positioned so that the two wires were parallel to the monitor's vertical pixel axis, a clear plastic ruler was placed on top of the film. The ruler was then aligned with the screen's horizontal pixel coordinate axis by ensuring that the top edge of the ruler was parallel and aligned with the horizontal line of the cross hair that was taped onto the monitor's screen. The test tool's film image was then digitized. The conversion factor was then determined from the digitized film image as follows: a single cursor (shaped like a cross hair) was superimposed on the displayed digitized test tool image at two different positions near the top edge of the ruler [Fig. 39], and at each location the cursor's horizontal pixel coordinates were recorded. The horizontal distance between these two cursor positions was then determined both in millimeters and in pixels. The conversion factor, C, was then determined from

$$C = \frac{d_{mm}}{d_{pixel}} \qquad (40)$$

where d_{mm} and d_{pixel} are the separation distance between the two cursor positions in millimeters and in pixels. Cursor coordinate selection was adjusted interactively via the program FSPOTCAL. The uncertainty in the conversion factor

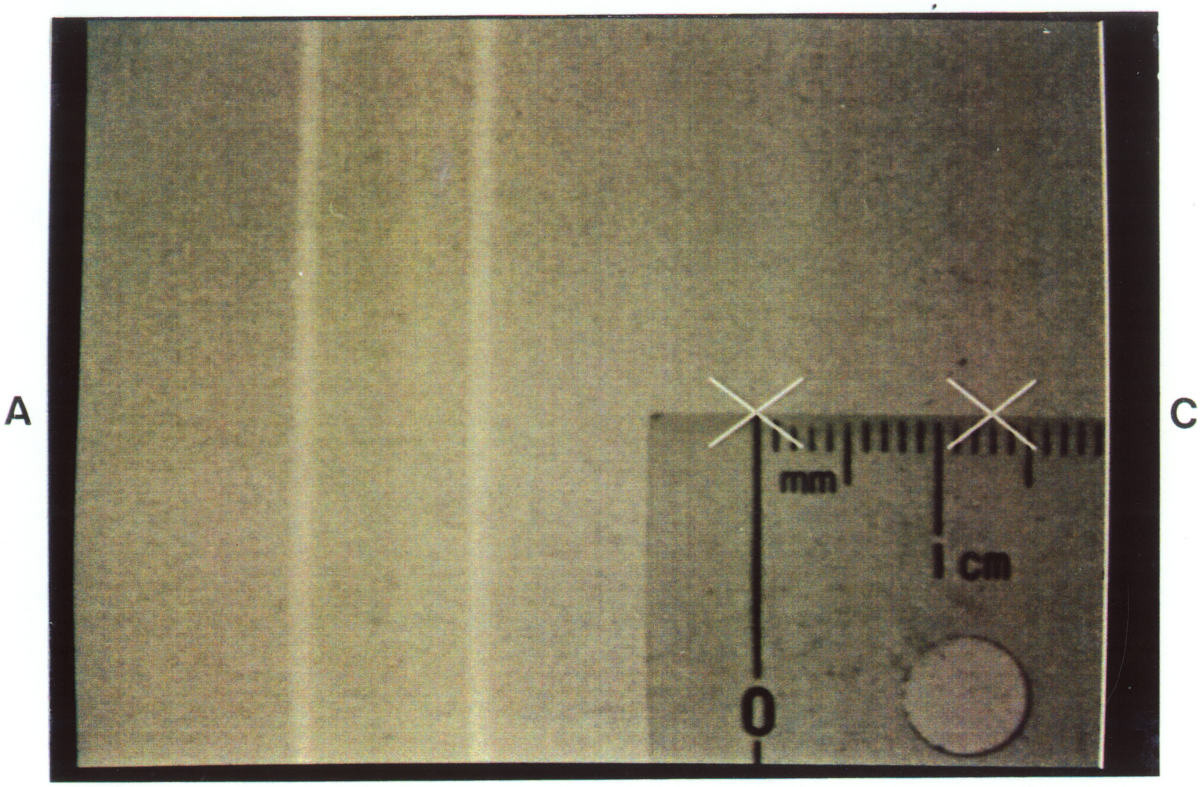

[Fig. 39]

Illustration of method that was used to calculate the conversion factor.

was calculated from

$$\delta C = \left[\left(\delta d_{mm} \cdot \frac{dd_{mm}}{dC} \right)^2 + \left(\delta d_{pixel} \cdot \frac{dd_{pixel}}{dC} \right)^2 \right]^{1/2}$$

$$= C \cdot \frac{\delta d_{pixel}}{d_{pixel}} \quad . \qquad (41)$$

Because the term d_{mm} in [Eq. 40] was a physical distance taken from a calibrated ruler, the uncertainty in this parameter was assumed to be negligible. The uncertainty in the distance d_{pixel} was calculated from the following equation

$$\delta d_{pixel} = \left[\left(\delta P_1 \cdot \frac{dP_1}{dd_{pixel}} \right)^2 + \left(\delta P_2 \cdot \frac{dP_2}{dd_{pixel}} \right)^2 \right]^{1/2}$$

$$= \left[(\delta P_1)^2 + (\delta P_2)^2 \right]^{1/2} \qquad (42)$$

where P_1 and P_2 are the horizontal pixel coordinates at the two cursor locations. The uncertainty at each of these two cursor locations was taken to be ± 1 pixel.

The average wire width on film as determined from digital imaging was then calculated from

$$w_{film} = C \cdot w_{image,corr}$$

$$= C \cdot w_{image} \cdot \cos(\theta_{mis}) \quad . \qquad (43)$$

As a consistency check, w_{film} (which for this example was 1.12 ± 0.07 mm, see [Table 20] for more details) was compared to the actual average width of the wires on film (which was 1.15 mm as determined from a magnifying glass having a built-in scale of 0.1 mm divisions and 7X magnification) and for all of the analyzed digitized film images, agreement was found within the error bars. The

conversion factor, C, as determined from [Fig. 41] was 0.11 mm/pixel (that is d_{mm} = 13 mm and d_{pixel} = 117 pixels).

IV.c.1.vii Geometric Magnification Calculation

In order to calculate the focal spot from w_{film}, the test tool's geometric magnification, M, had to be determined. This was done using an equation similar to that of [Eq. 13] in [section IV.a.1]. Recalling, that

$$M = 1 + \frac{d'}{d} \qquad (44)$$

where d' is the image distance (distance between the test tool and the film) and d is the object distance (distance between the focal spot and the test tool). The uncertainty in the test tool's geometric magnification was determined from

$$\delta M = \left[\left(\delta d' \cdot \frac{dd'}{dM}\right)^2 + \left(\delta d \cdot \frac{dd}{dM}\right)^2\right]^{1/2}$$

$$= \left[\left(\frac{d' \cdot \delta d}{d^2}\right)^2 + \left(\frac{\delta d'}{d}\right)^2\right]^{1/2} . \qquad (45)$$

The uncertainty in each measurement, δd and $\delta d'$, was estimated to be ± 3.2 mm (or ± 1/8").

IV.c.1.viii Focal Spot Determination

The focal spot size that produced the parallel wire test tool image on film was determined from the digitized test tool image by the following equation

$$f = \frac{w_{film} - w_{wire} \cdot M}{M - 1} \qquad (46)$$

where w_{film} is the wire width on film as determined from the digitized test tool image (in mm), w_{wire} is the physical wire diameter (in mm) and M was the test tool's geometric magnification. The wire diameter was verified by using a 7X magnifier containing a reticle scale of 0.01 mm divisions and was found to be 0.05 mm. The above equation has been derived in [Appendix F].

IV.c.2 Uncertainties in Focal Spot Determination

In the calculation of the focal spot, f, various factors were present that contributed to the overall uncertainty. This section, which considers the following equation

$$f = \frac{w_{image} \cdot C \cdot \cos(\Theta_{mis}) - w_{wire} \cdot M}{M - 1} \qquad (47)$$

to derive the various errors, will present both the statistical and systematic error contributions.

IV.c.2.i Statistical Error

The only statistical error contribution to the focal spot measurement arose from the manner in which the average wire width w_{image} was determined from the digitized image (see section IV.c.1.iv for details). The focal spot uncertainty due to this error was calculated from

$$(\delta f)_{sta} = \delta w_{image} \cdot \frac{dw_{image}}{df}$$

$$= \frac{w_{film}}{M - 1} \cdot \frac{\delta w_{image}}{w_{image}} \quad . \qquad (48)$$

The statistical uncertainty in the wire width, δw_{image}, was given by [Eq. 34].

IV.c.2.ii Systematic Errors

IV.c.2.ii.1 Physical Wire Width

Because the physical diameter of the test tool wires, w_{wire}, entered into the focal spot calculation [Eq. 47], the uncertainty in this known wire width also contributed to the overall focal spot uncertainty. The magnitude of the focal spot uncertainty as a result of this systematic error was determined from

$$\delta f_1 = \delta w_{wire} \cdot \frac{dw_{wire}}{df}$$

$$= \frac{M}{M - 1} \cdot \delta w_{wire} \quad . \qquad (49)$$

The uncertainty in the physical wire width, δw_{wire}, was estimated to be ± 0.005 mm.

IV.c.2.ii.2 Wire Width Conversion Factor

Before the focal spot dimensions could be determined, the calculated average wire width, w_{image}, which was in the digital imaging systems units (pixels), had to be converted to a

width in SI units. Because the conversion factor, C, had an uncertainty associated with it, this too contributed as a systematic error to the overall focal spot uncertainty. The contribution of this error to the overall focal spot uncertainty was calculated from

$$\delta f_2 = \delta C \cdot \frac{dC}{df}$$

$$= \frac{w_{film}}{M - 1} \cdot \frac{\delta C}{C} \qquad (50)$$

where δC has been given by [Eq. 41].

IV.c.2.ii.3 **Wire Misalignment Correction**

Because the digitized test tool wire images might not have been parallel to the monitor's vertical pixel coordinates axis, the calculated wire width w_{image} was corrected for the effect of this misalignment. Since this correction also had an associated uncertainty, this error also acted as a systematic error to the overall focal spot uncertainty. The magnitude of the overall focal spot uncertainty that was attributed to this effect was calculated from

$$\delta f_3 = \delta\cos(\theta_{mis}) \cdot \frac{d\cos(\theta_{mis})}{df}$$

$$= \frac{w_{film}}{M - 1} \cdot \frac{\delta\cos(\theta_{mis})}{\cos(\theta_{mis})} \quad . \qquad (51)$$

The uncertainty in this correction factor, $\delta\cos(\theta_{mis})$, was calculated from [Eq. 37].

IV.c.2.ii.4 Test Tool Geometric Magnification

Because the test tool's geometric magnification M also entered into the calculation of the focal spot [Eq. 47], the uncertainty in the magnification M also contributed a systematic error. The contribution of this error to the overall focal spot uncertainty was calculated from

$$\delta f_4 = \delta M \cdot \frac{dM}{df}$$

$$= \frac{w_{wire} - w_{film}}{(M-1)^2} \cdot \delta M \qquad (52)$$

where the uncertainty in the geometric magnification, δM, was calculated from [Eq. 45].

IV.c.2.ii.5 Wire Image Blurring

When the average wire width, w_{image} was determined from the digitized test tool film image, it was extracted from an image whose active region had previously undergone histogram equalization and vertical pixel averaging. Because of this image manipulation, the wire images had been blurred to some degree. Even though the net blurring effect at each edge of a given wire image was typically an increase of about 2 pixels, this effect did not have a large contribution in the focal spot measurement. This can be seen in [Fig. 40] from the close agreement between the enhanced edges of the two wire images and their actual edges. This blurring effect, which was not incorporated as a systematic error, was

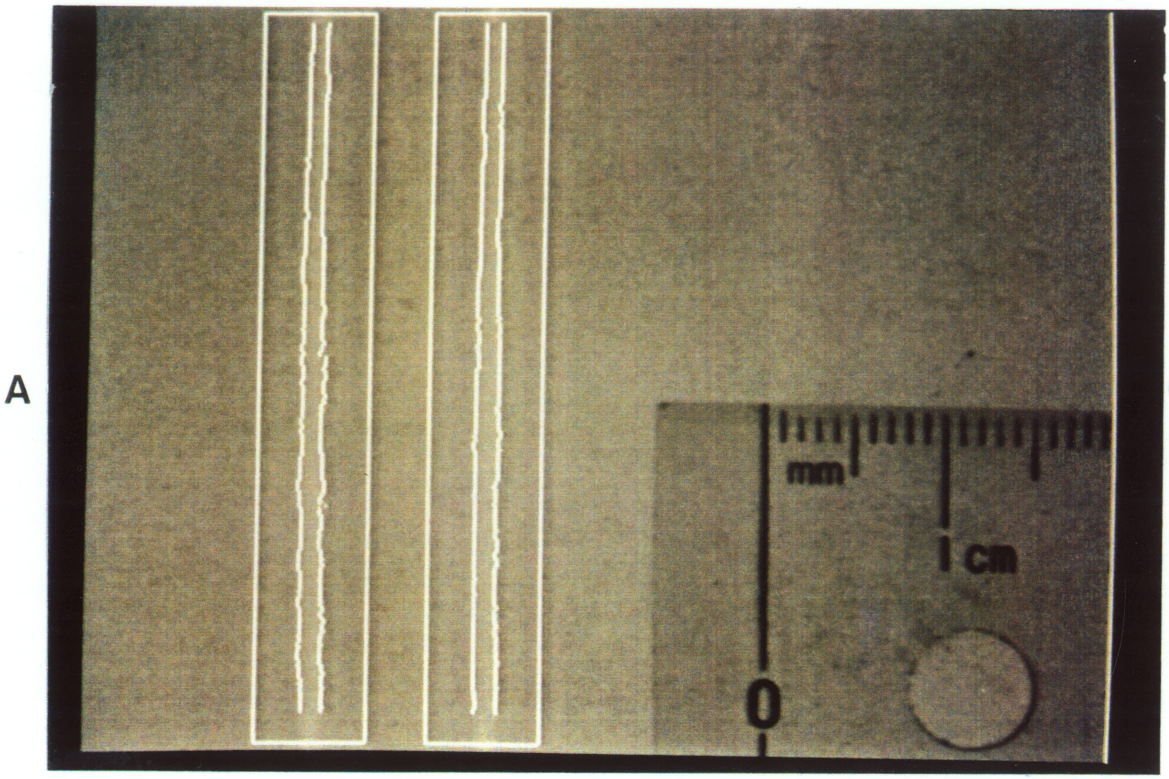

[Fig. 40]

Wire edge enhancement of both wire images.

experimentally found to be compensated for by defining the wire width, $w_{image,}$ as the FWHM of the pixel value distribution and not as the full width (see section IV.c.1.iii).

IV.c.2.ii.6 Test Tool Misalignment

When the test tool was set up prior to its exposure, it may have been set so that the plane containing the two wires was not perpendicular to the x-ray beam's central axis. This effect would have caused each wire to have a different test tool geometric magnification. Because this physical effect could not have changed the wire's object and image distance by more than 1 mm, the term δM in [Eq. 52] as calculated from [Eq. 45] would have been small (it should be pointed out that during test runs with a FFD of 101.6 cm (40") the wires object and image distances were both approximately 50.8 cm (20")), and thus the systematic error contribution to the overall uncertainty in the focal spot would have been negligible.

IV.c.2.ii.7 Pixel Width

Because the edges of a given wire are represented by a single pixel [Fig. 40], there will be an uncertainty of $\pm$ 0.5 pixels associated with each edge point, due to the width of a given pixel. Since the width of the wire on the digitized test tool film image is determined from two edge points (for a given horizontal row of pixels) then the uncertainty in the

wire's width due to this effect would be ± 0.7 pixels (calculated by adding in quadrature the uncertainty of ± 0.5 pixels twice). Because the statistical uncertainty in the average wire width estimate (which was typically between ± 0.8 and ± 1.0 pixels) inherently contains the above ± 0.7 pixel uncertainty, this effect was not included as an independent systematic error contribution.

IV.c.2.ii.8 Overall Systematic Error Contribution

The overall systematic error contribution to the focal spot uncertainty was calculated by adding in quadrature the first four systematic errors, that is

$$(\delta f)_{sys} = \left[\sum_{i=1}^{4} (\delta f_i)^2 \right]^{1/2} . \qquad (53)$$

IV.c.2.iii Overall Focal Spot Error

The overall error in the focal spot measurement was taken to be

$$\delta f = \left[(\delta f)_{sta}^2 + (\delta f)_{sys}^2 \right]^{1/2} . \qquad (54)$$

CHAPTER V

RESULTS AND DISCUSSION

V.a Data Representation

All of the focal spot data that was collected during test runs 1 through 7 is summarized in [Appendix G], [Appendix H] and [Appendix I] respectively. The data in these appendices is represented in the form of comparison plots to illustrate similarities in the focal spot data between the conventional focal spot measuring techniques and that of the digital imaging system. The ordinate of these comparison plots was taken to be the focal spot size and the abscissa the x-ray tube kVp settings (which was chosen to illustrate any kVp dependence in the focal spot data).

On a further note, all of the data in the above three appendices are the weighted mean results of two independent analyses that were performed two weeks apart. The digital imaging system's focal spot data in [Appendix G] and [Appendix I] are the results from test tool film images that utilized Kodak TMG double emulsion film and were taken at a FFD of 101.6 cm (40"). Because all of the focal spot data in [Appendix H] were taken at two different FFD settings, the FFD settings have been identified on each plot for greater clarity. In addition to the above, all of the focal spot data in [Appendix H] (with exception to test run 1) were obtained using Kodak TMG double emulsion film.

To comment on the various information that is contained within a given comparison plot, consider [Fig. 41] which is identical to a plot illustrated in [Appendix G]. As shown in [Fig. 41], the focal spot data representing the length of the focal spot were deliberately plotted at a kVp value that is 2 kVp lower then what was actually used. This was introduced for two reasons: 1) to simplify data comparison by reducing error bar cluttering; and 2) to separate the two focal spot dimensions. It is also seen in [Fig. 41] that two horizontal lines (one for each focal spot dimension) have been superimposed in each plot to signify the nominal focal spot's maximum NEMA tolerance values. These NEMA focal spot limits [Ref. 6] which have been tabulated in [Table 18] signify the maximum focal spot dimensions that are allowed by NEMA for a given nominal focal spot.

V.b Bar Resolution Pattern Comparison Results

All of the bar pattern focal spot results are summarized in [Appendix G]. It is seen from these 7 test runs that on the average the digital imaging system's focal spot data does appear to be in agreement with the bar pattern's focal spot data (two data points are said to be in agreement when their associated error bars overlap, that is both data points are within error of each other). It is also evident from this collected bar pattern data that on the average the size of the focal spot is independent of the tube's kVp setting. The

[Table 18]

NEMA Nominal Focal Spot Maximum Tolerance Values

Focal Spot Dimensions (mm)		
Nominal Focal Spot Size	NEMA Tolerance Value	
	Width	Length
0.10	0.15	0.15
0.15	0.23	0.23
0.20	0.30	0.30
0.25	0.40	0.40
0.30	0.45	0.45
0.40	0.60	0.85
0.50	0.75	1.10
0.60	0.90	1.30
0.80	1.20	1.60
1.00	1.40	2.00
1.20	1.70	2.40
1.40	1.90	2.80

following reasoning can be used to justify this finding: as seen in [Eq. 17] the focal spot dimensions as determined from the bar pattern test tool film image depend upon the line pair frequency of the bar group that has the three bars just resolvable. But, since the bar pattern test tool has only 11 bar groups (or line pair frequencies), for a given focal spot dimension the bar pattern can provide only one of 11 possible values. This implies that if the change in the focal spot size with tube kVp is less than the following difference:

$$\delta f = f_2 - f_1 \qquad (55)$$

where f_1 and f_2 are the focal spot values as determined from the bar group number that has the three bars just resolved and from the next lower bar group number, then the bar resolution pattern method will be insensitive to such a focal spot change.

Another observation that may be made from the data in [Appendix G] is that for most cases, the digital imaging system's focal spot measurements are consistently slightly greater than those of the bar pattern method. This observation can be justified as follows: when the focal spot dimensions are determined from a bar pattern test tool film image, the line pair frequency that was used in [Eq. 17] was that of the bar group that had the three bars just resolvable and not the three bars clearly visible. What this meant was that if the true focal spot value had a line pair frequency that was, for example in between that of bar group 7 and 8,

then from this method of bar detection it is the line pair frequency of bar group 8 that was used in the determination of the focal spot. The end result of this would be to provide a focal spot value that was slightly smaller then the true value.

Focal spot size comparison of the digital imaging system technique results, to the bar resolution pattern method results was made for the sake of completeness. Even though the subjectiveness of the bar resolution detection method and the limiting line pair frequency property of the bar pattern inhibited the bar pattern method from becoming a manufacturer's standard technique in the determination of focal spots.

The bar pattern method produced focal spot results that had on the average an overall error of ± 11%. The digital imaging system on the other hand produced results that had on the average an overall error of ± 6% [Table 19]. It should be noted that the overall error data presented in [Table 19] are the average results of test runs 1 through 7.

V.c Star Resolution Pattern Comparison Results

All of the star pattern focal spot results have been summarized in [Appendix H]. After close inspection of these comparison plots it is evident that on the average the digital imaging system's focal spot data does appear to be in good agreement with the star pattern's focal spot data at

[Table 19]

Digital Imaging System's Focal Spot Overall Error Summary

FFD Setting	Focal Spot Size	Focal Spot Dimensions	Average Overall Error (Tube kVp) 70	80	90
40"	Small	Width	± 7.1%	± 7.8%	± 8.0%
		Length	± 5.0%	± 5.4%	± 6.2%
40"	Large	Width	± 5.8%	± 6.9%	± 7.3%
		Length	± 6.0%	± 5.9%	± 6.1%
72"	Large	Width	± 6.4%	± 7.3%	± 7.5%
		Length	± 5.2%	± 5.7%	± 5.7%
Focal Spot Overall Error: (obtained by averaging above values)				± 6.4%	

both 101.6 cm (40") and 182.9 cm (72") FFD settings.

Contrary to the bar pattern's focal spot data, the star pattern's data as well as the digital imaging system's data does indicate that there is a slight decrease in the focal spot dimensions with an increase in the tube's kVp setting. This finding can be justified from the following phenomena: when a current is passed through the filament, electrons will be boiled off the filament and these electrons will undergo an acceleration towards the anode. The trajectories of these emitted electrons will now undergo deflections as a result of the tube's magnetic field that exists between anode and cathode. Now, when the tube's kVp (potential difference) is increased the deflections of these emitted electrons will be reduced due to their increased acceleration. This has the net effect of decreasing the size of the spot on the anode upon which they impinge. It should also be mentioned that as the tube kVp is increased the space charge effect is also diminished similarly contributing to a decreased focal spot size.

It appears from the comparison plots of [Appendix H] that the star pattern's focal spot data are consistently slightly greater than the digital imaging system's focal spot data. This trend may be attributed to the difficulty in determining the zero contrast diameter in the star pattern image on film. The poorest agreement in these comparison plots involved the large focal spot data, which had the largest zero contrast

diameters and were most difficult to accurately determine.

Another reason why the star pattern's focal spot data are slightly greater then the digital imaging system's may be attributed to the fact that the star pattern method involves measurment of the focal spot's dimensions from the focal spot's resolving power where more scattering occurs whereas the digital imaging system technique determines the focal spot dimensions from the actual size of the spot in a situation of diminished scattering.

Of the three conventional focal spot measuring techniques that were compared to the digital imaging system technique, the star pattern focal spot data provides the closest comparison on the basis that almost identical technique parameter generator settings and experimental conditions were used to collect the data. It was also observed that this focal spot data is in best agreement with the digital method.

The star pattern method produced focal spot results that had on the average an overall error of ± 5%. It should be noted that within these overall error calculations errors that might arise due to the manufacturing of the star pattern test tool (such as the error in the angle and width of the lead spokes) were considered negligible. The quoted uncertainty in the star pattern focal spot data was somewhat underestimated, since the assigned uncertainty in the zero contrast region's diameter took into account the uncertainty in the measurement itself and not the uncertainty in the

detection of the region's boundaries (which will vary with the individual that is performing the measurement).

V.d Pinhole Camera Comparison Results

All of the comparison plots that involved the pinhole camera focal spot data have been summarized in [Appendix I]. It is seen from these comparison plots that on the average there is good agreement between the pinhole camera focal spot data and the digital imaging system focal spot data. As was the case for the star pattern focal spot data, the pinhole camera data generally indicate a slight reduction in the focal spot dimensions when the tube kVp settings are increased.

From the comparison plots of [Appendix I] it appears that the digital imaging system focal spot data are consistently slightly larger than the pinhole camera data. This observation can be justified from the following: if we consider a pinhole camera and a parallel wire test tool whose pinhole and wire diameter dimensions are both "w", then from purely geometric considerations the penumbra region of the wire on film will be greater than that of the penumbra region of the pinhole, for the case where both test tools are placed with their respective centers on the x-ray beam's central axis and at the same distance from the focal spot and film. Thus, even though both methods may measure the true dimensions of the focal spot in a similar fashion (see [Eq.

24] and [Eq. 46]), the digital imaging system will evaluate a somewhat larger focal spot value due to the enlarged penumbra region. It should be remembered that during the digital imaging system's analysis the dimensions of the focal spot are determined from the calculated wire width of the digitized test tool film image (which is dependent on the penumbra region of the wire on film).

Another observation that is made from the comparison plots in [Appendix I] is that the worst agreement occurs in the focal spot length data. This finding was not surprising since one of the difficulties that exists in the pinhole camera method is in the determination of the length of the pinhole image (see Chapter I).

From all three conventional focal spot measuring techniques that were compared to the digital imaging system technique, the pinhole camera focal spot data would have provided the most different comparison based on the x-ray tube mAs settings required being quite different (for instance during the small focal spot data collection of test run 3, the mAs setting for the x-ray tube when operating at 70 kVp was at 80 when using the digital imaging system's test tool at an FFD of 101.6 cm (40") and was at 750 when using the pinhole camera). It is nonetheless seen that the focal spot data are in good agreement.

The pinhole camera method produced focal spot results that had on the average an overall error of ± 9%.

V.e Digital Imaging System Results

Since it is known that film image blurring can increase by the use of double emulsion film (see parallax unsharpness in section IV.c.1.i), which can in turn introduce additional uncertainty in the focal spot measurement, parallel wire and star pattern test tool film images were also collected, during test run 1, using single emulsion film (see Appendix H for results). The parallel wire test tool results for both single and double emulsion films have been plotted in [Fig. 42] and indicate that the digital imaging system technique of determining the focal spot is independent of whether the film is single or double emulsion type. Because of this finding, the remaining 6 test runs were performed using double emulsion film only. The use of double emulsion film was preferred over single emulsion film for the reason that lower tube mAs values (see Tables 12 through 15) could be used thus attaining focal spot data that was close to clinical imaging settings.

To determine whether the digital imaging system technique of measuring the focal spot size had any dependence on the film optical density of the test tool film image, parallel wire test tool images were collected during test run 1 at different tube mAs values (and thus different resultant film optical densities). The results of this test (performed using Kodak TMG double emulsion film at a FFD of 101.6 cm (40")) which are illustrated in [Fig. 43], indicate that the

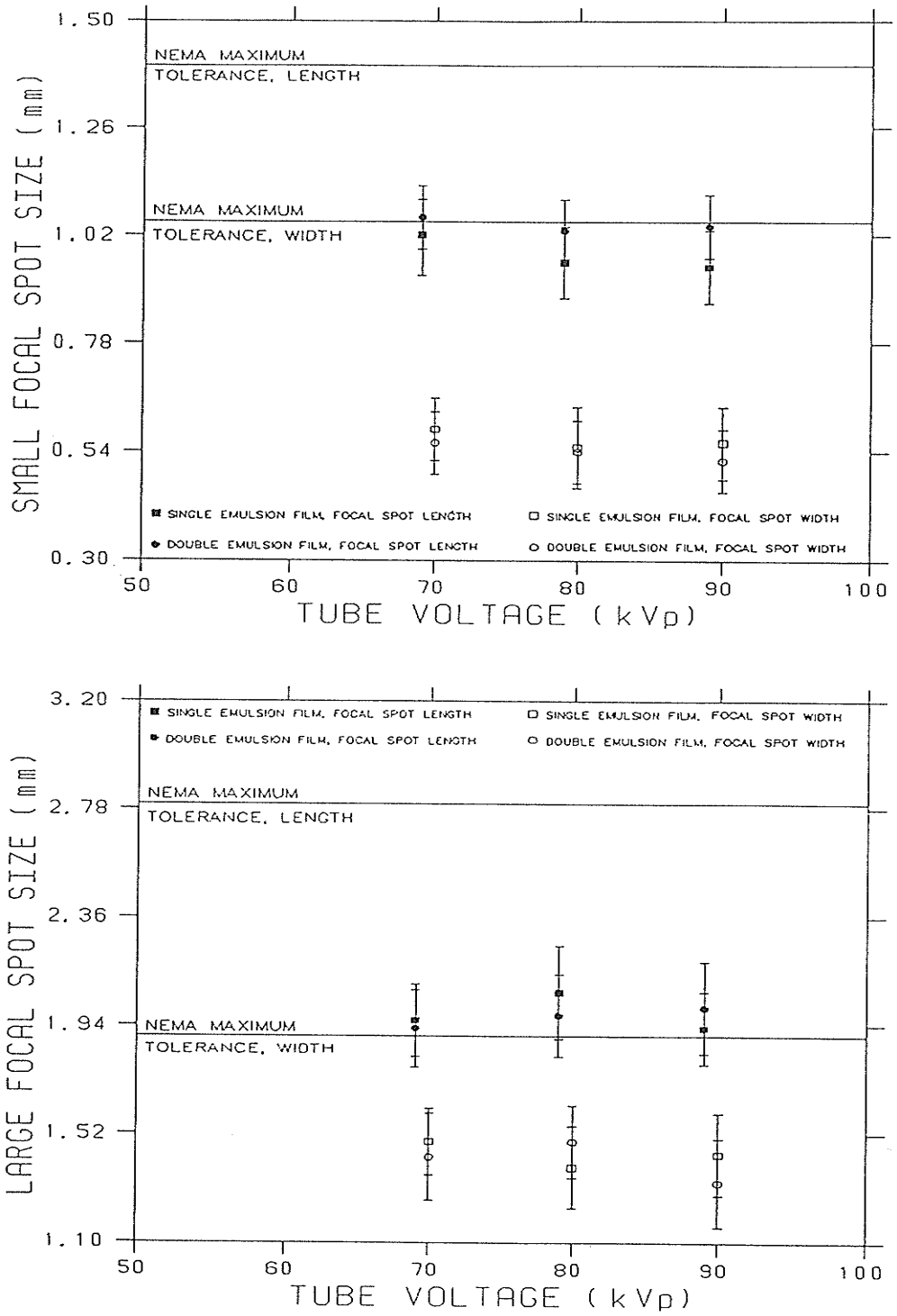

[Fig. 42]

Parallel wire test tool results of test run 1 while using single and double emulsion film at a 101.6 cm (40") FFD.

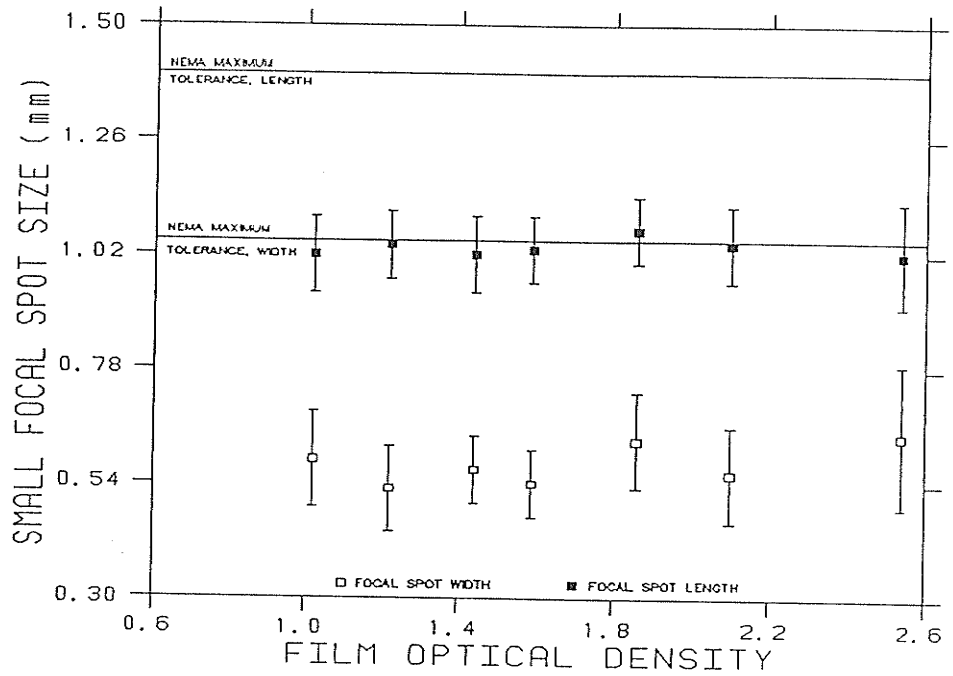

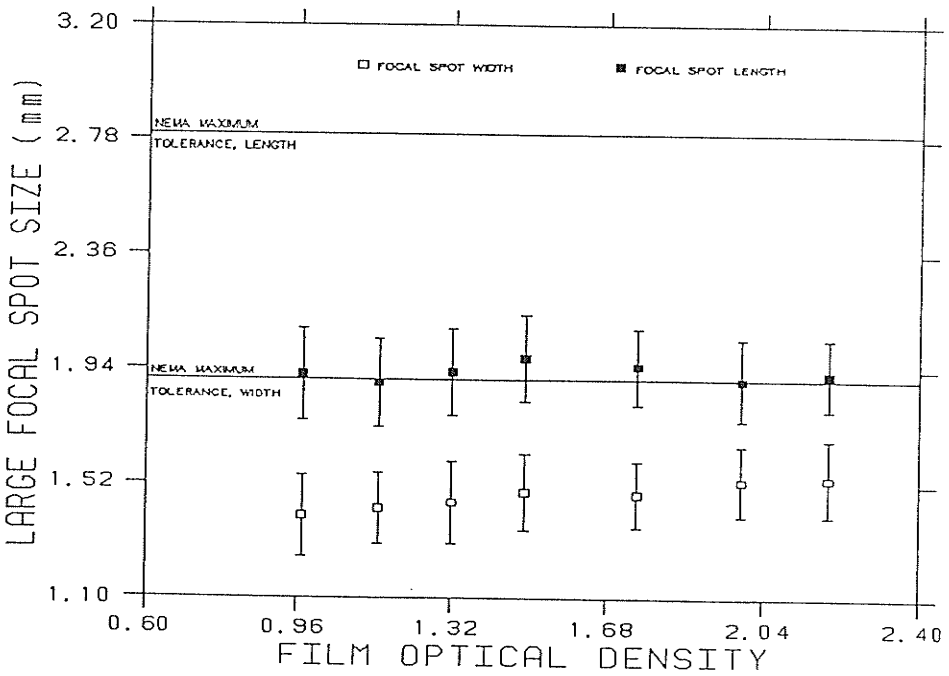

[Fig. 43]

Parallel wire test tool results of test run 1 when using different film optical densities.

digital imaging technique is independent of film optical density in the range between 1 and 2.5. This implies that this technique can be used on test tool film images that have film optical densities anywhere on the linear portion of the film's characteristic curve (see [Fig.16]).

The focal spot data in [Appendix H] was collected at 101.6 cm (40") and 182.9 cm (72") FFD settings, mainly to obtain data that was in accordance with standard diagnostic radiology focal spot-to-patient distances. To illustrate any comparisons between the focal spot data at 101.6 cm (40") and 182.9 cm (72") FFD setting, the digital imaging system's results are summarized in [Fig. 44] (which was the focal spot data from test run 1). After inspection of [Fig. 44], it becomes evident that the digital imaging system technique is capable of producing focal spot results that are consistent at both of these FFD settings. This finding not only illustrates the digital imaging technique's diversity in performing focal spot data at a wide range of FFD settings but it also confirms the effectiveness of the computer algorithm to extract the focal spot dimensions from the width of the wires in the digitized test tool film images. It should be noted that not only will the parallel wire test tool film images at a 182.9 cm (72") FFD setting have a much larger penumbra region (and thus more image blurring) than those film images at a 101.6 cm (40") FFD setting, but, the wire image itself in the digitized image (or film) will have

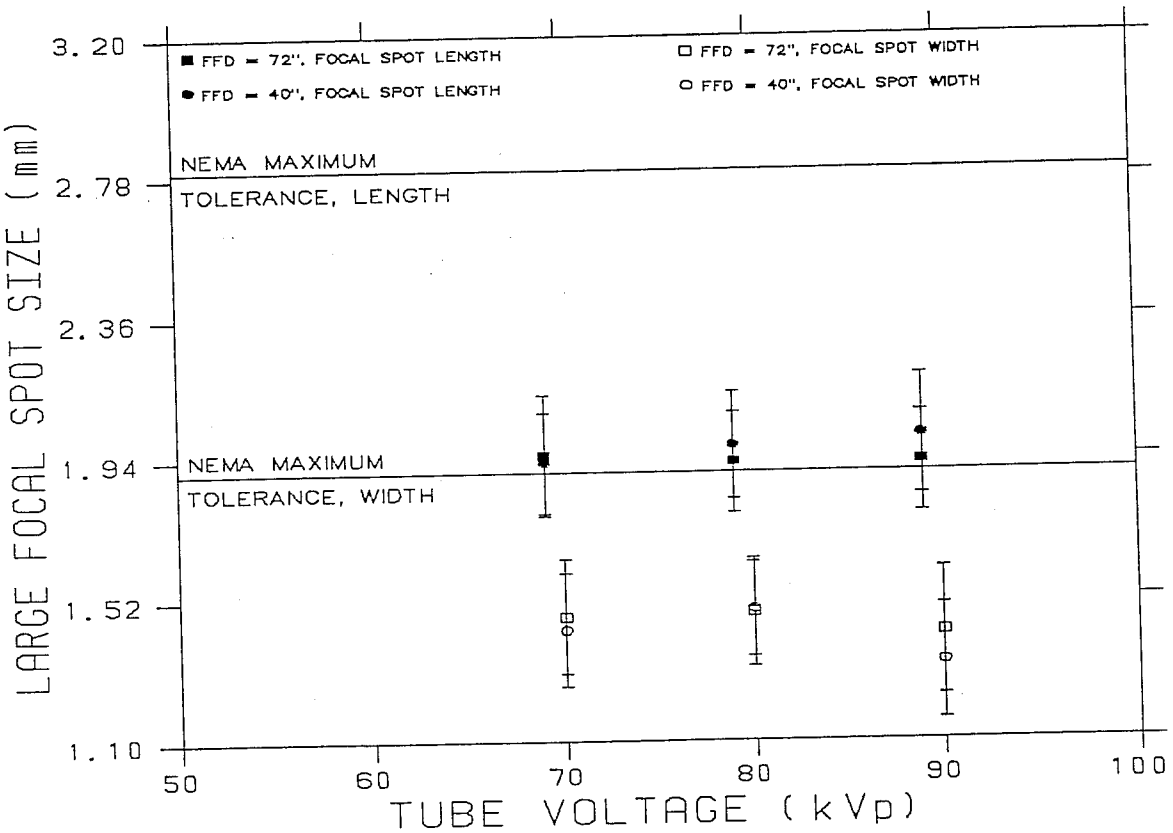

[Fig. 44]

Parallel wire test tool results of test run 1 when using different FFD settings with double emulsion film.

a reduced x-ray beam intensity at this distance thus making edge detection more difficult.

To illustrate a typical breakdown of the experimental data that was involved in a determination of the digital imaging system focal spot size, consider [Table 20] which tabulates the results for the test tool film image illustrated in [Fig. 29]. It is seen from this table of data that the correction of wire misalignment, which was typically about 2°, did not contribute very much change to the overall focal spot measurement. These effects would only have been significant if much larger misalignment angles had occurred. When the widths of the two wires in the digitized test tool film image are compared, the left wire's width appears to be narrower by 0.45 pixels. This difference in width arises from the fact that the left wire in [Fig. 29] was physically located nearer to the anode than was the right wire (recall that during this test the parallel wire test tool was placed perpendicular to the c-a axis so as to measure the small focal spot's length). After close inspection of the data in [Table 20] it is seen that the largest contribution to the absolute uncertainty in the focal spot measurement was due to the statistical variations in the width of the two wires in the digitized film image.

To reduce the statistical variations in the width of the wires thus reducing the overall uncertainty in the focal spot measurements, various attempts were made to optimize the

[Table 20]

Digital Imaging System Focal Spot Calculation Breakdown

Experimental Data	
Left wire misalignment angle:	1.561 ± 0.004 deg.
Right wire misalignment angle:	1.564 ± 0.003 deg.
Average wire misalignment angle:	1.563 ± 0.002 deg.
Cosine of average misalignment angle:	0.9996 ± 0.0001
Left wire width:	9.84 ± 0.93 pixels
Right wire width:	10.29 ± 0.77 pixels
Weighted mean of two wire widths:	10.10 ± 0.59 pixels
Pixel calibration factor:	0.111 ± 0.001 mm/pixel
Average wire width corrected for misalignment and converted to SI units	1.12 ± 0.07 mm
Test tool geometric magnification	2.000 ± 0.009

Error Analysis		
Parameter	Error in Parameter	Error in Focal Spot
Statistical error:		
Average wire width	± 0.066 mm	± 0.066 mm
Systematic errors:		
Calibration constant	± 0.001 mm/pixel	± 0.014 mm
Cos(misalign. angle)	± 0.0001	± 0.000 mm
Physical wire width	± 0.005 mm	± 0.010 mm
Test tool magn.	± 0.009	± 0.010 mm
Total systematic error		± 0.020 mm
Overall error:		± 0.069 mm

Focal spot size	1.02 ± 0.07 mm

digital imaging technique. The one parameter that was found to influence the overall uncertainty in the focal spot measurement was the width of the active region. This finding was not surprising since the results of the wire image enhancement after histogram equalization [Fig. 32] were very much dependent on the size of the background region within the active region. It is apparent that, the larger the background region within the active region the greater the influence this background will have on the smoothing routines. In order to obtain the active region width that gives the best overall results, a test was performed prior to test run 1 when using double emulsion film that was exposed at a FFD of 101.6 cm (40"), using a 70 kVp tube potential difference. The results of this test, which are summarized in [Table 21], indicated that an active region width of 55 pixels provided the best conditions.

Because the pixels that were located within the wire image had pixel values that were comparable to the values of the pixels that were located in the background region [Fig. 33a] of the active region, background subtraction methodolgy could not be successfully applied to the digitized test tool film images.

The reproducibility of the overall digital imaging system technique was determined by obtaining 7 test tool film images at identical tube mAs and kVp settings and then analyzing the digitized film images. The results of this test, which were

[Table 21]

Active Region Width Optimization

Active Region (pixels)	Focal Spot Percent Error			
	Small Focal spot		Large Focal Spot	
	Width	Length	Width	Length
30	± 9.8%	± 8.4%		
40	± 9.4%	± 6.8%	± 8.7%	± 7.5%
45	± 8.7%	± 6.7%	± 8.9%	± 7.4%
50	± 8.5%	± 6.5%	± 8.3%	± 7.3%
55	± 8.2%	± 6.5%	± 8.3%	± 7.2%
60	± 8.7%	± 6.6%	± 8.5%	± 7.5%
70	± 8.8%	± 7.1%	± 8.4%	± 7.6%

performed at 80 kVp and at a 101.6 cm (40") FFD setting, are summarized in [Table 22] and show that this method of focal spot measurement was reproducible to 2.9%. The consistency in a given focal spot measurement was also determined for the digital imaging technique by re-analyzing a single digitized test tool film image 7 times. The results of this test are presented in [Table 23] and indicate that a single measurement can typically be reproduced to 2.6%. The data in [Table 22] and in [Table 23] were obtained from the same Picker diagnostic x-ray tube. The overall reproducibility of the system could then be determined by adding in quadrature the above two effects, which is found to be about 4%.

All of the focal spot data that had been determined from test runs 1 through 7 were obtained from x-ray tubes that had nominal focal spot values between 0.6 mm and 1.4 mm. In order to check the limitations of the digital imaging technique to calculate focal spot sizes, tests were also performed on x-ray tubes that were dedicated to mammography which had nominal focal spot sizes between 0.1 mm and 0.3 mm. The results of these test runs have been summarized in [Table 24]. It was not possible to verify the results in this table with the conventional focal spot measuring techniques that were used before, for the following reasons:

(a) the smallest focal spot that could have been measured by the bar resolution pattern was 0.5 mm (which corresponded to a test tool bar separation of bar group 11). Because the largest spot of the mammography tubes

[Table 22]

Reproducibility of Digital Imaging Technique

Test	Focal Spot Measurements			
	Small Focal Spot		Large Focal Spot	
	Width (mm)	Length (mm)	Width (mm)	Length (mm)
1	0.54	1.03	1.49	1.98
2	0.57	1.01	1.51	1.93
3	0.59	1.00	1.40	2.12
4	0.58	1.00	1.48	1.98
5	0.57	1.06	1.43	1.99
6	0.56	1.03	1.48	1.98
7	0.55	1.05	1.42	2.11
Mean	0.57	1.03	1.46	2.01
S. Dev.	0.02	0.02	0.04	0.07
% Error	3.5	1.9	2.7	3.5
System Reproducibility: (calculated by averaging above row)				2.9%

[Table 23]

Consistency in Digital Imaging Technique

Test	Focal Spot Measurements			
	Small Focal Spot		Large Focal Spot	
	Width (mm)	Length (mm)	Width (mm)	Length (mm)
1	0.60	0.98	1.40	2.00
2	0.56	0.99	1.45	1.86
3	0.55	0.94	1.40	1.89
4	0.59	1.04	1.40	1.94
5	0.58	1.03	1.41	1.97
6	0.60	1.00	1.43	1.98
7	0.57	0.97	1.40	1.94
Mean	0.58	0.99	1.41	1.94
S. Dev.	0.02	0.03	0.02	0.05
% Error	3.4	3.0	1.4	2.6
Consistency in a single measurement: (calculated by averaging above row)				2.6%

[Table 24]

Focal Spot Results[7] of Test Runs 8, 9 and 10

Test Run Number	Nominal Focal Spot Size (mm)	NEMA Max. Tolerance (mm)	Focal Spot Size Width (mm)	Length (mm)
8	0.1	0.15	0.12 ± 0.02	0.14 ± 0.01
	0.3	0.45	0.31 ± 0.02	0.47 ± 0.02
9	0.1	0.15	0.12 ± 0.02	0.14 ± 0.02
	0.3	0.45	0.35 ± 0.02	0.48 ± 0.02
10	0.1	0.15	0.12 ± 0.02	0.15 ± 0.02
	0.3	0.45	0.34 ± 0.02	0.53 ± 0.03

[7]Both test runs were performed without phototiming. They both involved use of the grid and standard Mo filter. Test run 8 (9) (10) was performed at 25 (27) (25) kVp, at a FFD of 65.0 (63.3) (65.0) cm and at a tube mAs of 4.

was 0.3 mm this test tool was clearly unsuitable;

(b) the star resolution pattern that was used was of the 2° type. In order to make focal spot measurements on x-ray tubes with nominal focal spots in the range between 0.1 mm and 0.3 mm, a star pattern test tool with an angle of 1° must be used; and

(c) the pinhole camera that was used had a pinhole diameter of 0.075 mm. As it is seen from [Table 1] a pinhole diameter of 0.03 mm is recommended for very small focal spot sizes.

As seen in the results of [Table 24], the digital imaging technique can determine the small (large) focal spot dimensions to an average overall uncertainty of 15% (5%) for mammography x-ray tubes.

V.f Conclusion

The main goal of this work was to develop a technique that could be used to determine the focal spot dimensions of a wide range of focal spot sizes currently in use in diagnostic radiology x-ray machines in such a way as to eliminate the subjectiveness of the individual that is performing the measurement. This was done by digitizing a parallel wire test tool film image and then extracting the focal spot dimensions from the digitized film image via the application of the analysis program FSPOTCAL, which utilized digital imaging techniques. The focal spot results from this method indicate that not only are results comparable to the pinhole camera and star pattern methods possible, but they can be attained with an overall average uncertainty of the order of ± 6%.

In order to calculate the focal spot dimensions from the

three conventional focal spot test tools, the optical density of the test tool film images had to be between 0.8 - 1.2, 1.3 - 1.7 and 0.8 - 1.2 for the bar pattern, the star pattern and the pinhole camera respectively. Any deviation from these film optical density values might result in erroneous focal spot measurement results. The digital imaging system on the other hand has been shown to be independent of film optical density in the range of 1.0 - 2.5.

It also has been shown that the digital imaging technique can measure focal spots with nominal sizes between 0.1 mm to 1.4 mm, while using the same parallel wire test tool (which utilized two tungsten wires each of 0.05 mm diameter). The other three conventional focal spot measuring techniques, with the exception of the bar resolution pattern test tool, require the use of different range test tool models, depending on the focal spot size to be measured (in the star pattern test tool it is the spoke angle that is changed whereas on the pinhole camera test tool it is the pinhole diameter). The utilization of a single test tool to make focal spot measurements over a wide range of nominal values makes the technique more versatile.

When the conventional focal spot techniques are used to perform measurements, the various test tools are required to be set up at prescribed FFD's and using specified technique settings. This has the disadvantage of obtaining focal spot data that may not be at clinically used technique settings.

In the digital imaging technique, it has been shown that focal spot results can be obtained that are independent of the resultant film optical density (O.D) over the O.D. range 1.0 - 2.5 that encompasses most clinically used technique settings.

In the conventional focal spot techniques, single emulsion film is recommended. The disadvantage of this is that higher tube mAs values must be used to produce a useable test tool film image. The end result is that the focal spot measurement is taken at tube mAs values that are often beyond the normal clinically used range. The digital imaging system technique has been shown to produce results that are independent of whether the film is of single or double emulsion type.

In conclusion, the main advantage that the digital imaging system technique has over the existing recommended focal spot measuring techniques, is that it can perform focal spot measurements that are closer to normal clinical operating conditions and in a manner that removes the subjectiveness of the investigator that is performing the measurement.

REFERENCES

[1] National Council on Radiation Protection and Measurements (NCRP) Report No. 99, Quality Assurance for Diagnostic Imaging Equipment, NCPR Publications, 7910 Woodmont Ave., Siute 800, Bethesda, Maryland, USA, 20814, 1988, Pg. 65.

[2] American Association of Physicists in Medicine (AAPM) Report No. 4, Basic Quality Control in Diagnostic Radiology, AAPM Publications, 111 East Wacker Dr., Chicago, Illinois, USA, 60601, 1977, Pg. 24.

[3] National Electrical Manufactureres' Association (NEMA), Measurements of dimensions of focal spots of diagnostic x-ray tubes, NEMA Standard 9-11-1974, Publication No. XR-5-1989, New York, NY.

[4] Kemp F. H and Nichols A. F., Focal Spot Sizes, Br. J. Radiol., 31:485-488, 1958.

[5] Bookstein J. J. and Voegeli E., A critical analysis of magnification radiology, Radiol. 98:23-30, 1971.

[6] Christensen E. E., Introduction to the Physics of Diagnostic Radiology, (Philadelphia, Pa.: Lea & Febiger, Publisher, 1984), Pg. 273.

[7] International Commission of Radiological Units and Measurements (ICRU), Methods of evaluating radiological equipment and materials, Recommendations of the ICRU. NBS Handbook 89. Washington, DC: Government Printing Office, 1962.

[8] Arnold B. A., Bjarngard B. E. and Klopping J. C., A modified pinhole camera method for investigation of x-ray tube focal spots, Phys. Med. Biol. 18:540-549, 1973.

[9] Spiegler P. and Breckinridge W. C., Imaging of Focal Spot by Means of the Star Test Pattern, Radiol., 102: 679-684, 1972.

[10] Bernstein H., Bergeron R. T. and Klein D. J., Routine Evaluation of Focal Spots, Radiol., 111:421-425, 1974.

[11] Bookstein J. J., Effective Focal Spot Size, Radiol. 31-33, 1971.

[12] Rontgen, W., Uber eine neue Art von Strahlen (vorlaufige Mitteilung), Sitzungs-Berichte der Physikalisch-medicinischen Gesellschaft zu Wurzburg 9:132, 1895.

[13] Klickstein, H., William Conrad Rontgen: On a new kind of rays - a bibliographical study, in Mallinckrodt Classics of Radiology (St.Louis: Mallinckrodt Chemical Works, 1966), vol.1.

[14] Etter, L., The Science of Ionizing Radiation (Springfield,Ill., Charles C Thomas, Publisher, 1965).

[15] Glasser, O., Dr. W. C. Rontgen (2nd ed.: Springfield,Ill., Charles C Thomas, Publisher, 1958).

[16] Donizetti, P., Shadow and Substance: The Story of Medical Radiography (Oxford: Pergamon Press, Inc., 1967).

[17] Johns H. E. and Cunningham J. R., The Physics of Radiology, (Springfield, Ill., Charles C. Thomas, Publisher, 1983), Pg. 23.

[18] Johns H. E. and Cunningham J. R., The Physics of Radiology, (Springfield, Ill., Charles C. Thomas, Publisher, 1983), Pg. 50.

[19] Christensen E. E., Introduction to the Physics of Diagnostic Radiology, (Philadelphia, Pa.: Lea & Febiger, Publisher, 1984), Pg. 12.

[20] Chaney E., Hendee W. and Hare d., Performance evaluation of Phototimers, Radiology 118:715, 1976.

[21] Christensen E. E., Introduction to the Physics of Diagnostic Radiology, (Philadelphia, Pa.: Lea & Febiger, Publisher, 1984), Pg. 38.

[22] Rogers, T., Solid state rectification in x-ray transfers, Cathode Press 22:36, 1965.

[23] Morgan J., The development and application of multi-phase x-rays in medical radiography, Radiol. Technol. 40:57, 1968.

[24] Christensen E. E., Introduction to the Physics of Diagnostic Radiology, (Philadelphia, Pa.: Lea & Febiger, Publisher, 1984), Pg. 18.

[25] Botden P., Modern Trends in Diagnostic Radiologic Instrumentation, (Springfield, Ill., Charles C. Thomas Publisher, 1964).

[26] Johns H. E. and Cunningham J. R., The Physics of Radiology, (Springfield, Ill., Charles C. Thomas, Publisher, 1983), Pg. 63.

[27] Hendee W. R., Medical Radiation Physics, Year Book Medical Publishers, Inc., Chicago, Illinois, USA, 1976, Pg. 61.

[28] Johns H. E. and Cunningham J. R., The Physics of Radiology, (Springfield, Ill., Charles C. Thomas, Publisher, 1983), Pg. 49.

[29] Christensen E. E., Introduction to the Physics of Diagnostic Radiology, (Philadelphia, Pa.: Lea & Febiger, Publisher, 1984), Pg. 30.

[30] Johns H. E. and Cunningham J. R., The Physics of Radiology, (Springfield, Ill., Charles C. Thomas, Publisher, 1983), Pg. 67.

[31] Christensen E. E., Introduction to the Physics of Diagnostic Radiology, (Philadelphia, Pa.: Lea & Febiger, Publisher, 1984), Pg. 124.

[32] Christensen E. E., Introduction to the Physics of Diagnostic Radiology, (Philadelphia, Pa.: Lea & Febiger, Publisher, 1984), Pg. 126.

[33] Johns H. E. and Cunningham J. R., The Physics of Radiology, (Springfield, Ill., Charles C. Thomas, Publisher, 1983), Pg. 146.

[34] Johns H. E. and Cunningham J. R., The Physics of Radiology, (Springfield, Ill., Charles C. Thomas, Publisher, 1983), Pg. 150.

[35] Morgan J. A., The Art and Science of Medical Radiography, (Saint Louis, Missouri, The Catholic Hospital Association, Publisher, 1962), Pg. 46.

[36] Christensen E. E., Introduction to the Physics of Diagnostic Radiology, (Philadelphia, Pa.: Lea & Febiger, Publisher, 1984), Pg. 219.

[37] International Commission on Radialogical Protection (ICRP) Report No. 42, A Compilation of the Major Concepts and Quantities in Use by ICRP, Pergamon Press Inc., Elmsford, New York, USA, 10523, 1984, Pg. 2.

[38] Christensen E. E., Introduction to the Physics of Diagnostic Radiology, (Philadelphia, Pa.: Lea & Febiger, Publisher, 1984), Pg. 107 .

[39] Radiation Measurements Incorporated (RMI), Focal Spot Test Tool, RMI Publication, Middleton, Wisconsin, USA, 53562.

[40] Victoreen Nuclear Associates, 100 Voice Rd., Carle Place, New York, USA, 11514.

[41] Instruction Manual for Digital KV Meter ("Electronic kVp Cassette"), Canadian Scientific Products Ltd.

[42] Instruction Manual (Model 3036, Dosimeter-Ratemeter-Timer), Canadian Scientific Products Ltd.

[43] Radcal Corporation, Innovators in Instrumentation, 426 West Duarte Rd., Monrovia California, USA, 91016.

[44] Mind Computer Products (Assembler of IBM Compatible Computers), 892 Portage Ave., Winnipeg, Manitoba, Canada

[45] PCVISIONplus Frame Grabber User's Manual, Imaging Technology Inc., 1986.

[46] ITEX PCplus Programmer's Manual, Imaging Technology Inc., 1986.

[47] Victoreen Instruction Manual, X-ray Pinhole Camera - For Measuring the Dimensions of Focal Spots of X-ray Tubes, Victoreen Publications, 1980.

[48] Sarper R., AAPM The Physics of Medical Imaging: Recording System Measurement and Techniques, AAPM Publication 1979, Pg. 390.

[49] COHU Inc., Installation and Operation Instructions for 5000, 5100 and 5200 Series Low Light Level Cameras, COHU Publications 1984, San Diego, California, USA, 92138.

[50] NEC Home Electronics (USA) Inc., Multisync II Color Monitor User's Manual, NEC Corporation, Tokyo, Japan.

[51] Gonzalez R. C. and Wintz P, Digital Image Processing, (2nd ed.: Addison-Wesley Publishing Co., 1987), Pg. 144.

[52] Bevington P. R., Data Reduction and Error Analysis for the Physical Sciences, McGraw-Hill Book Co., 1969, Pg. 92.

APPENDIX A

TRUE MAGNIFICATION

The one assumption that was made in the calculation of geometric magnification (M) on film was that the focal spot was a point source. Even though this assumption may hold true when the focal spot dimensions are negligible in comparison to the focal spot-to-film distance, it does not hold true for the radiological distances that are often used. Thus, to properly calculate the true magnification (m) of an object on film the focal spot dimensions must also be considered.

In the following figure, which will be used in the derivation of m, 2R is the focal spot dimension, d is the focal spot-to-object distance, d' is the object-to-film distance, S_0 is the size of the object and S_i is the size of the image on film.

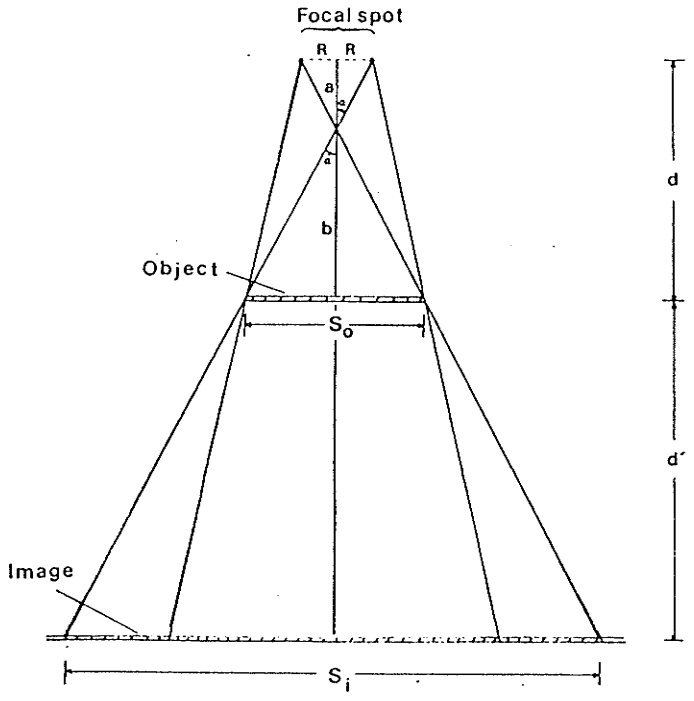

From the above figure, we have

$$\tan(\alpha) = \frac{R}{a} = \frac{S_0}{2b} = \frac{S_i}{2(d' + b)} \quad . \tag{A1}$$

Now from [Eq. A1] we have

$$\frac{b}{a} = \frac{S_0}{2R}$$

$$= \frac{S_0}{f} \tag{A2}$$

and

$$b = \frac{a \cdot S_0}{f} \tag{A3}$$

where f is the dimension of the focal spot, that is 2R.

Since

$$d = a + b$$

we have

$$\frac{d}{a} = 1 + \frac{b}{a} \tag{A4}$$

and after the substitution of [Eq. A2] into [Eq. A4] we find

$$a = \frac{d \cdot f}{f + S_0} \quad . \tag{A5}$$

Now from [Eq. A1] we also have

$$S_i = \frac{S_0 \cdot (d' + b)}{b} \tag{A6}$$

which is equal to the expression

$$S_i = \frac{d'}{d} \cdot (f + S_0) + S_0 \tag{A7}$$

after the substitution of [Eq. A3] and [Eq. A5].

From the definition of magnification, m, and [Eq. A7] we have

$$m = \frac{S_i}{S_0}$$

$$= \frac{f \cdot d'}{d \cdot S_0} + \frac{d'}{d} + 1 \quad . \tag{A8}$$

But since the geometric magnification, M, is calculated from

$$M = \frac{d + d'}{d} \tag{A9}$$

and thus

$$\frac{d'}{d} = (M - 1) \tag{A10}$$

the true magnification can then be shown to be

$$m = M + (M - 1) \cdot \frac{f}{S_0} \tag{A11}$$

once [Eq. A10] is substituted into [Eq. A8].

APPENDIX B

FOCAL SPOT CALCULATION WHEN USING BAR RESOLUTION PATTERN

When a bar resolution pattern is used to determine the dimensions of the focal spot, the following phenomenon is observed on the x-ray film image of the test tool.

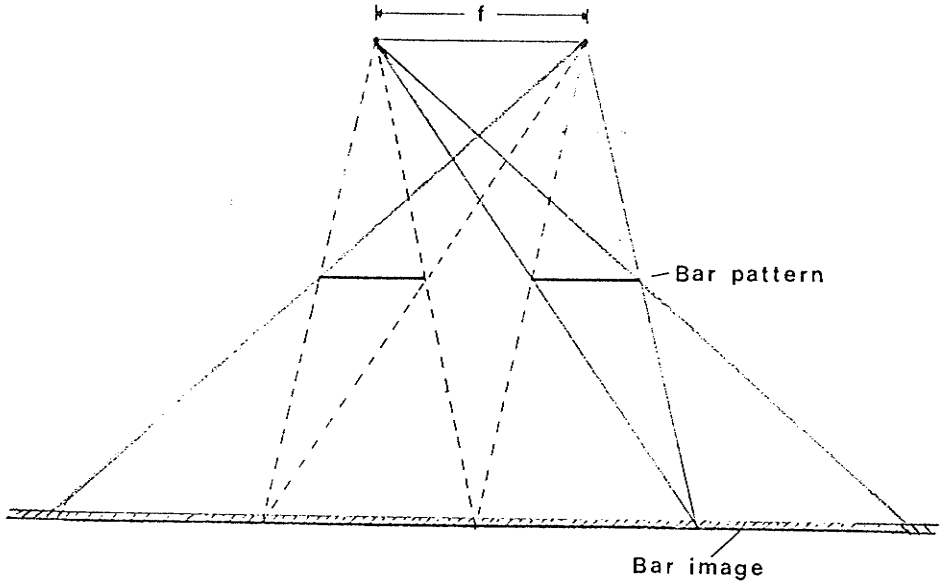

In the above figure a focal spot of dimensions f, which has been represented by two point sources separated by a small distance f, is shown to irradiate only two bars of a given bar group (recall that the width of each bar and the space between the bars are equal for a given bar group).

The focal spot measurement is made from the bar group image on film that is just resolved, that is when the separation distance between the two bar images on film is slightly greater than zero. The above figure illustrates the

limiting case when the separation distance is zero, which occurs when the magnified image of one of the bars from one point source equals the magnified image of the space between the two bars from the other point source. To derive a mathematical expression for this, consider the following figure which uses only a single bar:

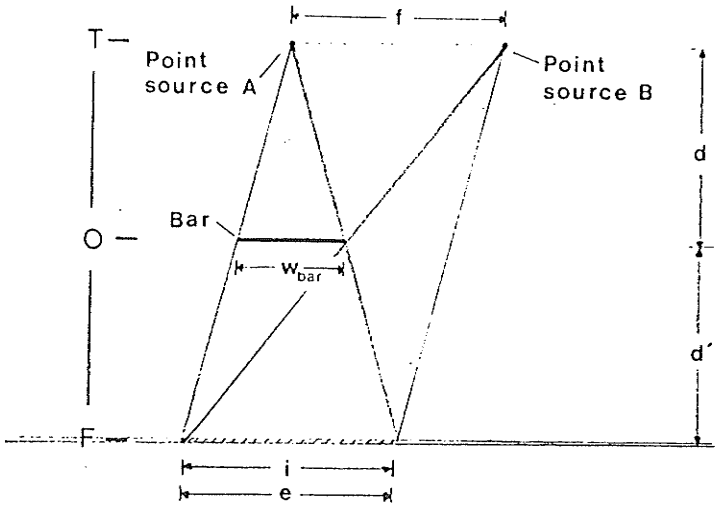

From the definition of magnification, we have

$$M = \frac{i}{w_{bar}} \qquad (B1)$$

where i is the image width of the bar on film due to point source A and w_{bar} is the physical width of the bar. Now from similar triangles we have

$$\frac{i}{w_{bar}} = \frac{TF}{TO} \qquad (B2)$$

from point source A and

$$\frac{e}{f} = \frac{OF}{TO} \qquad (B3)$$

from point source B.

Substituting the relation OF = TF - TO into [Eq. B3] we have

$$e = f\cdot(M - 1) \qquad (B4)$$

after seeing from [Eq. B2] and [Eq. B1] that M = TF/TO. In the above expression e is the image of the bar on film from point source B.

Now once again consider the top figure. The image size of the first bar on film as produced by point source A will be given by i. Since the separation distance between the two bars is equal to the width of a single bar, the image size of this separation distance on film from point source B will be given by e. Thus after equating e to i we find

$$f = \frac{w_{bar} \cdot M}{(M - 1)} . \qquad (B5)$$

Since the line pair frequency, l_f, of a given bar group is defined as

$$l_f = \frac{1}{2\cdot w_{bar}} \qquad (B6)$$

then [Eq. B5] can be rewritten as

$$f = \frac{M}{2l_f\cdot(M - 1)} . \qquad (B7)$$

APPENDIX C

FOCAL SPOT CALCULATION WHEN USING STAR RESOLUTION PATTERN

When a focal spot of dimensions f irradiates a star pattern test tool, the film image of a small section of the test tool will appear as follows:

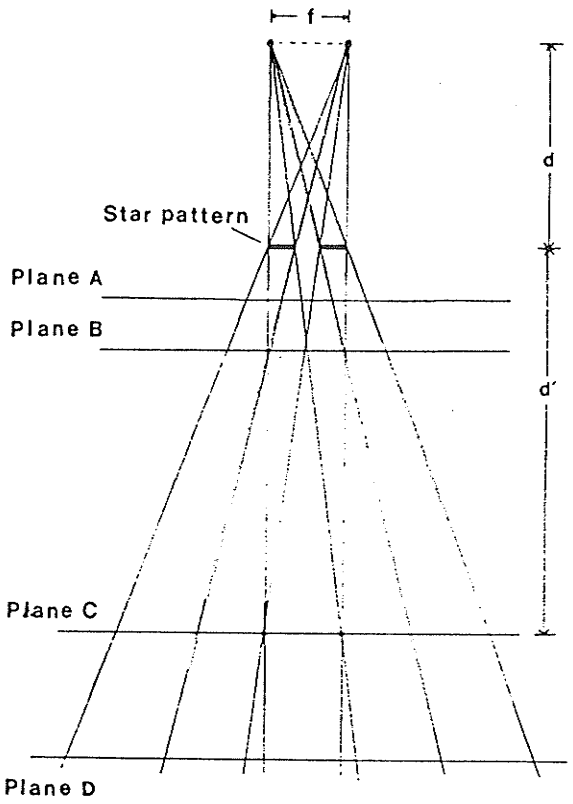

It is seen above that on the film, the penumbra of the two absorbing strips interacts and obscures the image of the gap between the two strips. For this to occur, the magnified image of the gap (seen in plane B) must be equal to the penumbra of either absorber (seen in plane C). Since the

penumbra region of the absorbers on film is given by e in [Appendix B] and since the magnified image of the gap is given by 2i where, i, is defined in [Appendix B], then after equating e to 2i we find

$$2 \cdot M \cdot w = f \cdot (M - 1) \qquad (C1)$$

where w is the physical width of the gap between the two absorbers. Rewriting [Eq. C1] we then have

$$f = \frac{2 \cdot w \cdot M}{(M - 1)} . \qquad (C2)$$

Because of the star pattern's construction (see [Fig. 23] for illustration), the width of the absorbers (lead wedges) which is also given by w, will vary depending on the distance from the center of the star pattern. Thus, for a distance r from the center of the star pattern the width of the absorbers will be given as

$$w = \frac{N}{360} \cdot 2\pi r \qquad (C3)$$

where N is the angle of the lead wedges on the star pattern test tool. After the substitution of [Eq. C3] into [Eq. C2] and then solving for f we find

$$f = \frac{N}{180} \cdot \frac{2\pi r \cdot M}{(M - 1)}$$

$$= \frac{N}{57.3} \cdot \frac{M \cdot d}{(M - 1)} \qquad (C4)$$

where d is the diameter, equal to 2r. Since the distance Md is determined from the test tool's film image and is equal

to the diameter, D, of the zero contrast region, then [Eq. C4] becomes

$$f = \frac{N}{57.3} \cdot \frac{D}{(M - 1)} \quad . \qquad (C5)$$

APPENDIX D

FOCAL SPOT CALCULATION WHEN USING THE PINHOLE CAMERA

When a pinhole camera is used to determine the dimensions of the focal spot, the geometry of the test tool with respect to the focal spot is as follows.

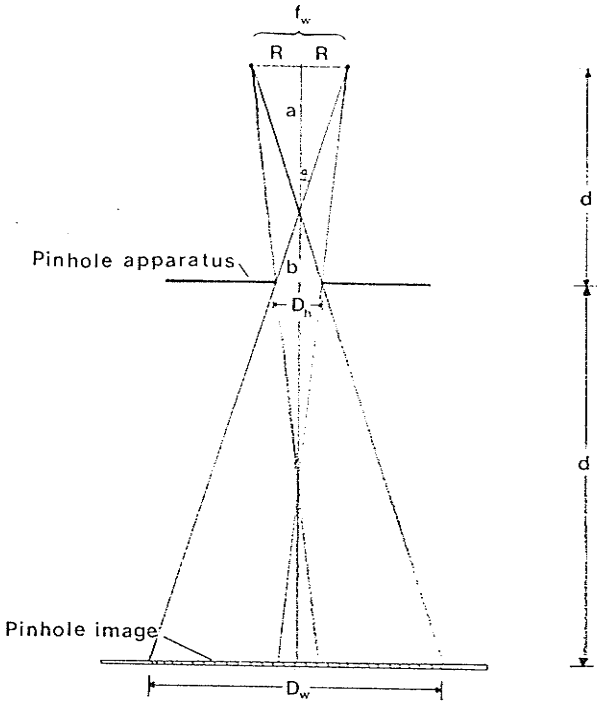

It should be noted that this figure is identical to the one shown in [Appendix A], with the only difference being that the object in question is now taken to be the camera's pinhole. From [Appendix A] then, the true magnification (m) of the pinhole on film is then given by

$$m = M + (M - 1)\cdot\frac{f_w}{D_h} \qquad (D1)$$

where M is the geometric magnification of the pinhole camera, D_h is the physical diameter of the pinhole and f_w is the

width of the focal spot.

From the definition of magnification, we have

$$m = \frac{D_w}{D_h} \qquad (D2)$$

where D_w is the diameter of the pinhole in the test tool's x-ray film image. Then by equating [Eq. D2] to [Eq. D1] we find

$$\frac{D_w}{D_h} = M + (M - 1)\cdot\frac{f_w}{D_h} \quad . \qquad (D3)$$

The width of the focal spot can then be determined from [Eq. D3] and is found to be

$$f_w = \frac{D_w - D_h \cdot M}{(M - 1)} \quad . \qquad (D4)$$

APPENDIX E

DIGITAL IMAGING ANALYSIS PROGRAM

In this appendix the program FSPOTCAL is presented in the form it was used to perform the data analysis. The program was written and compiled in the C computer language in such a manner to access the object code library of the ITEX PCplus software package. Because of the header files: pcpitex.h and pcpcnt.h, this code as it is shown can be compiled only at the Manitoba Cancer Treatment and Research Foundation where it was written and tested.

In the code that follows, various records were greater then 80 characters long and because of this these records were carried over to the following line. These records were left unchanged to avoid alteration of the information that is displayed on the computer terminal while the analysis program is activated. It should be noted that the user communicates interactively with the program via the computer terminal while image manipulation is performed on the display monitor.

```
/* ------------------------------------------------------
                The analysis program FSPOTCAL

    Written by: Konstantinos Chantziantoniou
    Version # : 21                  Date: August 24, 1989
   ------------------------------------------------------ */

#include <pcpitex.h>
#include <pcpcnt.h>
#include <stdio.h>
#include <math.h>
#include <limits.h>
```

```
 main( )
{
/* ------------------------------------------------------------
                    Variable assignments
   ------------------------------------------------------------ */

  FILE *in;
  FILE *inputdata;
  FILE *output;
  char name[20],comment[20],filename[20],filename1[20];
  char test,filedata[20],date[20],loca[20],film1[20];
  char fss[20],junk,film2[20],film3[20],film4[20],orin[20];
  char kvp[20],mas[20],dummy[70],outdata[20];
  int gain,offset,answer,answera,answerb,answerc,xcoord;
int ycoord,answerd,answere,answerf,answerg,x1,x2,y1,y2;
  int count,ker[49],ansdata,conti,answeri,xmin;
  int xcoord1,xcoord2,ycoord1,ycoord2,pixel,answerh,xmax;
  int ymax,ymin,kernel[9],center,lfwhm,rfwhm,lp[490];
  int rp[490],sonum,cw[490],counter,kern[9],x,y,dx,dy;
  int kerl[17],datum,ansdata1;
  int limit,dut1,dut2,data[9][480],type_key,automa;
  int tfnumber1,tfnumber2,pixelx,scale,active;
  float sigma,mean,sigmad,alpha,beta,gamma,meanl,sigmal;
  float meanr,sigmar,xp1,yp1,eta,mu,xq1,xq2,yq1,yq2;
  float meant,sigmat,width,swidth,a,b,da,db,gamma1;
  float gamma2,fsrange,fwdisterr,wfdisterr,starerr;
  float sxi,sxi2,syi,syi2,sxyi,delta,s1,s2,s3,sdelta;
  float fspot,sfspot,add1,add2,add3,add4,add5;
  float fwdist,wfdist,od1,od2,star1,star1err,star2;
  float star2err,dia1,dia1err,dia2,dia2err,dia3,dia3err;
  float dia4,dia4err,magn,magnerr,dia5,dia5err,dia6;
  float dia6err,dia7,dia7err,dia8,dia8err,magn1,magn1err;
  float pin1,pin1err,pin2,pin2err,dtotal,df1,df2,df3;
  float bar1,bar1err,bar2,bar2err,dtheta,dcos,scalex;
  float dscalex,dx1,dy2,uu,dthetal,dthetar,dfs1,dfs2,dfs3;
  float dfspot1,dfspot2,dfspot3,dfspot4,dfspot5,dfspot6;
  float dfspot7;

/* ------------------------------------------------------------
                    Statement assignments
   ------------------------------------------------------------ */

  #define question1  "What image data file do wish to view:"
#define question2  "State file comment:"
  #define fault      "You did not answer the question
correctly !"
  #define question3  "Save the entire screen (8-bit pixels)
into file :"
  #define question4  "Do you wish to digitize x-ray film (y
or n):"
  #define question5  "Do you wish to adjust the gain and
offset (y or n):"
```

```
  #define statement  "The default values of gain and offset
are:"
  #define statement1 "Enter the new gain value:"
  #define statement2 "Enter the new offset value:"
  #define statement3 "Are you finished adjusting the offsets
(y or n):"
  #define statement4 "The x-ray film has been digitized and
stored"
  #define statement10 "Do you wish to sharpen the image (y or
n):"
  #define statement11 "Do you wish to store a line of pixel
values (y or n):"
  #define statement13 "State two points on the
vertical/horizontal line:"
  #define statement14 "Point one x-coordinate:"
  #define statement15 "Point one y-coordinate:"
  #define statement16 "Point two x-coordinate:"
  #define statement17 "Point two y-coordinate:"
  #define statement19 "Do you wish to stretch the LUT values
(y or n):"
  #define statement20 "Do you wish to store modified image (y
or n):"
  #define statement21 "Which image file do you wish to use:"
#define statement22 "The min and max pixel values used were:"

  #define statement23 "Define two points on a diagonal to
designate active area:"
  #define statement24 "Is this rectangular active area
sufficient (y or n):"
  #define statement25 "Do you wish to perform a histogram
equalization ( y or n):"
  #define statement26 "Do you wish to perform horizontal
averaging ( y or n):"
  #define statement27 "Are you finished with code (y or n);"
#define statement28 "Which input data file do you wish to
use:"
  #define statement29 "Estimate wire thickness via curser to
determine wire maxima:"
  #define statement30 "Estimated wire width is:"
  #define statement31 "Do you wish to store the calculated
data (y or n):"
  #define statement32 "Which data file (xx.dat) do you wish
to use:"
  #define statement33 "Do you wish to continue (y or n):"
  #define statement34 "Estimate pixel scale factor via
curser:"
  #define statement35 "Distance on scale (in mm):"
  #define statement36 "Distance on scale (in pixels):"
  #define statement37 "Press any key to continue:"
  #define statement38 "Width of active area:"
  #define statement39 "Do you wish the default active area (y
or n):"
```

```
  #define statement40 "*** Note no histogram equalization has
been performed ***"


/* ------------------------------------------------------------
    Performs the IBM PC Vision Plus system initialization
   ------------------------------------------------------------ */

  sethdw(0x300,0xA0000L,DUAL);
  setdim(512,512,8);
  initialize();

  select_mem(MEM_A);      /* Selects frame memory A */

/* ------------------------------------------------------------
                      Start of program
   ------------------------------------------------------------ */

  conti = 'y';

  while ( conti == 'y')
   {

   cls();                  /* Clears computer terminal */

/* Reads in the input data file that contains the various
 information that is pertinent to the focal spot
   calculation and identification of experimental
   conditions. */

   printf("%53s",statement28);
   scanf("%s",filedata);
   printf("\n");

   fopen(filedata,"r")
   fscanf(inputdata,"%s",date);
   fscanf(inputdata,"%s",loca);
   fscanf(inputdata,"%d",&tfnumber1);
   fscanf(inputdata,"%d",&tfnumber2);
   fscanf(inputdata,"%s",kvp);
   fscanf(inputdata,"%s",mas);
   fscanf(inputdata,"%f",&fsrange);
   fscanf(inputdata,"%s",orin);
   fscanf(inputdata,"%s",film1);
   fscanf(inputdata,"%s",film2);
   fscanf(inputdata,"%s",film3);
   fscanf(inputdata,"%s",film4);
   fscanf(inputdata,"%f",&od1);
   fscanf(inputdata,"%f",&od2);
   fscanf(inputdata,"%s",fss);
   fscanf(inputdata,"%f %s %f",&fwdist,dummy,&fwdisterr);
```

```
    fscanf(inputdata,"%f %s %f",&wfdist,dummy,&wfdisterr);

    close(inputdata);

/* Stores the input data in the output data file. */

    printf("%62s",statement31);
    ansdata = getkey( );
    ansdata1 = ansdata;
    printf("\n");

    if ( ansdata == 'y')
      {
      printf("%56s",statement32);
      scanf("%s",outdata);

      output = fopen(outdata,"w");

      fprintf(output,"                                        Focal Spot
Results\n");
      fprintf(output,"
==============================\n");
      fprintf(output,"\n");
      fprintf(output,"          Date:%s",date);
      fprintf(output,"                    x-ray tube
location:%s \n",loca);
      fprintf(output,"          ----");
      fprintf(output,"
------------------- \n");
      fprintf(output,"\n");
      fprintf(output,"X-Ray Tube Information \n");
      fprintf(output,"----------------------- \n");
      fprintf(output,"\n");
      fprintf(output,"  mAs:%s\n",mas);
      fprintf(output,"  kVp:%s\n",kvp);
      fprintf(output,"  Nominal focal spot size (in
mm):%3.1f\n",fsrange);
      fprintf(output,"  Focal spot size
identification:%s\n",fss);
      fprintf(output,"\n");
      fprintf(output,"X-Ray Film Information \n");
      fprintf(output,"----------------------- \n");
      fprintf(output,"\n");
      fprintf(output,"  Type used:%s\n",film1);
      fprintf(output,"  Color sensitivity:%s\n",film2);
      fprintf(output,"  Was screen used ? %s\n",film3);
      fprintf(output,"  Single or double emulsion
used:%s\n",film4);
      fprintf(output,"  Optical density (base +
fog):%4.2f\n",od1);
      fprintf(output,"  Optical density (image
background):%4.2f\n",od2);
```

```
      fprintf(output,"\n");
      fprintf(output,"X-Ray Image Information\n");
      fprintf(output,"-----------------------\n");
      fprintf(output,"  Test number:%d\n",tfnumber1);
      fprintf(output,"  Frame number:%d\n",tfnumber2);
      fprintf(output,"\n");
      fprintf(output,"Experimental Setup\n");
      fprintf(output,"------------------\n");
      fprintf(output,"\n");
      fprintf(output,"  Wire focal spot target orientation
w.r.t cathode-anode axis:%s\n",orin);
      fprintf(output,"  Focal spot to wire plane distance(in
mm):    %6.1f +/- %3.1f\n",fwdist,fwdisterr);
      fprintf(output,"  Wire plane to film distance (in mm):
      %6.1f +/- %3.1f\n",wfdist,wfdisterr);
      fprintf(output,"\n");

      }

   dia1 = fwdisterr;
   dia2 = wfdisterr;

/* Performs the following functions: grabs the test tool
   film image, displays it on the monitors screen and stores
   it in frame memory. */

   printf("\n");
   printf("%56s",question4);
   answer = getkey( );
   printf("\n");

   sclear(255);              /* Clears imaging screen */

   rectangle(340,250,110,1,0); /* Places alignment cross
   rectangle(395,195,1,110,0);    hairs on imaging screen */

   if ( answer == 'y' || answer == 'n' )
     {
     if ( answer == 'y' )   /* Creates and displays image */
       {
       printf("\n");
       printf("%61s",question3);
       scanf("%s",name);
       printf("%31s",question2);
       scanf("%s",comment);
       printf("\n");

       grab(0);

       gain = 39;
       offset = 83;
```

```
    setgain(gain);          /* Sets default gain */
    setoffset(offset);      /* Sets default offsets */

    printf("%54s",statement);
    printf("%d,%d\n",gain,offset);

    printf("%63s",question5);
    answera = getkey( );
    printf("\n");

    if ( answera == 'y' )
      {
      answerb = 'n';
      while ( answerb == 'n' )
        {               /* Sets gain manually */
        printf("%37s",statement1);
        scanf("%d",&gain);
                        /* Sets offsets manually */
        printf("%39s",statement2);
        scanf("%d",&offset);

        setgain(gain);
        setoffset(offset);

        printf("%60s",statement3);
        answerb = getkey( );
        printf("\n");
        }
      }

    printf("\n");
    printf("%38s",statement37);
    type_key = getkey( );
    printf("\n");

    stopgrab(NO_WAIT);
            /* Saves digitized image in frame memory */
    saveim(0,0,511,511,EIGHT_BIT,name,comment);

    printf("\n");
    printf("%56s",statement4);
    printf("\n");
    printf("\n");

    readim(0,0,511,511,name,comment);
    }
  else   /* Displays digitized image from frame memory */
    {
    printf("\n");
    printf("%49s",question1);
    scanf("%s",name);
    printf("%31s",question2);
```

```
        scanf("%s",comment);
        printf("\n");

        readim(0,0,511,511,name,comment);
        }
      }
    else
      printf("%55s",fault);

    datum = 1;

    while (datum < 3)
      {
/* Defines the programs active area. */

      if ( datum == 1)
        {
        printf("%72s",statement29);
        printf("\n");

        cursorsetting1();

        printf("\n");                /* Sets wire width seed */
        printf("%36s",statement30);/* for horizontal pixel */
        scanf("%d",&limit);          /* averaging            */
        printf("\n");

        printf("%51s",statement34);
        printf("\n");

        cursorsetting1();

        printf("\n");                /* Determines pixel     */
        printf("%38s",statement35);/* calibration constant */
        scanf("%d",&scale);
        printf("%42s",statement36);
        scanf("%d",&pixelx);
        printf("\n");

        sclear(255);
        readim(0,0,511,511,name,comment);
        }

      printf("%69s",statement23);
      printf("\n");

      cursorsetting();

      printf("\n");

      if (datum == 1)
        {
```

```
    printf("%57s",statement39);
    automa = getkey();
    printf("\n");
    }

  if (automa == 'y')
    {
    if (datum == 1)
      {
      printf("%35s",statement14);
      scanf("%d",&xcoord1);
      printf("\n");
      }
    if (datum == 2)
      {
      printf("%35s",statement14);
      scanf("%d",&xcoord1);
      printf("\n");
      }

    ycoord1=5;  /* Sets default active area dimensions */
    ycoord2=475;

    dx=55;
    }

  if (automa == 'n')
    {
    if (datum == 1)
      {
      printf("%35s",statement14);
      scanf("%d",&xcoord1);
      printf("%35s",statement15);
      scanf("%d",&ycoord1);
      printf("%35s",statement16);
      scanf("%d",&xcoord2);
      printf("%35s",statement17);
      scanf("%d",&ycoord2);
      printf("\n");
      }
    if (datum == 2)
      {
      printf("%35s",statement14);
      scanf("%d",&xcoord1);
      printf("%35s",statement16);
      scanf("%d",&xcoord2);
      printf("\n");
      }

    dx=xcoord2-xcoord1;
    }
```

```
x=xcoord1;     /* Sets active area to any dimensions */
y=ycoord1;
dy=ycoord2 - ycoord1;

rectangle(x,y,dx,dy,255);

printf("%64s",statement24);
answerg = getkey( );
printf("\n");

while (answerg == 'n')
  {

  sclear(255);
  readim(0,0,511,511,name,comment);
  cursorsetting( );
  printf("\n");
  if (automa == 'y')
    {
    if (datum == 1)
      {
      printf("%35s",statement14);
      scanf("%d",&xcoord1);
      printf("\n");
      }
    if (datum == 2)
      {
      printf("%35s",statement14);
      scanf("%d",&xcoord1);
      printf("\n");
      }

    ycoord1=5;
    ycoord2=475;

    dx=55;
    }

  if (automa == 'n')
    {
    if (datum == 1)
      {
      printf("%35s",statement14);
      scanf("%d",&xcoord1);
      printf("%35s",statement15);
      scanf("%d",&ycoord1);
      printf("%35s",statement16);
      scanf("%d",&xcoord2);
      printf("%35s",statement17);
      scanf("%d",&ycoord2);
      printf("\n");
      }
```

```
        if (datum == 2)
          {
          printf("%35s",statement14);
          scanf("%d",&xcoord1);
          printf("%35s",statement16);
          scanf("%d",&xcoord2);
          printf("\n");
          }

        dx=xcoord2-xcoord1;
        }

      x=xcoord1;
      y=ycoord1;
      dy=ycoord2 - ycoord1;

      rectangle(x,y,dx,dy,255);
      printf("%64s",statement24);
      answerg = getkey();
      printf("\n");
      }

/* Performs Histogram Equalization. */

    if (fsrange > 0.4) /* For focal spots > 0.4 mm */
      {
      setlut(RED,5);
      histeq(RED,5,x,y,dx,dy);
      maplut(RED,5,x,y,dx,dy);
      linlut(RED,5);
      linlut(GREEN,5);
      linlut(BLUE,5);
      }
    else                    /* For focal spots < 0.4 mm */
      {
      printf("\n");
      printf("%69s",statement40);
      printf("\n");
      }

/* Performs vertical pixel averaging. */

    for (counter=0;counter<=16;counter++) kerl[counter]=1;
    kerl[9]=0;
    convol(x-1,y-1,dx+3,dy+9,4,0,ABS,1,17,kerl);

/* Finds the wire center and width for all of the horizontal
   row of pixels found within a given active area.  */

    x1=x+1;
    x2=x+dx-1;
    counter=0;
```

```
        for (count=(y+1);count<=(y+dy);count++)
          {
          counter=counter+1;
          findcenter(x1,x2,count,&center,limit);
          cw[counter]=center;
          findwirewidth(count,center,&lfwhm,&rfwhm,limit);
          lp[counter]=lfwhm;
          rp[counter]=rfwhm;
          }

        sclear(255);
        readim(0,0,511,511,name,comment);
        rectangle(x,y,dx,dy,255);

        counter=0;
        for (count=(y+1+5);count<=(y+dy-1-19);count++)
          {
          counter=counter+1;
          wpixel(lp[counter+5],count,255);
          wpixel(rp[counter+5],count,255);
          if (datum == 1 )
            {
            data[1][counter]=lp[counter+5];
            data[2][counter]=rp[counter+5];
            data[4][counter]=rp[counter+5]-lp[counter+5]+1;
            data[3][counter]=(rp[counter+5]-lp[counter+5]+1)/2;
            }
          if (datum == 2 )
            {
            data[5][counter]=lp[counter+5];
            data[6][counter]=rp[counter+5];
            data[8][counter]=rp[counter+5]-lp[counter+5]+1;
            data[7][counter]=(rp[counter+5]-lp[counter+5]+1)/2;
            }
          }

        datum = datum +1;
        printf("\n");
        }

/* Determines the wires misalignment angle. */

    sxi = 0;     /* Least squares fit of left wire centers */
    sxi2 = 0;
    syi = 0;
    syi2 = 0;    /* Note the 0.8 factor arises from the */
    sxyi = 0;    /* fact that the y-coord pixel dimensions */
    s1 = 0.0;    /* are 4/5 th of the x-coord pixels  */
    s2 = 0.0;    /* dimensions. So the y-coord pixels must */
    s3 = 0.0;    /* be multiplied by 0.8 to make the */
    sdelta = 0.0; /* y-coord scale the same as the */
```

```
    delta = 0.0;  /* x-coord scale. */
    a = 0.0;
    da = 0.0;
    b = 0.0;
    db = 0.0;

    dut1 = 1;
    while ( dut1 <= counter )
      {
      sxi = sxi + (long)data[3][dut1];
      sxi2 = sxi2 + (long)data[3][dut1]*data[3][dut1];
      syi = syi + (long)(dut1+ycoord1+5)*0.8;
      syi2 = syi2 +(long)(dut1+ycoord1+5)
             *(dut1+ycoord1+5)*0.8*0.8;
      sxyi = sxyi + (long)data[3][dut1]*(dut1+ycoord1+5)*0.8;
      s1 = s1 + (float)data[3][dut1]*data[3][dut1]
           /(dut1+ycoord1+5)/0.8;
      s2 = s2 + (float)1/(dut1+ycoord1+5)/0.8;
      s3 = s3 + (float)data[3][dut1]/(dut1+ycoord1+5)/0.8;
      dut1 = dut1 +1;
      }

    delta = counter*sxi2 - sxi*sxi;
    sdelta = s2*s1 - s3*s3;

                /* Linear eq'n is : y = b*x + a */

    a = (sxi2*syi - sxi*sxyi)/delta;
    da = sqrt(s1/sdelta);
    b = (counter*sxyi-sxi*syi)/delta;
    db = sqrt(s2/sdelta);

    gamma1 = atan(b);

    dthetal = db/(1 + b*b);
    dthetal = dtheta*180/3.1415927;

    gamma = gamma1;
    add1 = gamma1;

    cls( );          /* Clears computer terminal */

    printf("                                        Experimental
data\n");
    printf("
-----------------\n");
    printf("             Left wire was misaligned by:
  %6.3f +/-%6.3f degrees\n",gamma1,dthetal);

    gamma1 = cos(gamma1);
```

```
sxi = 0;  /* Least squares fit of right wire centers */
sxi2 = 0;
syi = 0;
syi2 = 0;
sxyi = 0;
a = 0.0;
b = 0.0;
s1 = 0.0;
s2 = 0.0;
s3 = 0.0;
sdelta = 0.0;
da = 0.0;
db = 0.0;

dut2 = 1;
while ( dut2 <= counter )
  {
  sxi = sxi + (long)data[7][dut2];
  sxi2 = sxi2 + (long)data[7][dut2]*data[7][dut2];
  syi = syi + (long)(dut2+ycoord1+5)*0.8;
  syi2 = syi2 + (long)(dut2+ycoord1+5)
       *(dut2+ycoord1+5)*0.8*0.8;
  sxyi = sxyi + (long)data[7][dut2]*(dut2+ycoord1+5)*0.8;
  s1 = s1 + (float)data[7][dut2]*data[7][dut2]
     /(dut2+ycoord1+5)/0.8;
  s2 = s2 + (float)1/(dut2+ycoord1+5)/0.8;
  s3 = s3 + (float)data[7][dut2]/(dut2+ycoord1+5)/0.8;
  dut2 = dut2 +1;
  }

delta = (float)counter*sxi2 - (float)sxi*sxi;
sdelta = (float)s2*s1 - (float)s3*s3;

a = (sxi2*syi - sxi*sxyi)/delta;
b = (counter*sxyi-sxi*syi)/delta;
da = sqrt(s1/sdelta);
db = sqrt(s2/sdelta);

gamma2 = atan(b);

dthetar = db/(1 + b*b);
dthetar = dthetar*180/3.1415927;

gamma = (gamma+gamma2)/2;
add2 = gamma2;
add3 = gamma;

dtheta = dthetal*dthetal + dthetar*dthetar;
dtheta = sqrt(dtheta);
dtheta = (float)1/2*dtheta;

printf("            Right wire was misaligned by:
```

```
  %6.3f +/-%6.3f degrees\n",gamma2,dthetar);
   printf("            Straight average of wire misalignment
is: %6.3f +/-%6.3f degrees\n",gamma,dtheta);

   gamma2 = cos(gamma2);

   gamma = (gamma1 + gamma2)/2;

   dcos = sqrt(1 - gamma*gamma)/2*sqrt(dthetal*dthetal +
        dthetar*dthetar);

   printf("            Cos(misalignment angle) is:
  %6.4f +/- %6.4f\n",gamma,dcos);

/* Determines the mean left and right wire widths in
   pixels. */

   meanl = 0.0;
   for (sonum=1;sonum<=counter;sonum++)
     {
     meanl = meanl + data[4][sonum];
     }

   meanl = meanl/counter;      /* Left wire width mean */
   sigmal = 0.0;
   sigmad = 0.0;
   sonum = 1;
   while ( sonum <= counter )
     {
     sigmal = data[4][sonum] - meanl;
     sigmad = sigmal*sigmal + sigmad;
     sonum =sonum +1;
     }

   sigmal = sigmad/(counter-1);
   sigmal =sqrt(sigmal);

   printf("\n");
   printf("            Left wire width is:
  %6.2f +/- %4.2f pixels \n",meanl,sigmal);

   meanr = 0.0;
   for (sonum=1;sonum<=counter;sonum++)
     {
     meanr = meanr + data[8][sonum];
     }

   meanr = meanr/counter;      /* Right wire width mean */

   sigmar = 0.0;
   sigmad = 0.0;
   sonum = 1;
```

```
    while ( sonum <= counter )
      {
      sigmar = data[8][sonum] - meanr;
      sigmad = sigmar*sigmar + sigmad;
      sonum =sonum +1;
      }

    sigmar = sigmad/(counter-1);
    sigmar =sqrt(sigmar);

    printf("            Right wire width is:
   %6.2f +/- %4.2f pixels \n",meanr,sigmar);

          /* Weighted mean of left and right wire widths */

    sigmat = 1/(sigmal*sigmal)+1/(sigmar*sigmar);
    sigmat = 1/sigmat;
    meant = meanl/(sigmal*sigmal)+meanr/(sigmar*sigmar);
    meant = meant*sigmat;
    sigmat = sqrt(sigmat);

    printf("            Weighted mean of two wire widths is:
   %6.2f +/- %4.2f pixels \n",meant,sigmat);


/* Determines the pixel calibration constant. */

    scalex = (float)scale/pixelx;
    dscalex = scalex*sqrt(2)/pixelx;
    printf("\n");
    printf("            Pixel calibration factor was:
   %6.3f +/- %4.3f mm/pixel \n",scalex,dscalex);

/* Determines the corrected average wire width. */

    width = meant*gamma*scalex;

    swidth = width*sigmat/meant;

    printf("            Wire width corrected for misalignment
is: %6.2f +/- %4.2f mm \n",width,swidth);
    printf("\n");

/* Determines the test tool geometric magnification. */

    magn = 0.0;
    magnerr = 0.0;

    magn = (fwdist + wfdist)/fwdist;

    magnerr = dia1*dia1*wfdist*wfdist/fwdist/fwdist
```

```
            /fwdist/fwdist;
    magnerr = magnerr + dia2*dia2/fwdist/fwdist;
    magnerr = sqrt(magnerr);

    printf("              Geometric magnification was:
   %6.3f +/-%6.3f \n",magn,magnerr);
    printf("\n");

    printf("\n");
    printf("%38s",statement37);
    ansdata = getkey( );
    printf("\n");

 /* Determines the statistical and systematic errors in
    the focal spot measurement. */

    junk = '%';

    cls( );              /* Clears computer terminal */

    printf("                              ---------- Error Analysis
----------\n");
    printf("              Parameter                 Uncertainty
    Focal Spot Uncertainty\n");
    printf("              ---------                 -----------
    ------------------------\n");
    printf("\n");
    printf("              Statistical\n");
    printf("              -----------\n");
    printf("\n");

 /* Wire width statistical error. */
    dfspot1 = swidth/(magn-1);

    printf("              Wire width                +/- %4.3f mm
          +/-%6.3f mm\n",swidth,dfspot1);
    printf("\n");
    printf("              Systematic\n");
    printf("              ----------\n");
    printf("\n");

 /* Calibration constant systematic error contribution. */

    dfspot2 = meant*gamma*dscalex/(magn - 1);
    printf("              Calib. factor             +/- %4.3f
mm/pixel         +/-%6.3f mm\n",dscalex,dfspot2);

 /* Wire misalignment angle systematic error contribution. */
    dfspot3 = meant*scalex*dcos/(magn - 1);
    printf("              Cos(misal.ang)            +/- %5.4f
         +/-%6.3f mm\n",dcos,dfspot3);
```

```
/* Physical wire width systematic error contribution. */

   dfspot4 = magn/(magn - 1)*0.005;
   printf("            Physical wire width    +/- 0.005 mm
         +/-%6.3f mm\n",dfspot4);

/* Geometric magnification systematic error contribution. */

   dfspot5 = -(0.05 - width)/(magn - 1)/(magn - 1)*magnerr;
   printf("            Magnification          +/- %4.3f
         +/-%6.3f mm\n",magnerr,dfspot5);

/* Total systematic error in focal spot measurement. */

   dfspot6 = dfspot2*dfspot2 + dfspot3*dfspot3 +
             dfspot4*dfspot4;
   dfspot6 = dfspot6 + dfspot5*dfspot5;
   dfspot6 = sqrt(dfspot6);
   printf("\n");
   printf("            Adding the above four errors in
quadrature       +/-%6.3f mm\n",dfspot6);

/* The focal spot value. */

   fspot = (width - 0.05*magn)/(magn - 1);

/* Absolute error in focal spot measurement. */

   dfspot7 = dfspot1*dfspot1 + dfspot6*dfspot6;
   dfspot7 = sqrt(dfspot7);
   printf("\n");
   printf("            Final result\n");
   printf("            ------------\n");
   printf("\n");
   printf("            Focal spot size is          %6.2f
+/-%5.2f mm (%4.2f
%c)\n",fspot,dfspot7,dfspot7/fspot*100,junk);
   printf("\n");

/* Stores the calculated data in the output file. */

   if ( ansdata1 == 'y')
     {

     fprintf(output,"\n");
     fprintf(output,"Focal Spot Size Determined Using Wire
Test Tool\n");

fprintf(output,"-----------------------------------------------
--\n");
     fprintf(output,"\n");
     fprintf(output,"                              Experimental
```

```
data\n");
     fprintf(output,"
-----------------\n");
     fprintf(output,"\n");
     fprintf(output,"  Left wire was misaligned by:
  %6.3f +/-%6.3f degrees\n",add1,dthetal);
     fprintf(output,"  Right wire was misaligned by:
  %6.3f +/-%6.3f degrees\n",add2,dthetar);
     fprintf(output,"  Straight average of wire misalignment
is: %6.3f +/-%6.3f degrees\n",add3,dtheta);
     fprintf(output,"  Cos(misalignment angle) is:
  %6.4f +/- %6.4f\n",gamma,dcos);
     fprintf(output,"\n");
     fprintf(output,"  Left wire width is:
  %6.2f +/- %4.2f pixels \n",meanl,sigmal);
     fprintf(output,"  Right wire width is:
  %6.2f +/- %4.2f pixels \n",meanr,sigmar);
     fprintf(output,"  Weighted mean of two wire widths is:
  %6.2f +/- %4.2f pixels \n",meant,sigmat);
     fprintf(output,"\n");
     fprintf(output,"  Pixel calibration factor was:
  %6.3f +/- %4.3f mm/pixel \n",scalex,dscalex);
     fprintf(output,"  Wire width corrected for misalignment
is: %6.2f +/- %4.2f mm \n",width,swidth);
     fprintf(output,"\n");
     fprintf(output,"  Geometric magnification was:
  %6.3f +/-%6.3f \n",magn,magnerr);
     fprintf(output,"\n");
     fprintf(output,"                                Error
analysis\n");
     fprintf(output,"
----------------\n");
     fprintf(output,"\n");
     fprintf(output,"  Parameter                     Uncertainty
   Focal Spot Uncertainty\n");
     fprintf(output,"  ---------                     -----------
   ----------------------\n");
     fprintf(output,"\n");
     fprintf(output,"  Statistical\n");
     fprintf(output,"  ------------\n");
     fprintf(output,"\n");
     fprintf(output,"  Wire width                     +/- %4.3f mm
         +/-%6.3f mm\n",swidth,dfspot1);
     fprintf(output,"\n");
     fprintf(output,"  Systematic\n");
     fprintf(output,"  -----------\n");
     fprintf(output,"\n");
     fprintf(output,"  Calib. factor                 +/- %4.3f
mm/pixel         +/-%6.3f mm\n",dscalex,dfspot2);
     fprintf(output,"  Cos(misal.ang)                +/- %5.4f
        +/-%6.3f mm\n",dcos,dfspot3);
     fprintf(output,"  Physical wire width           +/- 0.005 mm
```

```
          +/-%6.3f mm\n",dfspot4);
      fprintf(output,"  Magnification          +/- %4.3f
          +/-%6.3f mm\n",magnerr,dfspot5);
      fprintf(output,"\n");
      fprintf(output,"  Adding the above four errors in
quadrature       +/-%6.3f mm\n",dfspot6);
      fprintf(output,"\n");
      fprintf(output,"  Final result\n");
      fprintf(output,"  ------------\n");
      fprintf(output,"\n");
      fprintf(output,"  Focal spot size is          %6.2f
+/-%5.2f mm (%4.2f
%c)\n",fspot,dfspot7,dfspot7/fspot*100,junk);

      close(output);
      }

   printf("\n");
   printf("%45s",statement33);
   conti = getkey();
   printf("\n");
   }
}

/* ------------------------------------------------------
                Subroutine : Cursorsetting

   Displays the cursor on the image display screen.
   ------------------------------------------------------ */
Cursorsetting()
{

   int answerc,answerd,answere,xcoord,ycoord,value;
   #define statement5 "Do you wish to display cursor (y or
n):"
   #define statement6 "x-coordinate assignment:"
   #define statement7 "y-coordinate assignment:"
   #define statement8 "Are you finished with the cursor (y or
n):"
   #define statement9 "Do you wish to clear previous cursor
position (y or n):"
   #define statement18 "The pixel value at this coordinate
position is:"

   printf("%51s",statement5);
   answerc = getkey();

   if ( answerc == 'y' )
     {
     answerd = 'n';
     while ( answerd == 'n' )
       {
```

```
        printf("\n");
        printf("%36s",statement6);
        scanf("%d",&xcoord);
        printf("%36s",statement7);
        scanf("%d",&ycoord);
        printf("%59s",statement18);

        value = rpixel(xcoord,ycoord);

        printf("%d",value);
        printf("\n");

        dispcurs(xcoord,ycoord,FALSE);

        printf("%54s",statement8);
        answerd = getkey( );
        printf("\n");

        if ( answerd == 'n' )
          {
          printf("%67s",statement9);
          answere = getkey( );

          if ( answere == 'y' )
            clrcurs(xcoord,ycoord);
          }
        }
      }
}

/* ------------------------------------------------------
              Soubroutine : Cursorsetting1

   Displays curser along a horizontal row of pixels, this
   is used when determining the wire width seed and pixel
   calibration constant. The y-coord of the pixels on
   this horizontal row were all set at 250.
   ------------------------------------------------------ */
cursorsetting1( )
{

   int answerc,answerd,answere,xcoord,ycoord,value;

   #define statement5 "Do you wish to display cursor (y or
n):"
   #define statement6 "x-coordinate assignment:"
   #define statement8 "Are you finished with the cursor (y or
n):"
   #define statement9 "Do you wish to clear previous cursor
position (y or n):"
   #define statement18 "The pixel value at this coordinate
position is:"
```

```
    printf( "%51s",statement5);
    answerc = getkey( );

    if ( answerc == 'y' )
      {
      answerd = 'n';
      while ( answerd == 'n' )
        {
        printf( "\n" );
        printf( "%36s",statement6);
        scanf( "%d",&xcoord);
        printf( "%59s",statement18);

        value = rpixel(xcoord,250);

        printf( "%d",value);
        printf( "\n" );

        dispcurs( xcoord,250,FALSE);

        printf( "%54s",statement8);
        answerd = getkey( );
        printf( "\n" );

        if ( answerd == 'n' )
          {
          printf( "%67s",statement9);
          answere = getkey( );

          if ( answere == 'y' )
            clrcurs( xcoord,250);
          }
        }
      }
}

/* ------------------------------------------------------
                Soubroutine : Findcenter

   Finds the center of the wire for a given horizontal
   row of pixels by performing horizontal pixel averaging.
   ------------------------------------------------------ */

Findcenter( xx1,xx2,yy1,cwire,wlimit)
   int *cwire;
{
   int num,ymaxp,countt,pixell1,pixell2,pixell3,pixelll;
   int inc,n,numm,spx;

   num=0;
   ymaxp=0;
```

```
    wlimit = wlimit/2;
    countt = xx1 + wlimit;

    while ( countt <= (xx2-wlimit+1) )
      {
      n = 1;
      numm = 0;
      spx = 0;

      while ( numm < wlimit )
        {
        pixelll=rpixel(countt+numm,yy1);
        spx = spx + pixelll;
        numm = numm + 1;
        n = n +1;
        }

      numm = 1;

      while ( numm < wlimit )
        {
        pixelll=rpixel(countt-numm,yy1);
        spx = spx + pixelll;
        numm = numm + 1;
        n = n +1;
        }

      pixelll = spx/(n-1);

      if ( pixelll > ymaxp )
        {
        ymaxp = pixelll;
        inc = countt ;
        }

      countt = countt + 1;

      }
      *cwire=inc;
}

/* ------------------------------------------------------
              Subroutine : Findwirewidth

   This code will find the FWHM width of the wire for a
   given horizontal row of pixels.
   ------------------------------------------------------ */

Findwirewidth(yy1,wcen,fwhml,fwhmr,climit)
   int *fwhml,*fwhmr;
{
```

```
int numb,min1,min2,pix,pixm,miny1,miny2;
int stop,backyc,height;
float slope;
int numb1,numb2,min1a,min2a;

min1 = 0;
min2 = 0;

numb1 = climit/2;                    /* Finds left minimum */
pixm = rpixel(wcen,yy1);

stop = 0;
while ( stop == 0 )
  {
  pix = rpixel(wcen - numb1,yy1);
  if ( pix <= pixm )
    {
    min1 = wcen - numb1;
    pixm = pix;
    }
  else
    {
    stop = 1;
    }
  numb1 = numb1 +1;
  }

numb2 = climit/2;                    /* Finds right minimum */
pixm = rpixel(wcen,yy1);
stop = 0;
while ( stop == 0 )
  {
  pix = rpixel(wcen + numb2,yy1);
  if ( pix <= pixm )
    {
    min2 = wcen + numb2;
    pixm = pix;
    }
  else
    {
    stop = 1;
    }
  numb2 = numb2 +1;
  }

miny1 = rpixel(min1,yy1);
miny2 = rpixel(min2,yy1);

slope = (miny2 - miny1)/(min2 - min1);
backyc = slope*(wcen - min1) + miny1;
height = rpixel(wcen,yy1) -backyc;
height = height/2;
```

```
    height = rpixel(wcen,yy1) - height;

    numb = 1;                    /* Finds left FWHM point */
    pixm = height;
    stop = 0;
    while ( stop == 0 )
      {
      pix = rpixel(wcen - numb,yy1);
      if ( pix >= pixm)
        {
        min1 = wcen - numb;
        }
      else
        {
        stop = 1;
        }
      numb = numb +1;
      }

    numb = 1;                    /* Finds right FWHM point */
    stop = 0;
    while ( stop == 0 )
      {
      pix = rpixel(wcen + numb,yy1);
      if ( pix >= pixm )
        {
        min2 = wcen + numb;
        }
      else
        {
        stop = 1;
        }
      numb = numb +1;
      }

    *fwhml = min1;
    *fwhmr = min2;
  }

/* ------------------------------------------------------
                Subroutine : Storepixelline

    This code stores the pixel values of a horizontal line of
    pixels in a specified data file.
    ------------------------------------------------------ */

Storepixelline(a1,a2,a3)
{
  FILE *fname;
  char datafile[20];
  int number,pix;
```

```
  #define statement12 "Which data file (xx.dat) do you wish
to use:"

  printf("%56s",statement12);
  scanf("%s",datafile);
  printf("\n");

  fname = fopen(datafile,"w");

  number = a1;
  while ( number <= a2 )
    {
    pix = rpixel(number,a3);
    fprintf(fname," %d %d %d\n",number,a3,pix);
    number = number+1;
    }

  close(fname);
}

/* ------------------------------------------------------
                Subroutine : Storepixeldif

   This code stores the differences in the pixels of a
   given horizontal line of pixels in a specified data file.
   ------------------------------------------------------ */

Storepixeldif(b1,b2,b3)
{
  FILE *enter;
  char datadif[20];
  int numbers,pixdif,pix;

  #define statement12 "Which data file (xx.dat) do you wish
to use:"

  printf("%56s",statement12);
  scanf("%s",datadif);
  printf("\n");
  enter = fopen(datadif,"w");
  numbers = b1+1;
  while ( numbers <= b2 )
    {
    pix = rpixel(numbers,b3);
    pixdif = rpixel(numbers,b3) - rpixel(numbers-1,b3);
    fprintf(enter," %d %d %d %d\n",numbers,b3,pixdif,pix);
    numbers = numbers+1;
    }
  close(enter);
}
                /*    End of program    */
```

APPENDIX F

FOCAL SPOT CALCULATION WHEN USING PARALLEL WIRE TEST TOOL

The geometric representation of the parallel wire test tool image on film has been illustrated below.

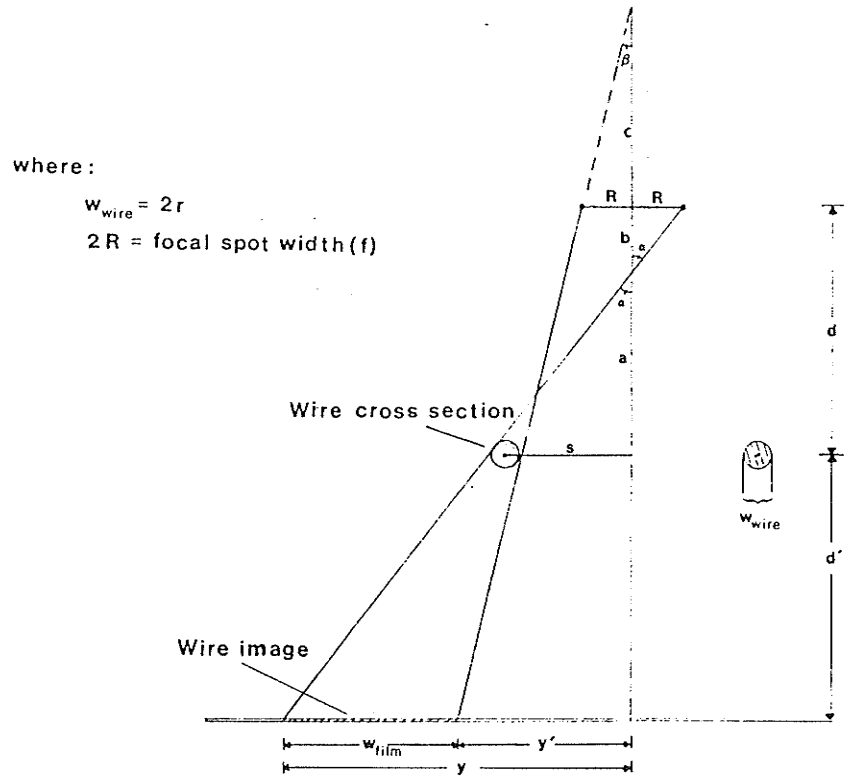

Before the above figure is used to derive the focal spot dimensions, the variable definitions will be made here:

R is the radius of the focal spot;
f is the width of the focal spot;
d is the test tool's object distance;
d'is the test tool's image distance;
s is the distance from the central x-ray beam axis to the wire center on the test tool;
r is the physical radius of the wires;
w_{wire} is the physical width of the wires; and
w_{film} is the wire image's width on film.

It should be noted here that the focal spot dimensions, f,

are assumed to be symmetric and that the focal spot is assumed to behave as two point sources that have a separation distance of f.

From the above figure it can be shown that

$$\tan(\alpha) = \frac{R}{b} = \frac{(s + r)}{a} = \frac{y}{(d' + a)} \quad . \tag{F1}$$

It can then be shown from [Eq. F1] that

$$y = \frac{(s + r)\cdot(d' + a)}{a} \tag{F2}$$

and

$$\frac{R}{(s + r)} = \frac{b}{a} \quad . \tag{F3}$$

Now since

$$d = a + b$$

we then can show that

$$\frac{d}{a} = 1 + \frac{b}{a}$$

$$= \frac{s + r + R}{s + r} \tag{F4}$$

after the substitution of [Eq. F3]. Rearranging [Eq. F4] into the form

$$a = \frac{d\cdot(s + r)}{s + r + R} \tag{F5}$$

and then substituting this expression into [Eq. F2] allows one to rewrite [Eq. F2] as

$$y = \frac{d' \cdot (s + r + R) + (s + r)}{d} \quad . \qquad (F6)$$

From the above figure it can also be shown that

$$\tan(\beta) = \frac{R}{c} = \frac{(s - r)}{(d + c)} = \frac{y'}{(d' + d + c)} \quad . \qquad (F7)$$

From [Eq. F7] we then have the relations

$$y' = \frac{(s - r) \cdot (d' + d + c)}{(d + c)} \qquad (F8)$$

and

$$\frac{R}{(s - r)} = \frac{c}{(d + c)} \quad . \qquad (F9)$$

Rearrange [Eq. F9] into the form

$$c = \frac{R \cdot d}{(s - R - r)} \qquad (F10)$$

and then substituting this expression into [Eq. F8] we can show that

$$y' = \frac{(d' + d) \cdot s - (d' + d) \cdot r - d'R}{d} \quad . \qquad (F11)$$

Because the width of the wires image on film is shown to be

$$w_{film} = y - y' \qquad (F12)$$

in the above figure, then after the substitution of [Eq. F6] and [Eq. F11] into [Eq. F12], we can show that

$$w_{film} = \frac{2r \cdot (d + d')}{d} + \frac{2Rd'}{d} \quad . \qquad (F13)$$

Since we have defined

$$w_{wire} = 2r \qquad (F14)$$

and

$$f = 2R \tag{F15}$$

then after the substitution of [Eq. F14] and [Eq. F15] into [Eq. F13] we can solve for the width of the focal spot, which is

$$f = w_{film} \cdot \frac{d}{d'} + w_{wire} \cdot 1 + \frac{d}{d'} \quad . \tag{F16}$$

Because the geometric magnification of the test tool is

$$M = 1 + \frac{d'}{d} \tag{F17}$$

and thus

$$\frac{d}{d'} = \frac{1}{(M - 1)} \tag{F18}$$

we can then substitute [Eq. F18] into [Eq. F16] to express the focal spot dimensions as

$$f = \frac{w_{film} - w_{wire} \cdot M}{(M - 1)} \quad . \tag{F19}$$

APPENDIX G

BAR RESOLUTION PATTERN COMPARISON RESULT

G.a Results from test run 1

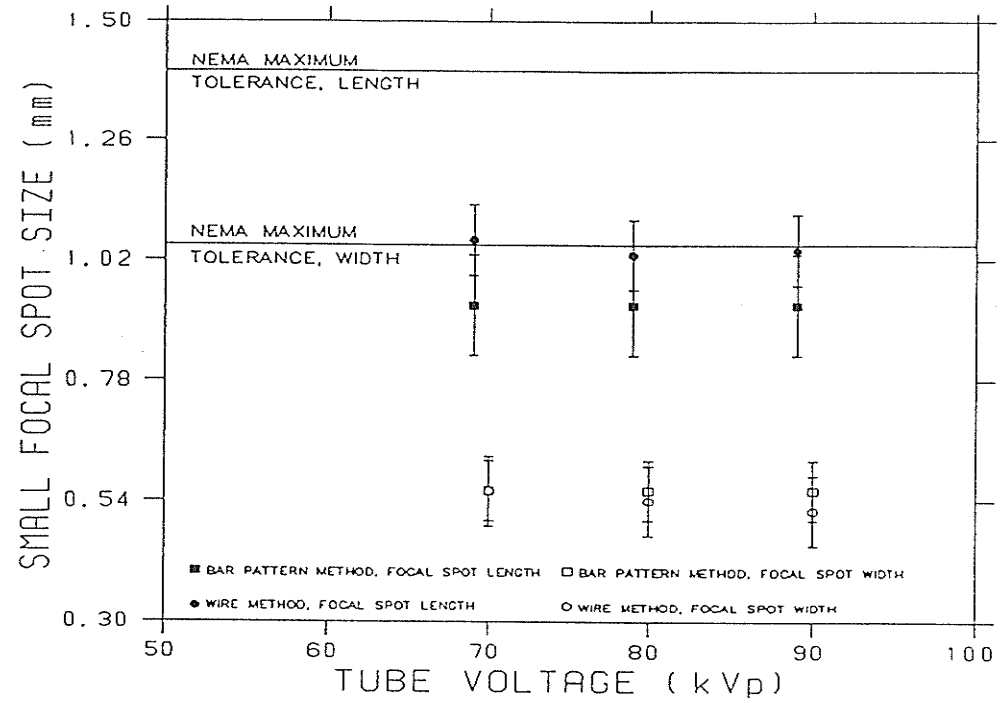

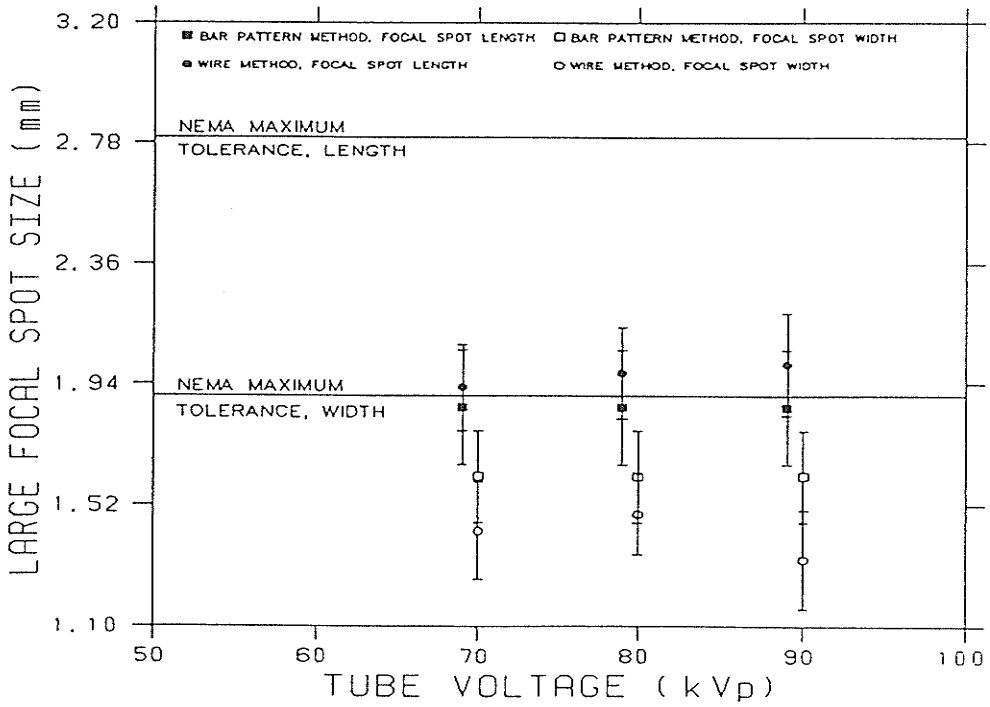

G.b Results from test run 2

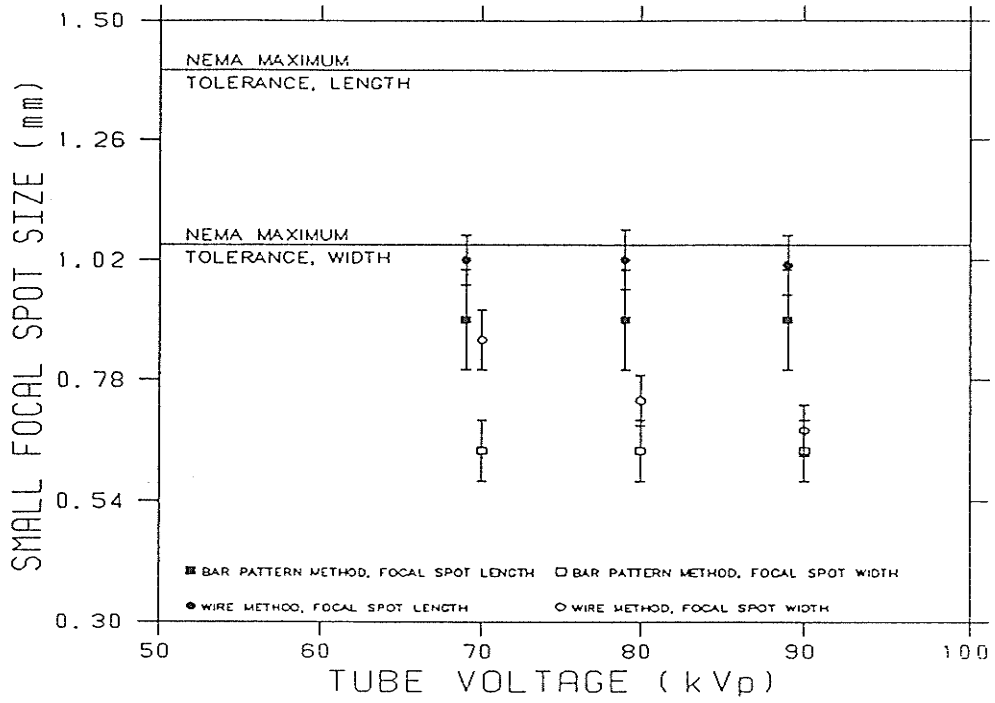

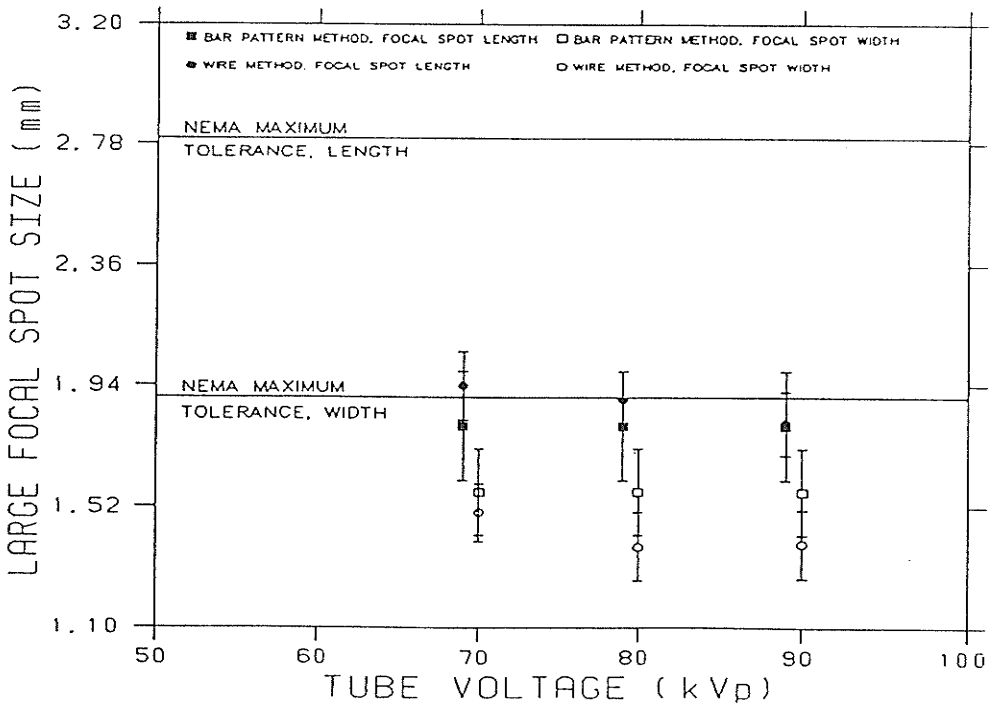

G.c Results from test run 3

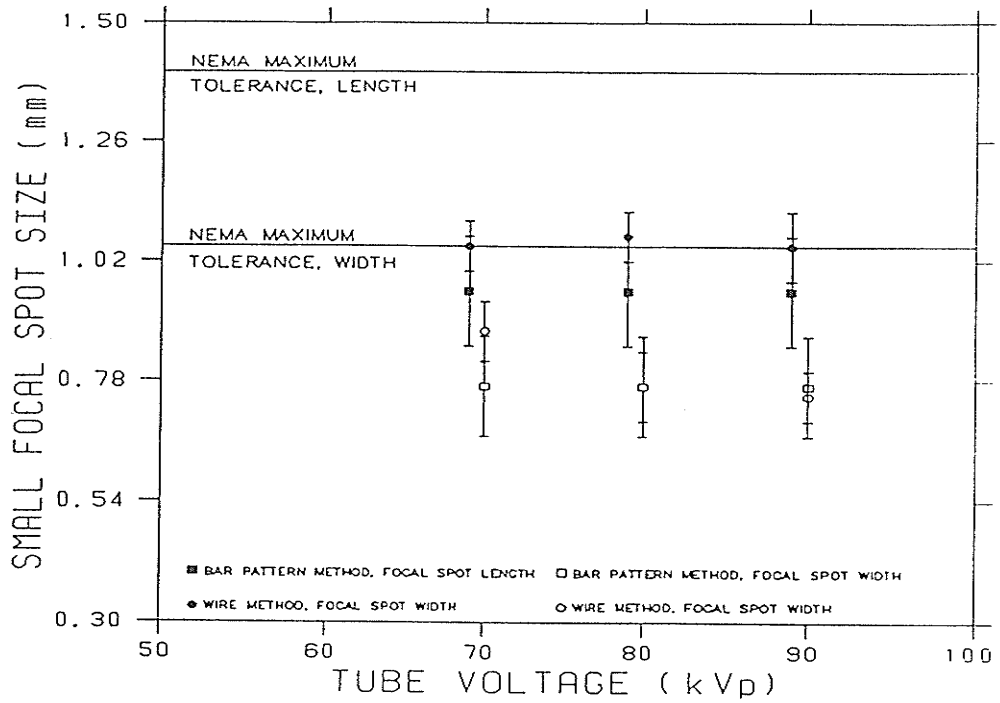

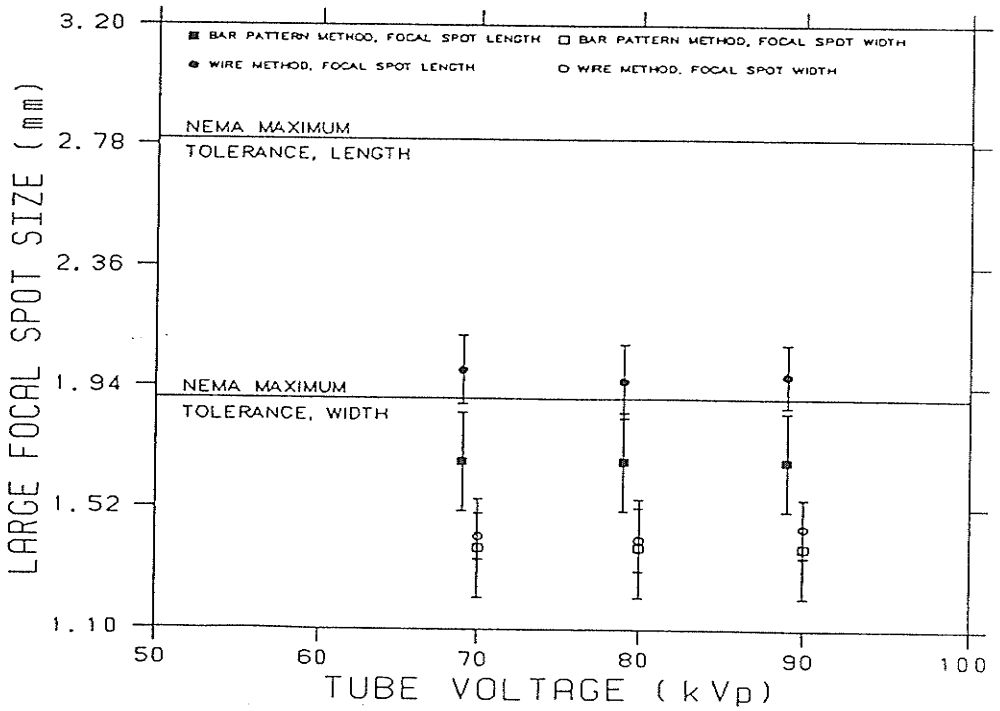

G.d Results from test run 4

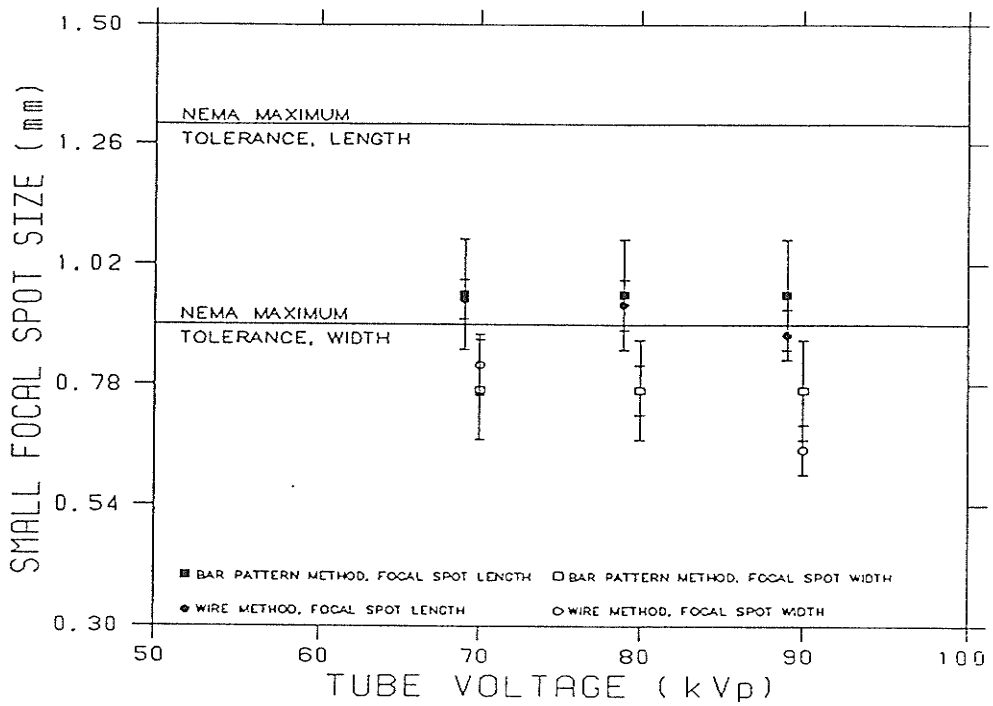

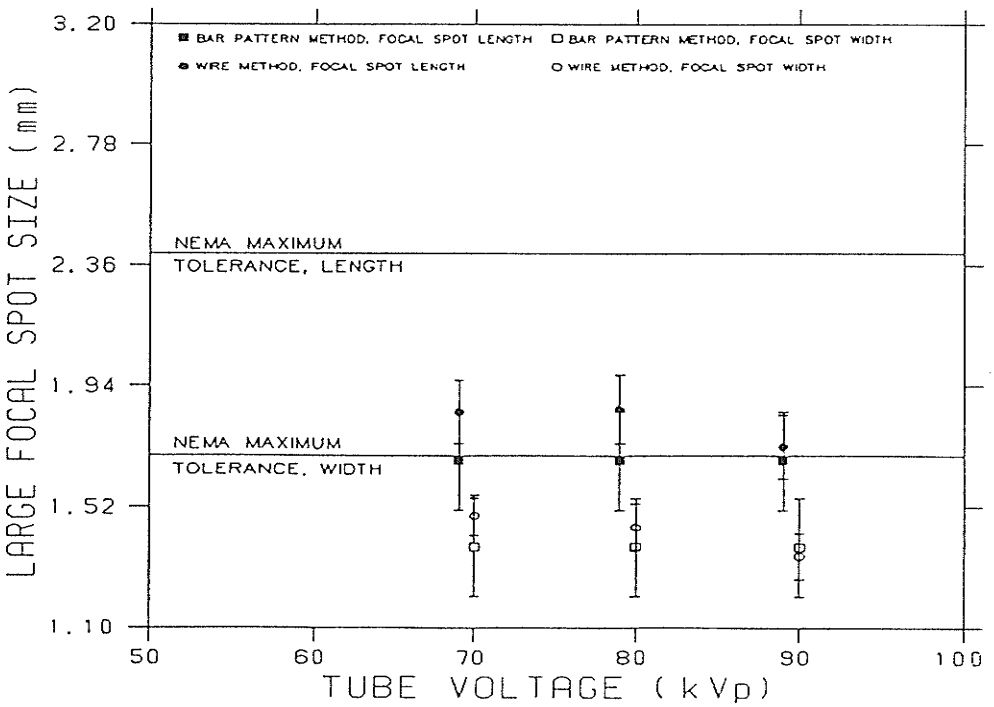

G.e Results from test run 5

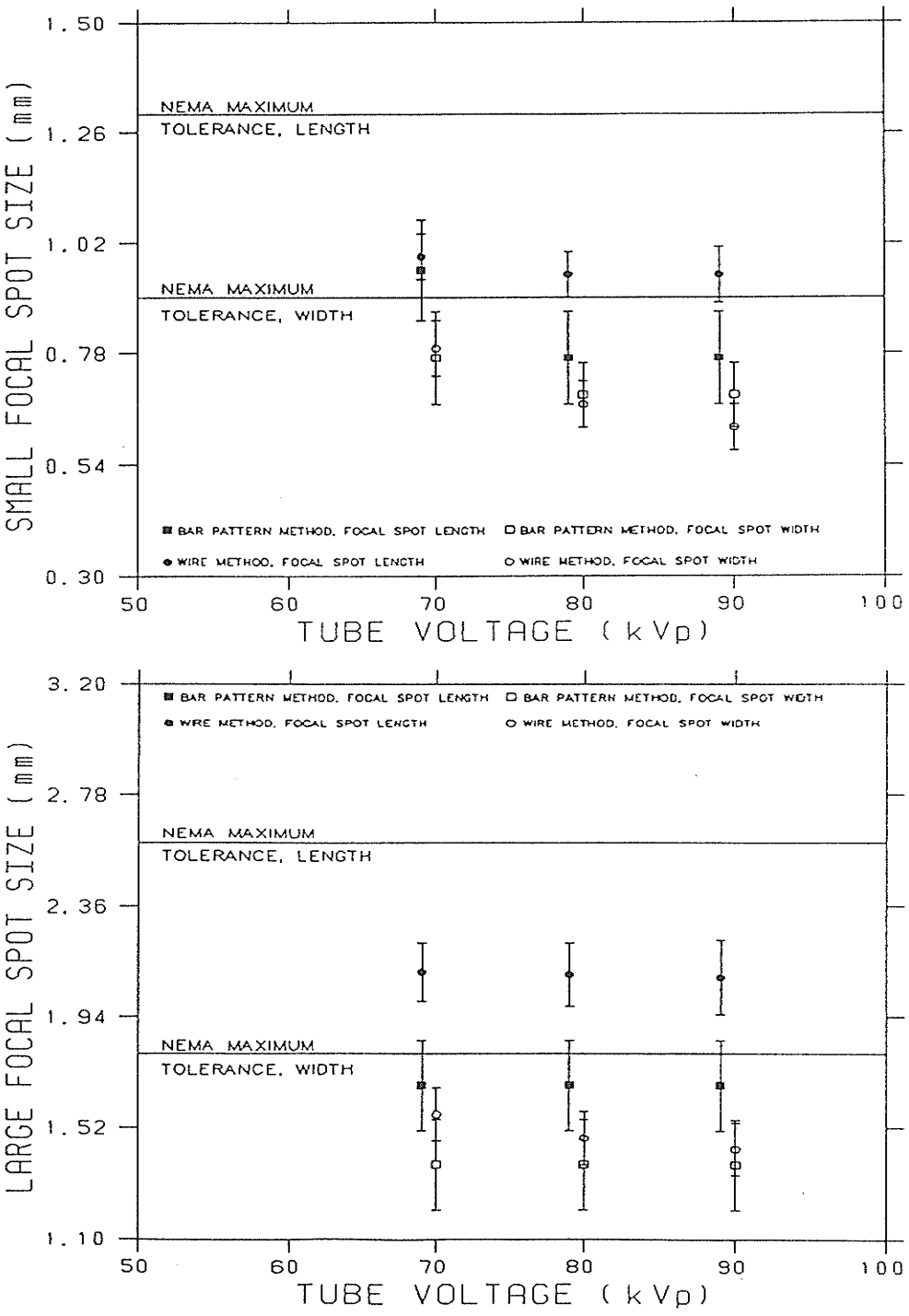

G.f Results from test run 6

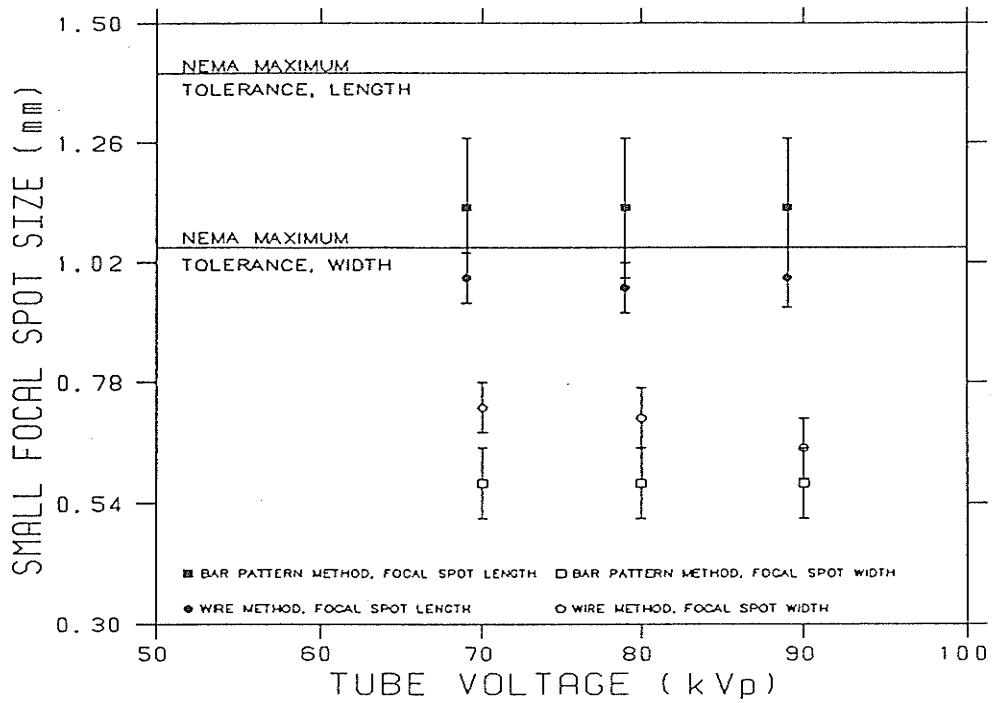

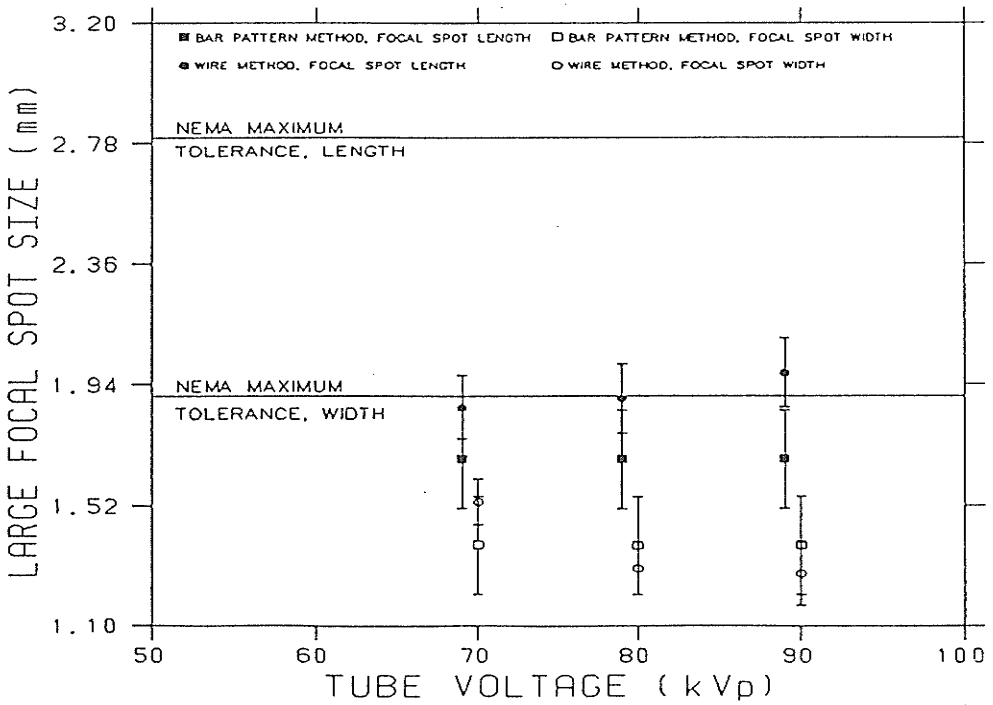

G.g Results from test run 7

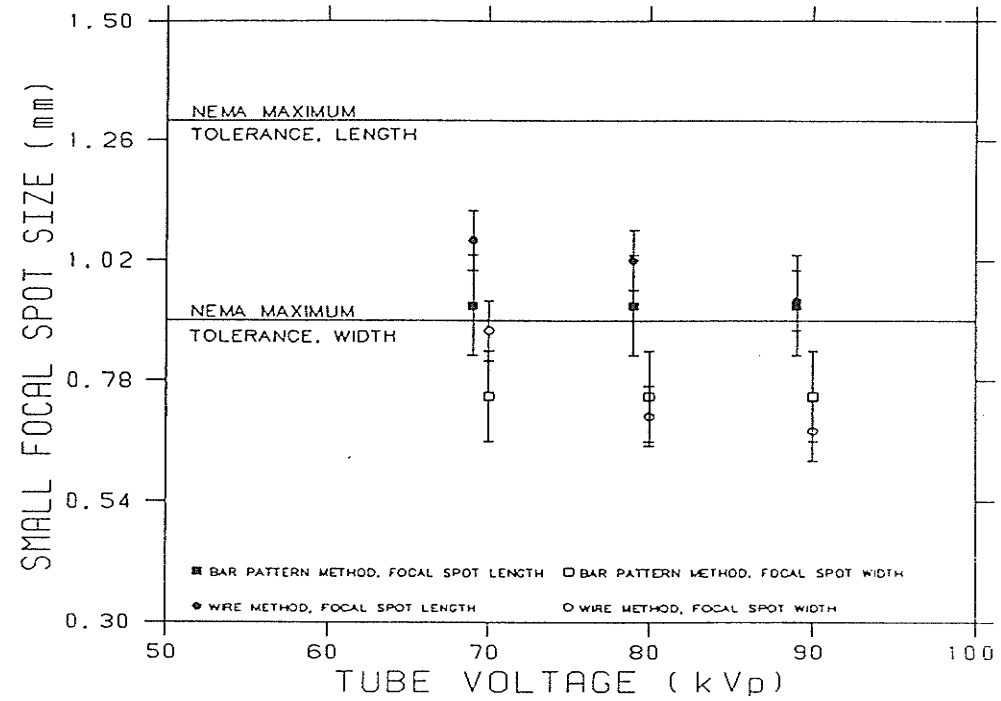

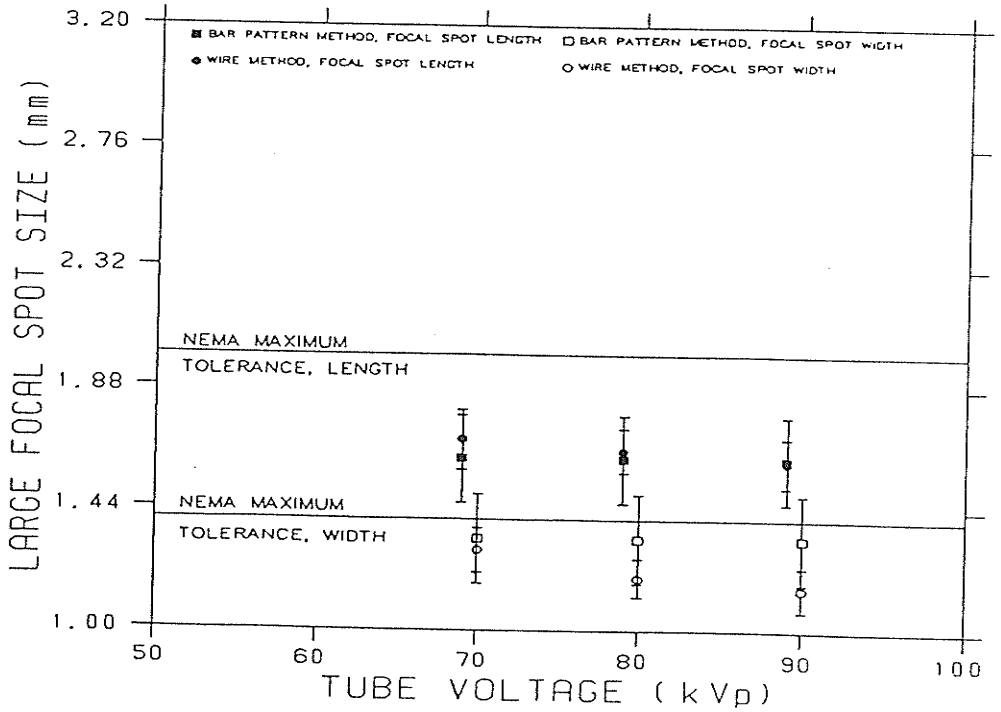

APPENDIX H

STAR RESOLUTION PATTERN COMPARISON RESULTS

H.a Results from test run 1

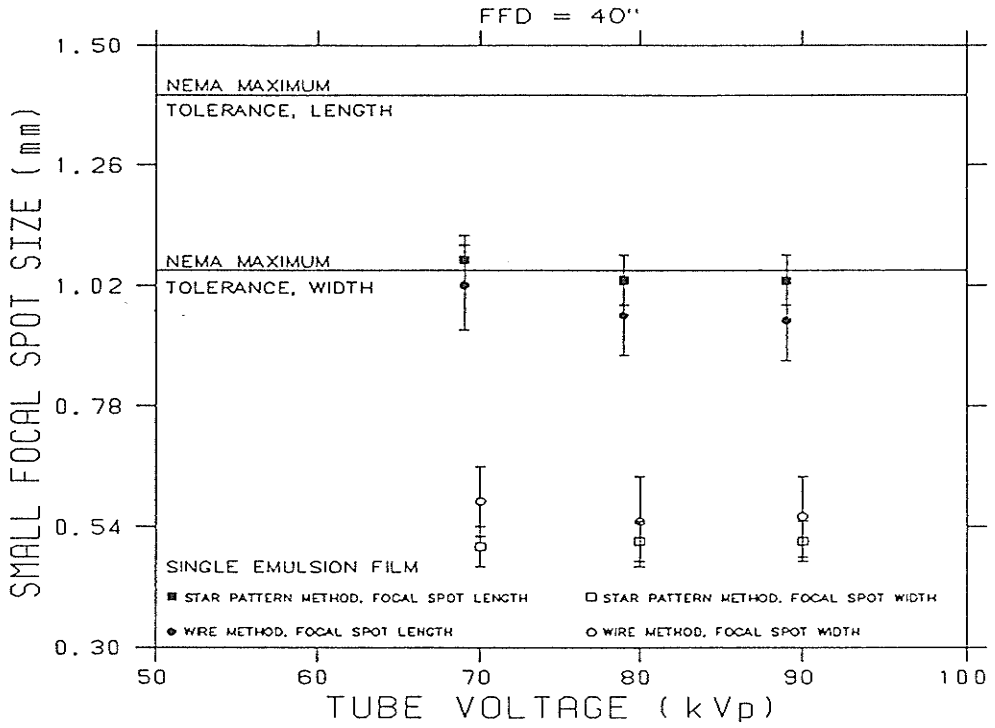

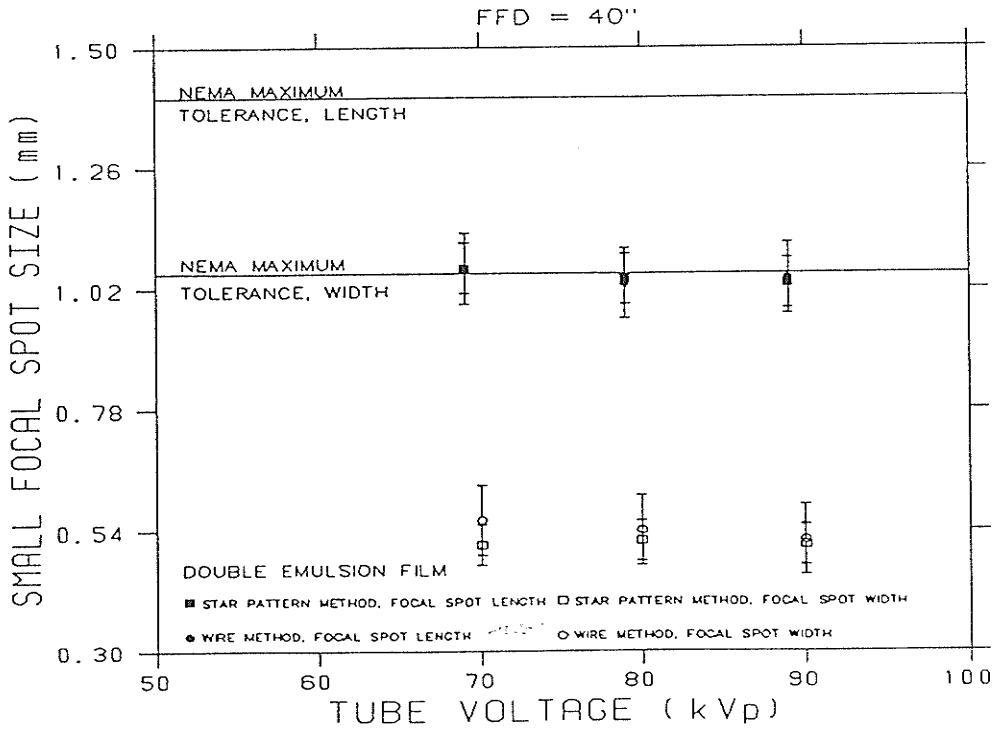

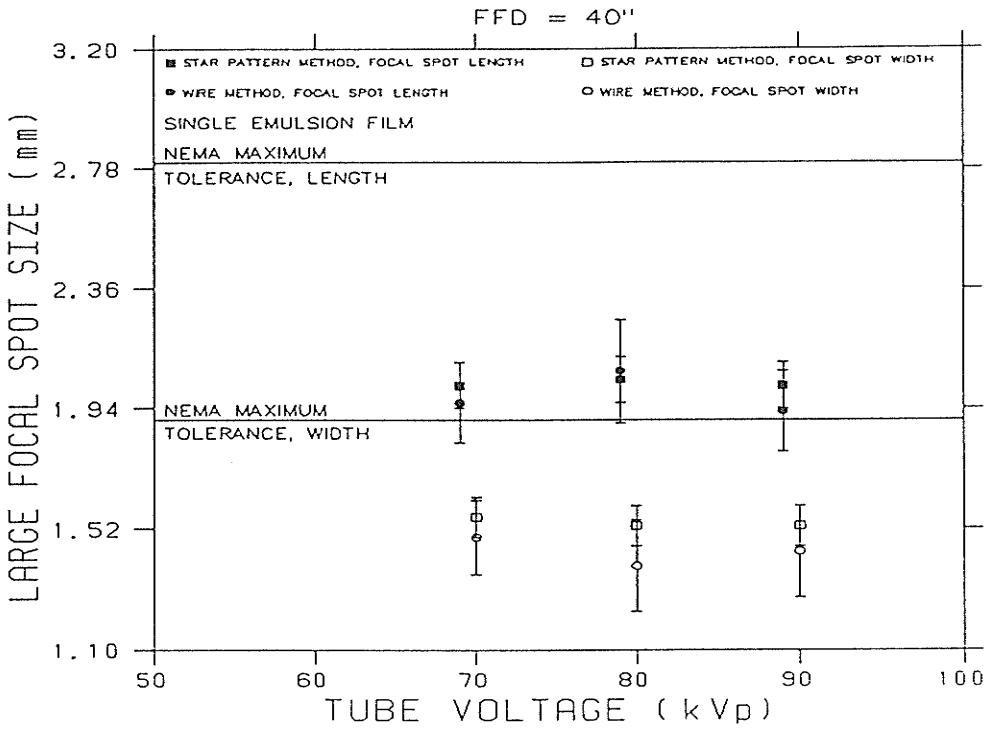
FFD = 40"
STAR PATTERN METHOD, FOCAL SPOT LENGTH
STAR PATTERN METHOD, FOCAL SPOT WIDTH
WIRE METHOD, FOCAL SPOT LENGTH
WIRE METHOD, FOCAL SPOT WIDTH
SINGLE EMULSION FILM
NEMA MAXIMUM
TOLERANCE, LENGTH
NEMA MAXIMUM
TOLERANCE, WIDTH
LARGE FOCAL SPOT SIZE (mm)
3.20
2.78
2.36
1.94
1.52
1.10
50
60
70
80
90
100
TUBE VOLTAGE (kVp)

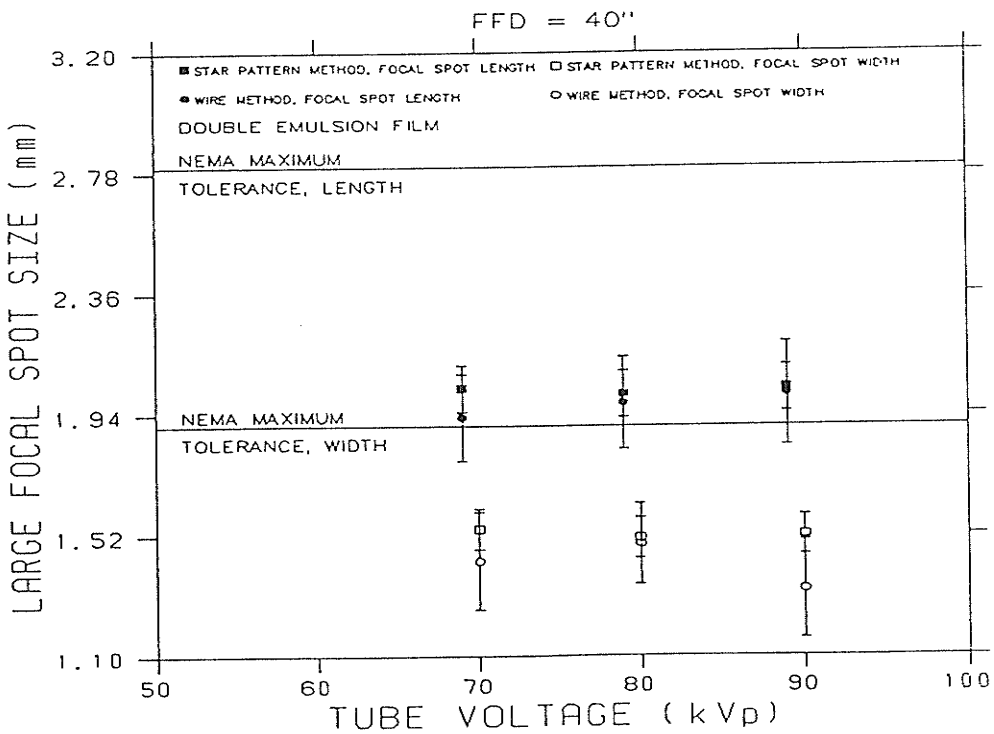
FFD = 40"
STAR PATTERN METHOD, FOCAL SPOT LENGTH
STAR PATTERN METHOD, FOCAL SPOT WIDTH
WIRE METHOD, FOCAL SPOT LENGTH
WIRE METHOD, FOCAL SPOT WIDTH
DOUBLE EMULSION FILM
NEMA MAXIMUM
TOLERANCE, LENGTH
NEMA MAXIMUM
TOLERANCE, WIDTH
LARGE FOCAL SPOT SIZE (mm)
3.20
2.78
2.36
1.94
1.52
1.10
50
60
70
80
90
100
TUBE VOLTAGE (kVp)

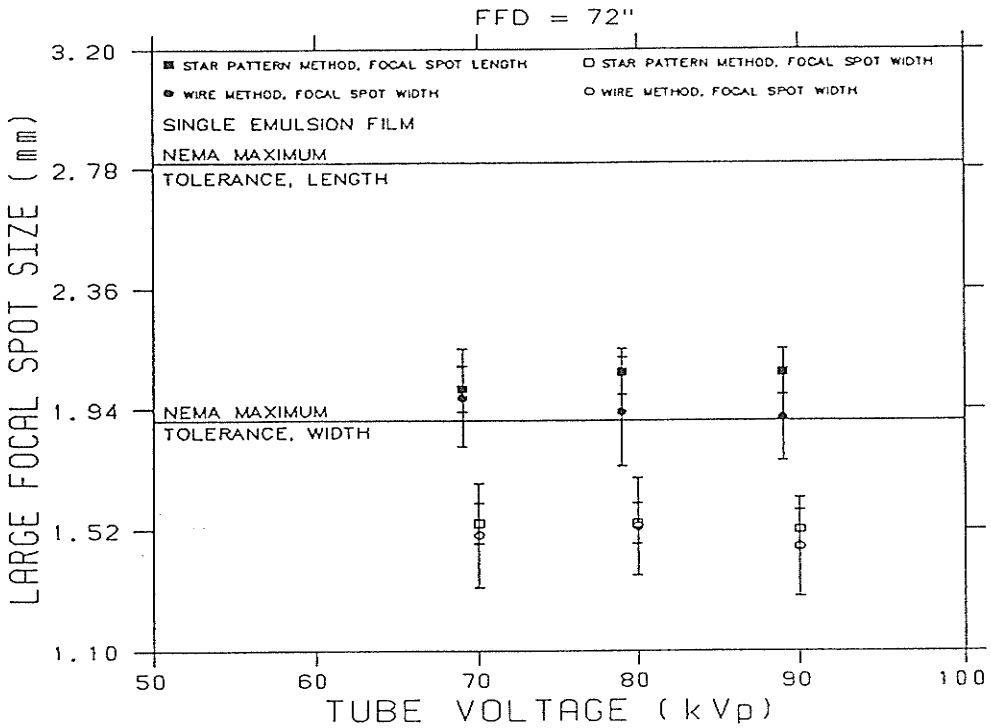
FFD = 72"
STAR PATTERN METHOD, FOCAL SPOT LENGTH
STAR PATTERN METHOD, FOCAL SPOT WIDTH
WIRE METHOD, FOCAL SPOT WIDTH
WIRE METHOD, FOCAL SPOT WIDTH
SINGLE EMULSION FILM
NEMA MAXIMUM
TOLERANCE, LENGTH
NEMA MAXIMUM
TOLERANCE, WIDTH
LARGE FOCAL SPOT SIZE (mm)
3.20
2.78
2.36
1.94
1.52
1.10
50
60
70
80
90
100
TUBE VOLTAGE (kVp)

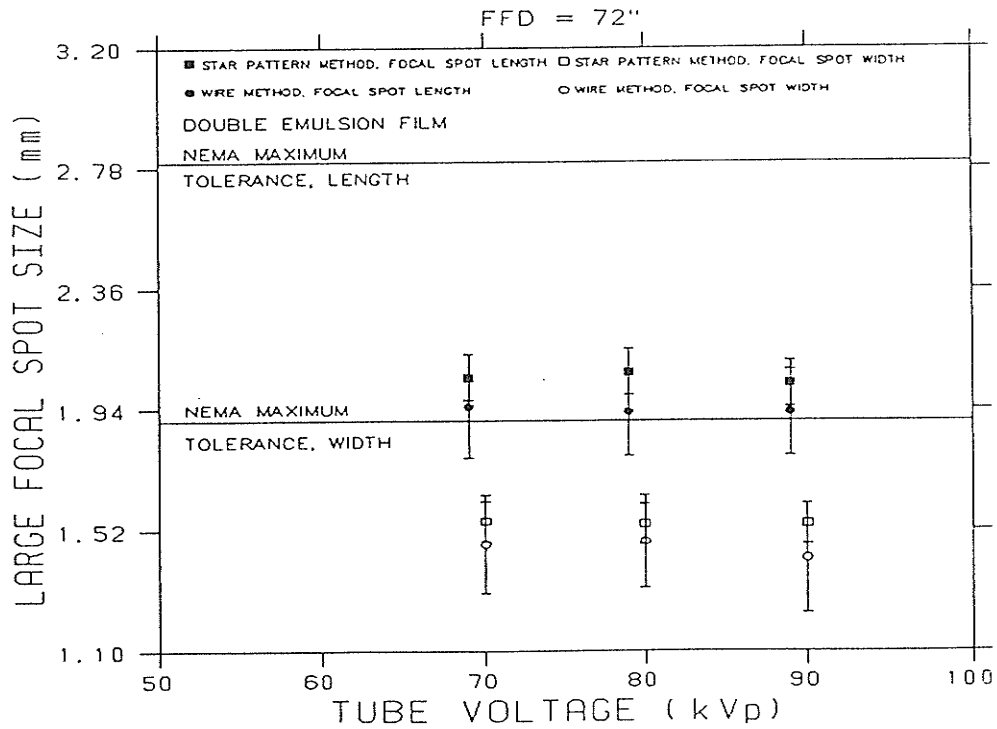
FFD = 72"
STAR PATTERN METHOD, FOCAL SPOT LENGTH
STAR PATTERN METHOD, FOCAL SPOT WIDTH
WIRE METHOD, FOCAL SPOT LENGTH
WIRE METHOD, FOCAL SPOT WIDTH
DOUBLE EMULSION FILM
NEMA MAXIMUM
TOLERANCE, LENGTH
NEMA MAXIMUM
TOLERANCE, WIDTH
LARGE FOCAL SPOT SIZE (mm)
3.20
2.78
2.36
1.94
1.52
1.10
50
60
70
80
90
100
TUBE VOLTAGE (kVp)

H.b Results from test run 2

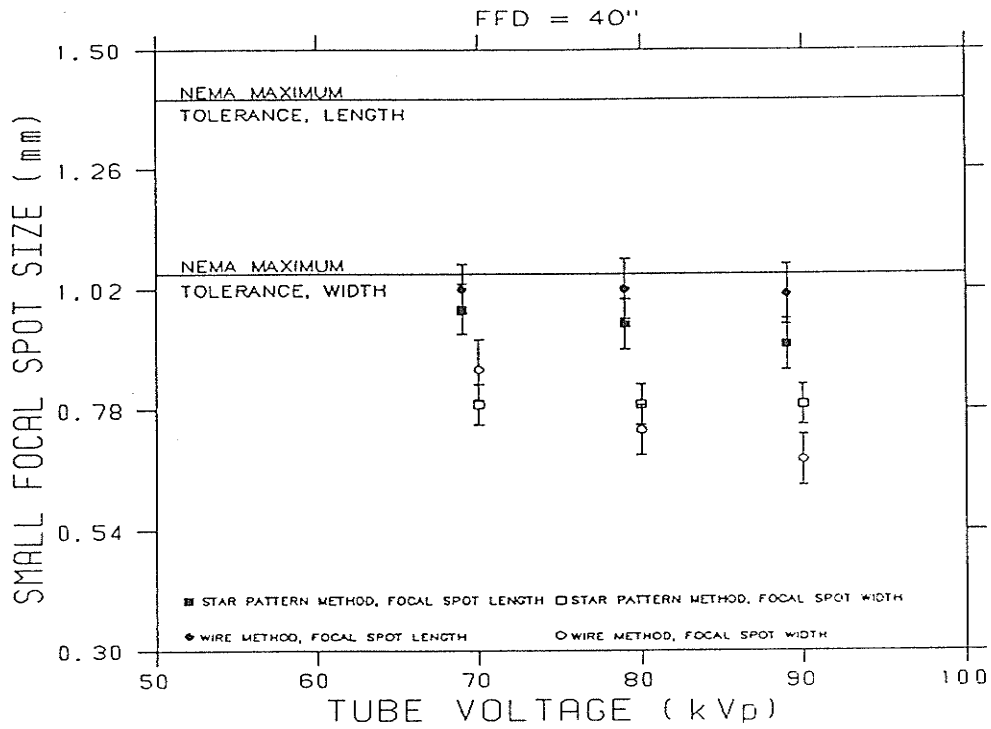

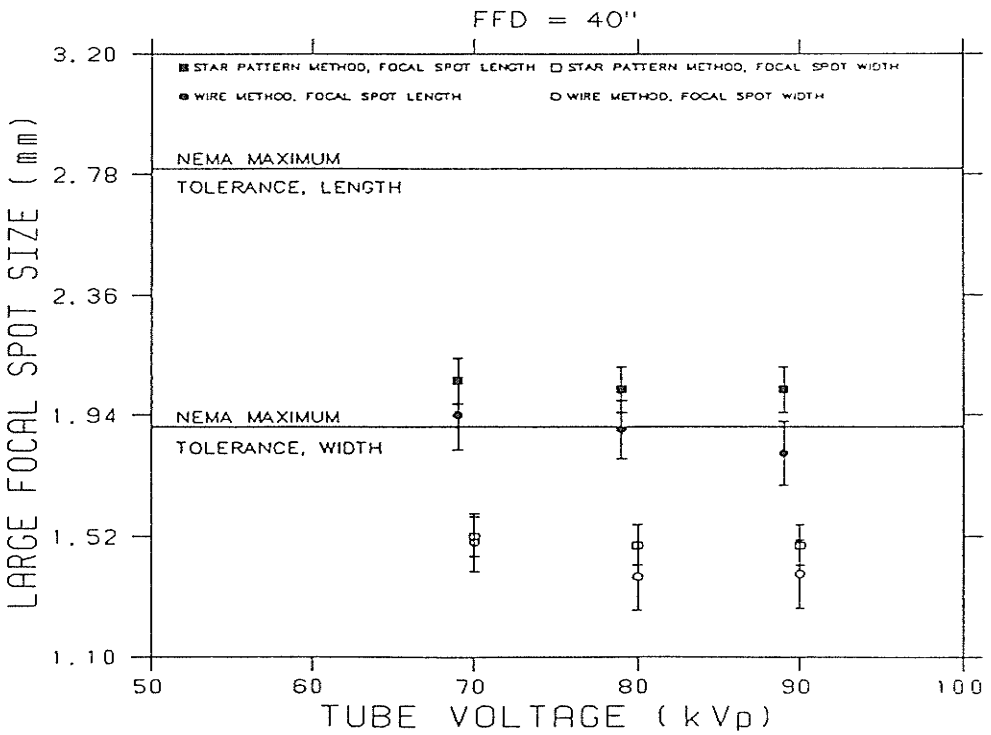

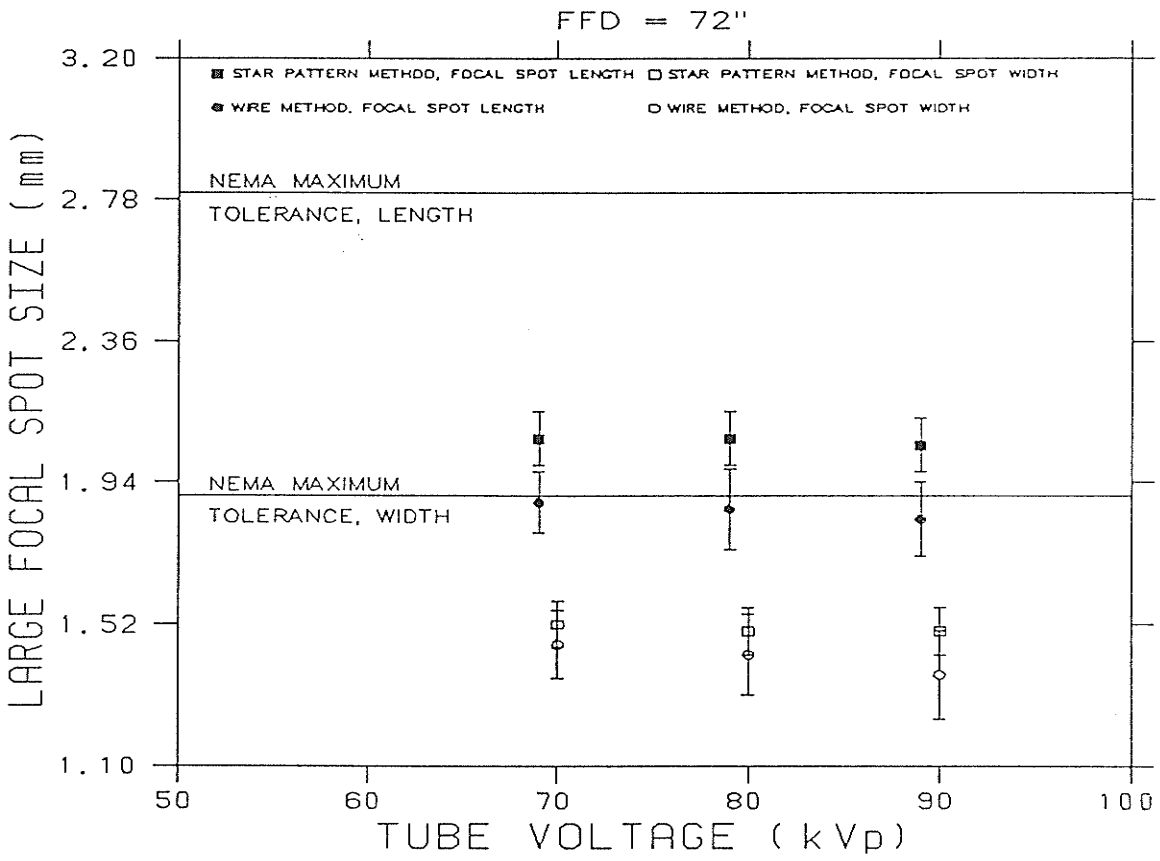
FFD = 72"
STAR PATTERN METHOD, FOCAL SPOT LENGTH
STAR PATTERN METHOD, FOCAL SPOT WIDTH
WIRE METHOD, FOCAL SPOT LENGTH
WIRE METHOD, FOCAL SPOT WIDTH
NEMA MAXIMUM
TOLERANCE, LENGTH
NEMA MAXIMUM
TOLERANCE, WIDTH
LARGE FOCAL SPOT SIZE (mm)
3.20
2.78
2.36
1.94
1.52
1.10
50
60
70
80
90
100
TUBE VOLTAGE (kVp)

H.c Results from test run 3

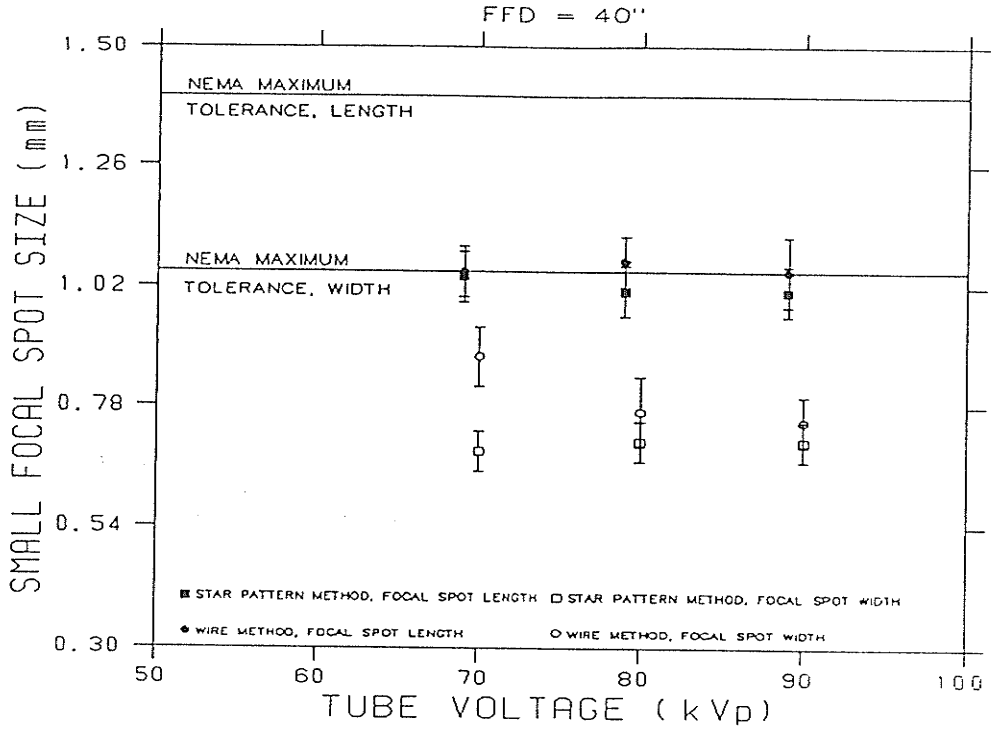

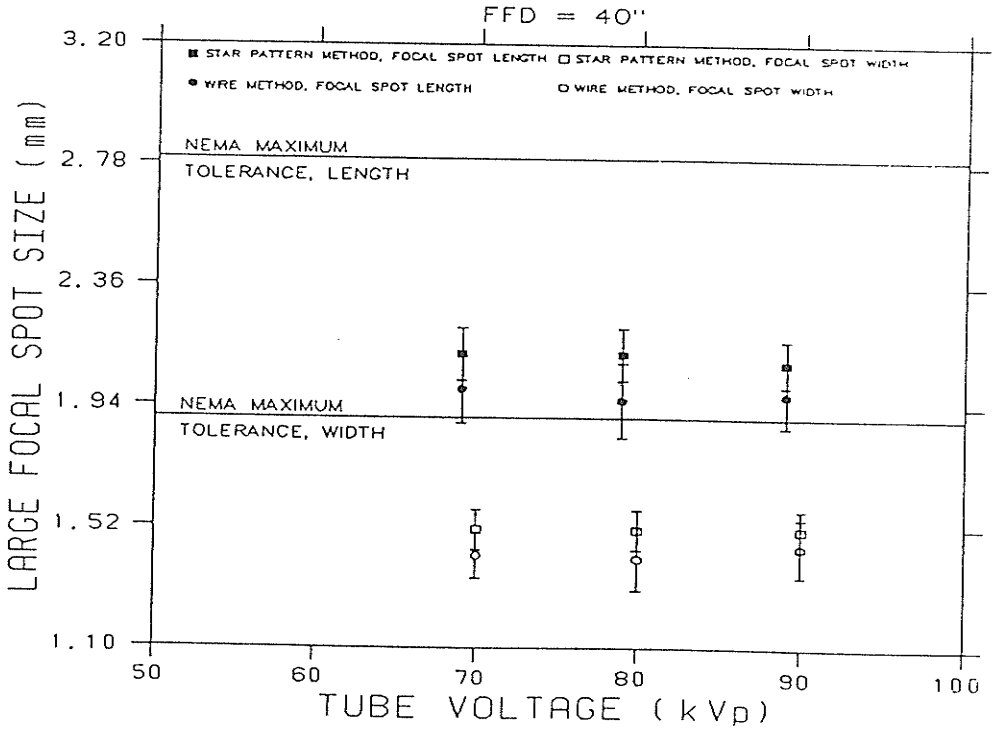

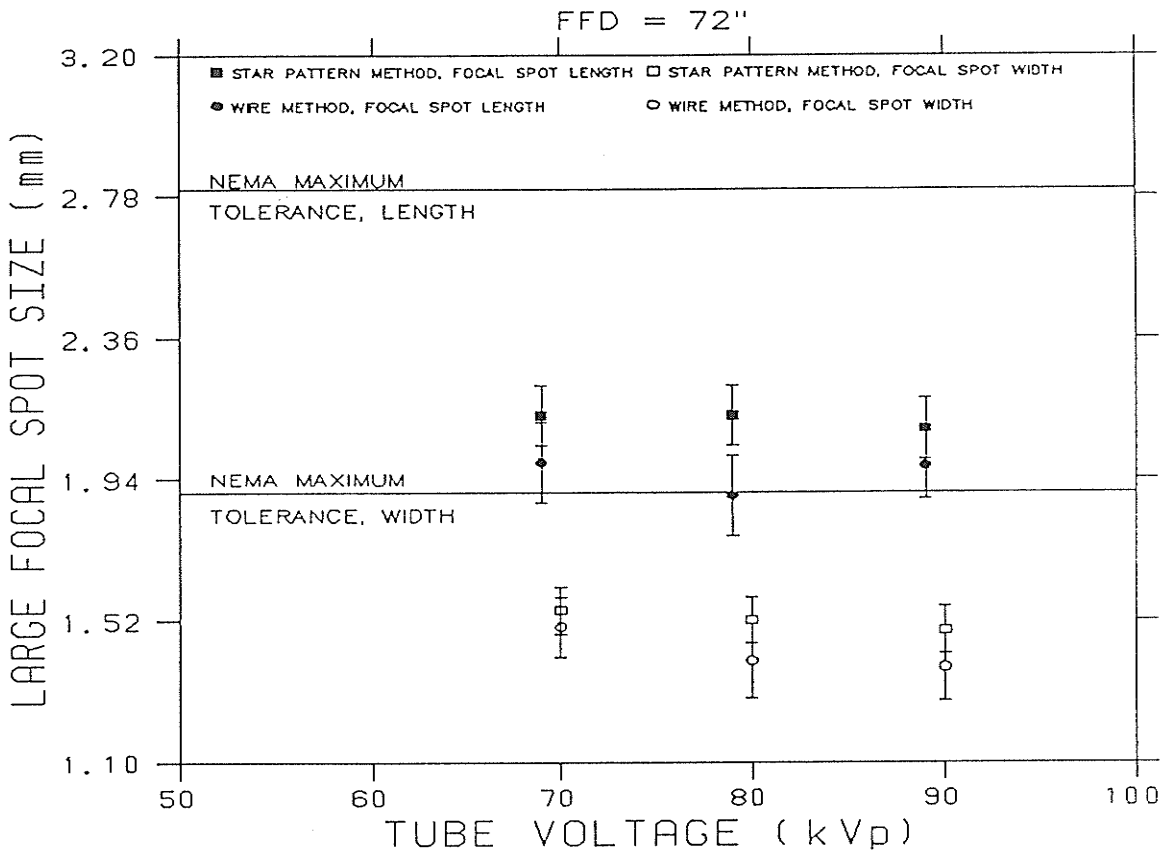
FFD = 72"
STAR PATTERN METHOD, FOCAL SPOT LENGTH
STAR PATTERN METHOD, FOCAL SPOT WIDTH
WIRE METHOD, FOCAL SPOT LENGTH
WIRE METHOD, FOCAL SPOT WIDTH
NEMA MAXIMUM
TOLERANCE, LENGTH
NEMA MAXIMUM
TOLERANCE, WIDTH
LARGE FOCAL SPOT SIZE (mm)
3.20
2.78
2.36
1.94
1.52
1.10
50
60
70
80
90
100
TUBE VOLTAGE (kVp)

H.d Results from test run 4

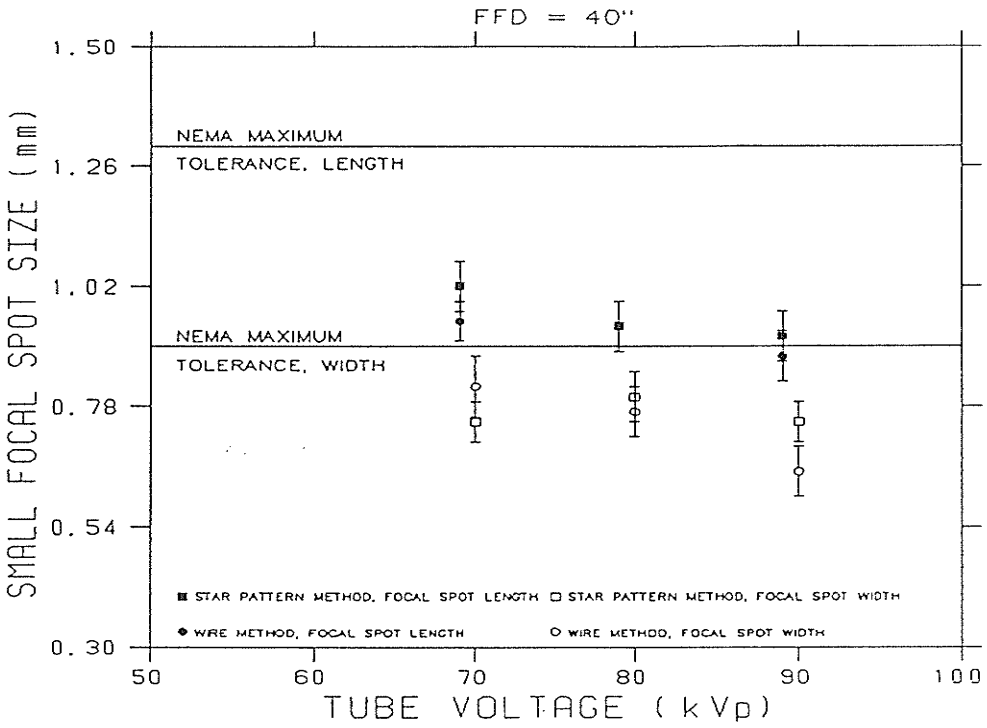

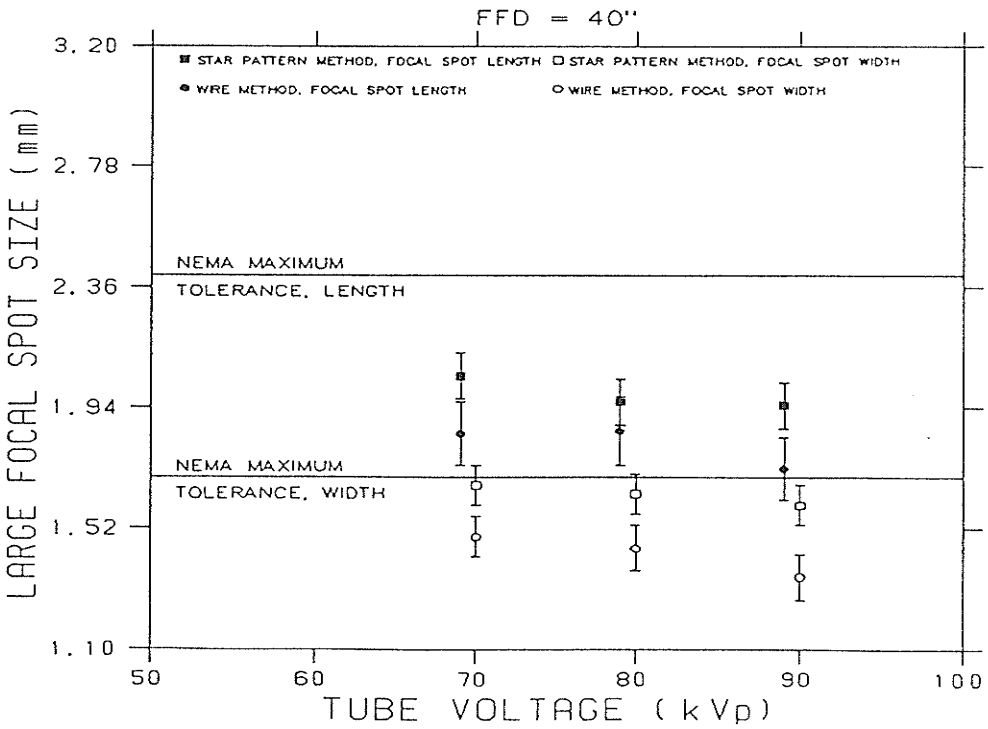

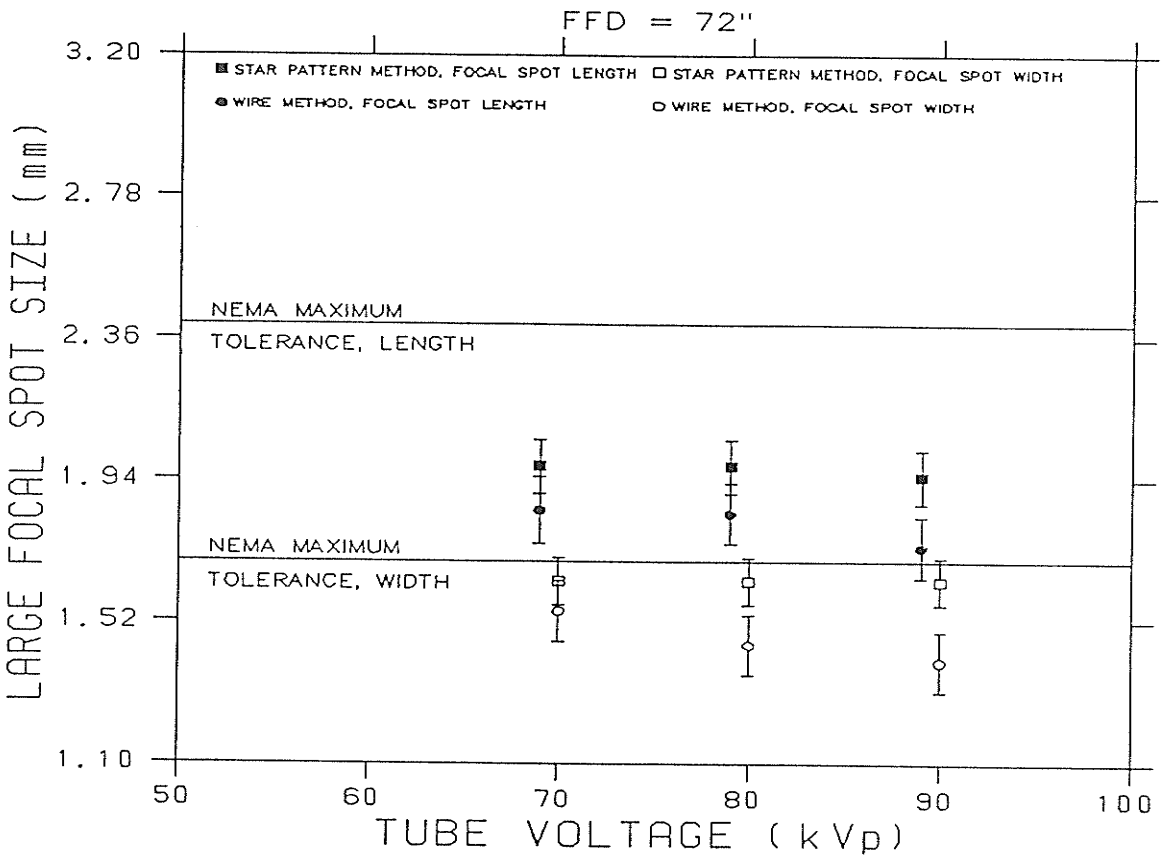
FFD = 72"
STAR PATTERN METHOD, FOCAL SPOT LENGTH
STAR PATTERN METHOD, FOCAL SPOT WIDTH
WIRE METHOD, FOCAL SPOT LENGTH
WIRE METHOD, FOCAL SPOT WIDTH
NEMA MAXIMUM TOLERANCE, LENGTH
NEMA MAXIMUM TOLERANCE, WIDTH
LARGE FOCAL SPOT SIZE (mm)
3.20
2.78
2.36
1.94
1.52
1.10
50
60
70
80
90
100
TUBE VOLTAGE (kVp)

H.f Results from test run 5

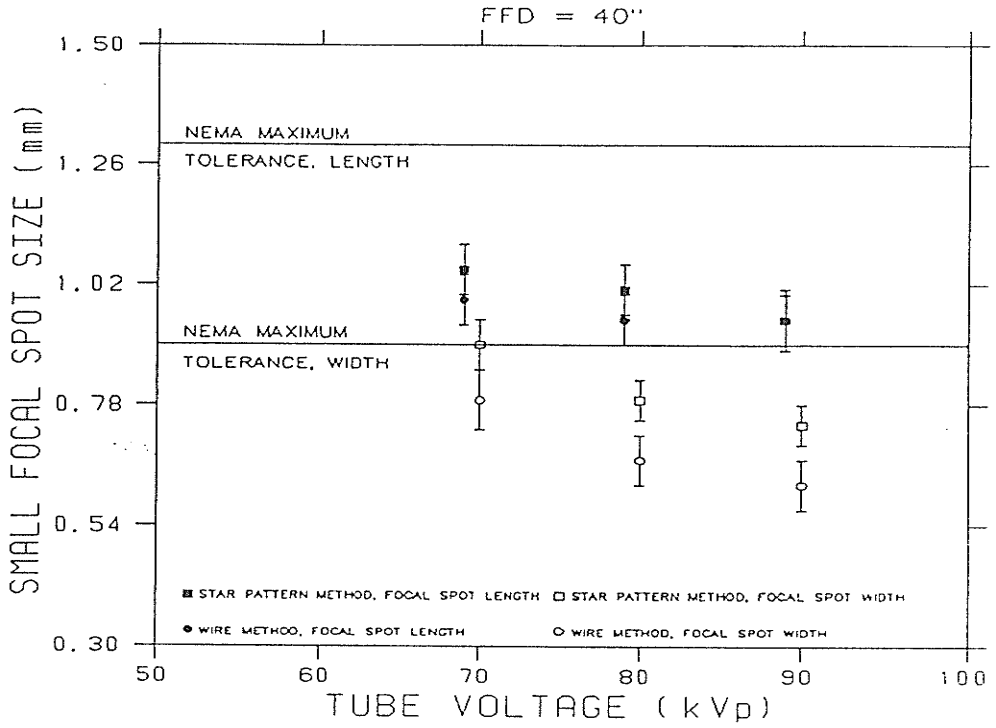

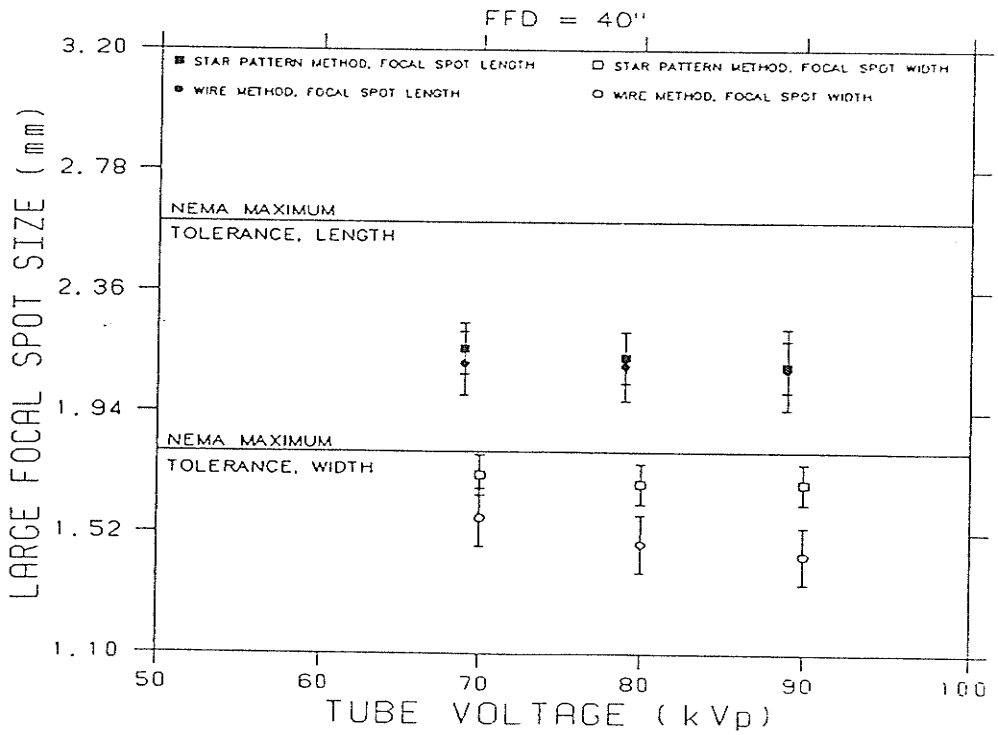

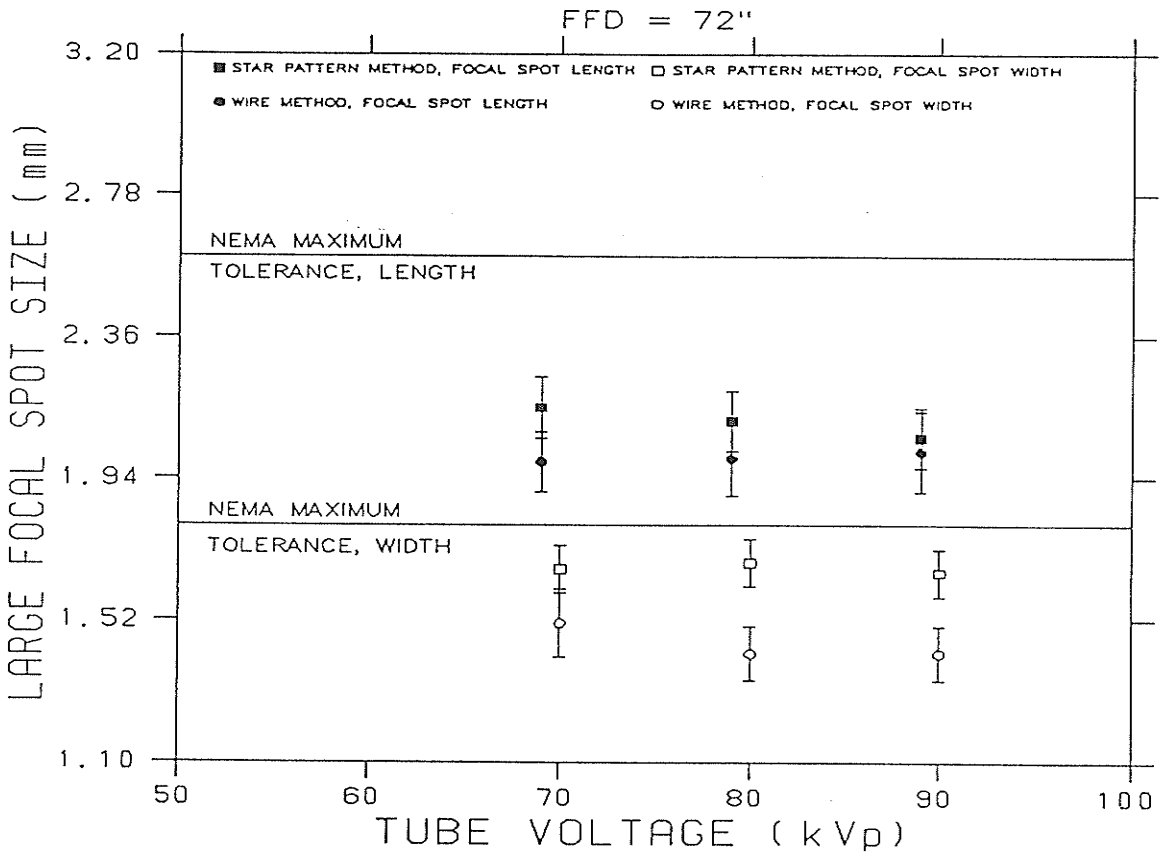
FFD = 72"
STAR PATTERN METHOD, FOCAL SPOT LENGTH
STAR PATTERN METHOD, FOCAL SPOT WIDTH
WIRE METHOD, FOCAL SPOT LENGTH
WIRE METHOD, FOCAL SPOT WIDTH
NEMA MAXIMUM TOLERANCE, LENGTH
NEMA MAXIMUM TOLERANCE, WIDTH
LARGE FOCAL SPOT SIZE (mm)
3.20
2.78
2.36
1.94
1.52
1.10
50
60
70
80
90
100
TUBE VOLTAGE (kVp)

H.g Results from test run 6

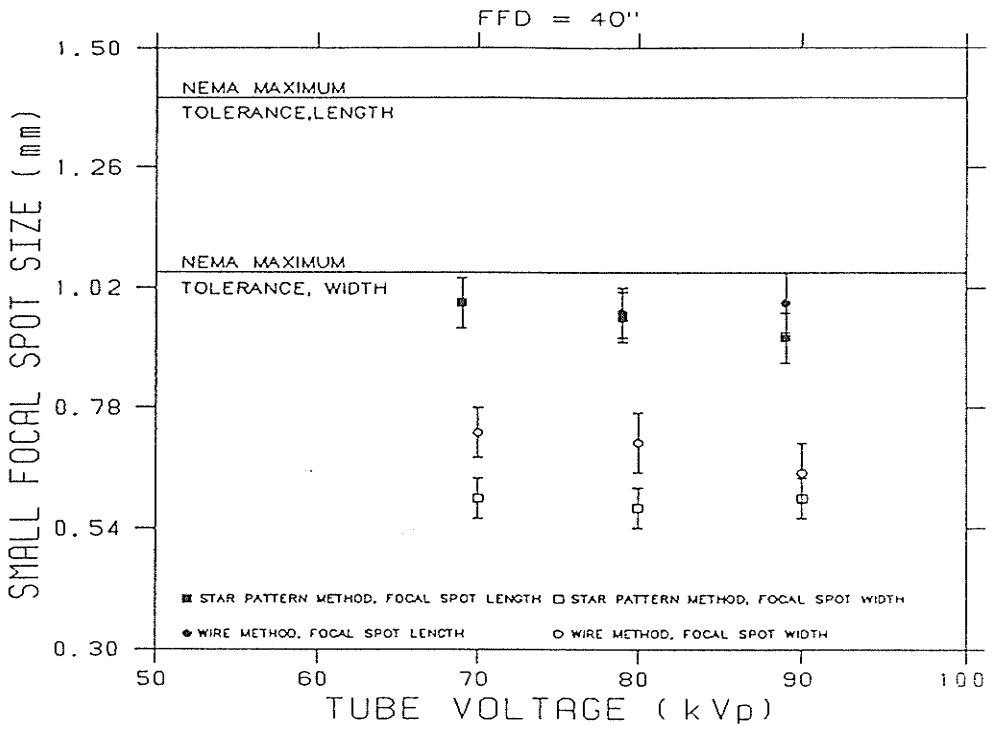

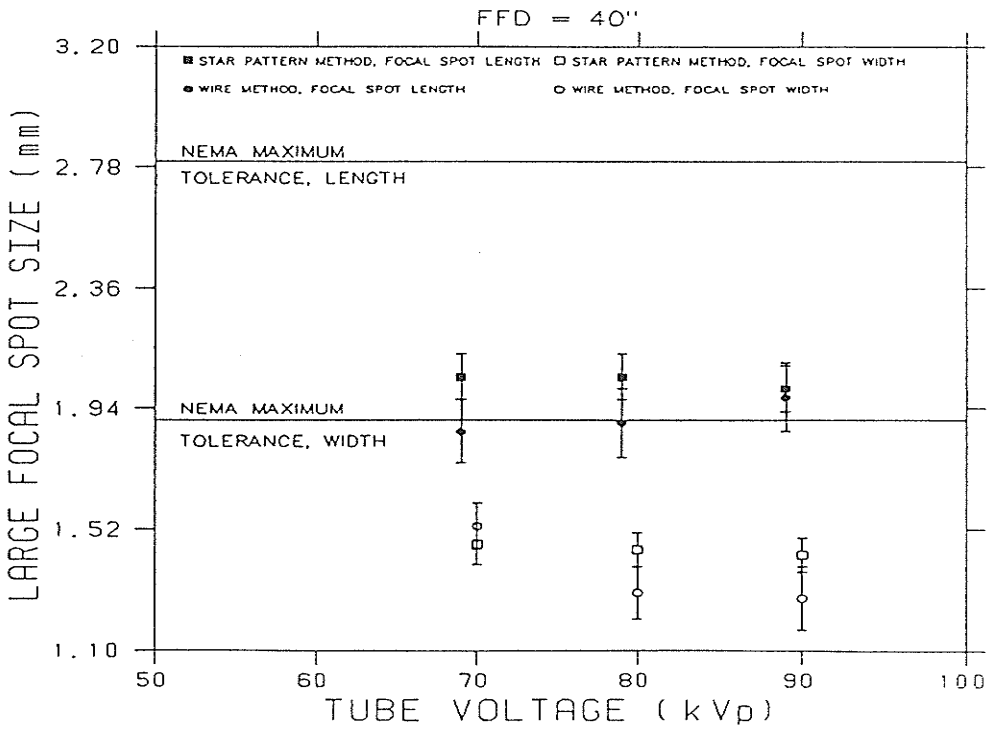

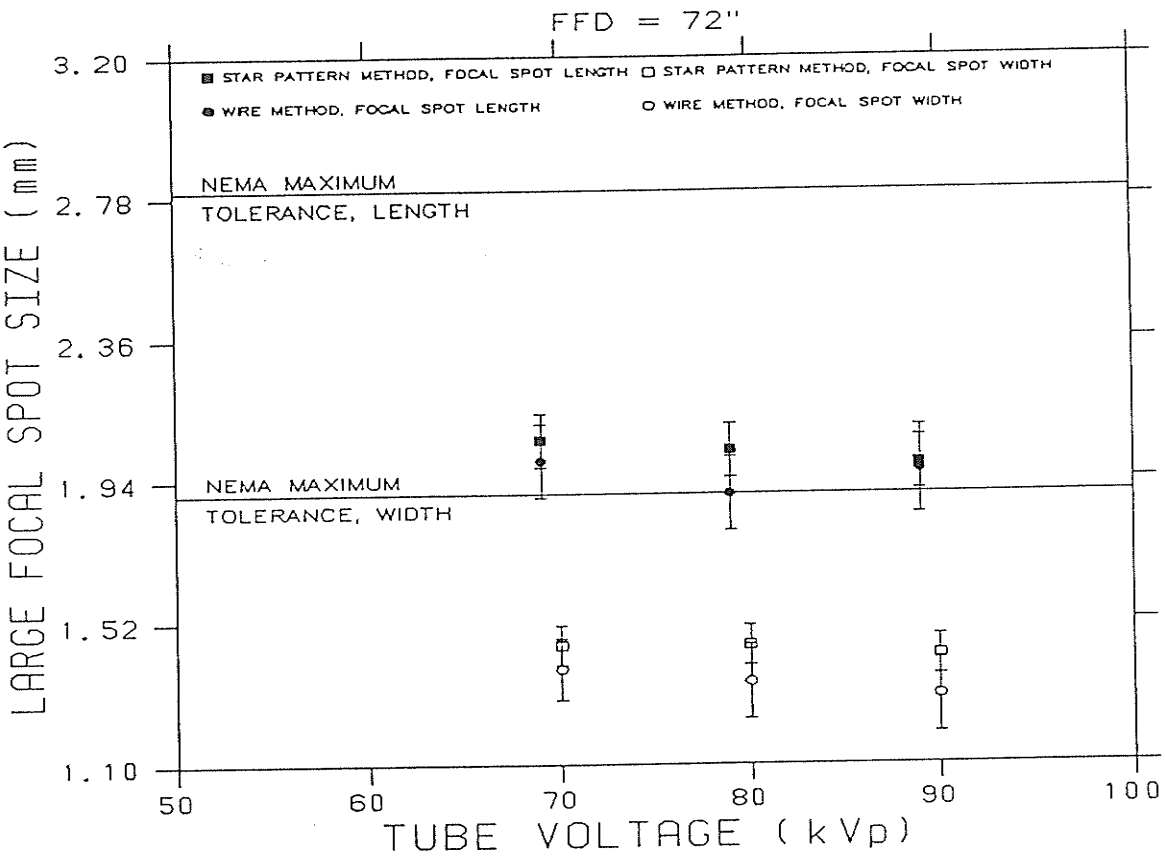
FFD = 72"
STAR PATTERN METHOD, FOCAL SPOT LENGTH
STAR PATTERN METHOD, FOCAL SPOT WIDTH
WIRE METHOD, FOCAL SPOT LENGTH
WIRE METHOD, FOCAL SPOT WIDTH
NEMA MAXIMUM TOLERANCE, LENGTH
NEMA MAXIMUM TOLERANCE, WIDTH
LARGE FOCAL SPOT SIZE (mm)
3.20
2.78
2.36
1.94
1.52
1.10
50
60
70
80
90
100
TUBE VOLTAGE (kVp)

H.h Results from test run 7

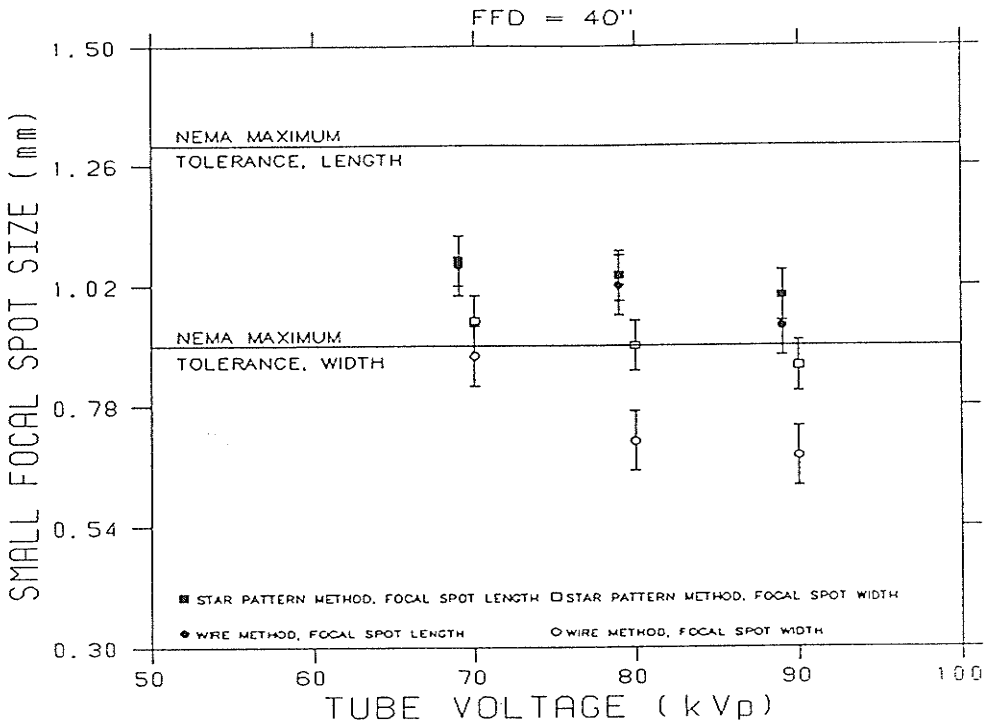

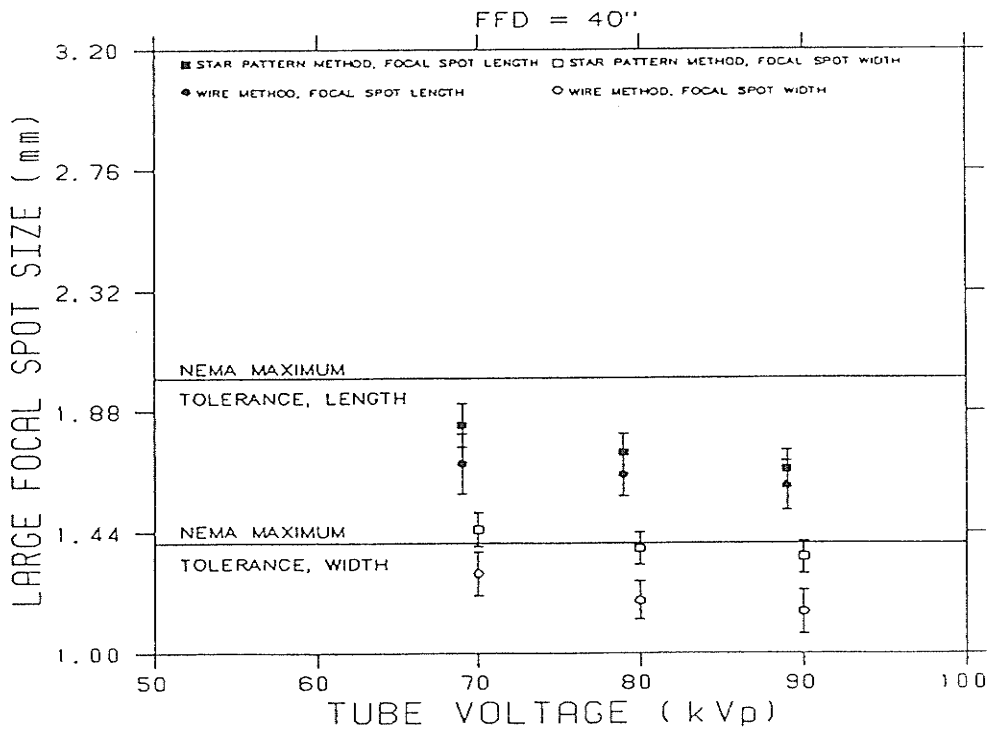

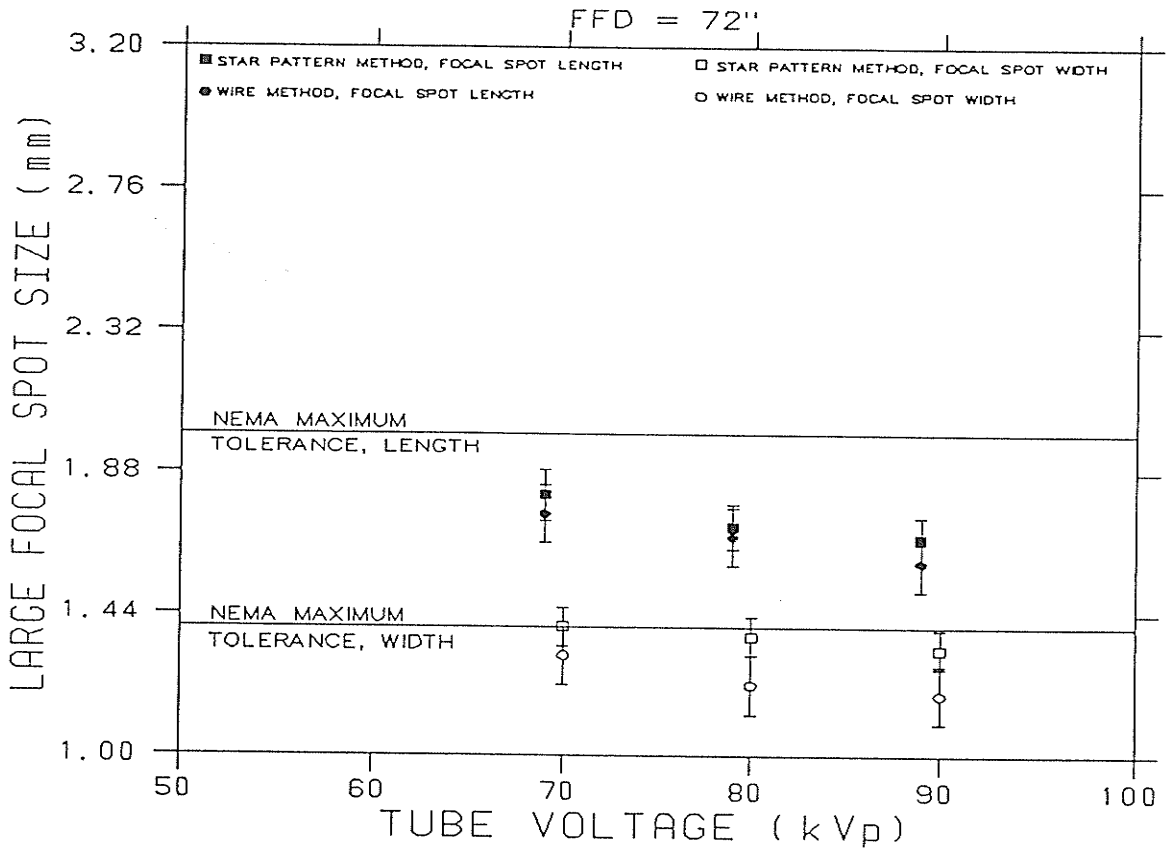
FFD = 72"
STAR PATTERN METHOD, FOCAL SPOT LENGTH
WIRE METHOD, FOCAL SPOT LENGTH
STAR PATTERN METHOD, FOCAL SPOT WIDTH
WIRE METHOD, FOCAL SPOT WIDTH
NEMA MAXIMUM TOLERANCE, LENGTH
NEMA MAXIMUM TOLERANCE, WIDTH
LARGE FOCAL SPOT SIZE (mm)
3.20
2.76
2.32
1.88
1.44
1.00
50
60
70
80
90
100
TUBE VOLTAGE (kVp)

APPENDIX I

PINHOLE CAMERA COMPARISON RESULTS

I.a Results from test run 1

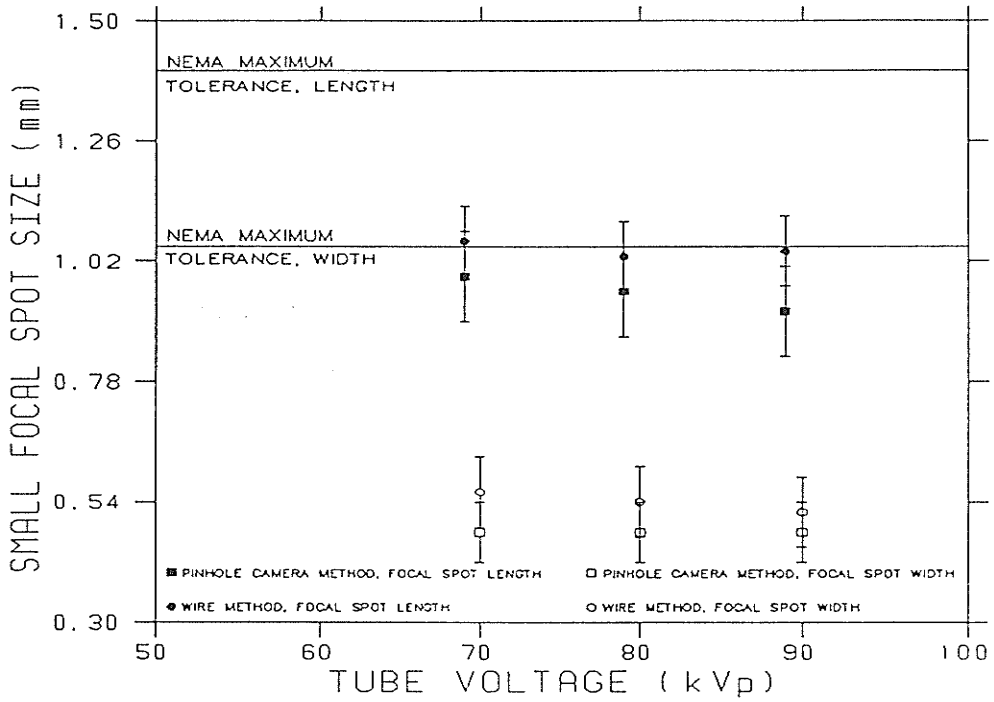

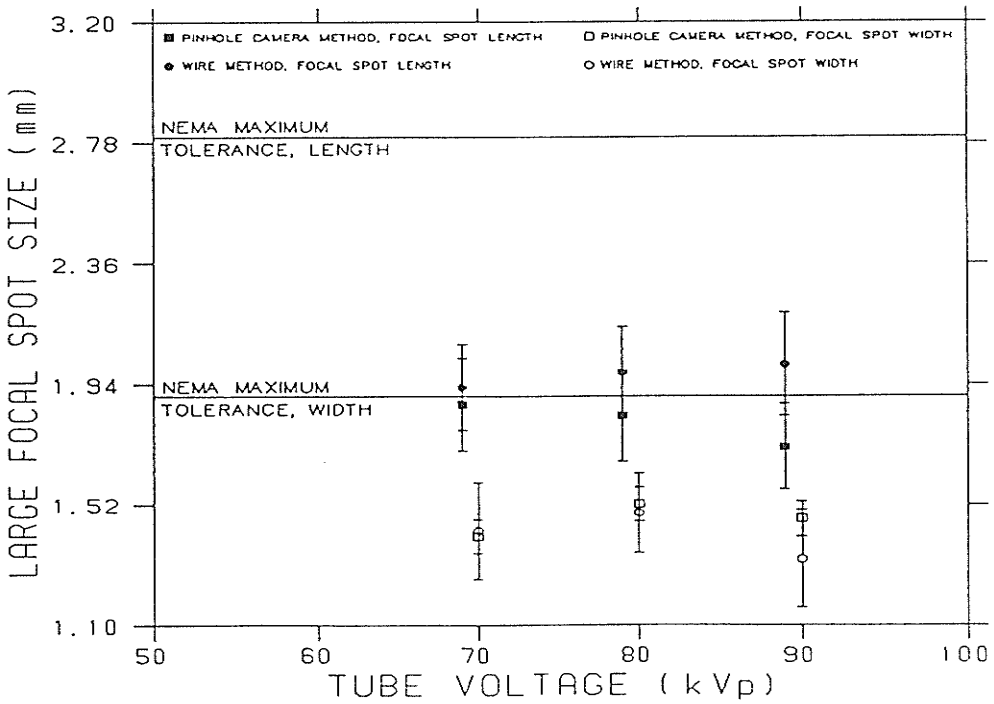

I.b Results from test run 2

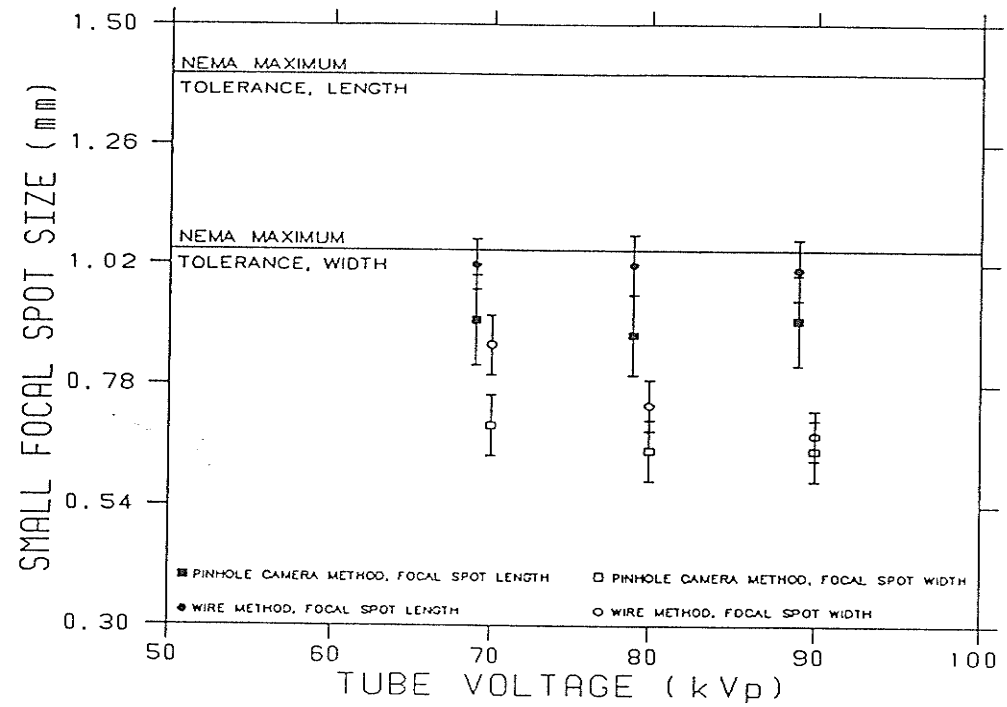

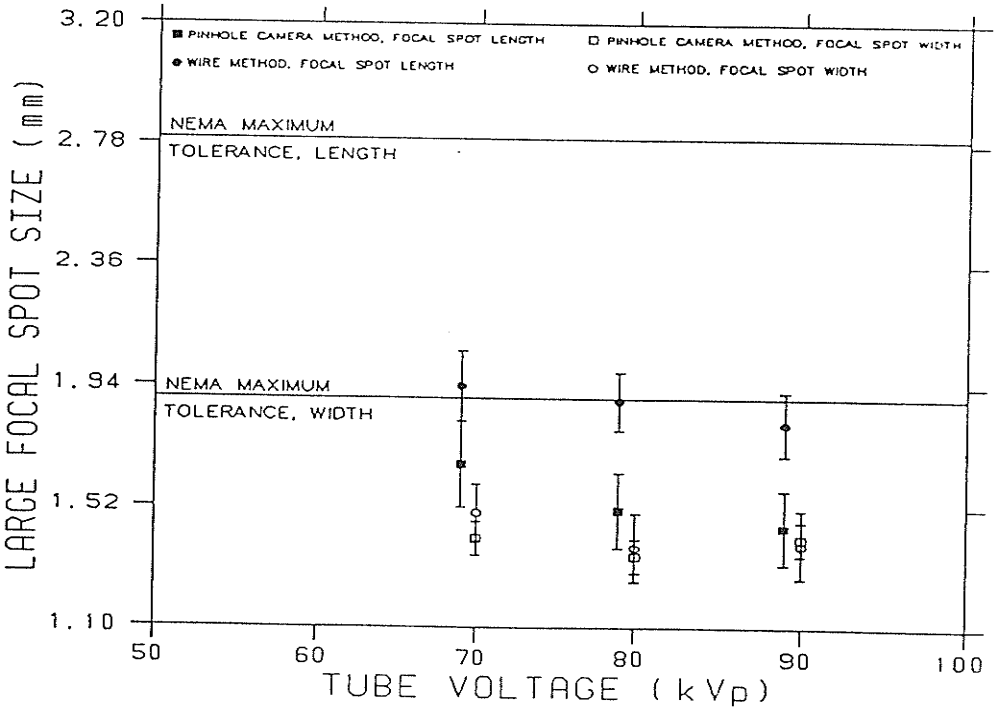

I.c Results from test run 3

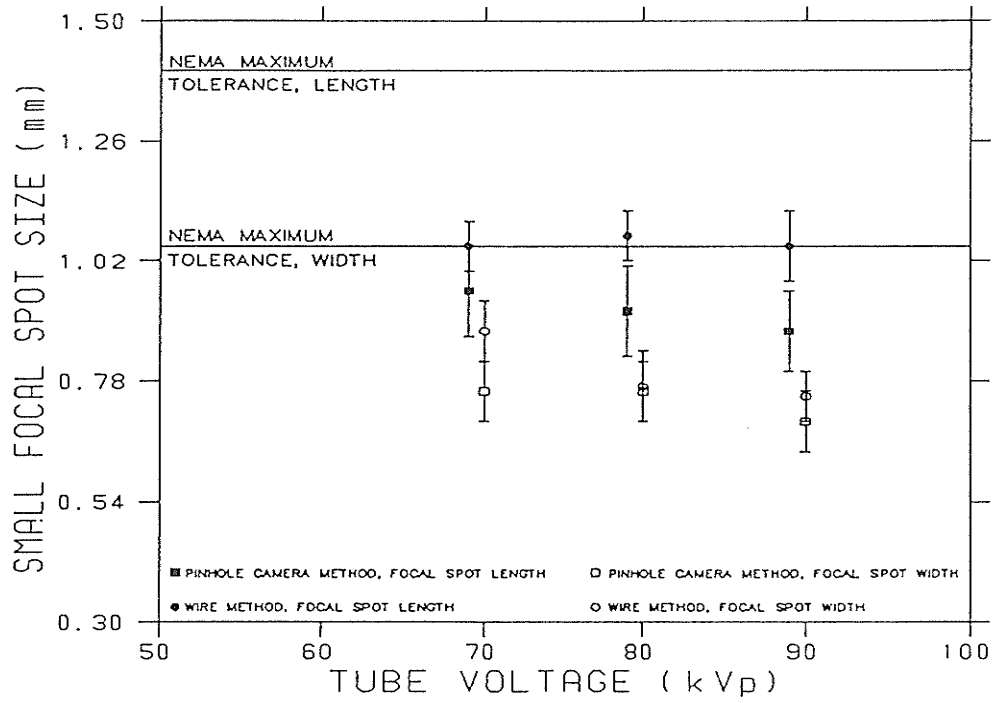

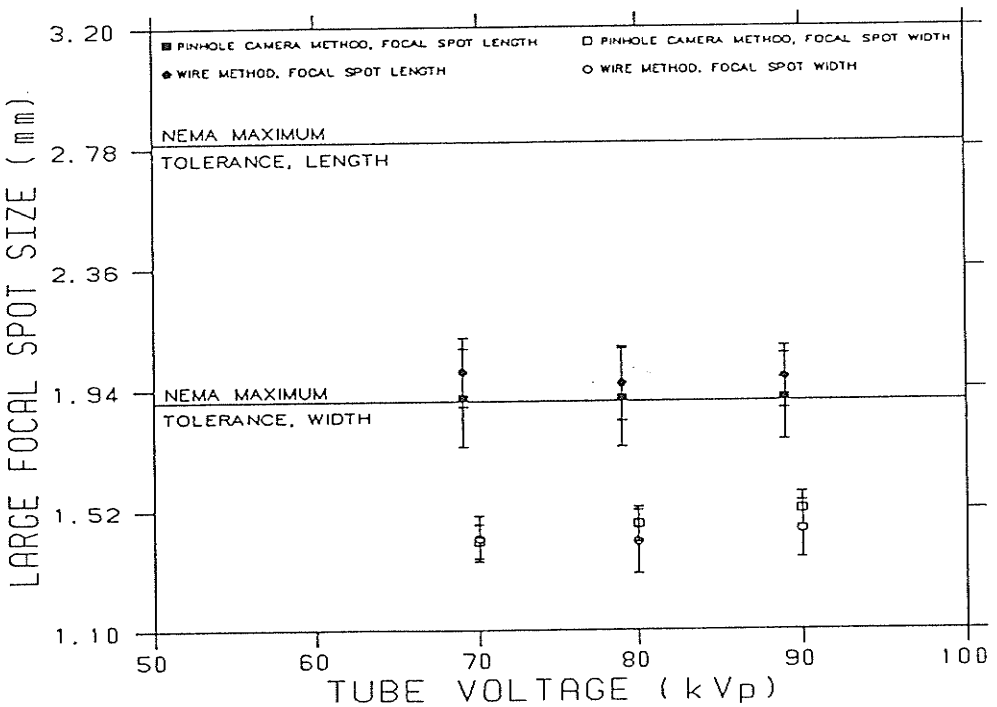

I.d Results from test run 4

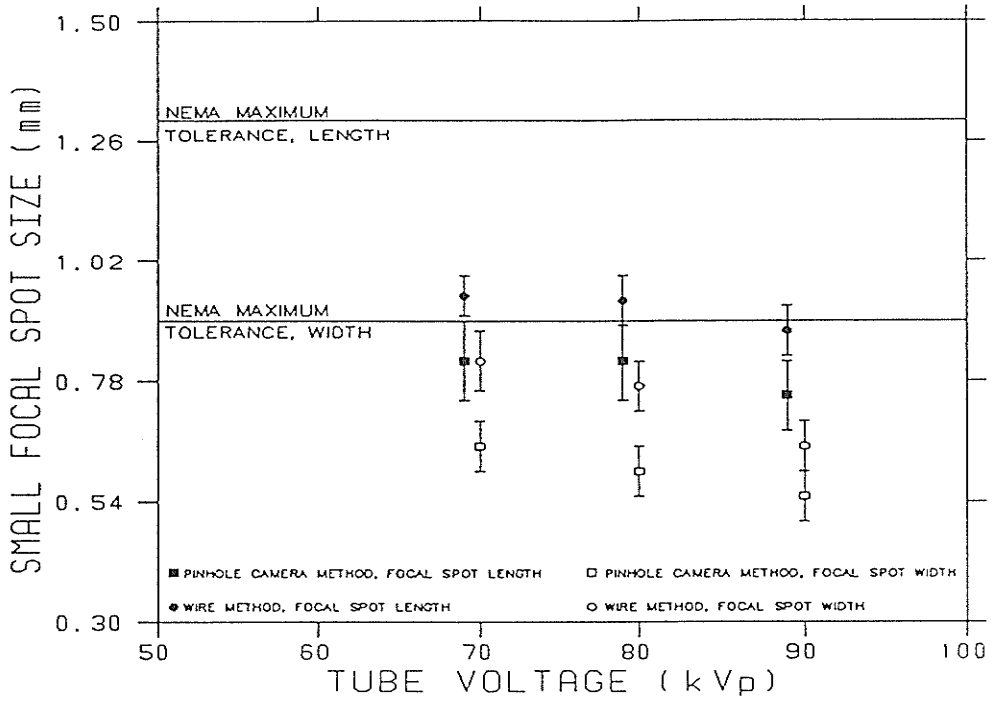

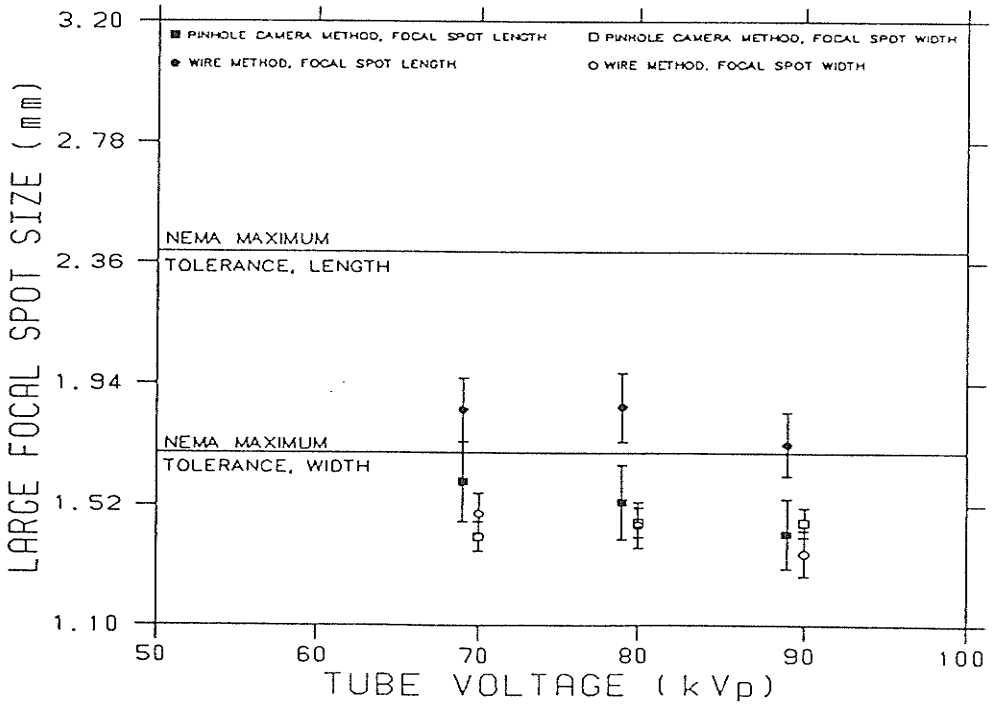

I.e Results from test run 5

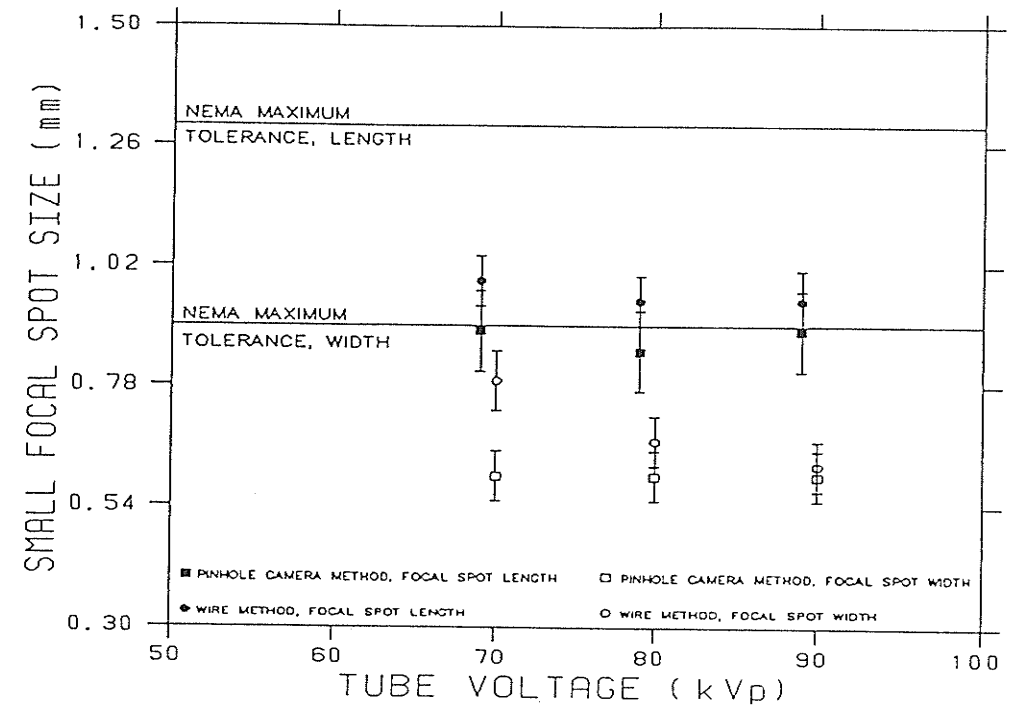

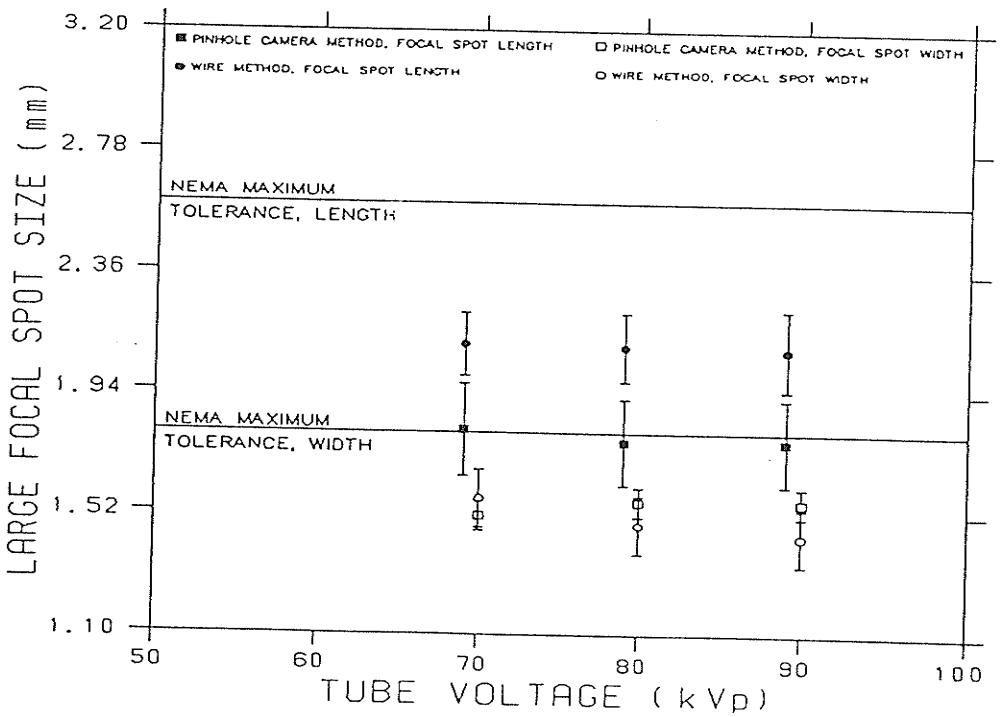

I.f Results from test run 6

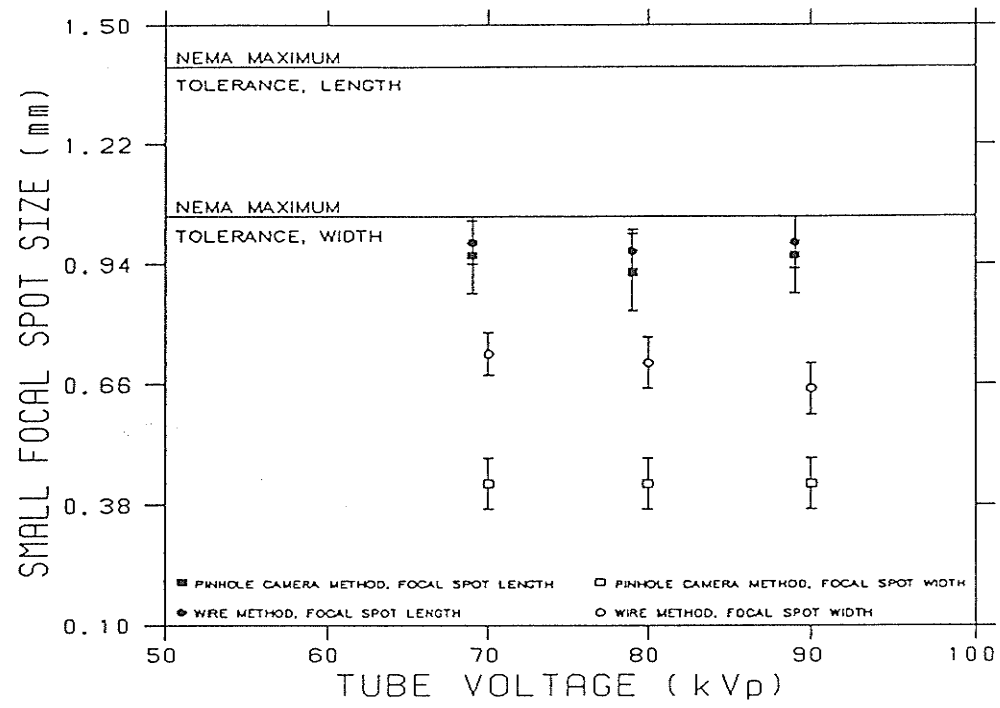

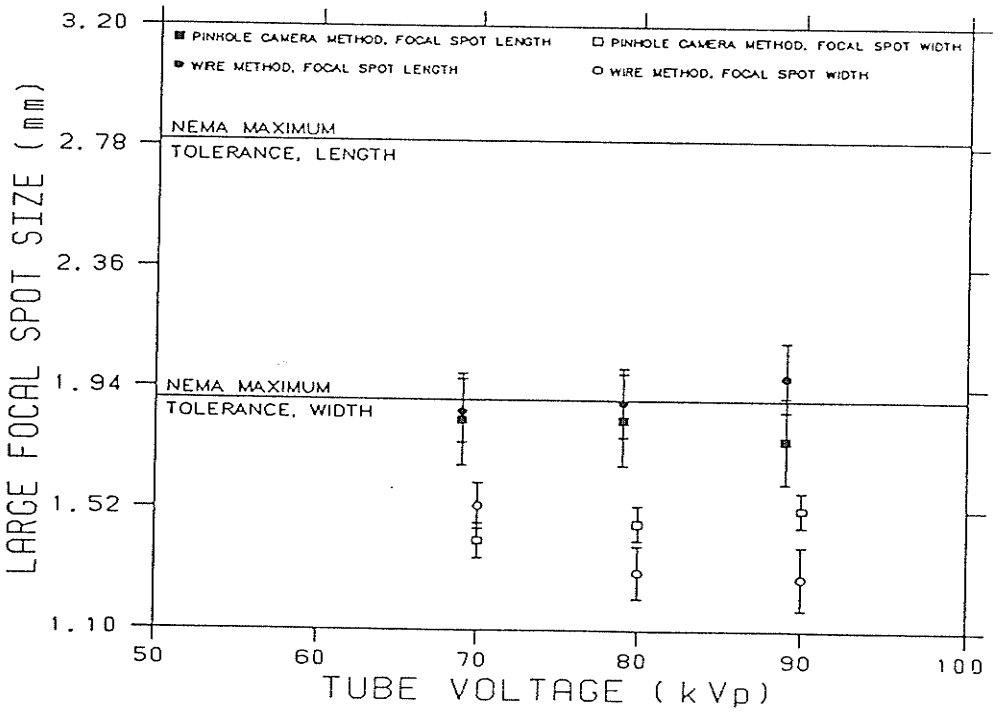

I.g Results from test run 7